Biochemical and Physiological Investigations on Adenosine Monophosphate Deaminase and Haloacid Dehalogenase Superfamily Members from *Plasmodium spp.*

A Thesis Submitted for the Award of the Degree of

Doctor of Philosophy

By

Lakshmeesha K N

Thesis Supervisor: Prof. Hemalatha Balaram

Molecular Biology and Genetics Unit,

Jawaharlal Nehru Centre for Advanced Scientific Research

(Deemed to be University)

Bangalore-560064, India

July, 2019

Biochemical and Physiological Investigations on Adenosine Monophosphate Deaminase and Haloacid Dehalogenase Superfamily Members from *Plasmodium spp.*

- Lakshmeesha K N

July 2019

Declaration

I hereby declare that this thesis entitled, **"Biochemical and Physiological Investigations on Adenosine Monophosphate Deaminase and Haloacid Dehalogenase Superfamily Members from *Plasmodium spp*."** is an authentic record of research work, which has been carried by me under the supervision of Prof. Hemalatha Balaram at the Molecular Biology and Genetics Unit, Jawaharlal Nehru Centre for Advanced Scientific Research, Bangalore, India and this work has not been submitted elsewhere for the award of any other degree.

In keeping with the general practice of reporting scientific observations, due acknowledgements have been made wherever the work described has been based on the findings of other investigators. Any omission, which might have occurred by oversight or misjudgment, is regretted.

Lakshmeesha K N

JNCASR, Bengaluru

Molecular Biology and Genetics Unit
Jawaharlal Nehru Centre for Advanced Scientific Research
Jakkur, Bengaluru-560064, India

Hemalatha Balaram, Ph.D.

Professor

Certificate

This is to certify that the work described in this thesis entitled **"Biochemical and Physiological Investigations on Adenosine Monophosphate Deaminase and Haloacid Dehalogenase Superfamily Members from *Plasmodium spp*."** is the result of investigations carried out by Mr. Lakshmeesha K N in the Molecular Biology and Genetics Unit, Jawaharlal Nehru Centre for Advanced Scientific Research, Bengaluru, India under my supervision, and that the results presented in this thesis have not been previously formed the basis for the award of any other diploma, degree or fellowship.

Prof. Hemalatha Balaram,

JNCASR, Bengaluru

Date

♦Telephone: 91-80-22082812 ♦Telefax: 91-80-22082766 ♦Email: hb@jncasr.ac.in

Acknowledgements

I hereby express my heartfelt regards to Prof. Hemalatha Balaram, for providing me with a valuable opportunity to work in her lab and also for her guidance without which this project would have been a difficult venture. She has been very supportive and gave me the independence to carry out research and helped me grow as an individual. I also thank her for inspiring me to develop the habit of reading.

I would like to thank all the faculty of MBGU, Prof. Anuranjan Anand, Prof. Ranga Uday Kumar, Prof. MRS Rao, Prof. Tapas Kundu, Prof. Maneesha Inamdar, Prof. Kaustuv Sanyal, Prof. Namita Surolia, Dr. Ravi Manjithaya, Dr. Jayanta Haldar, Dr. Meher Prakash, Dr. James Chelliah, Dr. Sheeba Vasu and Dr. Kushagra Bansal, whose course work and inputs helped me immensely in understanding some of the fundamental concepts in biology. I am highly indebted to Dr. Ramesh (our beloved Ramesh Sir) who taught us not only science but also discipline and ethics in science, during our practical course. My regards to Mr. Mohan who also taught us practicals in MS lab.

I also thank my viva examiners Prof. HS Savithri and Prof. B Gopal from IISC for their inputs and constructive criticisms. I am indebted to Prof. Rajan Dighe lab (Simna), Prof. PN Rangarajan lab (Krishna), for providing me strains and plasmids and Prof. P Balaram and Dr. Venkatesh for fruitful discussions. I am extremely thankful to Prof. T Govindaraju and Dr. Kota Arun Kumar for a productive collaboration which was very critical for the completion of my study.

I thank Mr. Sourav Roy and Dr. Vasudeva S P, for mentoring and teaching me during my lab rotation. Also, I would like to thank all my lab members (past and present) Vinay, Bharath, Sanjeev, Vijay, Arpit, Santosh, Prasoona, Jyothi, Umesh, Manu, Sonia, Vidhi, Debarati, Keerthana, Aparna, Arpitha, Meenakshi, Asutosh, Veena, Pavitra, Resmi, Neelakshi, Anusha, Sarika, Satya, Rashi (chotu), Nivedita, Irene, Pragya, Divya, Ruchika, Dhanlakshmi ma'am, Rahul (Ms student), Rahul (Post Doc) and Rahul (POBE), Subrata, Avishek, Srijana, Dr. Reghu Ravindran, Bala, and all the summer interns Kavya, Hamna, Palak, Mridul, Shadab for providing a great working environment and for their valuable suggestions. The scientific and philosophical discussions on the coffee table and heated political debates I had with my lab mates have got etched in my memory. Each one with their unique personality traits and idiosyncrasies has made a lasting impression in my mind. They have been great friends, mentors and critiques and have played a huge role in molding my personality.

My gratitude to Dr. Ravi Manjithaya, in whose lab I did my second lab rotation. Part of the work in my thesis was possible because of the skills I learned in his lab. I would like to thank all 'Autophagy lab' members; especially Piyush, Farheen, Amol, Sunaina, Shashank, Vishwa, Gaurav, Suresh, Veena and Sridevi for their extensive help.

I thank Anita ma'am, Suma ma'am and Dr. Prakash for their help and support. I would like to

thank JNCASR for providing a conducive environment to work. I would like to thank JNCASR and CSIR for funding.

I would like to thank batch mates and friends in MBGU and other departments especially Amrutha, Arnab, Abihk, Nikhil, Adma, Gopal, Raagesh, Deepak, Rebu, Arun, Mir mira and Vybhav for making my stay pleasant.

Thanks are due to my family members, my father Mr. K Nagappa, my mother Mrs. Kamala, my brother Sudhindra and sister-in-law Poornima and her family, and my in-laws Mr. Hanumantha Reddy, Mrs. Vandana, Vikram and Subbi for their love and support. Thanks to my friends in Mysore, Sumanth, Pavan H K, Pavan M S, Santosh, Milan, Srikanth, Lokesh, Sanjay, Prashanth, Nataraj, Dr. Raghavendra, who have always encouraged and supported me. Special thanks to Chaithra for tolerating my temper tantrums and to Vibodh for being a bundle of joy. I express my gratitude to Late Prof. Ramachandra Rao, a stranger who became a guiding beacon in my life.

- Lakshmeesha K N

Synopsis

Malaria caused by the parasitic protozoan *Plasmodium* is the most deadly of diseases causing 435,000 deaths worldwide (WHO, 2018). Although the PlasmoDB database is replete with information on the genome and proteome of the organism, most proteins have uncharacterized or putative status. Lack of proper understanding of the biochemistry of the organism has been a major impediment to the efforts put forth towards mitigation of this menacing disease. With genetic manipulation being highly challenging, understanding the physiological significance of these uncharacterized/putative proteins becomes a non-trivial task. In addition to efforts on development of efficient vaccines, studies are being conducted to develop strategies, targeting various aspects of parasite's physiology both in human and in the insect host (mosquito). One of the major approaches one can adopt is the exploitation of the differences between the host and parasite metabolism. Energetic requirements in *Plasmodium* that are solely dependent on glycolysis (Mehta et al., 2006) and an inability to synthesize precursors of purine nucleotides *de novo* (Downie et al., 2008) (due to absence of *de novo* pathway enzymes) are a couple of attractive features which are of interest to a biochemist working on *Plasmodium*.

The current study focuses on the preliminary characterization of a purine nucleotide cycle enzyme, AMP deaminase (AMPD hereafter) and members of the Haloacid Dehalogenase superfamily (HADSF) from *Plasmodium falciparum* and *Plasmodium berghei*. Purine nucleotide cycle performs inter-conversion of IMP and AMP with the release of fumarate and ammonia as by-products, that have physiological consequences. The pathway also plays a chief role in maintaining the adenylate energy charge (AEC) ratio, which is critical for cell survival (Chapman and Atkinson, 1973). This is achieved by regulating the levels of AMP. AMPD is a catabolic enzyme which deaminates AMP to IMP that can be further channelized to GMP production or AMP synthesis depending on the cellular requirement for respective mononucleotides. AMP can also be catabolized to adenosine and inorganic phosphate by specific/promiscuous 5´ nucleotidases, which are a common occurrence in the HAD superfamily. In a cellular context, AMP can be regarded as the central hub for the regulation of AEC. AMP deaminase, as well as nucleotidases, play a key role in maintaining the levels of this metabolite (Fig. 1). Failure in the regulation of AMP levels results in accumulation of this metabolite which has been shown to inhibit the *de novo* purine biosynthetic pathway that subsequently leads to defective protein synthesis (Akizu et al., 2013). AMP accumulation also drives the adenylate kinase reaction in the direction towards ATP depletion, which is physiologically not productive. Given the importance of nucleotide metabolism in the malarial parasite, it becomes imperative to have a substantial understanding of the modes and players involved in the regulation of nucleotide levels. Here, we have made an attempt to understand the role of AMPD and putative nucleotidases belonging to HAD superfamily from the parasitic protozoan *Plasmodium*.

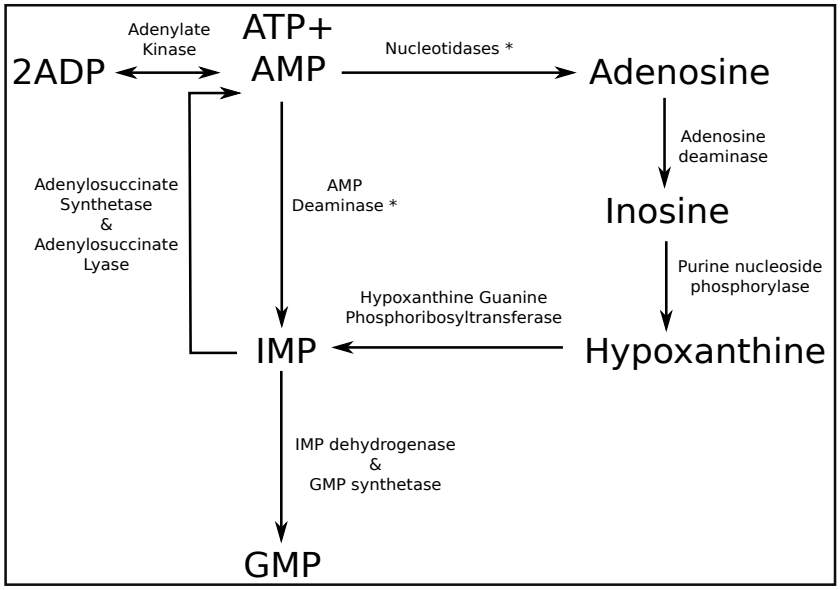

Figure 1: Regulation of AEC by enzymes involved in purine nucleotide metabolism Schematic representation of the regulation of AEC by modulation of AMP levels by AMPD and nucleotidases. * indicates enzymes under current study.

The current work is a continuation of my MS (Master of Science) project which was aimed at purification and preliminary characterization of AMPD, and this Ph.D. thesis consists of two parts – the first one dealing with attempts towards expression of recombinant *Plasmodium falciparum* AMPD (PfAMPD), characterization of the recombinant protein, generation and characterization of AMPD knockout parasites in the *P. berghei* model system. The second part comprises expression, purification, preliminary biochemical characterization and genetic ablation of HADSF members from *Plasmodium falciparum* and *Plasmodium berghei*.

A general introduction consisting of a concise description of *Plasmodium* life cycle, malaria epidemiology, host-pathogen interaction, parasite physiology and metabolism, plausible drug targets, and intervention strategies is provided at the beginning of the thesis that sets the basis for the work undertaken. This constitutes chapter one.

Chapter two provides a detailed description of the materials and methods employed for the study on *Plasmodium* AMPD. This involves various strategies adopted for the production of recombinant protein along with methods used for ablation of AMPD gene in *P. berghei*, the rodent malaria model. The results of these experiments are provided in a consolidated manner and are elaborately discussed in chapter three. Chapter two also provides a detailed description of the materials and methods employed for the study of *Plasmodium* HADSF members. This comprises bioinformatic analysis on HADSF members and a detailed account on gene cloning, expression and purification of candidate proteins belonging to HAD superfamily, *in vitro* characterization and methods used for genetic ablation of HADSF genes in *P. berghei*. The results of these experiments are compiled and discussed in detail in chapter four.

Chapter three provides a comprehensive account of the first part of the thesis - 'Studies on *Plasmodium* AMP deaminase'. The introductory section provides a preamble for the studies conducted on AMP deaminase. Apart from elaborating on the aspects of nucleotide metabolism in *Plasmodium falciparum*, purine nucleotide cycle, adenylate energy charge and its regulation, this section also includes bioinformatic analysis on AMP deaminase. This section also contains a description of the unique features of AMP deaminase, its catalytic mechanism and concludes with the objectives laid down for subsequent studies.

Various strategies, vectors and expression systems were used for the heterologous production of recombinant PfAMPD (PF3D7_1329400). Expressing and purifying functional AMPD was extremely difficult and hence a multitude of approaches had to be sought. A large investment in the form of time and resources had to be made to empirically establish conditions that were ambient for the production of a functional protein. The rationale for selection, along with probable causes for failure of each strategy/expression system has been addressed in detail. Among all the expression systems employed (*E. coli*, *S. cerevisiae*, *P. pastoris* and cell-free system), PfAMPD was recombinantly expressed in *S. cerevisiae,* only after harmonizing the codons in the PfAMPD gene according to the codon usage of the yeast system. But, obtaining a soluble protein demanded much more. The protein being highly unstable, readily degraded *in vivo* and displayed a significant improvement in stability when tagged with GFP at the C-terminus. Despite all the efforts, low levels of expression prevented us from purifying the protein in large scale.

Characterization of PfAMPD was performed by evaluating the ability of wildtype and mutant forms of PfAMPD to complement the deficiency of its homologue in a knockout yeast strain (*Δamd1*). The *Δamd1* strain shows a strong growth defect phenotype when challenged by the addition of S-adenosyl methionine in the growth medium (Saint-Marc et al., 2009). A detailed description of the principle behind this complementation assay and the different modes by which rescue can be achieved has been addressed here. Also, discussed, is the importance of various residues in the functionality of PfAMPD protein based on analysis of sequence, structure and literature available on AMPD from other organisms and evidence from our complementation assay. The prime focus here is to bring forth the similarities and key differences between PfAMPD and its homologues from *S. cerevisiae*, *Arabidopsis* and human.

Two strategies were employed to determine the localization of AMPD, 1) endogenous tagging of the *P. berghei* AMPD gene with GFP at the C-terminus and 2) episomal expression of C-terminal GFP-tagged PbAMPD using centromeric plasmid pBCEN5 (Iwanaga et al., 2010). Unfortunately, the endogenous tagging strategy failed as a consequence of a point mutation in the GFP sequence rendering it non-fluorescent. Attempts to express GFP-tagged PbAMPD from an episomal vector also met with failure as multiple transfection experiments did not yield drug-resistant parasites. However, drug-resistant parasites were obtained when transfection was done with pBCEN5 expressing catalytically inactive mutant of PbAMPD. *Plasmodium* is completely dependent on host for its purine source and operates predominantly via the HGXPRT (hypoxanthine-guanine-xanthine phosphoribosyltransferase) route to make IMP, which is then converted to AMP via the

ADSS (adenylosuccinate synthetase) and ASL (adenylosuccinate lyase) pathway and GMP via the IMPDH (IMP dehydrogenase) and GMPS (GMP synthetase) reactions. AMP thus generated will be utilized for various cellular processes including DNA synthesis during cell division. In such a metabolic context, increased expression of an enzyme that catabolizes AMP might result in the futile cycling of AMP/IMP interconversion, probably leading to a deficit of AMP that would have a deleterious effect on actively dividing cells. This hypothesis, explains our inability to get drug-resistant parasites when transfection was performed with a plasmid expressing active AMPD that leads to higher levels of the enzyme in the cell. In addition to this, results pertaining to *in vivo* work done towards determining the essentiality of AMPD in *P. berghei* (PBANKA_1344400) demonstrate the dispensable nature of this protein during the intra-erythrocytic stages of the parasite's life cycle, including gametocyte stages.

The second part of this thesis - 'Studies on HADSF members', addresses a completely different class of enzymes, the 'nucleotidases'. Although unrelated to AMP deaminase the aspect under study still revolves around the metabolism of nucleotides and its consequence on the parasite's physiology. Chapter four consists of an introduction section comprising bioinformatic analysis and objectives laid down towards the characterization of HADSF members (PF3D7_1118400, PF3D7_1226100 (PfHAD3) and PF3D7_0715000 (PfPGP)). Apart from providing a descriptive account of the structural and functional features of this superfamily of proteins, a brief account of earlier studies carried out by our group on HADSF members (PVX_123945 *aka* PvHAD2 and PF3D7_1206100 *aka* PfISN1) from *Plasmodium* is also discussed (Srinivasan and Balaram, 2007; Srinivasan et al., 2015).

All the HAD members in the current study were expressed and purified using the *E. coli* expression system. Identification of physiologically relevant substrates by an unbiased substrate screen, determination of key properties such as oligomeric state, optimum pH, preferred divalent metal ion are the key features discussed. It was not surprising to find that one of the HADSF members, PF3D7_1118400 (referred to as PfHADx here onwards, where 'x' implies unknown relevant physiological substrate) displayed substrate promiscuity acting on a broad category of monophosphates such as purine/pyrimidine monophosphates as well as phosphorylated cofactors and sugar phosphates. The second HAD member PfHAD3 turned out to be completely insoluble when expressed in *E. coli* and hence could not be characterized biochemically. Although the other HAD member under study, PfPGP, was earlier proposed to have implication in vitamin B1 metabolism (Knöckel et al., 2008), its sequence homology with phosphoglycolate phosphatases from yeast and human prompted us to re-investigate its properties. Surprisingly, even this enzyme was found to be in the insoluble fraction. But, its homologue from *P. berghei,* PBANKA_1421300 (PbPGP), was expressed in soluble form and upon further biochemical characterization displayed stark contrast in its choice of substrates when compared to PfHADx. PbPGP was found to have very high activity on 2-phosphoglycolate and 2-phospho L-lactate in addition to generic substrates para-nitophenyl phosphate (pNPP) and β-glycerophosphate. This enzyme function is vital as it is involved in dephosphorylation of toxic metabolites generated as a consequence of enzymatic

side reactions. In addition to substrate identification and preliminary kinetic characterization, data pertaining to active site mutants confirmed that the proteins under study are indeed HADSF members.

The question of essentiality is again invoked in the case of HADSF members. Presence of multiple HADSF members in an organism and their established role as repertoires for evolution along with implications in house-cleaning and drug resistance (Kuznetsova et al., 2006; Titz et al., 2007) renders them attractive for reverse genetic approaches. In a manner similar to AMPD, individual HADSF members were also genetically ablated using linear plasmid constructs generated by recombineering strategy. Knockout studies were conducted on HADSF members PBANKA_1441100 (PbHAD2) (homologue of PVX_123945 *aka* PvHAD2), PBANKA_1441000 (PbHAD3) (homologue of PF3D7_1226100 *aka* PfHAD3), PBANKA_0929700 (PbHADx) (homologue of PF3D7_1118400 *aka* PfHADx) and
PBANKA_1421300 (PbPGP) (homologue of PF3D7_0715000 *aka* PfPGP). Of these four HADSF members, knockout parasites were generated for all except PbPGP even after multiple attempts, suggesting its essentiality. To rule out the possibility of the locus being refractory for genetic recombination, GFP tagging was attempted and homogenous population of transfectants was obtained. Having established that the locus is amenable for genetic manipulation, a conditional knockdown strategy at protein level making use of a regulatable fluorescent affinity tag (RFA) (Muralidharan et al., 2011) was adopted. Though a homogenous population of transfectants was obtained, significant levels of knockdown could not be achieved. This kind of scenario has earlier been described for yoelipain where the authors were unable to knockout/disrupt the gene suggesting its essentiality. However, attempts at lowering the protein level led to insufficient decrease and hence a phenotype was not observed (Pei et al., 2013). Likewise, PbPGP is essential during the asexual stages of the parasite life cycle.

Apart from the aforementioned chapters an overall discussion summarizing key conclusions of the study carried out along with future prospects has been provided. An appendix listing primers, additional experimental data, list of equations, the composition of reagents/media used and copyright permissions are also included. The literature referred to in the thesis are listed in the 'Bibliography' section. In its entirety, this thesis is a consolidated account addressing the role of two distinct classes of enzymes, AMPD and HADSF members, aimed at providing a better understanding of nucleotide metabolism and serendipitously identifying a conserved detoxifying mechanism in the malaria parasite *Plasmodium*. The study conducted on AMPD and the study on PGP has been published (Nagappa et al., 2019a,b).

List of Publications

1. How a purine salvage enzyme singles out the right base. **Lakshmeesha Kempaiah Nagappa**, Sundaram Balasubramanian and Hemalatha Balaram. **Journal of Biological Chemistry** (invited Editors' Pick Highlight), 2019.

2. Biochemical and physiological investigations on adenosine 5' monophosphate deaminase from *Plasmodium spp.* **Lakshmeesha Kempaiah Nagappa***, Dipti Singh*, Sandeep Dey, Kota Arun Kumar, Hemalatha Balaram. **Molecular Microbiology**, 2019.

3. Phosphoglycolate phosphatase is a metabolic proof-reading enzyme essential for cellular function in *Plasmodium berghei*. **Lakshmeesha Kempaiah Nagappa**, Pardhasaradhi Satha, Thimmaiah Govindaraju, Hemalatha Balaram. **Journal of Biological Chemistry**, 2019.

4. Septins are involved at the early stages of macroautophagy in *S. cerevisiae*. Gaurav Barve, Shreyas Sridhar, Amol Aher, Mayurbhai H. Sahani, Sarika Chinchwadkar, Sunaina Singh, **K. N. Lakshmeesha**, Michael A. McMurray, Ravi Manjithaya. **Journal of Cell Science**, 2018.

5. Role of W181 in modulating kinetic properties of *Plasmodium falciparum* hypoxanthine guanine xanthine phosphoribosyltransferase. Sourav Roy*, Tarak Karmakar*, **Lakshmeesha K. Nagappa***, Vasudeva S. Prahlada Rao, Sundaram Balasubramanian, Hemalatha Balaram. **Proteins**, 2016.

6. Kinetic mechanism of *Plasmodium falciparum* hypoxanthine-guanine-xanthine phosphoribosyltransferase. Roy S, **Nagappa LK**, Prahladarao VS, Balaram H. **Molecular and Biochemical Parasitology**, 2016.

7. Slow ligand-induced conformational switch increases the catalytic rate in *Plasmodium falciparum* hypoxanthine guanine xanthine phosphoribosyltransferase. Roy S, Karmakar T, Rao VS, **Nagappa LK**, Balasubramanian S, Balaram H. **Molecular Biosystems**, 2015.

8. Prediction of substrate specificity and preliminary kinetic characterization of the hypothetical protein PVX_123945 from *Plasmodium vivax*. Srinivasan B, **Nagappa LK***, Shukla A*, Balaram H. **Experimental Parasitology**, 2015.

***Equal contribution**

Manuscript under preparation

1. Insights into physiological role of haloacid dehalogenase superfamily members from *Plasmodium spp.* **Lakshmeesha Kempaiah Nagappa et al.**

List of Abbreviations

2,3 BPG – 2, 3 bis phosphoglycerate

2-PGA – 2 Phosphoglyceric acid

3-PGA – 3 Phosphoglyceric acid

ADP – Adenosine diphosphate

ADSS – Adenyloscuccinate synthetase

AEC – Adenylate energy charge

AEC – Aminoethyl carbazole

AICAr – Aminoimidazole carboxamide ribonucleoside

AMP – Adenosine 5' monophosphate

AMPD – AMP deaminase

APRT – Adenine phosphoribosyltransferase

AQUA – Advanced quick assembly

ASL – Adenyloscuccinate lyase

AtAMPD – *Arabidopsis thaliana* adenosine monophosphate deaminase

ATP – Adenosine triphosphate

α-GP – Alpha glycerophosphate

β-GP – Beta glycerophosphate

cAMP – 5' 3' Cyclic adenosine monophosphate

CAS – CRISPR associated

cDNA – Complementary deoxyribonucleic acid

CF11 – Cellulose fibrous 11

CMP – Cytidine monophosphate

CRISPR – Clustered regularly interspaced short palindromic repeats

dAMP – Deoxy adenosine monophosphate

DAPI – 4',6-diamidino-2-phenylindole

DDD – DHFR degradation domain

ddH2O – Double distilled water

DEPC – Diethylpyrocarbonate

dGMP – Deoxy guanosine monophosphate

dIMP – Deoxy Inosine monophosphate

DNA – Deoxyribonucleic acid

dNTPs – Deoxy Nucleoside triphosphate

DTT – Dithio threitol

ECL – Enhanced chemiluminescence

EDTA - Ethylene diamino tetraaceticacid

EEFs - Exo-erythocytic forms

F 1,6 bP – Fructose 1, 6 – bis phosphate

F-6-P – Fructose 6 phosphate

FAD – Flavin adenine dinucleotide

FMN – Flavin mononucleotide

G-1-P – Glucose 1 phosphate

G-3-P – Glycerol 3 phosphate

G-6-P – Glucose 6 phosphate

GCUA – Graphical Codon Usage Analyser

GFP – Green fluorescent protein

GMP – Guanosine monophosphate

GMPS – GMP synthetase

GTP – Guanosine triphosphate

HA – Hemagglutinin

HAD – Haloacid dehalogenase

HADSF – Haloacid dehalogenase superfamily

hDHFR – Human dihyrofolate reductase

HGPRT – Hypoxanthine guanine phosphoribosyltransferase

HGXPRT – Hypoxanthine guanine xanthine phosphoribosyltransferase

HRP – Horseradish peroxidase

HsAMPD – *Homo sapiens* adenosine monophosphate deaminase

IFA - Immunofluorescence assay

IgG – Immunoglobulin G

IMP – Inosine 5' monophosphate

IPTG – Isopropyl thiogalactoside

ISN1 – IMP specific nucleotidase 1

kb – Kilobases

kDa – Kilo Dalton

LB – Lineweaver Burk

LB – Luria Bertani

M-6-P – Mannose 6 phosphate

MM – Michaelis Menten

NAD – Nicotinamide adenine dinucleotide

NAM – Nicotinic acid mononucleotide

Ni-NTA – Nickel-nitrilotriacetic acid

NLS – Nuclear localization signal

NMN – Nicotinamide mononucleotide

OD – Optical density

ORF – Open reading frame

PAC – *Plasmodium* artificial chromosome

PAGE – Polyacrylamide gel electrophoresis

PBS – Phosphate buffered saline

PBST – Phosphate buffered saline with tween-20

PCR – Polymerase chain reaction

PEG – Polyethylene glycol

PEP – Phosphoenolpyruvate

PfAMPD – *Plasmodium falciparum* adenosine monophosphate deaminase

PGAL – Phosphoglyceraldehyde

PLP – Pryidoxal phosphate

PM1KO – Plasmepsin 1 knockout

PMSF – Phenylmethyl sulfonyl fluoride

pNPP – para-nitrophenylphosphate

PRPP – Phosphoribosylpyrophosphate

QC – Quality control

R-5-P – Ribose 5 phosphate

RBC – Red blood corpuscles

RLU – Relative luciferase units

RNA – Ribonucleic acid

rpm – Rotations per minute

RPMI – Roswell Park Memorial Institute

RT-PCR – Reverse transcription PCR

SAM – S–adenosyl methionine

sAMP – Succinyl adenosine monophosphate

ScAMPD – *Saccharomyces cerevisiae* adenosine monophosphate deaminase

SD – Synthetically defined

SDS – Sodium dodecyl sulphate

SDS-PAGE – Sodium dodecyl sulphate–polyacrylamide gel electrophoresis

SFLD – Structure function linkage database

TAE – Tris acetate EDTA

TB – Terrific broth

TIM – Triosephosphate isomerase

TMP – Thymidine monophosphate

TNE – Tris NaCl EDTA

UMP – Uridine monophosphate

UTR – Untranslated region

WT – Wild type

XMP – Xanthosine 5' monophosphate

yFCU – Yeast cytosine deaminase/uridine phosphoribosyltransferase

YPD – Yeast extract peptone dextrose

List of Figures

List of Tables

Contents

Chapter 1

Introduction

This chapter provides a concise description of *Plasmodium* life cycle, malaria epidemiology, parasite pathophysiology and metabolism, some of the plausible drug targets, and current intervention strategies and challenges faced.

1.1 Malaria - a global burden

Malaria caused by the parasitic protozoan *Plasmodium* is the most deadly of diseases causing 435,000 deaths worldwide (WHO, 2018). The disease affects both human and non-human vertebrate hosts and is transmitted by female mosquitoes of the genus *Anopheles*. The parasite has been in existence along with its host for millions of years and has evolved mechanisms to escape from the host immune system and has also developed resistance to existing anti-malarial drugs (Carter and Mendis, 2002; Antony and Parija, 2016). Human malaria is caused by five species of *Plasmodium* namely *P. falciparum, P. vivax, P. malaria, P. ovale and P. knowlesi* (Cowman et al., 2016). The disease is predominantly seen in tropical and subtropical parts of the globe with a large population carrying the parasite in South Asia, while recording high numbers of fatality in Africa most of which are children. Even though the development of the insecticide DDT marked a milestone in the path towards the eradication of malaria, this achievement was not sustainable as a consequence of the emergence of resistance in mosquitoes. Due to the elimination of malaria in parts of Europe and America, the eradication programme did see a dip in interest (Greenwood and Mutabingwa, 2002). However, the battle is still going on in malaria-endemic regions such as India, Sub-Saharan Africa and parts of south-east Asia.

1.2 Life cycle of the malaria parasite

The malaria parasite completes its life cycle in two hosts, the mosquito vector and vertebrate host (primates, rodents, birds and reptiles). The infection initiates when a carrier female *Anopheles* mosquito injects haploid sporozoites while taking a blood meal from a healthy vertebrate host. The sporozoites enter the bloodstream, reach the liver and establish infection in the hepatocytes. Inside the hepatocytes, the sporozoites transform into merozoites that upon release into the bloodstream infect erythrocytes and initiate the asexual cycle. RBCs are ideal hosts for the parasite as they lack major histocompatibility complexes (MHC) on the cell surface, thereby aiding the parasite in evading the host immune system. The intra-erythrocytic development of *Plasmodium* has four distinct stages, rings, trophozoites, schizonts and merozoites. The time duration for one intra-erythrocytic cycle differs among different species of *Plasmodium*. *P. falciparum* completes one erythrocytic asexual cycle in approximately 48 hours while it is 24 hrs for *P. berghei*. Once the liver stage merozoites invade erythrocytes the parasite is harboured inside a membranous parasitophorous vacuole. The progress through various intra-erythrocytic stages is marked by morphological changes. During the ring stage, the parasite starts to feed on the hemoglobin content of the erythrocyte and matures into a trophozoite that is characterized by the presence of a dark hemozoin pigment (a polymer of heme) in the food vacuole. The parasite nucleus now undergoes division giving rise to multiple daughter nuclei that is a characteristic feature of the schizont stage. During cytokinesis, each of the nuclei acquires a bit of cytoplasm forming merozoites. Post-lysis of the erythrocyte, merozoites emerge and repeat the asexual cycle

by invading fresh erythrocytes. A small proportion of schizonts cycling through the asexual stages commit to sexual development and differentiate into male or female gametocytes. The number of male gametocytes is lower in comparison to their female counterpart as each male gametocyte can give rise to eight male gametes whereas each female gametocyte produces only one female gamete. Sexual dimorphism is clearly evident in the case of *P. falciparum* gametocytes whereas it is not distinct in *P. berghei*. The gametocytes are taken up by a female *Anopheles* mosquito during its blood meal from an infected individual. The gametocytes mature in the mosquito host to form male and female gametes, followed by fertilization in midgut to give rise to a diploid zygote. The zygote further differentiates into a motile ookinete that invades the epithelium of the midgut. This is followed by transformation into a sessile oocyst that harbours hundreds of sporozoites. The sporozoites egress into the hemolymph and eventually reach the salivary gland ducts where they await further transmission to a new vertebrate host (Phillips et al., 2017). This is represented in Fig. 1.1.

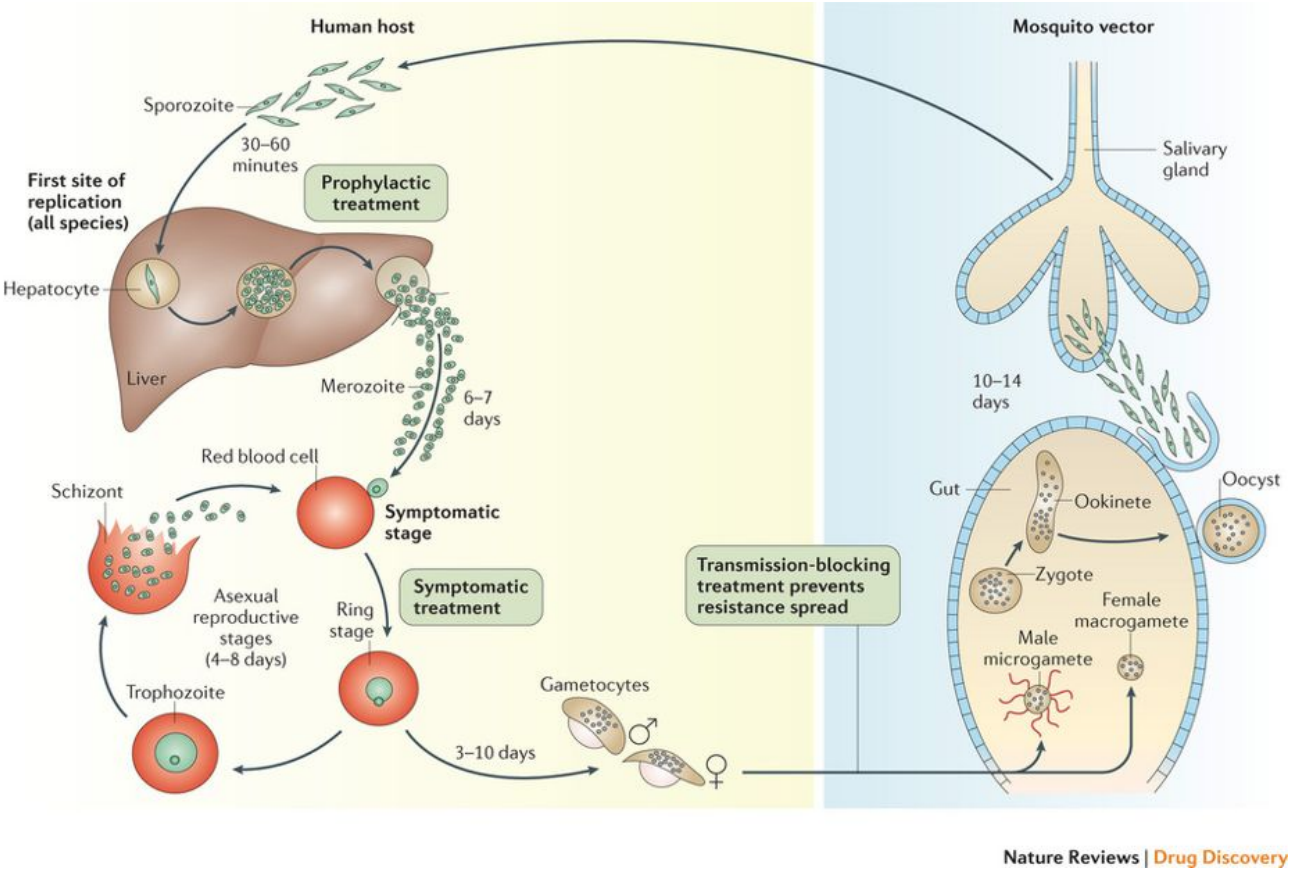

Figure 1.1: The *Plasmodium* life cycle

The parasite infects the vertebrate host when an infected female *Anopheles* mosquito takes a blood meal. Sporozoites from the salivary gland of the mosquito are injected into the blood-stream of the host which, later reach the liver and undergo maturation by a process called hepatic schizogony which, gives rise to a large number of merozoites that are released into the bloodstream. These merozoites now begin their intra-erythrocytic life cycle starting with the invasion of erythrocytes, followed by an actively metabolizing trophozoite stage. They then undergo schizogony to give rise to 12-16 merozoites which rupture the RBC and enter the bloodstream to infect new erythrocytes. This cycle takes about 48 hours in case of *P. falciparum* and 24 hours in case of *P. berghei*. Some of the merozoites mature into gametocytes that can be taken up by the mosquito during a blood meal. The gametocytes mature into male and female gametes in the mosquito gut and fuse to form a zygote which develops into an ookinete. The ookinete traverses the gut wall and becomes oocyst, which ruptures upon maturation and releases sporozoites that migrate to the salivary gland of the mosquito. The zygote is the only diploid cell in the parasite's life cycle. Figure reproduced with permission from "Malaria", Phillips M A et al, 2017, Copyright © Springer Nature.

1.3 Malaria pathophysiology

Most malaria cases occur as febrile fever after an incubation period of usually 10-15 days post-infection (del Prado et al., 2014). Parasite infections before the onset of illness can often be overcome by either host immunity (in malaria-endemic areas) or chemoprophylactic intervention involving treatment with antimalarials (del Prado et al., 2014; Liehl et al., 2015; Cowman et al., 2016). Although only a small fraction of *Plasmodium* infections result in severe malaria the actual numbers are enormous due to high entomological inoculation rate (EIR - this is an index of frequency of infectious bites an individual receives). This number ranges from a nominal five per year in Asia and South America to a staggering 1000 per year in sub-Saharan Africa (Greenwood and Mutabingwa, 2002). Severe malaria is characterized by anaemia due to lysis of erythrocytes and is also associated with acidosis leading to respiratory distress. In cases of cerebral malaria, parasites get sequestered in small blood vessels of the cranium often leading to coma and death. In pregnant women, malaria leads to maternal anaemia, fetal growth restriction and fetal loss. Infections involving *P. vivax* are less severe than that of *P. falciparum* as they do not sequester in the vasculature (del Prado et al., 2014). However, *P. vivax* is known to form dormant liver-stage hypnozoites which upon activation result in periodic relapses of blood stage infections (Mikolajczak et al., 2015).

1.4 Targetting *Plasmodium* metabolism

Ever since the discovery of *Plasmodium* as the causative agent of the dreaded disease malaria by Charles Louis Alphonse Laveran; focus has been laid on the development of several approaches to tackle the menace caused by this apicomplexan parasite. While the development of an effective antimalarial vaccine remains elusive (Mahmoudi and Keshavarz, 2017), another interesting area

of focus is the metabolism of this parasite. Perturbation of metabolic pathways is a promising intervention strategy and hence understanding the complex network of enzymes carrying out these reactions and the associated metabolic flux is highly essential. Absence of enzymes needed for *de novo* amino acid and purine synthesis in the metabolic arsenal of the parasites make the organism dependent on the host and is a weakness that can be exploited. Nevertheless, preference of different host cells i.e. mature erythrocytes by *P. falciparum* and reticulocytes by *P. berghei* and avian malaria parasites add another layer of complexity towards understanding parasite metabolism (Olszewski and Llinás, 2011). Efforts have been ongoing in this regard and numerous drug targets have been identified through small-molecule screening, and reverse genetics approaches (Guiguemde et al., 2010; Bushell et al., 2017; Zhang et al., 2018). This includes enzymes involved in various aspects of parasite physiology such as glucose and energy metabolism, nucleic acid synthesis, lipid metabolism, hemoglobin degradation, co-factor and co-enzyme synthesis etc. (Yeh and Altman, 2006). A short list of *Plasmodium* drug targets involved in nucleotide metabolism is provided below in 'Table 1.1'. Recently, computational approaches have been adopted that combine transcriptomics (gene expression) data and flux-balance analysis to predict putative essential genes that can be potential drug targets (Huthmacher et al., 2010) (Table 1.2). Also, information from genome wide knockout / gene disruption studies revealing essential genes, that are potential drug targets is compiled in the database 'Phenoplasm' (http://phenoplasm.org/) (Sanderson and Rayner, 2017). All these approaches aid in the discovery of new therapeutics and take us closer towards disease eradication.

Table 1.1: List of *Plasmodium* drug targets involved in nucleotide metabolism

Drug targets involved in nucleotide metabolism			
Enzyme	**Gene ID**	**Inhibitors**	**References**
Adenosine deaminase	PF10_0289	L-nucleoside analogs	Gero et al., 2003
GMP synthetase	PF10_0123	Psicofuranine	McConkey, 2003
Hypoxanthine guanine phosphoribosyltransferase	PF10_0121	Immucillin phosphates and acyclic nucleoside phosphonates & bisphosphonates	Keough et al, 2009 Kaiser et al, 2017 Špaček et l, 2017
IMP dehydrogenase	PFI1020c	Bredinin, Mycophenolic acid	Webster and Whaun, 1982 Veletzky, 2014
Purine nucleoside phosphorylase	PFE0660c	Immucillins	Madrid et al., 2008
Dihydroorotase	PF14_0697	6-L- thiodihydroorotate	Seymour et al., 1997
Orotidine-5'-phosphate decarboxylase	PF10_0225	Pyrazofurin	Seymour et al., 1994
Dihydrofolate reductase - Thymidylate synthase	PFD0830w	Folate based inhibitors	Jiang et al., 2000
Dihydroorotate dehydrogenase	PFF0160c	Leflunomide, DSM1	Phillips and Rathod, 2010
Orotate phosphoribosyltransferase	PF3D7_0512700	5'-Fluoroorotate, Pyrazofurin	Cassera et al., 2011

The references cited in this table are listed in page 203.

Table 1.2: List of predicted *Plasmodium* drug targets through flux-balance analysis

Enzyme name	Compartment	Pathway
Adenylate cyclase	Apicoplast	Purine metabolism
Fumarase	Cytosol	Citrate cycle
2-C-methyl-D-erythritol 4-phosphate cytidylyltransferase	Apicoplast	Biosynthesis of isopentenyl diphosphate
4-hydroxy-3-methylbut-2-enoyl-diphosphate synthase		
CDP-ME kinase		
Pantetheine-phosphate adenylyltransferase	Cytosol	CoA biosynthesis
Pyridoxal 5-phosphate synthase		Vitamin B6 metabolism
Geranyl-diphosphate synthase		Terpenoid biosynthesis
Farnesyl-diphosphate synthase		
2-Octaprenylphenol hydroxylase	Mitochondrion	Ubiquinone biosynthesis
Ubiquinone biosynthesis methyltransferase		
Uroporphyrinogen decarboxylase	Apicoplast	Porphyrin metabolism
Coproporphyrinogen oxidase		
UMP-CMP kinase		Pyrimidine metabolism
Aspartate carbamoyltransferase	Cytosol	
Orotate phosphoribosyltransferase		
Cysteine desulfurase	Apicoplast/ mitochondrion	Fe-S-protein biogenesis
tRNA ligase (Ile, Lys, Met, Trp, Tyr)	Cytosol/ apicoplast/ mitochondrion	Aminoacyl-tRNA biosynthesis
Glutathione synthase	Cytosol	Glutathione metabolism
Riboflavin kinase		Riboflavin metabolism
Glucosamine 6-phosphate synthase	Apicoplast	Aminosugars metabolism
Mannose-6-phosphate isomerase	Cytosol	Fructose and mannose metabolism
Cytochrome-c oxidase	Mitochondrion	Oxidative phosphorylation
Choline-phosphate cytidylyltransferase	Cytosol	Glycerophospholipid metabolism
Deoxyhypusine synthase		Activation of eiF5A

Table reproduced and modified from "Antimalarial drug targets in *Plasmodium falciparum* predicted by stage-specific metabolic network analysis", Carola Huthmacher et al., 2010, distributed under the terms of the Creative Commons Attribution License to BioMed Central Ltd.

1.4.1 *Plasmodium* nucleotide metabolism

Nucleotide synthesis in the parasitic protozoan *P. falciparum* is characterized by the absence of *de novo* purine biosynthetic pathway and the pyrimidine salvage pathway (Fig. 1.2). Hence, the parasite is forced to acquire the purine bases from its host and generate its cellular purine nucleotide pool by salvage pathway enzymes. The parasite residing inside the RBC has transporters that mediate uptake of nucleosides and nucleobases. Though the erythrocyte also lacks *de novo* purine biosynthetic pathway it salvages adenosine from plasma and generates AMP through the action of adenosine kinase. Since erythrocyte adenosine kinase has high catalytic efficiency, levels of adenosine in the RBC are low. Nevertheless, this can also be imported into the parasite (Belen Cassera et al., 2011). Adenosine can be acted upon by adenosine deaminase to give inosine and further catalyzed by purine nucleoside phosphorylase (PNP) to give rise to hypoxanthine (Belen Cassera et al., 2011). The predominant nitrogen base salvaged by the parasite is hypoxanthine, that gets converted to IMP. This reaction is catalysed by hypoxanthine-guanine-xanthine phosphoribosyltransferase (HGXPRT) which can act on hypoxanthine, guanine and xanthine to form IMP, GMP and XMP respectively. IMP thus formed is used to synthesize AMP or GMP (Downie et al., 2008). IMP is converted to sAMP by adenylosuccinate synthetase (ADSS) and further converted to AMP by adenylosuccinate lyase (ASL). IMP can also be oxidized to give XMP by IMP dehydrogenase and then amidated to give GMP through the action of GMP synthetase (GMPS). Though the parasite lacks the enzymes APRT and adenosine kinase, it has the ability to import adenine nucleotide monophosphate from the erythrocytes by nucleotide transporters present on parasite plasma membrane (Cassera et al., 2008). However, it is not clear if this uptake of AMP is of any significant magnitude. Presence of purines in high concentration in the RBC and pyrimidines in low concentration correlates with the metabolic adaptation of the parasite in having a salvage pathway for purines and retaining *de novo* pathway for pyrimidine synthesis. The prime feature about the enzymes involved in purine nucleotide synthesis is that the enzymes HGXPRT, ADSS, ASL, IMPDH, and GMPS are all essential for parasite survival (Sanderson and Rayner, 2017; Zhang et al., 2018). The *de novo* pathway for pyrimidine synthesis is similar to that seen in humans (Belen Cassera et al., 2011).

Host adenosine deaminase acts on adenosine and 2' deoxyadenosine while the parasite enzyme acts on an additional substrate 5' methylthioadenosine that is formed during polyamine synthesis. This difference in substrate specificity has resulted in the development of *Plasmodium* adenosine deaminase specific inhibitor 5' methylthio-coformycin (a transition-state analogue) that operates at sub-nanomolar concentration and has more than 20000 fold higher specificity for the parasite enzyme than the human counterpart. (Belen Cassera et al., 2011).

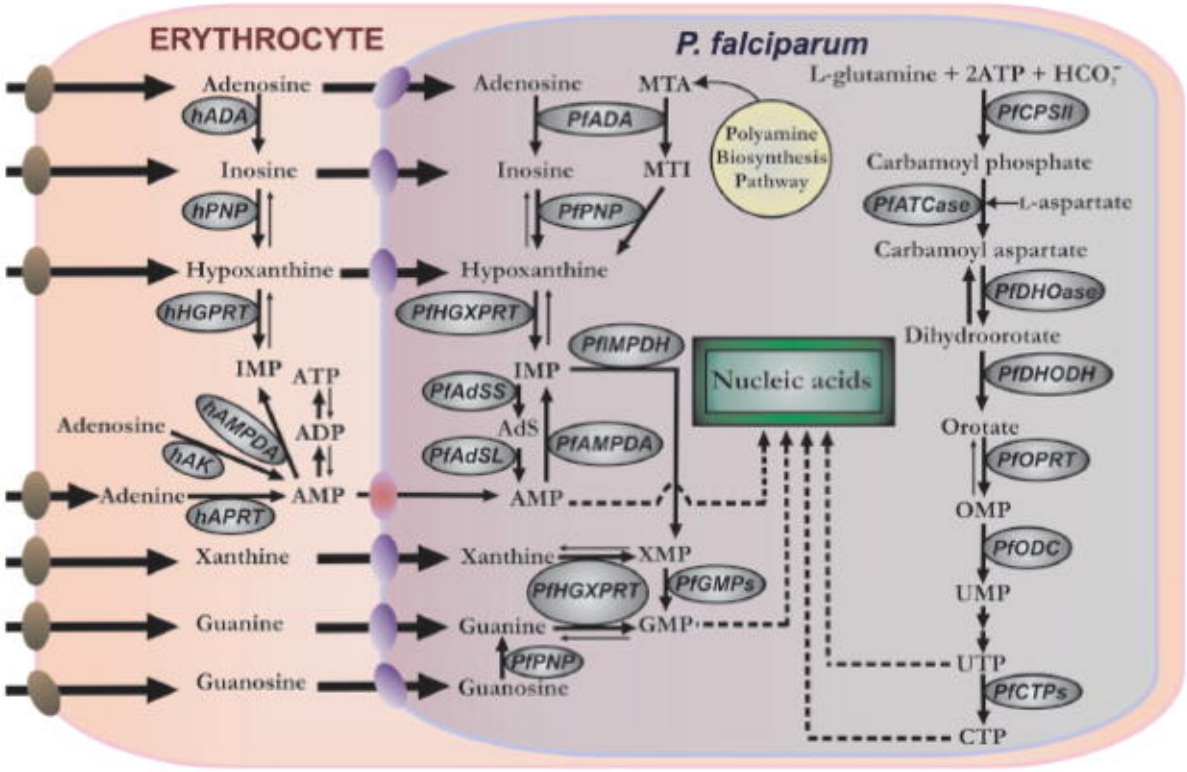

Figure 1.2: Purine and pyrimidine metabolism in *Plasmodium*

Purine pathway: AMP, adenosine 5-monophosphate; ADP, adenosine 5-diphosphate; ATP, adenosine 5-triphosphate; IMP, inosine 5-monophosphate; XMP, xanthosine 5-monophosphate; GMP, guanosine 5-monophosphate; hADA, human adenosine deaminase; MTA, methylthioadenosine; MTI, methylthioinosine; AdS, adenylsuccinate; hPNP, human purine nucleoside phosphorylase; hHGPRT, human hypoxanthine-guanine phosphoribosyltransferase; hAK, human adenosine kinase; hAMPDA, human adenosine 5-monophosphate deaminase; hAPRT, human adenine phosphoribosyltransferase; PfADA, *P. falciparum* adenosine deaminase; PfPNP, *P. falciparum* purine nucleoside phosphorylase; PfHGXPRT, *P. falciparum* hypoxanthine-guanine-xanthine phosphoribosyltransferase; PfAMPDA, *P. falciparum* adenosine 5-monophosphate deaminase; PfIMPDH, *P. falciparum* inosine 5-monophosphate dehydrogenase; PfGMPs, *P. falciparum* guanosine 5-monophosphate synthase; PfAdSS, adenylosuccinate synthetase; PfAdSL, adenylosuccinate lyase. Pyrimidine pathway: OMP, orotidine 5'-monophosphate; UMP, uridine 5'- monophosphate; UTP, uridine 5'-triphosphate; CTP, cytidine 5'-triphosphate; PfCPSII, *P. falciparum* carbamoyl phosphate synthetase II; PfATCase, *P. falciparum* aspartate carbamoyltransferase; PfDHOase, *P. falciparum* dihydroorotase; PfDHODH, *P. falciparum* dihydroorotate dehydrogenase; PfOPRT, *P. falciparum* orotate phosphoribosyltransferase; PfODC, *P. falciparum* orotidine 5'-monophosphate decarboxylase; PfCTPs, *P. falciparum* cytidine 5'-triphosphate synthase. Figure reproduced with permission from "Purine and pyrimidine pathways as targets in *Plasmodium falciparum*", Cassera M B et al, Copyright © Bentham Science Publishers.

PNP from mammalian host acts on multiple substrates namely, inosine, deoxyinosine, guanosine and deoxyguanosine, resulting in the formation of hypoxanthine or guanine and the byproduct α-D-(deoxy) ribose 1'-phosphate. Immucillin-H inhibits both parasite and human PNP and its addition to culture medium kills parasites under purine limiting growth conditions. It was found that the parasite enzyme has a high affinity for inosine and guanosine as compared to its human

counterpart in addition to recognizing 5' methylthioinosine as substrate, indicating its involvement in polyamine metabolism. This key difference was exploited to develop a specific inhibitor 5-methylthio-Immucillin-H (Belen Cassera et al., 2011). PNP knockout *P. falciparum* parasite line shows significant growth retardation when compared to that of the wildtype suggesting essentiality of PNP (Madrid et al., 2008). Interestingly, in *P. yoelii* PNP knockout parasites not only displayed attenuation and got cleared off the host system, but mice injected with these parasites conferred immunity against a lethal dose of wildtype *P. yoelii* parasites (Ting et al., 2008).

HGXPRT is a key enzyme in purine salvage, catalyzing the transfer of 5' phosphoribosyl moiety from 5' α-D-phosphoribosyl pyrophosphate to N9 of 6-oxopurines (Hypoxanthine, Xanthine and Guanine); leading to the formation of 5' nucleotide monophosphate and inorganic pyrophosphate as a by-product. The enzyme HGPRT has been kinetically characterised from human and it has been reported that the forward reaction occurs in an ordered sequential manner (Giacomello and Salerno, 1978). Here binding of PRPP to the enzyme is the first event followed by the binding of nitrogen base and PPi is the first product to be released ahead of the nucleotide monophosphate. Also, kinetic studies have provided evidence that this enzyme follows a steady-state kinetic mechanism which is characterized by a rapid catalytic conversion step and a rate-limiting product release step, thereby showing a burst phase in the pre-steady state, as observed in kinetic characterization by rapid quench technique (Xu et al., 1997). On the other hand, PfHGXPRT has shown an offbeat kinetic behavior by exhibiting hysteretic properties. This has been supported by the data obtained from steady-state, pre-steady-state kinetics and ligand binding kinetic studies. The wild type PfHGXPRT enzyme in unactivated condition shows an initial lag of 100 seconds for xanthine phosphoribosylation which vanishes upon full activation by incubation of the enzyme with either of its activators i.e. IMP (a product of the reaction) or PRPP in the form of magnesium complex (a substrate for the reaction). Pre-steady-state kinetic studies report the absence of a burst phase indicating phosphoribosylation is slower than product release (Roy et al., 2015a,b). The human and *Plasmodium* enzyme differ in their substrate specificity where only *Plasmodium* enzyme is able to recognize xanthine as substrate. Similar to PNP, several immucillin phosphates and acyclic immucillin phosphonates have been developed that inhibit PfHGXPRT at nanomolar level (Li et al., 1999; Hazleton et al., 2012).

ADSS is the enzyme that channelizes IMP produced by HGXPRT towards adenine nucleotide pool. This enzyme catalyzes the addition of an aspartate moiety on to IMP leading to the production of succinyl AMP (sAMP) using a molecule of GTP during the process. Biochemical and structure-function studies have been carried out on this enzyme revealing ordered binding of substrates while ADSS from other organisms display random mechanism. Also, *P. falciparum* ADSS is activated by fructose 1, 6-bisphosphate, that is known to inhibit the human enzyme (Raman et al., 2004; Mehrotra et al., 2010). These key differences are vital leads for drug discovery. Hadacidin, an aspartate analogue affects parasite growth *in vitro* by inhibiting ADSS as this is an essential enzyme involved in AMP synthesis (Raman et al., 2004; Crowther et al., 2011).

ASL catalyzes the cleavage of sAMP to fumarate and AMP (as a part of purine nucleotide cycle) and also the cleavage of succinyl aminoimidazole carboxamide (sAICAR) to aminoimidazole carboxamide (AICAR) and fumarate (as a part of the *de novo* pathway). Although the de novo pathway is absent in the parasite ASL has retained activity on sAICAR (Bulusu et al., 2009). Interestingly, the addition of AICAR to parasite culture has been reported to inhibit parasite growth through inhibition of ASL. This involves conversion of AICAR to its nucleotide form ZMP (Bulusu et al., 2011b).

IMPDH is a key protein catalyzing the oxidation of IMP to XMP. Although much literature is not available on *Plasmodium* IMPDH, IMPDH in humans is involved in neoplastic transformation, lymphocyte activation, cancer cell differentiation, eye development and pigment synthesis, control of circadian clock and delay of embryonic development (Collart and Huberman, 1990; Konno et al., 1991; Collart et al., 1992; Nagai et al., 1992). Multiple drugs such as ribavirin, selenazofurin, tiazofurin, mycophenolic acid and bredinin are available against IMPDH and are used for anti-tumor, antiviral and immunosuppressant therapies (Shu and Nair, 2008).

XMP generated by IMPDH is utilized by GMP synthetase that catalyses its conversion to GMP using glutamine as the amino group donor and a molecule of ATP. GMPS in *Plasmodium* is a two-domain type enzyme, comprising of glutaminase domain (GATase) that deamidates glutamine to glutamate and channels the NH_3 group to the ATP pyrophosphatase (ATPpase) domain where a high energy AMP-XMP intermediate (adenylation reaction) is formed. The overall reaction ends with the formation of GMP, XMP, AMP, PPi and glutamate. Extensive structure-function studies on *Plasmodium* GMPS have revealed aspects such as active-site coupling, ammonia tunnelling, and cross-talk between GATase and ATPpase domains that aid in the development of inhibitors. GMPS is a known drug target in infections caused by other pathogenic organisms such as *Candida, Cryptococcus, Aspergillus and Trypanosoma* in addition to being an anti-cancer target (Bhat et al., 2008; Rodriguez-Suarez et al., 2007; Ballut et al., 2015; Bianchi-Smiraglia et al., 2015).

1.4.2 *Plasmodium* central carbon metabolism

In vitro studies have clearly demonstrated that parasites display gluttony for glucose (Fig. 1.3). Mature RBCs, that lack mitochondria, rely on glucose to meet their energetic demands and consumption of glucose occurs at a rate of 5 mol /24 h/10^9 RBCs (Jensen et al., 1983). However, as a result of parasite invasion, this rate spikes up by almost a hundredfold during trophozoite and schizont stage (Roth, 1990). Only a small fraction of this consumed glucose gets completely oxidised to CO_2 and most of it (>90 %) is converted to lactate (Olszewski and Llinás, 2011). This is supported by the fact that parasites are microaerophilic and their growth is retarded upon exposure to atmospheric oxygen levels (Scheibel et al., 1979). The glycolytic flux of the parasite is akin to that of a cancerous cell. To accommodate its glycolytic demands the parasite exports a hexose transporter to the surface of its plasma membrane (Slavic et al., 2011). Although analysis of the parasite genome shows the absence of enzymes involved in gluconeoge-

nesis, phosphoenolpyruvate carboxykinase (PEPCK) encoded in the genome can shunt carbon from the TCA cycle or amino acid metabolism towards gluconeogenesis. Since the parasite does not generate polymeric glucose reserves such as glycogen or starch, it requires a constant supply of glucose from the host. This reliance on glucose is observed even in mosquito stages as the hemolymph of the vector has abundant glucose and the transporter (PB000562.01.0) involved in uptake is expressed in all mosquito stages (Olszewski and Llinás, 2011).

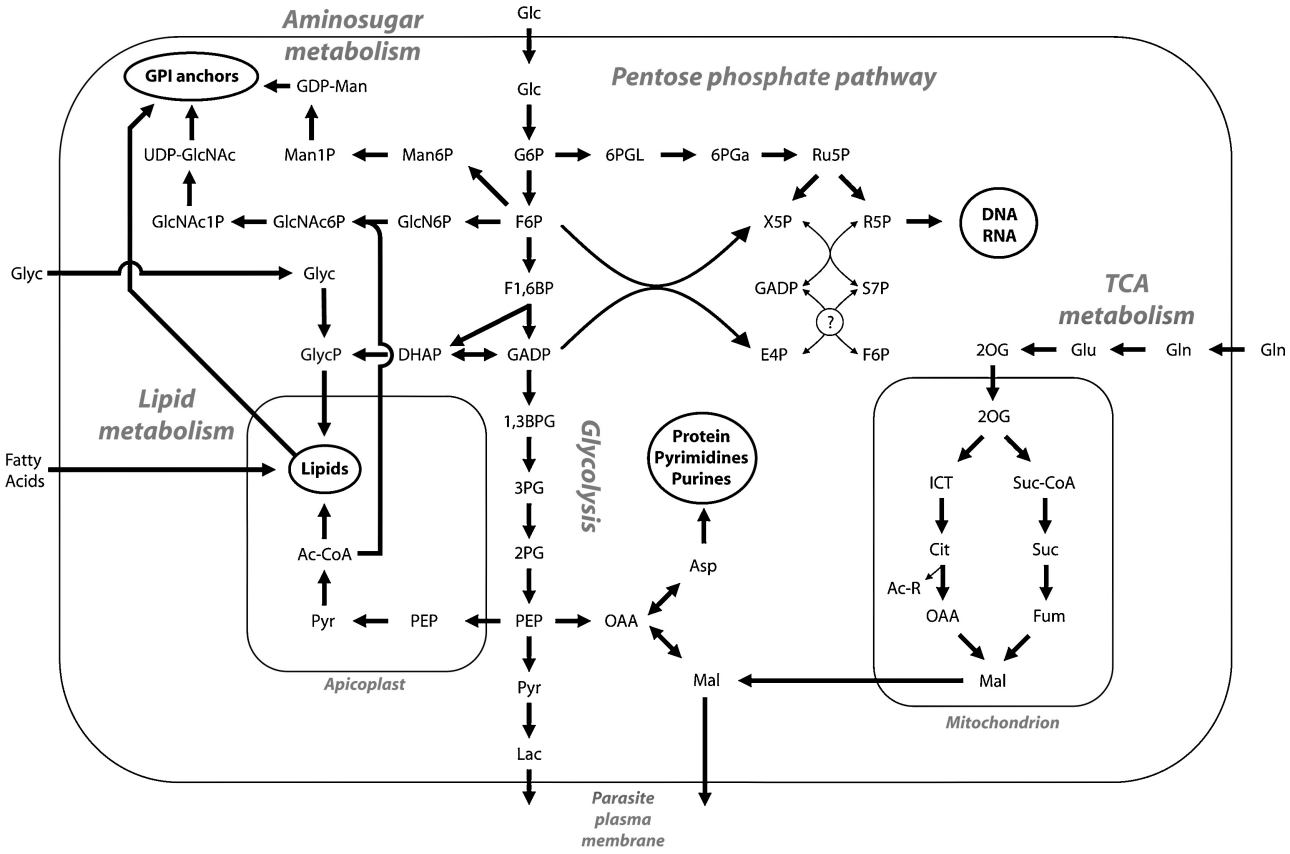

Figure 1.3: Central carbon metabolism of *Plasmodium* parasites

Glc, glucose; G6P, glucose-6-phosphate; F6P, fructose-6-phosphate; F1,6BP, fructose-1,6-bisphosphate; DHAP, dihydroxyacetone-phosphate; GADP, glyceraldehyde-3-phosphate; 1,3BPG, 1,3-bisphosphoglycerate; 3PG, 3-phosphoglycerate; 2PG, 2-phosphoglycerate; PEP, phosphoenolpyruvate; Pyr, pyruvate; Lac, lactate; AcCoA, acetyl-CoA; Ac-R, either acetate or acetyl-CoA; GlycP, glycerol-3-phosphate; Glyc, glycerol; Man6P, mannose-6-phosphate; Man1P, mannose-1-phosphate; GDP-Man, GDP-mannose; GlcN6P, glucosamine-6-phosphate; GlcNAc6P, N-acetyl-glucosamine-6-phosphate; GlcNAc1P, N-acetyl-glucosamine-1-phosphate; UDP-GlcNAc, UDP-N-acetyl-glucosamine; 6PGL, 6-phosphoglucono-δ-lactone; 6PGa, 6-phosphogluconate; Ru5P, ribulose-5-phosphate; R5P, ribose-5-phosphate; X5P, xylulose-5-phosphate; S7P, sedoheptulose-7-phosphate; E4P, erythrose-4-phosphate; Asp, aspartate; Gln, glutamine; Glu, glutamate; 2OG, 2-oxoglutarate; ICT, isocitrate; Cit, citrate; OAA, oxaloacetate; Mal, malate; Suc-CoA, succinyl-CoA; Suc, succinate; Fum, fumarate; GPI, glycophosphatidylinositol. Figure reproduced with permission from "Central carbon metabolism of Plasmodium parasites", Kellen L. Olszewski and Manuel Llinás, 2011, Copyright © Elsevier B.V.

Pentose phosphate pathway is an important conserved pathway whose chief function is to generate ribose-5-phosphate for nucleic acid synthesis and NADPH that is required for maintenance of redox balance and is used in various anabolic pathways. Although all the necessary enzymes that constitute the pathway have been found to be present in the parasite, transaldolase remains an exception whose homolog has not yet been identified (Gardner et al., 2002). Interestingly glucose 6-phosphate dehydrogenase (G6PDH) deficiency is associated with malaria resistance. The reason for this being the oxidative damage to host cell membrane targeting it for phagocytosis. The parasite also produces various modified sugars such as amino sugars, sugar alcohols etc. which decorate critical proteins such as circumsporozoite protein, multiple merozoite surface proteins and GPI anchored proteins (Olszewski and Llinás, 2011).

Mitochondrial TCA cycle is a vital pathway with respect to cellular energetics. Carbon sourced from various precursors such as sugars, amino acids and fatty acids can feed into this pathway and get oxidised to CO_2 while generating ATP, NADH and $FADH_2$ in the due process. Nevertheless, the parasite's energy requirements are met largely through glycolysis itself and a low flux is reported through the TCA cycle during intra-erythrocytic stages which get enhanced in the mosquito stages (Ke et al., 2015). The parasite mitochondrion lacks the pyruvate dehydrogenase complex and the job of conversion of pyruvate to acetyl-CoA is carried out by an essential enzyme, branched chain keto acid dehydrogenase (BCKDH) (Oppenheim et al., 2014). It has been shown that except for fumarate hydratase and malate-quinone oxidoreductase all other enzymes of the TCA cycle in the malarial parasite are not essential (Ke et al., 2015). Also, it has been demonstrated that fumarate generated from the purine nucleotide cycle feeds into the TCA anaplerotically and also ends up in the amino acid pool (aspartate in particular) that gets reused in AMP biosynthesis by the enzyme ADSS (Bulusu et al., 2011a) and other processes such as pyrimidine and protein biosynthesis. Other than pyruvate coming from glucose, glutamine is the chief metabolite that was found to be incorporated in all TCA cycle intermediates through labelling studies (Elford et al., 1985). This is mediated by the enzymes glutamate synthase and glutamate dehydrogenase (Aparicio et al., 2010). Given that there is a lot of movement of metabolites across the mitochondrial membrane and the cytosol, key carrier proteins are annotated in the *Plasmodium* genome. This includes dicarboxylate/tricarboxylate carrier (DTC), oxoglutarate-citrate carrier (OGC) and mitochondrial pyruvate carrier (MPC). Given their importance in carbon metabolism these carriers have been recognized as key drug targets in cancer and diabetes (DeFronzo and Tripathy, 2009; Timón-Gómez et al., 2013). This might be true for the parasite as well.

1.5 Reverse genetics approaches towards understanding the parasite physiology

Malaria which is caused by the parasitic protozoans of the *Plasmodium* genus is one of the leading infectious diseases causing a large number of deaths worldwide. The death toll is severe in developing countries. Though many drugs are available to curb the menace caused by *Plasmodium*, the parasite has come up with resistance to most of them. And recently, resistance to artemisinin has emerged that has been a major issue of concern (Dondorp et al., 2009). Hence, the identification of new drug targets is of top priority. This needs a proper understanding of different stages of the parasite life cycle, and associated physiological changes (de Koning-Ward et al., 2015). The advent of transfection in *Plasmodium* dates back to 1993 where a luciferase reporter was transiently transfected in *P. gallinaceum* (Goonewardene et al., 1993), which has been followed by many major developments such as usage of DHFR from *P. berghei, T. gondii* and human as selection markers in gene knockout studies (Wu et al., 1996; Crabb and Cowman, 1996; Waters et al., 1997), GFP as reporter (VanWye and Haldar, 1997), complementation using PAC (*Plasmodium* artificial chromosome) (Sultan et al., 2001), piggyback transposon mutagenesis (Balu et al., 2005), conditional knockdown using degradation domain tagging (Armstrong and Goldberg, 2007; Muralidharan et al., 2011), recombineering (Pfander et al., 2011), Cre-LoxP conditional gene deletion system , Zinc-finger nucleases (Straimer et al., 2012) and the latest PlasmoGEM recombineering (Gomes et al., 2015; Schwach et al., 2015) and CRISPR-Cas9 genome editing system (Ghorbal et al., 2014). All these approaches involve DNA recombination mediated by homology arms.

The haploid nature of the parasite is advantageous as only one allele has to be manipulated to see the phenotype. At the same time, is also disadvantageous as it will be a hurdle to ablate essential genes. Transfection in *Plasmodium* is a challenging process as the foreign DNA is required to pass through four membranes i.e., erythrocyte membrane, parasitophorous vacuolar membrane, parasite plasma membrane and nuclear membrane, resulting in lower transfection efficiencies. *P. falciparum,* which is transfected during the ring stage has transfection efficiency of 10^{-6} – 10^{-8} as compared to *P. berghei*, which has a better efficiency of 10^{-2} – 10^{-4}. The recently developed nucleofection method, with its patented technology, has improved the transfection efficiency in *P. falciparum* by almost 1000 folds (Janse et al., 2006). In our current study, we have employed the PlasmoGEM recombineering technique for knocking out genes from *P. berghei* and DHFR degradation domain based regulatable affinity tag system for a conditional knockdown. Where *Plasmodium* transfection is concerned, one cannot avoid the 'catch 22' situation. *P. falciparum* has multiple selection markers, but has lower transfection efficiency and the studies are limited to intraerythrocytic stages, while *P. berghei* transfections efficiencies are better than that of *P. falciparum* but suffer from the compulsion of recycling a single selection marker (HDHFR/yFCU) for multiple genetic manipulations (Orr et al., 2012). Nevertheless, a new basticidin resistance marker has been developed for *P. berghei* which seems promising, in spite of its limited use only

under *in vitro* growth conditions (Soga et al., 2018).

1.6 Current intervention strategies and challenges

WHO has been striving for the eradication of malaria since the 1950s (Greenwood and Mutabingwa, 2002). Even though it has faced many setbacks in achieving this goal, promising results were obtained as four countries have been certified to have eliminated malaria namely, United Arab Emirates (2007), Morocco (2010), Turkmenistan (2010), and Armenia (2011). For a long time there were no approved vaccines against malaria, but the RTS,S/AS01 vaccine that was subjected to a large scale clinical trial in seven African countries, showed promising results (RTS, 2015). But the occurrence of rebound infections indicates that the efficacy of this vaccine can wane out in the population over time (Olotu et al., 2016). Now this vaccine under the commercial name 'Mosquirix' is being utilized in national immunization programmes in Ghana, Kenya, and Malawi. The composition of this vaccine is as follows, central repeat region of *Plasmodium falciparum* circumsporozoite protein (CSP); T-cell epitope of the CSP; and the hepatitis B surface antigen (HBsAg). This vaccine prevents malaria at the very first stage by inhibiting the infection of liver cells by the sporozoite.

Depending on the level of transmission, the predominant species of *Plasmodium* and status of drug resistance in a given area, there are four types of malaria risks and this has been summarized in the table below (del Prado et al., 2014):

Table 1.3: Malaria risk and type of prevention

	Malaria risk	Type of prevention
Type 1	Low-transmission settings	Only mosquito bite prevention
Type 2	*P. vivax* or *P. falciparum* with no evidence to resistance to chloroquine	Mosquito bite prevention and chemoprophylaxis with chloroquine
Type 3	*P. vivax* or *P. falciparum* and chloroquine resistance. This includes Nepal, Sri-Lanka, Tayikistán, and parts of Colombia and India	Mosquito bite prevention and chemoprophylaxis with chloroquine and proguanil
Type 4	High risk-transmission settings by *P. falciparum* and antimalarial drug resistance or moderate/low-transmission with high antimalarial drug resistance	Mosquito bite prevention and mefloquine or doxycycline or atovaquone/proguanil

Insecticide-treated nets (ITNs), long-lasting insecticidal nets (LLINs) or pyrethroid-treated nets, and indoor residual spraying with insecticides are the most effective modes of malaria prevention.

Since these modes are not implemented in an efficient manner *Plasmodium* infections persist among populations and if not diagnosed and treated in time become lethal (del Prado et al., 2014). Chloroquine, akin to other quinine derivatives that are also used as prophylactic measure inhibits parasite growth by blocking heme polymerization wherein toxic heme is converted into its polymeric form, hemozoin. Artemisinin combination therapy (ACT - available in multiple combinations such as artemether plus lumefantrine, artesunate plus amodiaquine, artesunate plus mefloquine, artesunate plus sulfadoxine-pyrimethamine, and dihydroartemisinin plus piperaquine) is the best treatment that is currently available for malaria, inhibits parasite growth by causing oxidative stress (Eastman and Fidock, 2009; del Prado et al., 2014). The emergence of resistance to this drug in Cambodia, Myanmar, Thailand, and Viet Nam is a matter of concern and its spread will have devastating consequences on public health (Dondorp et al., 2009).

The latest venture in the field of malaria is the advent of gene drive technology to design and generate genetically modified mosquito that either replace the existing population with one that does not act as a vector (population replacement) (Carballar-Lejarazú and James, 2017; James et al., 2018) or in a self destructive mode wipe out the entire existing population of vectors in a few generations (population elimination) (Kyrou et al., 2018; James et al., 2018). Using CRISPR-Cas9 technology the 4-exon 5-intron boundary of the *Anopheles gambiae* gene doublesex (Agdsx) was disrupted and the resultant allele did not affect male fertility while females that were homozygous for this disrupted allele displayed intersex phenotype and were sterile. This allele spread in the complete laboratory population of mosquitoes within 7-11 generations and was associated with lower egg production and an eventual population collapse (Kyrou et al., 2018). Though promising this approach is not free from apprehension as wiping out an entire population of insects will have ecological implications as male mosquitoes are involved in pollination as well. Another issue of concern raised is that mosquitoes are part of the food chain and destroying a species might impact its dependents negatively. Also, the chances of the gene drive component getting horizontally transferred to other species due to intra-specific mating in *Anopheles gambiae* complex, and other ecological consequences have to be accessed carefully (James et al., 2018). Taken together, a refined and specific approach that aids towards the eradication of malaria seems to be the need of the hour. Numerous labs around the globe are working on *Plasmodium* physiology taking different approaches towards understanding aspects such as parasite cell signalling, cytoskeletal elements and parasite movement, host-parasite interaction, transmission and vector biology etc. In similar lines, understanding key aspects of the parasite metabolism will open up new avenues in the struggle towards the eradication of malaria.

1.7 Objectives of the current study and structure of the thesis

This thesis is focused on understanding biochemical properties and physiological roles of enzymes involved in nucleotide and carbon metabolism in the malaria parasite *Plasmodium*. The study has been carried out on AMP deaminase, a purine nucleotide cycle enzyme and four members of

HAD superfamily. The chief objectives were to produce recombinant proteins and to perform *in vitro* biochemical characterization, in addition to addressing the question of essentiality of these gene products during different stages the parasite life cycle. The thesis consists of a common chapter entailing materials used and methodologies adopted (Chapter 2). This is followed by two chapters, one on studies on AMP deaminase (Chapter 3) and the other pertaining to studies on HADSF members (Chapter 4). Both chapters comprise of an introduction section with detailed objectives followed by an elaborate discussion of the observations made and results obtained during the course of the study. The thesis work is summarized along with a discussion of future prospects, after these two chapters. Taken together, this thesis work adds new information to the existing knowledge base on nucleotide and carbon metabolism in *Plasmodium,* discovering potential drug targets.

Chapter 2

Materials and Methods

This chapter comprises the details of materials and various methodologies/procedures employed for the characterization of recombinant PfAMPD. Expression systems such as *E. coli*, *S. cerevisiae*, *P. pastoris* and cell-free system were employed to achieve this objective. Characterization of the protein was done by a functional complementation assay in AMPD knockout yeast using mutants generated by following 'AQUA cloning' protocol. Also, included are the steps by which linear knockout vectors were generated for obtaining GFP tagged and knockout *P. berghei* parasite cell line. This chapter also comprises the details of materials and methods employed for the characterization of recombinant HADSF members. *E. coli* expression system was employed to achieve this objective. Characterization of HADSF members was done by *in vitro* biochemical assays. Also, included are the steps by which linear knockout vectors were generated for obtaining GFP tagged, knockout and conditional knockdown *P. berghei* parasite cell lines for specific HADSF members. The contents of this chapter are also part of two publications (Nagappa et al., 2019a,b).

2.1 Materials

Chemicals and reagents were procured from Sigma Aldrich, USA; Fischer Scientific; Spectrochem and SRL, India. Media components were purchased from Himedia, Mumbai. Primers were custom synthesized from Sigma Aldrich, India. Restriction enzymes, reverse transcriptase, Phusion DNA polymerase, Taq DNA polymerase and T4 DNA ligase were obtained from New England Biolabs, USA and used according to the instructions of the manufacturer. Trizol™ was from Invitrogen, USA. Antibiotics ampicillin, tetracycline and chloramphenicol were bought from USB chemicals. G418 was bought from Sigma Aldrich, USA and Zeocin from Invitrogen, USA. Plasmid isolation, PCR clean-up and gel extraction kits were from Qiagen. *E. coli* strain XL-1 blue, and expression strain Rosetta (DE3) pLysS and plasmids pET21b, pET22b, pET23d, pQE30, pETduet-1 and pMALP-2x were from Novagen. pJAZZ library clones (PbG02_B-44h05 for PbAMPD, PbG02_B-53b06 for PbPGP and PbG01-2362a01 for PbHAD3), pJAZZ final knockout constructs (PbGEM-265660 for PbHAD2 and PbGEM-290712 for PbHADx), plasmids, pSC101BAD, R6K zeophes and R6K GFP mut3 were procured from PlasmoGem, Sanger Institute, UK. *E. coli* TSA cells were obtained from Lucigen and pir strains were from PlasmoGem. Plasmid pBCEN5 was a gift from Dr. Shiroh Iwanaga, Japan. Plasmid pCM189 and Wild type *(BY4742; MATa; ura3Δ0; leu2Δ0; his3Δ1; lys2Δ0)*, *Δamd1 (BY4742; MATa; ura3Δ0; leu2Δ0; his3Δ1; lys2Δ0; YML035c::kanMX4), Δade1 (BY4741; MATa; ura3Δ0; leu2Δ0; his3Δ1; met15Δ0; YAR015W::kanMX4)* and *Δade2 (BY4741; MATa; ura3Δ0; leu2Δ0; his3Δ1; met15Δ0; YOR128C::kanMX4) S. cerevisiae* strains were from Euroscarf and gift from Dr. Ravi Manjithaya, JNCASR, Bangalore. Plasmid pYES2C/T was a kind gift from Prof. P N Rangarajan, IISC, Bangalore. Pichia pastoris strain X-33 and plasmids pGAPZ and pGAPZαA were gifted by Prof. Rajan Dighe and Prof. P N Rangarajan, IISC, Bangalore. Codon harmonised PfAMPD gene was synthesized and procured from Shinegene, China. *P. falciparum* 3D7 and *P. berghei* ANKA strain were procured from MR4. PM1 knockout strain of *P. falciparum* and pGDB plasmid were a kind gift from Dr. Vasant Muralidharan, University of Georgia, USA. RPMI-1640 and Albumax were from Sigma Aldrich, USA and Gibco, respectively. P5 Nucleofection kit was from Lonza, Germany. Infusion assembly kit was from TaKaRa Bio, USA. Random primer kit was from BRIT, India. Male/female BALB/c mice aged 6-8 weeks were used for culturing and transfection of *P. berghei*. Blood required for parasite culture was collected from healthy individuals having O+ve blood group with prior consent. New Zealand white female rabbit was provided by the in-house animal facility to generate antigen-specific antibodies. Permission for *in vitro* parasite culture and animal work was obtained from the Institutional Bio-safety Committee and Animal Ethics Committee. Gene sequencing by Sanger sequencing method was carried out in the in-house central instrumentation facility, JNCASR, Bangalore and Eurofins, Bangalore. Sequences of oligonucleotides used and media and reagent composition have been provided in the appendix. Fitting of enzyme kinetics data was performed using GraphPad Prism V5 and visualization of protein structures was done using PyMol.

2.2 Methods (Studies on AMPD)

2.2.1 RNA isolation, cDNA synthesis and RT PCR

Saponin released *P. falciparum* cell pellet from 40 mL of *in vitro* culture was treated with 1 mL Trizol™ reagent at room temperature for 15 minutes and then centrifuged for 30 minutes at 18000 × g to remove the cell debris. The supernatant was transferred to a fresh tube and 200 µL of chloroform was added and kept at room temperature for 15 minutes. This was centrifuged at 18000 × g for 30 minutes at 4 ℃ for phase separation. The top layer was aspirated to a fresh tube and 400 µL of isopropanol was added and kept at -20 ℃ for 4 hrs. This was centrifuged at 18000 × g for 30 minutes at 4 ℃ to obtain an RNA pellet. This pellet was washed once with 75 % ethanol made in diethylpyrocarbonate (DEPC) treated water and allowed to air dry. The pellet was resuspended in 20 µL of DEPC treated water and stored at -80 ℃.

For RNA isolation from *P. berghei*, blood was harvested from mice at 10 - 15 % parasitemia and collected in heparin (200 units mL^{-1}). The cells were lysed by resuspending them in 10 volumes of erythrocyte lysis buffer (155 mM NH_4Cl, 12 mM $NaHCO_3$ and 0.1 mM EDTA) and kept at 4 ℃ for 5 minutes. The cells were harvested by centrifugation at 500 × g for 10 minutes, the supernatant was discarded and the pellet was used for RNA isolation. The steps used for RNA isolation were identical to that described for *P. falciparum*. The cDNA was synthesized using gene-specific reverse primer (P1 for *P. falciparum* and P83 for *P. berghei*) and Moloney Murine Leukemia Virus (MMLV) reverse transcriptase according to manufacturer's protocol. This cDNA was used as the template for PCR amplification of AMPD gene.

For RNA isolation from yeast, a single colony of *S. cerevisiae* containing pYES2/CT_PfAMPD_$(His)_6$ was inoculated in 5 mL of liquid SD – Ura (– indicates without) medium containing 2 % glucose as carbon source. This was grown for 12 hours at 30 °C, 150 rpm. The cells were harvested by centrifugation at 1200 × g for 3 minutes. The cells were resuspended in 5 mL SD – Ura medium containing 2 % galactose as carbon source and incubated at 30 °C, 150 rpm for 16-20 hours. The cells were harvested by centrifugation at 1200 × g for 3 minutes and the supernatant was discarded. The cells were resuspended in 0.25 mL of Trizol™ reagent and 0.5 mm acid washed glass beads were added to about half of the volume of the suspension. This was subjected to 5 cycles of vigorous vortexing (30 seconds) and incubated on ice (30 seconds). After the fifth cycle, 0.75 mL of Trizol™ reagent was added to the suspension and mixed thoroughly. The rest of the steps were as described for *Plasmodium*. For *P. pastoris*, single colony containing pGAPZαA_PfAMPD was inoculated into 5 mL YPD and grown for 24 hrs. The RNA isolation protocol was as described for *S. cerevisiae*. The cDNA was synthesized using gene-specific reverse primer (P19 for *S. cerevisiae* and P21 for *P.* pastoris) and Moloney Murine Leukemia Virus (MMLV) reverse transcriptase according to manufacturer's protocol. This cDNA was used as the template for PCR amplification of AMPD gene.

2.2.2 Generation of plasmid constructs

All clones were generated in XL-1 blue strain of *E. coli* cells (Table 2.1 lists the plasmid constructs used in the study). Using cDNA as template PfAMPD gene was PCR amplified using primers P2 and P3. The PCR product was digested with EcoRI and HindIII and cloned into double digested pETDuet-1 vector. Similarly, the truncated versions of PfAMPD gene were PCR amplified using the full-length clone as template and primer pairs P4, P5 for Δ59; P6, P7 for Δ94 and P8, P9 for Δ178. All PCR products were digested using EcoRI and HindIII enzymes and, cloned into double digested pETDuet-1 vector. Using full-length clone of PfAMPD (pETDuet-1_PfAMPD) as a template and primers P18, P19, PfAMPD gene was PCR amplified, digested with KpnI and XbaI enzymes followed by cloning into double digested pYES2/CT plasmid.

Initial sequence analysis was done by submitting PfAMPD gene sequence to the server, Graphical Codon Usage Analyser (GCUA) (Fuhrmann et al., 2004) to determine the codon compatibility of PfAMPD gene with the *P. pastoris* expression system. It was found that the gene sequence was highly adapted for the *Pichia* system and consisted of only two rare codons - 2^{nd} and 174^{th}. Synonymous mutations were made to eliminate these two rare codons by incorporating the changed codons in forward primer P20 and internal primers (P22 and P23). Overlap PCR strategy was employed for this purpose where partial amplicons were generated using primer pairs P20, P23 and P21, P22. These partial amplicons were purified by gel extraction and used as template for amplifying PfAMPD gene with two altered codons. Full-length PfAMPDA was amplified using the primers P20 and P21 and cloned into *Pichia* expression vector pGAPZαA (for secretory expression) between XhoI and XbaI sites. Clones were confirmed by PCR, insert release and sequencing. Also, PfAMPDA was sub-cloned from pGAPZαA_PfAMPD to pGAPZ A (for intracellular expression) plasmid between restriction sites XhoI and XmaI. Clones were confirmed by PCR and insert release. Both constructs were used for protein expression.

Using genomic DNA from yeast as template, yeast AMPD gene was PCR amplified using primers P14 and P15. The PCR product was digested with SacI and XhoI enzymes and cloned into double digested pYES2/CT plasmid. Yeast AMPD gene was also cloned into pCM189 vector between sites BamHI and PstI, for which the gene was amplified using the primers P16 and P17. The PfAMPD gene was harmonized for yeast codon usage using Eugene codon optimization tool. The harmonized gene was synthesized by Shinegene China. The synthesized gene was provided as a clone in pMD19 plasmid. This synthesized gene was subcloned into *E. coli*, *S. cerevisiae* and *P. pastoris* expression vectors and checked for expression and solubility of the protein. Though the gene was harmonised for yeast expression system, protein expression was attempted in *E. coli* and yeast using a series of bacterial vectors as well as yeast expression vectors. Harmonised PfAMPD (hPfAMPD) gene segment was released from pMD19_hPfAMPD vector using the enzymes KpnI and XhoI and subcloned into a pYES2/CT plasmid which was cut at the same restriction sites. eGFP was amplified using primers P24, P25 and pRS306 as template, double digested using enzymes BamHI and XhoI and ligated into the double di-

gested pYES2/CT vector. Cloning of GFP tagged yeast and PfAMPD was done by ligating three DNA segments i.e vector, gene fragment and GFP fragment. ScAMPD was amplified using primers P26, P27 followed by digestion with SacI and KasI enzymes. eGFP was amplified by using primers P28, P29 followed by digestion with KasI and XhoI enzymes. These two fragments were ligated with SacI, XhoI digested pYES2/CT plasmid. Similarly, PfAMPD was amplified using primers P30, P31 and pMD19_hAMPD as template, followed by digestion with KpnI and XbaI enzymes. eGFP was amplified by using primers P32, P33 followed by digestion with XbaI and XhoI enzymes. These two fragments were ligated with KpnI, XhoI digested pYES2/CT plasmid. PCR product for pYES2/CT_$(His)_6$_hPfAMPD_GFP construct, was generated using primers P65, P66 and pYES2/CT_hPfAMPD_GFP (pYES2/CT clone containing harmonised PfAMPD gene with C-terminal GFP tag) as template. The PCR product was digested with enzymes KpnI and XhoI and cloned into a digested pYES2/CT plasmid. PCR product for pYES2/CT_hPfAMPD_GFP_$(His)_6$ construct, was generated using primers P64, P67 and pYES2/CT_hPfAMPD_GFP as template. The PCR product was digested with enzymes KpnI and XhoI and cloned into a digested pYES2/CT plasmid.

An N-terminal Strep-tag and C-terminal GFP tag construct (pYES2/CT_StrepTag-II_hPfAMPD_GFP) was also made. Using pYES2/CT_PfAMPD_GFP as template PCR was performed using primers P96 and P65. The purified PCR product was digested with KpnI and XhoI enzymes and ligated to similarly digested pYES2/CT plasmid.

2.2.3 Site-directed mutagenesis and PfAMPD N-terminal truncations

Using pYES2/CT_hPfAMPD_GFP (pYES2/CT clone containing harmonised PfAMPD gene with C-terminal GFP tag) plasmid as template site-directed mutagenesis was performed by following overlap extension PCR and AQUA cloning protocol (Beyer et al., 2015). Partial amplicons for each mutant were obtained by PCR using Gal promoter-forward primer/ mutagenic-reverse primer and Cyc terminator-reverse primer/ mutagenic-forward primer pairs. The fragments were gel purified and mixed with double digested (KpnI and XhoI) and gel purified pYES2/CT vector in the molar ratio 1:3:3:: vector:insert1:insert2. This mix was used to transform competent XL1-Blue *E. coli* cells and plated on LB plates containing 100 µg mL^{-1} ampicillin. The clones were confirmed by PCR, restriction digestion and sequencing. These constructs were used to perform functional complementation in *Δamd1* yeast by serial dilution and spotting assay. PfAMPD lacking 60 and 180 residues from N-terminal end, hPfAMPD_*ΔN60* and hPfAMPD_*ΔN180* were PCR amplified using primer pairs P34, P65 and P35, P65; respectively. The PCR product was double digested (KpnI and XhoI) and cloned into a digested pYES2/CT plasmid.

Table 2.1: List of plasmid constructs generated

Sl. No.	Name of construct	Comments
1	pETDuet-1_$(His)_6$_PfAMPD	For expression in *E. coli*
2	pETDuet-1_$(His)_6$_PfAMPD *Δ59*	
3	pETDuet-1_$(His)_6$_PfAMPD *Δ94*	
4	pETDuet-1_$(His)_6$_PfAMPD *Δ178*	
5	pET23d_PfAMPD_$(His)_6$	
6	pYES2/CT[a]	Vector control
7	pYES2/CT_PfAMPD_$(His)_6$	For expression in *S. cerevisiae* and complementation assay
8	pYES2/CT_ScAMPD_$(His)_6$	Positive control for complementation assay
9	pGAPZαA_PfAMPD	For secretory expression in *P. pastoris*
10	pGAPZ A_PfAMPD	For intracellular expression in *P. pastoris*
11	pMD19_hPfAMPD	Codon harmonised PfAMPD synthesized by Shinegene, China
12	pQE30_$(His)_6$_hPfAMPD_$(His)_6$	For expression in *E. coli* with codon harmonised gene
13	pET22b_(PelB)_hPfAMPD_$(His)_6$	
14	pET21b_$(His)_6$_hPfAMPD_$(His)_6$	
15	pET21b_(MBP)_hPfAMPD_$(His)_6$	
16	pGAPZ A_hPfAMPD_$(His)_6$	For intracellular expression in *P. pastoris* with codon harmonised gene
17	pYES2/CT_hPfAMPD_$(His)_6$	For expression in *S. cerevisiae* and complementation assay through codon harmonised gene
18	pCM189_hPfAMPD_$(His)_6$	
19	pCM189_ScAMPD_$(His)_6$	Positive control for complementation assay
20	pCM189[a]	Vector control
21	pYES2/CT_GFP	
22	pYES2/CT_hPfAMPD_GFP	For expression in *S. cerevisiae* and complementation assay through codon harmonised gene and microscopy
23	pYES2/CT_ScAMPD_GFP	Positive control for complementation assay
24	pYES2/CT_$(His)_6$_hPfAMPD_GFP	To determine stability conferred by C-terminal GFP tag
25	pYES2/CT_hPfAMPD_GFP_$(His)_6$	
26	pYES2/CT_*ΔN60*_hPfAMPD_GFP	For characterization by complementation assay
27	pYES2/CT_*ΔN180*_hPfAMPD_GFP	
28	pYES2/CT_hPfAMPD_H245A/H247A_GFP	
29	pYES2/CT_hPfAMPD_F319L_GFP	
30	pYES2/CT_hPfAMPD_Y323L_GFP	
31	pYES2/CT_hPfAMPD_D454N_GFP	
32	pYES2/CT_hPfAMPD_M504R_GFP	
33	pYES2/CT_hPfAMPD_M504H_GFP	
34	pYES2/CT_hPfAMPD_H517A_GFP	
35	pYES2/CT_hPfAMPD_E520A_GFP	
36	pYES2/CT_hPfAMPD_H539A_GFP	
37	pYES2/CT_hPfAMPD_D594A_GFP	
38	pYES2/CT_hPfAMPD_D595A_GFP	
39	pYES2/CT_hPfAMPD_E608D_GFP	
40	pYES2/CT_hPfAMPD_T621A_GFP	
41	pYES2/CT_hPfAMPD_D623Y_GFP	
42	pYES2/CT_StrepTag-II_hPfAMPD_GFP	For recombinant expression and purification
43	pGDB_PfAMD	For conditional knockdown in *P. falciparum*
44	pBCEN5_GFP[a]	Vector control
45	pBCEN5_PbAMPD_GFP	For localization studies
46	pBCEN5_PbAMPD_H245A/H247A_GFP	

[a]These are procured plasmids and not generated in the study

2.2.4 Bacterial transformation and expression

Competent *E. coli* cells were prepared by following the method described earlier (Chung et al., 1989). The transformation was carried out as described in 'Molecular cloning' by Sambrook and Russel (Sambrook and Russell, 2001). For expression, a single colony was inoculated into 5 mL LB media with ampicillin (100 µg mL^{-1}) and chloramphenicol (34 µg mL^{-1}) and grown overnight at 37 ℃, 180 rpm. The overnight culture was added to a secondary culture (terrific broth) at 1 % inoculum in the presence of the antibiotics ampicillin and chloramphenicol and incubated at 37 ℃, 180 rpm till the A_{600} reached 0.6. The culture was then induced using IPTG at a concentration of 1 mM and further incubated at 37 ℃, 180 rpm for four more hours. 1 mL culture was lysed by resuspending in 1 × loading dye and separated on SDS-PAGE followed by Western blot. Anti - $(His)_6$ antibody from mouse was used to probe the blot followed by anti-mouse antibody from goat conjugated to horseradish peroxidase (HRP) as secondary antibody. The blot was developed using aminoethyl carbazole (AEC) and hydrogen peroxide as substrates.

2.2.5 Generation and purification of anti PfAMPD antibody

pET23d_PfAMPD_$(His)_6$ construct (Nagappa, 2014) was used for the production of the antigen in *E. coli*. The protein was expressed in Rosetta (DE3) pLysS strain and purified under denatured conditions. The protein was ethanol precipitated and run on SDS-PAGE, followed by Coomassie staining. The full-length protein band and the major degradation band at around 35 kDa was cut and minced into small bits and electroelution was performed using SDS-PAGE buffer containing 25 mM Tris HCl, 192 mM glycine, 0.1% SDS, followed by electrodialysis using 15 mM ammonium bicarbonate buffer containing 0.0125% SDS. This sample was lyophilized and then resuspended in 1×PBS and quantified calorimetrically by Bradford's method. This was used as antigen to immunize New Zealand White rabbit in order to generate antibodies. The immunization schedule was as follows. Pre-immune serum was collected on day 0. This was followed by a primary injection consisting of 400 µg antigen with Freund's complete adjuvant mixed in 1:1 v/v ratio. A booster dose of antigen was given on day 15 consisting of 250 µg antigen with Freund's incomplete adjuvant mixed in 1:1 v/v ratio. Another booster dose was given on day 30 comprising of 200 µg antigen with Freund's incomplete adjuvant. A test bleed of around 5 mL was done on day 37, followed by a major bleed of around 25 mL on day 40. Another booster dose consisting of 200 µg antigen with Freund's incomplete adjuvant was given on day 70, followed by a major bleed of around 30 mL on day 78. Blood collected from the rabbit was allowed to clot overnight at 4 ℃. Later it was centrifuged and the supernatant antiserum was collected and stored in aliquots at -20 ℃.

Since PfAMPD protein was insoluble conventional antibody purification protocol could not be followed. Hence strip affinity protocol was followed to purify antigen-specific antibody, which was subsequently used for indirect immunofluorescence using confocal microscopy. Denatured and purified PfAMPD was precipitated by adding ethanol to a final concentration of 90 % and

stored overnight at -20 ℃. The precipitate was centrifuged, dried and resuspended in 1 × SDS-PAGE loading dye and boiled for 5 minutes. The sample was subjected to SDS-PAGE and Western transfer. The blot was PonceauS stained and the bands of interest were cut and blocked using 5 % skimmed milk in 1 × PBS. The blots were then incubated with antiserum overnight at 4 ℃ and washed three times with 1 × PBS containing 0.1 % Tween20. Antibody bound to the blot was eluted using 100 mM Tris-glycine, pH 2.5 and immediately neutralized using 1 M Tris HCl, pH 8.0. This was repeated and the fractions eluted were concentrated using centrifugal concentrators.

2.2.6 Co-expression of PfAMPD with chaperones

BL21 DE3 strain of *E. coli* was transformed with pETDuet-1_$(His)_6$_PfAMPD and selected on LB-ampicillin agar plate. A single colony was picked and was used to prepare chemically competent cells by the method of Chung et al (Chung et al., 1989). These cells were now transformed individually with each of the five plasmids from the chaperone kit and selected on LB-ampicillin-chloramphenicol plates. Induction of PfAMPD was carried out using 0.5 mM IPTG. Samples were collected after 6 hours of induction and were analysed by SDS-PAGE and Western blotting where the expression was checked by probing the blot with an anti-PfAMPD antibody raised in rabbit as primary antibody and anti-rabbit IgG raised in goat conjugated with HRP as the secondary antibody.

2.2.7 Expression of PfAMPD in *S. cerevisiae*

Saccharomyces cerevisiae transformation was performed according to the protocol described by Gietz and Schiestl (Gietz and Schiestl, 2007). For expression, a single colony was inoculated into 5 mL SD-Ura (synthetically defined minus uracil) medium containing glucose (2%) as carbon source and incubated at 30 ℃, 180 rpm for 15-20 hrs. The overnight culture was harvested by centrifugation, washed once with sterile water and resuspended in 5 mL of SD-Ura medium containing galactose (2 %) as carbon source and incubated at 30 ℃, 180 rpm. 1 mL aliquots were taken at different time points and TCA was added to the cells (final concentration 12 %) and stored at -80 ℃ overnight for precipitation. The aliquots were thawed and the cells were harvested by centrifugation at 12000 × g. The supernatant was discarded and the pellet was washed in 250 µL 80 % cold acetone twice. After the second wash, acetone was removed and the pellet was air dried, resuspended in 1 % SDS/0.1 N NaOH solution. The lysates were boiled in the presence of 1 × loading dye and separated on SDS-PAGE followed by Western blotting. Anti - $(His)_6$ antibody or anti - GFP antibody raised in mouse was used to probe the blot followed by anti-mouse antibody from goat conjugated to (HRP) as secondary antibody. The blot was developed using AEC and hydrogen peroxide as substrates.

2.2.8 Expression of PfAMPD in *Pichia pastoris* strain X-33

Around 1 µg of pGAPZαA_PfAMPD (or pGAPZ A_PfAMPDD) was linearized using AvrII restriction enzyme and used to transform electro-competent *Pichia pastoris* X-33 cells. Electroporation was performed according to the condensed *Pichia* transformation protocol (Lin-Cereghino et al., 2005). After electroporation, the cells were spread on YPD agar plates containing 200 µg mL^{-1} zeocin and incubated at 30 °C for 2 days. Few colonies were picked and plated on YPD plates containing 400 µg mL^{-1} zeocin for selection of multi-copy integrants. Transformants were confirmed by PCR. For expression, a single colony was inoculated into 5 mL YPD medium and grown at 30 °C, 150 rpm for 12 hours. This was used to inoculate a secondary culture of 100 mL YPD medium at 0.2 A_{600} mL^{-1}. The secondary culture was grown at 30 °C, 150 rpm and aliquots of 1 mL were collected at different time points. Both media supernatant and cells were processed and analysed by SDS-PAGE and Western blotting. Sample processing was similar to that described for *S. cerevisiae*. These were subjected to electrophoresis and Western blotting where the expression was checked by probing the blot with anti-PfAMPDA antibody raised in rabbit as primary and anti-rabbit IgG raised in goat conjugated with HRP as the secondary.

2.2.9 Expression of PfAMPD using cell-free protein expression systems

TNT® T7 coupled wheat germ extract from Promega was used to produce recombinant PfAMPD. The kit was used as per the manufacturer's instruction. The template was pET23d_PfAMPD_$(His)_6$ vector (Nagappa, 2014). The luciferase construct supplied with the kit was used as control and was validated by luciferase assay using a tube luminometer. The samples were analysed by Western blotting using anti-$(His)_6$ antibodies. The experiment was also repeated with linearized constructs containing harmonised PfAMPD gene.

2.2.10 Serial dilution and spotting of *S. cerevisiae* cells

Single colonies were inoculated into 5 mL SD-Ura medium containing glucose as carbon source and grown overnight at 30 ℃, 180 rpm. The cells were harvested by centrifugation at 5000 × g and washed once with sterile water. A_{600} was determined and serial dilutions were made starting from 1 A_{600} mL^{-1} to 10^{-3} A_{600} mL^{-1}. 2 µL from each dilution was spotted on SD-Ura plate containing galactose as carbon source with or without 50 µg mL^{-1} S - adenosylmethionine (SAM). The plates were allowed to air dry and incubated at 30 ℃ (37 ℃ for temperature sensitivity studies) for 60-72 hrs. The plates were observed for cell growth and photographically documented.

2.2.11 Generation of *Plasmodium* transfection vectors

2.2.11.1 Generation of linear vectors for knockout and tagging of PbAMPD gene

Target specific genetic manipulation in *P. berghei* involves homologous recombination between chromosomal DNA and a selection marker containing foreign DNA. In order to perform a knock-out, a minimum of 0.5 kb of both 5´ and 3´ flanking regions of the gene of interest, have to be cloned flanking a selection cassette. When this construct is used to transfect the parasite the homology arms will facilitate double crossover recombination and the gene of interest will be replaced by the selection cassette. The conventional cloning process using restriction enzymes and ligase is faced with a lot of hindrances because of the high AT richness of the *Plasmodium* genome. Plasmids containing such high AT-rich segments are not stably maintained in *E. coli* cells. To overcome this obstacle PlasmoGem has generated a representative *P. berghei* genomic DNA library (PbG01) (average length of insert 9 kb) in pJAZZ-OK, a bacteriophage N15 based low copy number linear cloning vector, which can be maintained in *E. coli* TSA cells (Godiska et al., 2009; Pfander et al., 2011; Gomes et al., 2015).

Generation of linear vectors (either for knockout or tagging) was done by following the recombineering technology. The library clone for *P. berghei* AMPD (PbG02_B-44h05) was obtained from PlasmoGem. The library clone obtained from PlasmoGem was validated by PCR using P68 and P69 primers which bind to 5´ UTR and in the gene, respectively. Restriction digestion was set up in a 10 µL reaction containing 1 × cutsmart buffer, 1 µL StuI enzyme, 1 µg plasmid and volume made up with H_2O. The PCR product was analysed by electrophoresis on 0.8 % agarose gel with 0.5 µg mL^{-1} ethidium bromide in 1 × TAE buffer. The Zeo-PheS bacterial +ve/-ve selection cassette was amplified using specific primer pairs (P72, P73 for knockout construct generation and P74, P75 for tagging construct generation) and plasmid pR6K-Zeo-PheS as template for the PCR. The PCR product was analysed by agarose gel electrophoresis. The PCR product was purified by gel extraction procedure using the Qiagen gel extraction kit. The TSA cells containing PfAMPD library clone were transformed with pSC101gbdA plasmid and selected on tetracycline plate. A single colony was picked and inoculated into 5 mL TB medium and grown at 30 °C, 180 rpm overnight. This was used to inoculate a secondary culture of fresh 5 mL TB (1% inoculum). The cells were allowed to grow till A_{600} of 0.4 and induced with 100 µL of 10 % arabinose for 40 minutes at 37 °C, 180 rpm. The culture was chilled on ice for 10 minutes. 1.4 mL of culture was transferred to a chilled Eppendorf tube and centrifuged at 5000 × g for 3 minutes. The pellet was resuspended in 1 mL ice-cold water and centrifuged at 5000 × g for 3 minutes. The supernatant was discarded and the wash step was repeated three times. The cells were finally resuspended in 50 µL ice-cold water and mixed with 250 ng of the PCR product (selection cassette with 50 bp flanking homology arms). This was transferred to a chilled 1 mm electroporation cuvette and electroporated at 1800 V, 10 µF, 600 Ω using Bio-RAD Gene Pulsar Xcell. Electroporated cells were recovered in 1 mL TB and incubated at 37 °C, 180 rpm for 70 minutes and plated on TB zeocin plate (zeocin 100 µg mL^{-1}) and incubated at 37 °C for 16 hrs. The colonies were screened

by colony PCR using specific primer pairs (P68, P76 for knockout intermediate vector and P70, P71 for tagging intermediate vector). The positive clones were cultured and plasmid isolated from them was serially diluted (1:10) using sterile water and used to transform fresh TSA cells. Two rounds of transformation were done to eliminate parental copy of the library clone and to retain only the recombined one that was confirmed by PCR. The positive recombinant plasmid i.e., the intermediate vector was used for the Gateway LR Clonase reaction. The reaction was set up in 20 µL volume using 1 × LR clonase buffer, intermediate vector and *Plasmodium* selection marker containing plasmid in 1:3 molar ratio, 2 µL of LR clonase mix and volume made up with TE buffer. The reaction was incubated at 25 °C for 16 hours. 5 µL of this reaction was mixed with 50 µL of electrocompetent cells prepared according to the protocol described in 'Molecular Cloning' by Sambrook and Russel. Electroporation was performed at 1800 V, 10 µF, 600 Ω using Bio-RAD Gene Pulsar Xcell. Electroporated cells were recovered in 1 mL TB incubated at 37 °C, 180 rpm for 70 minutes and plated on a plate containing yeast extract (5 g L^{-1}), NaCl (5 g L^{-1}), 4-chloro-DL-phenylalanine (2 g L^{-1}), 2 % agar and 0.4 % glucose with 30 µg mL^{-1} kanamycin. The plates were incubated at 37 °C for 18 hours. The colonies were screened by PCR using Taq polymerase and specific primer pairs (P68, P78 for final knockout vector and P70, P71 for final tagging vector). The plasmid was isolated from positive clones and confirmed by restriction digestion using the restriction enzyme XbaI.

The intermediate vectors, knockout and, GFP tagging final constructs were confirmed by PCR and restriction digestion. The final tagging and knockout vectors were subjected to NotI digestion, purified and used for transfection. The entire procedure is schematically described in Fig. 2.1

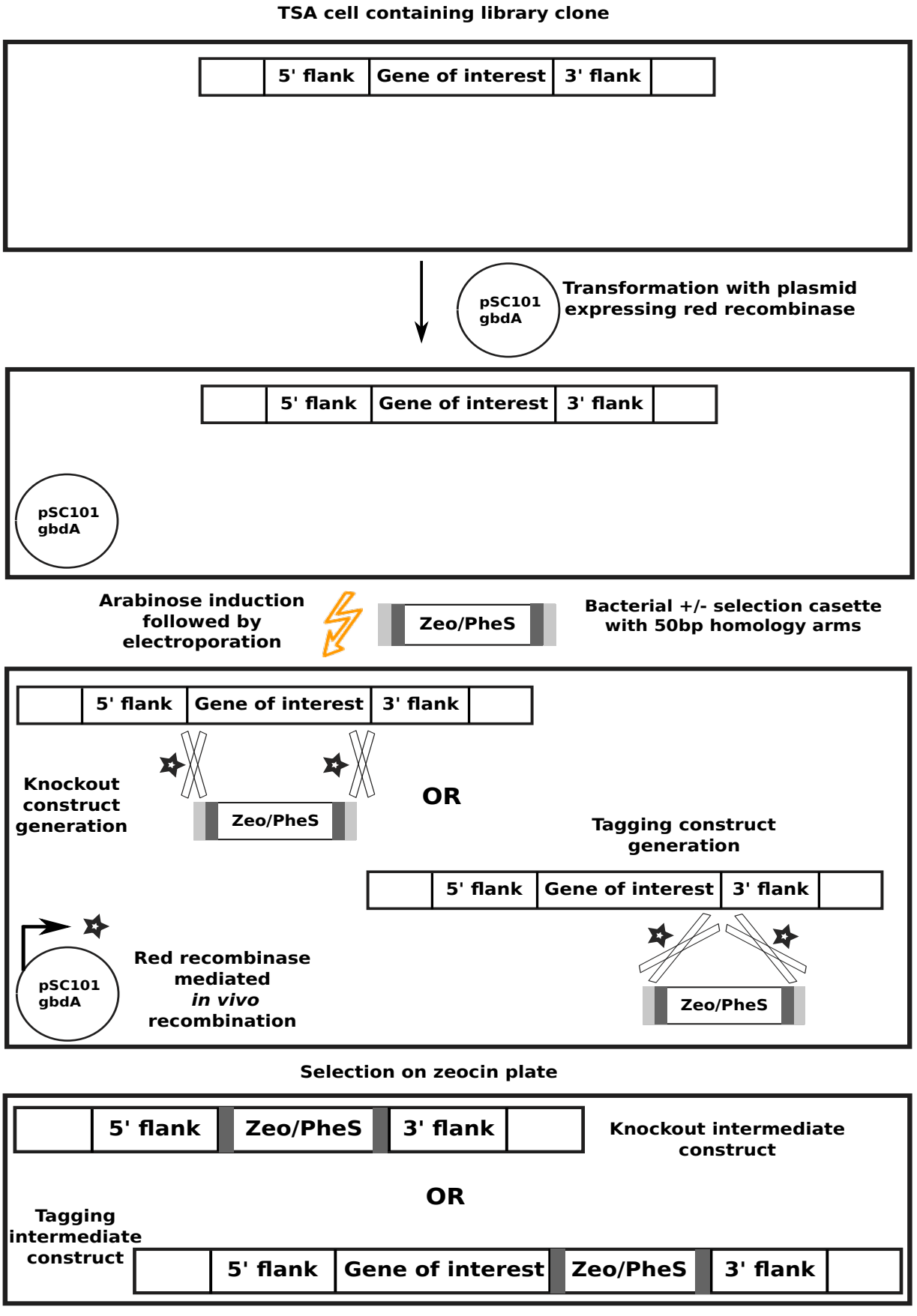
TSA cell containing library clone
5' flank
Gene of interest
3' flank
pSC101
gbdA
Transformation with plasmid
expressing red recombinase
5' flank
Gene of interest
3' flank
pSC101
gbdA
Arabinose induction
followed by
electroporation
Zeo/PheS
Bacterial +/- selection casette
with 50bp homology arms
5' flank
Gene of interest
3' flank
Knockout
construct
generation
Zeo/PheS
OR
Tagging construct
generation
5' flank
Gene of interest
3' flank
pSC101
gbdA
Red recombinase
mediated
in vivo
recombination
Zeo/PheS
Selection on zeocin plate
5' flank
Zeo/PheS
3' flank
Knockout intermediate
construct
OR
Tagging
intermediate
construct
5' flank
Gene of interest
Zeo/PheS
3' flank

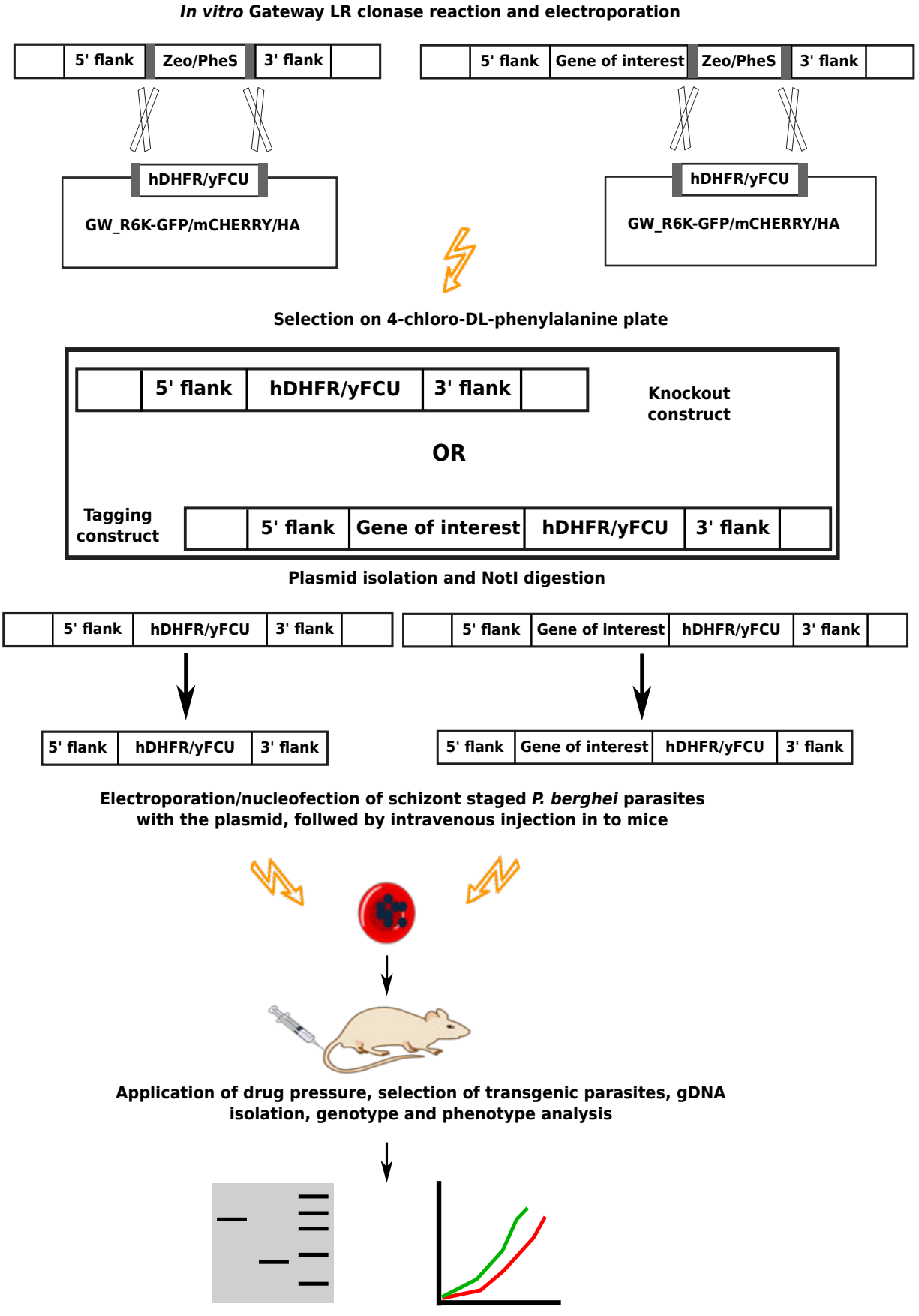
In vitro Gateway LR clonase reaction and electroporation
5' flank
Zeo/PheS
3' flank
hDHFR/yFCU
GW_R6K-GFP/mCHERRY/HA
5' flank
Gene of interest
Zeo/PheS
3' flank
hDHFR/yFCU
GW_R6K-GFP/mCHERRY/HA
Selection on 4-chloro-DL-phenylalanine plate
5' flank
hDHFR/yFCU
3' flank
Knockout construct
OR
Tagging construct
5' flank
Gene of interest
hDHFR/yFCU
3' flank
Plasmid isolation and NotI digestion
5' flank
hDHFR/yFCU
3' flank
5' flank
Gene of interest
hDHFR/yFCU
3' flank
5' flank
hDHFR/yFCU
3' flank
5' flank
Gene of interest
hDHFR/yFCU
3' flank
Electroporation/nucleofection of schizont staged *P. berghei* parasites with the plasmid, follwed by intravenous injection in to mice
Application of drug pressure, selection of transgenic parasites, gDNA isolation, genotype and phenotype analysis

Figure 2.1: Schematic representation of the generation of knockout / tagging construct by recombineering method

Library clone for a given gene of interest will have the complete coding sequence along with few kilobases of 5´ and 3´ flanking regions cloned between NotI restriction sites. This vector can be easily manipulated by recombinases. In order to modify a gene of interest, a library clone is selected and transformed with a plasmid encoding lambda phage Red recombinase under an inducible promoter. This is then transformed with a PCR product containing a bacterial positive-negative selection cassette (Zeo-PheS) generated using primers such that the cassette is flanked by 50 bp nucleotides homologous to the 5´ and 3´ region of the gene of interest. Upon induction of recombinase, the PCR product undergoes homologous recombination with the library clone via the 50bp homology arms; thereby replacing the gene of interest with the selection cassette. This plasmid, where the target gene has been replaced by a bacterial selection marker, is called the intermediate vector. This intermediate vector is subjected to an *in vitro* recombination reaction using Gateway LR clonase which replaces the bacterial selection marker with *Plasmodium* selection marker hDHFR-yFCU. This is facilitated by the attR1 and attR2 sites flanking the bacterial selection marker and the attL1 and attL2 sites flanking the *Plasmodium* selection marker. The att sites are attachment sites for the LR clonase (mix of Integrase, Integration Host Factor and Excisionase) which mediates recombination. This recombination is an irreversible process and correct recombination products are selected by transforming TSA cells and negatively selecting against PheS. The modified library clone is subjected to NotI digestion to release the insert containing *Plasmodium* selection marker flanked by homology arms of the gene of interest. This is used to transfect *P. berghei* where, by double crossover, the gene of interest will be replaced by the selection marker, thus knocking out the gene of interest. The knockouts are selected by feeding the mice with pyrimethamine treated water, which will inhibit the growth of wild type parasites, thereby selecting for only the parasites with the antibiotic cassette. Tagging construct and parasite are generated in a similar manner as depicted.

For generating pBCEN5_PbAMPD_GFP vector, *P. berghei* AMPD gene was amplified by PCR using cDNA obtained from *P. berghei* strain in which PbAMPD was endogenously tagged with GFP as template and primers P84, P85; followed by cloning into BamHI digested pBCEN5 plasmid using InFusion assembly kit from TaKaRa. The clone was confirmed by PCR and sequencing. Construct containing H245A/H247A mutant of PbAMPD (pBCEN5_PbAMPD_H245A/H247A_GFP) was generated by AQUA cloning protocol as described earlier. Partial amplicons were generated using primer pairs P86, P88 and P87, P89 and pBCEN5_PbAMPD_GFP vector as template.

2.2.11.2 Generation of conditional knockdown vector for PfAMPD gene

Apart from generating linear knockout vectors for *P. berghei* transfection, a circular conditional knockdown vector was also generated to probe the essentiality of PfAMPD. The conditional knockdown approach comes in handy while manipulating essential genes in a haploid organism like *Plasmodium*. This can be done at transcriptional, post-transcriptional and at the post-translational level. Here we have made use of a regulatable affinity tag which can be used to regulate the levels of the protein by causing premature degradation (Fig. 2.2). This was achieved by tagging the protein of interest with *E. coli* dihydrofolate reductase degradation domain (DDD) (Muralidharan et al., 2011). Using genomic DNA as template around 1.3 kb of the 3´ end of PfAMPD gene was amplified using primers P97 and P98. The PCR product was purified by

gel extraction procedure using the Qiagen gel extraction kit. The purified PCR product and plasmid pGDB were digested using enzymes AvrII and XhoI. The digested plasmid was purified by Qiagen gel extraction kit and the PCR product was subjected to PCR clean up by Qiagen kit. The purified vector and insert (in a molar ratio of 1:3) were subjected to ligation using T4 DNA ligase at 16 °C for 16 hours. The ligation mix was used to transform chemically competent *E.coli* XL-1 Blue cells. Transformants were selected on LB-ampicillin plates and screened by colony PCR using Taq polymerase. The positive clones were used to isolate plasmid which was further validated by restriction digestion and sequencing.

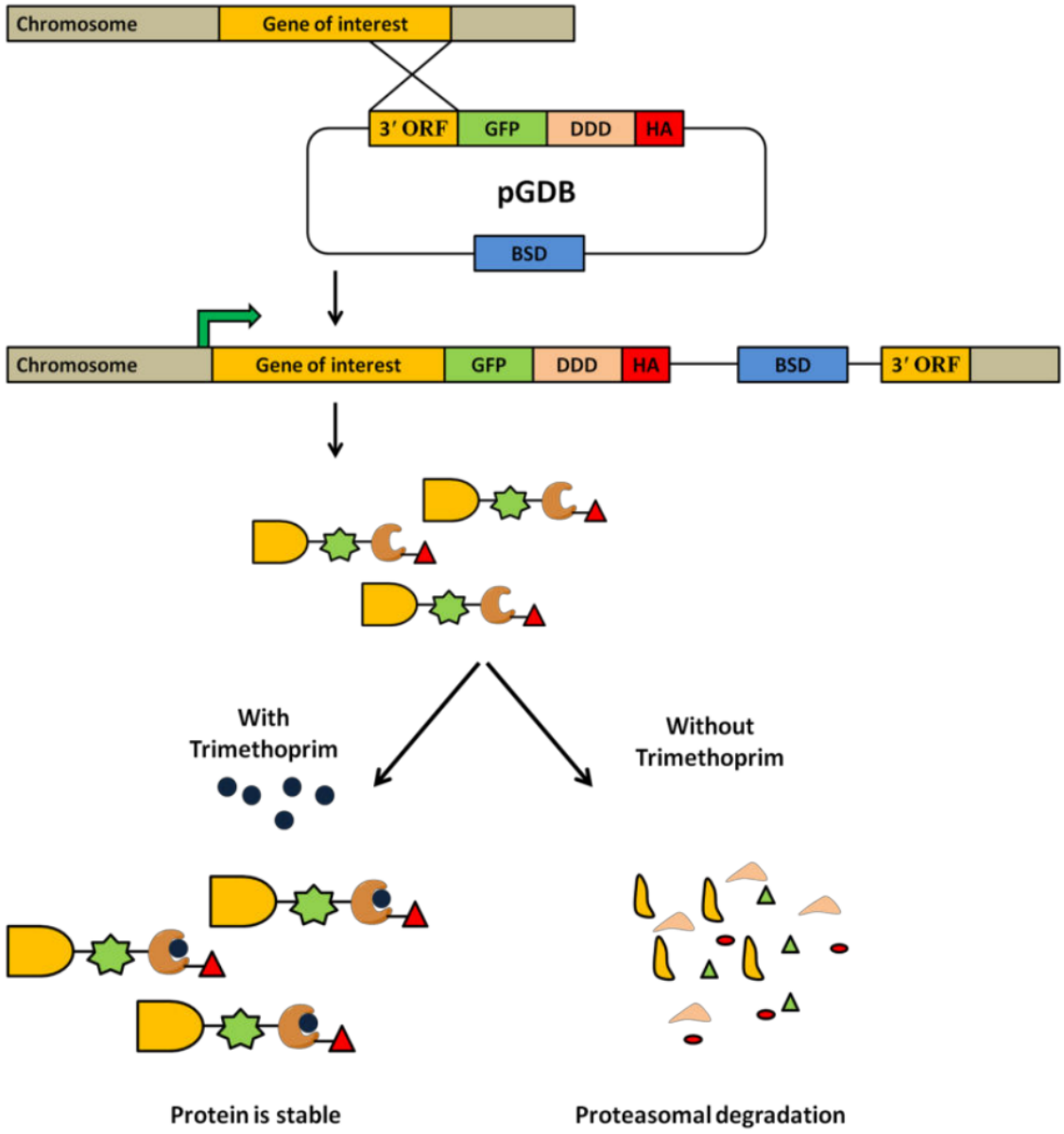

Figure 2.2: Schematic representation for generating a conditional knockdown by using post-translational degradation domain tagging strategy

The DHFR degradation-domain based conditional knockdown requires cloning of around 1 kb of 3´ end of the gene of interest into the circular plasmid pGDB such that the ORF is in frame with GFP, DDD and HA-tag encoded in the plasmid. This approach serves three purposes, namely-tagging of the protein of interest with GFP which helps in localization experiments, tagging with DDD helps in conditional knockdown of protein levels and also to vary the levels of the protein by varying the ligand concentration and the HA tag which can be used for pull-down experiments to identify interacting partners. The circular plasmid when transfected into the parasite; undergoes single crossover recombination through the 3´ end of the gene of interest and gets integrated into the chromosome. The parasites bearing the plasmid can be selected using the antibiotic blasticidin as the plasmid encodes the gene which confers resistance. For regulating protein levels the ligand trimethoprim which is a folate analogue can be used in a dose-dependent manner. Hence normal 3D7 strain parasites cannot be used for this experiment. A knockout strain, PM1KO where the non-essential gene encoding Plasmepsin 1 has been replaced by human DHFR which is resistant to trimethoprim is used to perform conditional knockdown using the DDD strategy. Around 80% reduction in levels of the protein can be achieved by this strategy but some proteins do not tolerate the tag due to its huge size.

2.2.12 *Plasmodium* culture and transfection

2.2.12.1 Maintenance of *P. falciparum* culture and transfection

Fresh blood (O+ve blood group) was collected from healthy human volunteers and stored in the presence of the anticoagulant, acid citrate dextrose solution at 4 ℃ overnight. Plasma was separated and discarded. The erythrocytes were washed with 1 × PBS three times and stored at 4 ℃ in incomplete RPMI-1640 medium containing 25mM HEPES at 50% hematocrit in the presence of the antibiotic gentamycin at 2.5 μg mL^{-1}. *P. falciparum* parasites were grown in complete RPMI medium (20 mM glucose, 0.2 % sodium bicarbonate, 0.5 % Albumax and 50 μM hypoxanthine) at 5 % hematocrit under micro-aerophilic conditions using a candle jar set up at 37 ℃. Parasitemia was checked regularly by making Giemsa stained smears. 5-10 % parasitemia was maintained and media change was given daily (Trager and Jensen, 1976).

Plasmid for transfection was purified using Qiagen endotoxin-free maxi-prep kit and the final DNA pellet was resuspended in cytomix. Preloading protocol was followed for the transfection experiment. 400 μL of 50 % hematocrit blood was taken in a 15 mL Falcon tube and centrifuged at 400 × g to pellet the erythrocytes. The supernatant was removed and approximately 100 μg of plasmid DNA was added to the erythrocyte pellet and resuspended. The volume was made up to 350 μL with cytomix. The mixture of RBC and DNA was transferred to a pre-chilled 2 mm cuvette and electroporated by using either exponential decay programme (0.31 Kv & 950 μF) or square wave protocol (365 V for 1 ms separated by 0.1 s eight times). Parameters such as time constant and droop percentage were noted down for exponential decay and square wave protocols, respectively. The cuvette was placed at room temperature and 1 mL RPMI-1640 medium was added. The electroporated cells were transferred to a 15 mL Falcon tube and 10 mL complete RPMI-1640 medium was added. The cells were harvested by centrifugation and the pellet was

resuspended in 10 mL complete medium. To this, 1mL of schizont stage parasite culture with at least 8 % parasitemia was added. The culture was maintained under micro-aerophilic conditions. Medium change was given after 12 hrs to remove RBC debris. Subsequently, regular medium change was done on a daily basis and fresh erythrocytes were added (100 µL of 50 % hematocrit) once every 3 days. Parasitemia was monitored weekly once for a period of 40 days.

2.2.12.2 Maintenance of *P. berghei* culture and transfection

Glycerol stock of wild type *P. berghei ANKA* parasites was injected into a healthy male BALB/c mouse (6-8 weeks old). The parasitemia was monitored by drawing blood from tail snip and observing Giemsa stained blood smears under the microscope (100 × oil immersion objective). Transfection of the parasites was done by modifying the protocol described by Janse et al. (Janse et al., 2006). Wild type *P. berghei* parasites were cultured in a healthy male BALB/c mouse and once the parasitemia reached 30-40 %, parasites were harvested. Around 1 mL of blood was collected in 0.5 mL of heparin solution (200 units mL^{-1}) made in incomplete RPMI-1640 medium. This was subjected to density gradient centrifugation by overlaying on 0.5 mL of 60 % nycodenz made in 1 × PBS in Eppendorf tubes at 200 × g for 7 min. The layer of schizonts separated at the interface was collected and washed with incomplete RPMI-1640 medium thrice. The washed parasites were resuspended in transfection solution (82 µL solution P5, 18 µL supplement solution and 10 µL plasmid) and transferred to a fresh nucleofection cuvette and electroporated using Amaxa 4D nucleofector (FP167 program) (Janse et al., 2006). Immediately after nucleofection 50 µL incomplete medium was added to the parasites, mixed well and injected into two healthy BALB/c mice through intravenous mode. Drug pressure was applied after around 3-4 days of injection by providing pyrimethamine (7 mg in 100 mL) in drinking water. Parasitemia was monitored by making Giemsa stained smears using blood drawn by tail snip regularly followed by microscopic examination. Drug-resistant parasites were harvested in heparin solution. Glycerol stocks were made by mixing 300 µL of 30 % glycerol and 200 µL of the harvested blood and stored in liquid nitrogen.

2.2.13 Genomic DNA isolation and genotyping of transgenic parasites

The harvested parasites were treated with cold 1 × erythrocyte lysis buffer for 5 min at 4 ℃ and centrifuged at 500 × g for 10 minutes. The supernatant was discarded and the pellet was used for either Western blotting or DNA isolation immediately or stored at -80 ℃ for future use. For DNA isolation, the parasite pellet was resuspended in 350 µL of TNE (Tris, NaCl and EDTA) buffer. To this 10 µL (10 mg mL^{-1} stock) RNAseA and 50 µL of 10 % SDS were added and volume was made up to 0.5 mL with TNE buffer. This was incubated at 37 ℃ for 10 minutes followed by Pronase treatment for 1 hr (10 µL of 10mg mL^{-1} stock). 1 mL of Tris-saturated phenol was added to the sample and mixed gently by inverting. The sample was centrifuged for 5 minutes at 10000 × g and the supernatant was carefully removed and treated with 1 mL of 1:1 phenol-chloroform

solution and centrifuged for 5 minutes at 10000 × g. The resultant supernatant was treated with 1 mL of chloroform-isoamyl alcohol solution and centrifuged at 10000 × g for 5 minutes. The supernatant was mixed with 1/10 volume of 3 M sodium acetate (pH 4.5) and 1 mL of absolute ethanol. The sample was mixed by inverting gently in order to precipitate the DNA. The sample was centrifuged at 10000 × g for 1 min and the supernatant was discarded. The DNA pellet was washed once with 70 % ethanol solution, air dried and resuspended in 50 µL DNAse free water. This was used for genotyping of parasites by PCR. Southern blotting was done on DNA from knockout parasites by following the protocol described in 'Molecular cloning' (Sambrook and Russell, 2001). *P. berghei* DHFR 3' UTR was PCR amplified using primers P81, P82. This PCR product was used to generate the probe for Southern blot using random primer kit and ^{32}P labeled dATP from BRIT, India.

2.2.14 Localization studies in *Plasmodium*

For *P. berghei*, parasites were harvested in heparin solution and centrifuged at 2100 × g for 5 min and the supernatant was discarded. The cells were resuspended in 1 × PBS containing Hoeschst 33342 (1 µg mL^{-1}) and incubated at room temperature for 15 min. The cells were centrifuged at 2100 × g for 5 min and the supernatant was discarded. The cells were washed once with 1 × PBS and the pellet was resuspended in 70 % glycerol. Cells were mounted on a glass slide using coverslips, then sealed and stored at 4 ° C. The cells were observed under oil immersion objective (100×) using Ziess LSM 510 Meta confocal microscope.

In the case of *P. falciparum,* 0.5 ml of parasite culture (5 % parasitemia) was pelleted and washed with 1 × PBS. This was fixed with 4 % paraformaldehyde and 0.0075 % glutaraldehyde for 30 minutes at room temperature followed by washing with 1 × PBS. Fixed parasites were permeabilized with 0.08 % Triton X-100/1 × PBS for 9 minutes and washed with 1 × PBS. Permeabilized cells were blocked in 3 % BSA made in 1 × PBS for 1 h at room temperature on a tumbler. Anti-PfAMPD antibody raised in rabbit (1:500 dilution in 3 % BSA made in 1 × PBS) was added to the cells and kept for tumbling for 1 h at room temperature followed by 1 × PBS wash. A secondary antibody conjugated to Alexa 488 (1:1000 dilution in 3 % BSA made in 1 × PBS) was added to the cells and kept for tumbling for 1 h at room temperature. Also, propidium iodide (1 µg mL^{-1}) was added at this step. The cells were then washed with 1 × PBS and resuspended in 70 % glycerol. Cells were mounted on a glass slide using the poly L-lysine coated coverslips, then sealed and stored at 4 ℃. The cells were observed under oil immersion objective (100×) using Ziess LSM 510 Meta confocal microscope.

2.2.15 Generation of cell lysates for Western blotting

For *P. berghei*, blood was harvested in heparinised RPMI medium and RBCs were lysed by treating with 1 × erythrocyte lysis buffer at 4 ℃ for 5 min. The sample was centrifuged and the

supernatant was discarded. The parasite pellet was lysed by resuspending it in equal volumes of 2 × SDS-PAGE loading dye in the presence of protease cocktail inhibitor. The sample was incubated in boiling water bath for 5 min, centrifuged to separate the debris and the supernatant was separated on a 12 % SDS-PAGE. Western blotting was performed by semi-dry transfer method on to a PVDF membrane.

2.2.16 Determination of growth rate of wildtype and *Δampd P. berghei*

Glycerol stocks of wildtype and clone C1 of *Δampd P. berghei* were injected into two separate mice and parasitemia was monitored by examination of Giemsa stained smears. Once parasitemia reached 0.5-1 %, blood was harvested in heparin solution and 10^5 parasites were injected into 5 fresh mice for both wildtype and *Δampd P. berghei*. Parasitemia was monitored by counting parasites in Giemsa stained smears regularly starting from day 1 post-injection and growth rate was determined by plotting percentage parasitemia on the y-axis against time (number of days) on the x-axis. The mortality rate among mice infected with either wildtype or *Δampd P. berghei* parasites was also determined by plotting percentage survival of mice on the y-axis against time (number of days) on the x-axis.

2.2.17 Enumeration of gametocytes in wildtype and *Δampd P. berghei*

Glycerol stocks of wildtype and clone C1 of *Δampd P. berghei* were injected to two separate mice and parasitemia was monitored by examination of Giemsa stained smears. Blood was harvested in heparin solution once parasitemia reached 10-20 % and 4×10^6 parasites were injected into 2 fresh mice for both wildtype and *Δampd P. berghei*. Parasitemia was monitored by counting parasites in Giemsa stained smears on day 2 post-injection. On day three all mice were fed with water containing sulfadiazine (30 mg in 100 mL) *ab libitum*. Giemsa stained smears were made on day 3 post sulfadiazine treatment and gametocytes were enumerated and female to male gametocyte ratio was also determined for wildtype and *Δampd P. berghei* parasites.

2.3 Methods (Studies on HADSF members)

2.3.1 Cloning, expression and purification of HADSF members

All expression plasmids with the desired gene of interest were generated in XL-1 blue strain of *E. coli* cells. Oligonucleotide sequences are provided in the appendix. The HAD members PfHAD3, PfPGP and PfHADx were amplified from the genomic DNA using respective primers and Phusion polymerase in reactions set up according to the protocol given by the manufacturer. The PCR product was purified by gel extraction procedure using the Qiagen gel extraction kit. The purified PCR products of genes PfHAD3, PfPGP and PfHADx were double digested

using enzyme combinations NheI-XhoI, NcoI-XhoI and NdeI-XhoI, respectively. PfHAD3 and PfPGP were cloned into pET23d vector whereas PfHADx was cloned into pET22b. The clones were confirmed by PCR, restriction digestion and sequencing. Also, the *P. berghei* homologue (PbPGP) of PfPGP was cloned into pET22b vector between NdeI and XhoI sites. Confirmed clones were used to transform Rosetta DE3 pLysS strain of *E. coli* cells.

A single colony of transformed Rosetta DE3 pLysS was inoculated into 10 mL of TB medium containing ampicillin (100 μg mL^{-1}) and chloramphenicol (34 μg mL^{-1}) and incubated at 37 ℃ at 180 rpm for 12 - 15 hours. The overnight culture was inoculated (1 mL / 100 mL) into 800 mL TB containing ampicillin and chloramphenicol. The cells were allowed to grow at 37 ℃, 180 rpm till 0.6 A_{600} was reached and thereafter induced with IPTG at a final concentration of 0.3 mM. Induction was carried out at 18 ℃, 180 rpm for 15 hrs. The cells were harvested by centrifugation at 4000 × g for 15 minutes at 4 ℃. The harvested cells were resuspended in 25 mL of lysis buffer (20 mM Tris HCl, pH 8, 100 mM NaCl, 1 mM DTT, 0.1 mM PMSF and 10 % w/v glycerol) and the cell suspension was lysed by passing through French pressure cell at 1000 psi for 7 cycles. The lysate was centrifuged at 18000 × g for 30 minutes at 4 ℃. The supernatant was collected, mixed with 0.5 mL packed volume of Ni-NTA agarose beads and incubated at 4 ℃ for 3 hours on a rotating rod. The suspension was then transferred to a glass column and the flow-through was collected. The beads were washed using lysis buffer containing increasing concentrations of imidazole. Pellet from a centrifuged cell lysate, the unbound fraction (flow through), wash fractions and eluates were analysed by 12 % SDS-PAGE and gel stained with Coomassie Brilliant Blue R-250.

For HADx, positive fractions from Ni-NTA chromatography were dialysed against 20 mM Tris HCl, pH 8, DTT 1 mM, PMSF 0.1 mM and 10 % w/v glycerol. Anion exchange chromatography was performed by injecting the dialysed sample onto Q – Sepharose column equilibrated with 20 mM Tris HCl, pH 8, containing 10 % glycerol and 1 mM DTT, connected to Akta Basic High-Performance Liquid Chromatography (HPLC) apparatus from Amersham Biosciences. Gradient elution was performed using elution buffer (20 mM Tris HCl, pH 8, containing 10 % glycerol and 1 mM DTT) containing increasing concentrations of NaCl. The progress of protein elution was monitored using a UV detector at 280 nm. Protein that eluted around 150-250 mM NaCl was collected in fractions of 2 mL each and 50 μL of each was analysed on 12 % SDS-PAGE, stained with Coomassie Brilliant Blue. Positive fractions were pooled and dialysed against 20 mM Tris HCl, pH 8, containing 10 % glycerol and 1 mM DTT. The dialysed sample was concentrated using centrifugal concentrator with 10 kDa cut-off membrane and protein was estimated by the method of Bradford using BSA as standard.

PbPGP was expressed and purified as described above except for a change in buffer pH, that was kept at pH 7.4. The fractions from Ni-NTA chromatography containing PbPGP were concentrated and subjected to further purification by size-exclusion chromatography on Sephacryl S-200 column (1.5 cm x 60 cm).

2.3.2 Far-UV CD spectra of PfHADx and determination of the oligomeric status of PfHADx and PbPGP by analytical size-exclusion chromatography

The CD spectrum of PfHADx was acquired in order to determine the gross secondary structure of the protein. The protein was dialysed against 10 mM potassium phosphate pH 7. About 250 µL of 10 µM protein was used for spectral analysis performed between 200-300 nm at 0.5 nm pitch and 50 nm min^{-1} scan speed. 10 mM potassium phosphate pH 7, was used as blank. The spectra were acquired in triplicates and subtracted from the blank.

The oligomeric state of PfHADx and PbPGP was determined by analytical size-exclusion chromatography using Sephacryl S-200 (1 cm x 30 cm) column attached to an AKTA Basic HPLC system. The column was equilibrated using 100 mM Tris HCl, pH 7.4 and 100 mM KCl at 0.8 mL min^{-1} flow rate and calibrated using the molecular weight standards; β-amylase (200 kDa), alcohol dehydrogenase (150 kDa), bovine serum albumin (66 kDa), carbonic anhydrase (29 kDa) and cytochrome C (12.4 kDa). 100 µL of PfHADx and PbPGP at 1 mg mL^{-1} concentration was injected into the column separately and eluted with equilibration buffer with monitoring at 280 nm. The molecular mass of PfHADx and PbPGP was estimated by interpolating the elution volume on a plot of the logarithm of molecular weight standards on the y-axis and elution volume on the x-axis. Gel-filtration was performed with and without NaCl in the equilibration buffer for PbPGP.

2.3.3 Enzyme assays

A comprehensive substrate screen comprising of various classes of molecules such as nucleoside phosphates, sugar phosphates, co-enzymes, amino acid phosphates, etc. was performed. The assay was carried out in 100 mM Tris HCl, pH 7.4, 2 mM substrate, 1 mM $MgCl_2$ in a volume of 100 µL. The reaction mix was pre-incubated at 37 ℃ for 1 minute, the assay was initiated using 2 µg enzyme and the reaction was allowed to proceed at 37 ℃ for 5 minutes. The reaction was stopped by the addition of 20 µL of 70 % trichloroacetic acid (TCA) and 1 mL of freshly prepared Chen's reagent (water, 6 N sulphuric acid, 2.5 % ammonium molybdate and 10 % L-ascorbic acid mixed in the ratio 2:1:1:1) was added, mixed thoroughly and incubated at 37 ℃ for 1.5 hours (Chen et al., 1956). The color developed was measured against blank (reaction mix to which enzyme was added after the addition of TCA) at 820 nm. Specific activity was calculated using the ε value of 25000 M^{-1} cm^{-1}.

pH optimum of PfHADx was determined by performing the assay in a mixed buffer containing 50 mM each of glycine, MES, Tris at different pH, 1 mM $MgCl_2$ and 2 mM GMP as the substrate in 100 µL volume. The reaction mix was pre-incubated at 37 ℃ for 1 minute and the assay was initiated using 2 µg enzyme and the reaction was allowed to proceed at 37 ℃ for 2 minutes, stopped using TCA and processed using Chen's reagent as described above. pH optimum of

PbPGP was determined similarly with a couple of changes in the protocol i.e. 1 mM of pNPP as substrate and initiation of reaction with 0.2 µg enzyme.

Preferred divalent metal ion was identified by using 10 mM pNPP as substrate and different salts such as $MgCl_2$, $MnCl_2$, $CaCl_2$, $CuCl_2$, and $CoCl_2$ at a final concentration of 1 mM in a 250 µL reaction mix containing 50 mM Tris HCl, pH 8. The reaction was initiated with 2 µg of PfHADx or 0.26 µg of PbPGP and conversion of pNPP to p-nitrophenol was continuously monitored at 405 nm at 37 ℃ temperature. The slope of the initial 20 seconds of the progress curve was used to calculate specific activity using an ε value of 18000 M^{-1} cm^{-1}.

2.3.4 Synthesis of 2-phospholactate

This was part of a collaborative study wherein the synthesis was carried out by Dr. Pardhasaradhi Satha under the supervision of Prof. T. Govindaraju, New Chemistry Unit, JNCASR. Synthesis of both D and L phospholactate was carried out following the available procedure (Collard et al., 2016). Methyl-L-lactate or methyl-D-lactate (1 mL, 9.60 mmol) was dissolved in trimethyl phosphate (10 mL), $POCl_3$(10 mL) was added and stirred overnight at 0 ℃. The reaction mixture was added to ice (100 g) with constant stirring followed by the addition of saturated lithium hydroxide solution and the pH was adjusted carefully to 9.5, and stirring continued for 3 hours. The resultant reaction mixture was centrifuged and the supernatant was separated and washed with chloroform (2 × 150 mL). The aqueous layer (150 mL) was saponified with 5 N KOH (22 mL) overnight at room temperature. The pH of the reaction was adjusted to 9.5 using concentrated HCl and thereafter, acetone (500 mL) was added and the reaction mixture was maintained 0 ℃ for 2 hours. The supernatant was decanted carefully, and the resultant precipitate was isolated by centrifugation. The pellet was washed with acetone (2 × 50 mL) and dried under vacuum. The pellet (1 g) was redissolved into 100 mL of water and loaded on to an anion-exchange column (DOWEX 1X8 200-400 mesh, Cl^- form). The column was washed with water (100 mL) followed by 10 mM HCl (50 mL) and 25 mM HCl (100 mL), and fractions collected by elution with 50 mM HCl (200 mL) were lyophilised. The fractions containing 2-phospho L-lactate or 2-phospho D-lactate were identified by detecting the enzymatic release of phosphate using shrimp alkaline phosphatase, pooled, lyophilised again and thoroughly characterized by ^1H, ^{13}C, ^{31}P NMR and mass spectrometry (Data shown in the appendix).

2.3.5 Kinetic studies

Kinetic parameters for PfHADx were determined by performing substrate titration studies using AMP, GMP, IMP, XMP, dAMP, dGMP, dIMP, UMP, TMP, CMP, and phosphoglyceraldehyde. The assay was carried out in 100µL reaction containing 50 mM MES, pH 6.5, 1 mM $MgCl_2$, and varied amount of substrate. The assay was initiated by addition of 2 µg of enzyme and reaction was allowed to proceed for 2 min at 37 °C. The reaction was stopped by the addition of 20 µL

of 70 % TCA and 1 mL of freshly prepared Chen's reagent was added, mixed thoroughly and incubated at 37 °C for 1.5 hours. The colour developed was measured against blank at 820 nm. Specific activity was calculated using an ε value of 25000 M^{-1} cm^{-1}.

In case of PbPGP, K_m values for 2-phosphoglycolate, 2-phospho L-lactate and β-glycerophosphate were determined by measuring initial velocity at varying substrate concentrations ranging from 0.5 mM to 15 mM for 2-phosphoglycolate and 2-phospho L-lactate and 0.25 mM to 30 mM for β-glycerophosphate. The concentration of $MgCl_2$ was fixed at 5 mM with the reaction buffer being 200 mM Tricine-NaOH, pH 7.4. The reaction in a volume of 100 µL was initiated with 1.89 µg of the enzyme, allowed to proceed at 37 ℃ for 2 minutes, stopped using TCA and processed using Chen's reagent as described above. Specific activity was plotted as a function of substrate concentration and the data points were fitted to the Michaelis-Menten equation using GraphPad Prism V5 to determine the kinetic parameters.

2.3.6 Inhibition kinetics of PfHADx

PfHADx showed inhibition by one of the products of its catalysis i.e. inorganic phosphate. Phosphate (potassium phosphate pH 8) was varied (0-1 mM) at different concentrations of pNPP (0-10 mM) and the activity was determined. The data points were fit to a competitive inhibition equation to determine the K_i. Also, double reciprocal plots were plotted to determine the mode of inhibition based on the intersection pattern.

2.3.7 Generation of active site mutants for PfHADx and PbPGP

Site-directed mutagenesis was performed following AQUA cloning protocol (Beyer et al., 2015). PCR products for D29N mutant of PfHADX was generated using primers P9, P14 and P13, P10 whereas, the PCR product for PbPGP D49N mutant was generated using primers P11, P14 and P13, P12. For both mutants, respective wild type genes cloned in pET plasmids served as template. The clones were confirmed by colony PCR, restriction digestion and sequencing. The validated clones were transformed into Rosetta™(DE3)pLysS cells for the purpose of protein expression. The mutants were purified by nickel-NTA and dialysed against 20mM Tris HCl, pH 8. Activity check was performed using pNPP as substrate.

2.3.8 Generation of *Plasmodium berghei* transfection vectors

pJAZZ final knockout constructs for PbHAD3 and PbHADx (PbGEM-265660 and PbGEM-290712 respectively) and library clones for PbPGP and PbHAD2 (PbG02_B-53b06 and PbG01-2362a01 respectively) were procured from PlasmoGem, validated by PCR and restriction mapping. Final knockout constructs for PbPGP and PbHAD2 and tagging construct for PbPGP

were generated following the protocol described earlier in section '2.2.11'. Generation of conditional knockdown (RFA-tagging) construct for PbPGP, involved the insertion of bacterial positive/negative selection cassette (obtained by PCR amplification using R6K_zeopheS plasmid as template) just before the stop codon of PbPGP in the parental clone. *E. coli* TSA cells expressing lambda Red recombinase were used for this purpose. The intermediate vector thus generated was used in an *in vitro* LR clonase reaction with modified donor plasmid GW_R6K_RFA where the bacterial positive/negative selection cassette was replaced by a *Plasmodium* selection marker derived from the donor plasmid. The intermediate and the final RFA tagging vectors were confirmed by PCR and restriction digestion.

For the generation of modified donor plasmid GW_R6K_RFA, the GFP sequence in the plasmid GW_R6K_GFPmut3 was replaced by regulatable fluorescent affinity (RFA) tag (GFP, DHFR degradation domain and HA-tag) which was PCR amplified by using pGDB plasmid as template and primers P41 and P42. The PCR product was digested with enzymes SacII and ApaI and ligated with double digested GW_R6K_GFPmut3 plasmid. The ligation mix was used to transform chemically competent *E. coli* pir strain and plated on LB agar plate containing tetracycline (10 µg mL^{-1}). The clones were confirmed by DNA sequencing.

2.3.9 Generation and purification of PfHADx specific polyclonal antibodies

The purified PfHADx protein was used as antigen to immunize New Zealand White rabbit in order to generate antibodies. The immunization protocol was as described for PfAMPD. Antibody titre was determined by dot blot. 2 µg of antigen was spotted on a nitrocellulose membrane and allowed to dry for 15 min. The nitrocellulose membrane was blocked with 5 % skimmed milk for 1 h on a rocker at room temperature. 5 % skimmed milk was removed and 2.5 % skimmed milk containing different dilutions of the primary antibody was added. This was incubated on a rocker for 1h at room temperature. The blots were washed for 15 min in 1 x PBS containing 0.1 % Tween-20. 2.5 % skimmed milk containing 1:4000 dilution of secondary antibody was added and kept on a rocker for 1 h at room temperature. Blots were again washed for 15 min in the washing solution. Blots were developed using the coloring reagent aminoethyl carbazole. Antibody purification was done by 'strip-affinity' protocol described earlier in section '2.2.5'.

2.3.10 Localization studies in *Plasmodium*

Localization of PfHADx was determined in *P. falciparum* by indirect immunofluorescence and for PbPGP was done by live cell imaging as per the protocol described earlier in section '2.2.14'.

2.3.11 Conditional knockdown of PbPGP in *P. berghei*

Glycerol stock of PbPGP RFA-tagged parasites was injected into a healthy BALB/c mouse. Parasitemia was monitored by microscopic observation of Giemsa-stained smears of blood drawn

from a tail snip. Trimethoprim pressure was maintained throughout the growth period. Upon parasitemia reaching 5–10%, about 500 µl of infected blood was collected in 500 µl of RPMI 1640 solution containing heparin. 100 µl of this parasite containing suspension was injected into a fresh mouse that was fed with trimethoprim (30 mg in 100 ml) in drinking water and a second 100 µl to another mouse that was not fed trimethoprim. Parasites were harvested from both mice after 6 days and subjected to Western blotting. The entire experiment was repeated twice.

Glycerol stock of PbPGP RFA-tagged *P. berghei* was injected into a healthy BALB/c mouse, and parasitemia was monitored by Giemsa-stained smears. Blood was harvested in heparin solution when parasitemia reached 0.5–1 % and 1.7 x 10^5 parasites were injected into two batches of mice (n = 5). One batch was fed with drinking water containing trimethoprim (30 mg in 100 ml) and the other with water lacking trimethoprim. Parasitemia was monitored regularly starting from day 2 post-injection by counting parasites in Giemsa-stained smears. The growth rate was determined by plotting the percentage of parasitemia on the y-axis against time (number of days) on the x-axis. The mortality rate among infected mice fed trimethoprim containing water or not was also determined by plotting the percentage of survival of mice on the y-axis against time (number of days) on the x-axis.

Chapter 3

Studies on AMP deaminase

This chapter is aimed at providing a concise understanding of nucleotide metabolism in the malaria parasite *Plasmodium*. Also provided, is an account on Adenylate Energy Charge (AEC) and its regulation, which is a critical parameter in the context of cellular energetics. A brief account on aminohydrolase superfamily including its key biochemical and structural features is also elaborated. Analysis of *Plasmodium* AMP deaminase sequence is added to provide a preliminary understanding of the protein's features and a detailed account of the literature available on AMPD, in general, is summarized. PfAMPD was recombinantly expressed in *Saccharomyces cerevisiae* using a codon harmonised gene. Nevertheless, protein expression levels were not sufficient to carry out downstream processes. Characterization of the protein was done through functional complementation assay in a knockout yeast strain and residues critical for enzyme function were identified by site-directed mutagenesis. As transfection of *P. berghei* with an episomal vector over-expressing GFP-tagged functional AMPD did not yield transgenic parasites, a construct expressing an inactive mutant was transfected. Transfectants expressing this non-functional protein with a C-terminal GFP tag were used to localize the protein in cytosol. The PbAMPD gene was deleted using a linear vector generated by recombineering technique. Transgenic parasites generated using this plasmid did not show any difference in intra-erythrocytic growth rate when compared with wildtype. The findings from the study conducted on PfAMPD have been *published in 'Molecular Microbiology'* (Nagappa et al., 2019b).

3.1 Introduction

3.1.1 Purine nucleotide cycle

Purine nucleotide cycle is a branch pathway of the purine nucleotide biosynthetic pathway. It comprises of three enzymes namely adenylosuccinate synthetase, adenylosuccinate lyase and AMP deaminase. These three catalyze the inter-conversion of AMP and IMP. IMP synthesized from either *de novo* or salvage pathway gets converted to succinyl-AMP by the action of the enzyme adenylosuccinate synthetase. Succinyl-AMP is hydrolysed to give AMP and fumarate. AMP gets deaminated back to IMP by AMP deaminase (Fig. 3.1). The by-products of this cycle are fumarate and ammonia. Fumarate is known to feed into the tricarboxylic acid cycle through anaplerosis (Bulusu et al., 2011a). However, the fate of ammonia is still under debate. It is not clear whether it is a metabolic waste or acceptor of H^+ ions, acting as a buffer system (Lowenstein, 1972). *In vivo* gene manipulation studies have shown that the ADSS/ASL pathway of AMP generation is essential for the malaria parasite (Sanderson and Rayner, 2017). This is because the ADSS/ASL pathway is the only route for AMP synthesis in *Plasmodium* and unlike other organisms such as yeast, *Toxoplasma*, *Leishmania*, *Trypanosoma*, etc., the parasite lacks APRT or AK that can directly salvage adenine or adenosine to generate AMP. Unlike ADSS and ASL the essentiality AMPD had not been investigated till date.

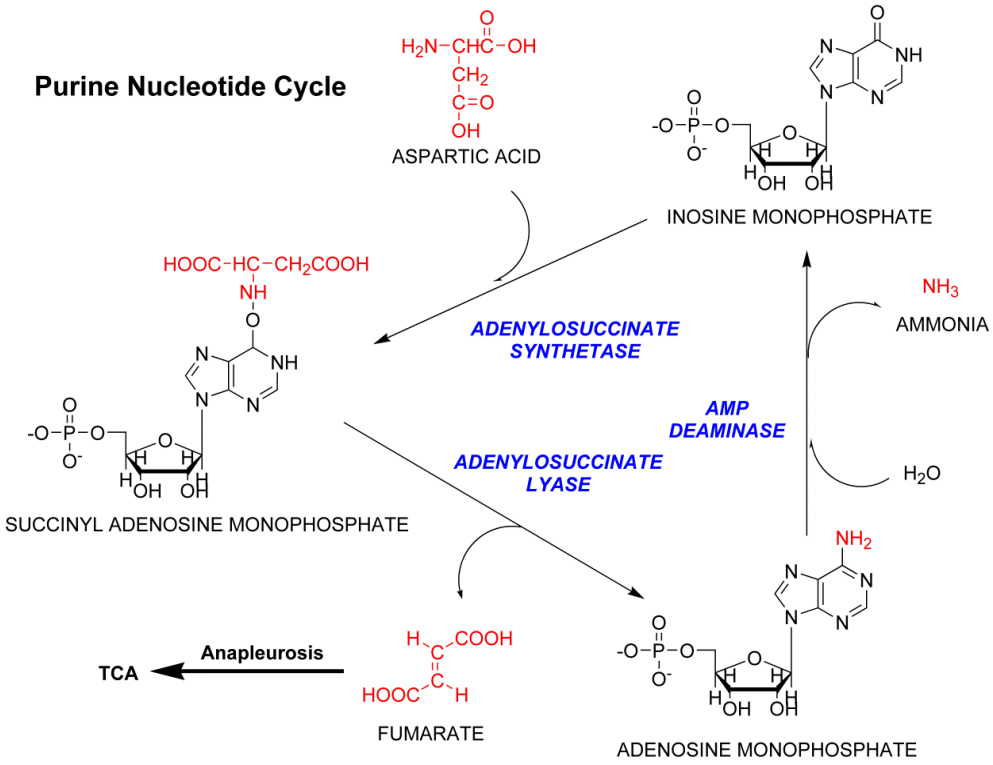

Figure 3.1: Purine nucleotide cycle – enzymes and metabolites involved

3.1.2 Adenylate Energy Charge and its regulation

Apart from the inter-conversion of IMP and AMP, another important role of the purine nucleotide cycle is to maintain 'Adenylate Energy Charge' (AEC) of the cell. AEC is a measure of the cell's adenylate pool, which can perform phosphorylation. It is basically an index representing the proportion of high energy phosphoanhydride bonds present in the total adenine nucleotide pool of a cell. Its mathematical representation was given by Daniel E. Atkinson as follows:

$$AEC = \frac{[ATP] + 0.5[ADP]}{[ATP] + [ADP] + [AMP]}$$

The AEC of a cell is basically the ratio of the sum of the molar concentration of ATP and half the molar concentration of ADP to the total adenylate pool (Atkinson, 1968; Chapman et al., 1971). This ratio is highly regulated and fluctuates within a narrow range (0.5-0.85). AEC value is affected by various ATP generating and ATP consuming processes. Apart from this, the purine nucleotide cycle enzyme, AMPD and the adenylate kinase reaction are known to modulate AEC of a cell (Chapman and Atkinson, 1973). Anabolic and catabolic pathways have a direct impact on AEC as they are involved in either consumption or generation of ATP. But AMPD and adenylate kinase reactions regulate AEC in a more sophisticated manner, which is described below. Purine nucleotide cycle can be divided into two arms; an AMP generating arm and an AMP depleting arm. The former comprises of two enzymes adenylosuccinate synthetase (ADSS) and adenylosuccinate lyase (ASL) which convert IMP to AMP along with the generation of a fumarate molecule. The latter arm, which has a single enzyme AMP deaminase (AMPD), converts AMP back to IMP. Under conditions when AEC drops below optimum, the ADSS-ASL arm is down-regulated and AMPD arm is up-regulated. This results in stalling of AMP production and conversion of existing AMP to IMP; thereby the AEC value is restored to normal at the expense of net loss of the adenylate pool concentration. When there is an increase in AEC the ADSS-ASL arm generates AMP which accumulates as there is a simultaneous down regulation of AMPD; resulting in bringing down the AEC to normal values (Hellsten et al., 1999). Extensive metabolite profiling experiments have given substantial evidence validating this mechanism employed by cells to maintain AEC (Kalsi et al., 2003; Lanaspa et al., 2012; Li et al., 2013). AMP deaminase is an interesting candidate as it can modulate AEC by being part of purine nucleotide cycle, in addition, to independently regulating the equilibrium of the adenylate kinase reaction. Adenylate kinase catalyzes a reversible reaction; where two ADP molecules are converted to one ATP and one AMP (2ADP $\leftrightarrow$ ATP + AMP) (Fig. 3.2). This reaction maintains the three way equilibrium between ATP, ADP and AMP levels in a cell. The ATP generated will be utilized by energy consuming processes, while AMP gets deaminated to IMP by AMPD. When there is excessive ATP catabolism, the increased generation of ADP drives the adenylate kinase reaction towards ATP production and helps in replenishing ATP pools. This reaction becomes very critical for tissues like skeletal muscle as their energy requirement is high. In conditions where AMPD is not

operating (either due to a mutation in case of the genetic disorder such as myoadenylate deaminase deficiency or in case of a knock-out cell where the gene has been deleted) AMP accumulation takes place and this drives the adenylate kinase reaction towards ATP depletion. This leads to several consequences of which, most prominent in the literature is fatigue and muscle weakness reported in subjects suffering from myoadenylate deaminase deficiency, an autosomal recessive genetic disorder (Sabina et al., 1984; Mineo et al., 1985; Hellsten et al., 1999; Isackson et al., 2005). Insufficient production of ATP and accumulation of AMP synergistically bring down the AEC of the cell in the absence of AMPD activity. Homeostasis of the AEC of a given cell is highly dependent on the flux through the two arms of purine nucleotide cycle as well as the adenylate kinase reaction which in turn is regulated by AMPD.

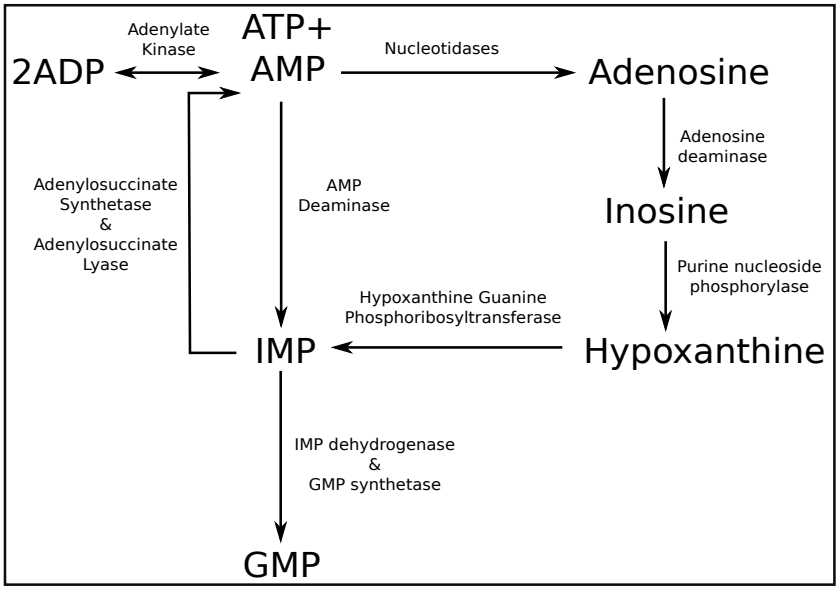

Figure 3.2: Regulation of AEC by enzymes involved in purine nucleotide metabolism

Schematic representation of the regulation of AEC by modulation of AMP levels by AMPD and nucleotidases.

3.1.3 Adenosine 5´ Monophosphate Deaminase – sequence, structure-function and mechanism

AMPD is absent in prokaryotes and archaea while it is encoded by a single gene in most of the eukaryotes. Three isoforms present in mammals are skeletal muscle AMPD (AMPD1), soft tissue AMPD (AMPD2) and erythrocytic AMPD (AMPD3). Sequence analysis and earlier reports show that AMPD consists of a highly divergent N-terminal sequence with a conserved C-terminal core containing the catalytic residues (Fig. 3.3). Publications available so far have reported biochemical characterization of N-terminal truncated forms of AMPD as this region is known to be highly disordered with high propensity for proteolytic degradation (Bauschjurken and Sabina, 1995) and till date only one crystal structure is available in the PDB database (Fig. 3.4A) (Han et al., 2006).

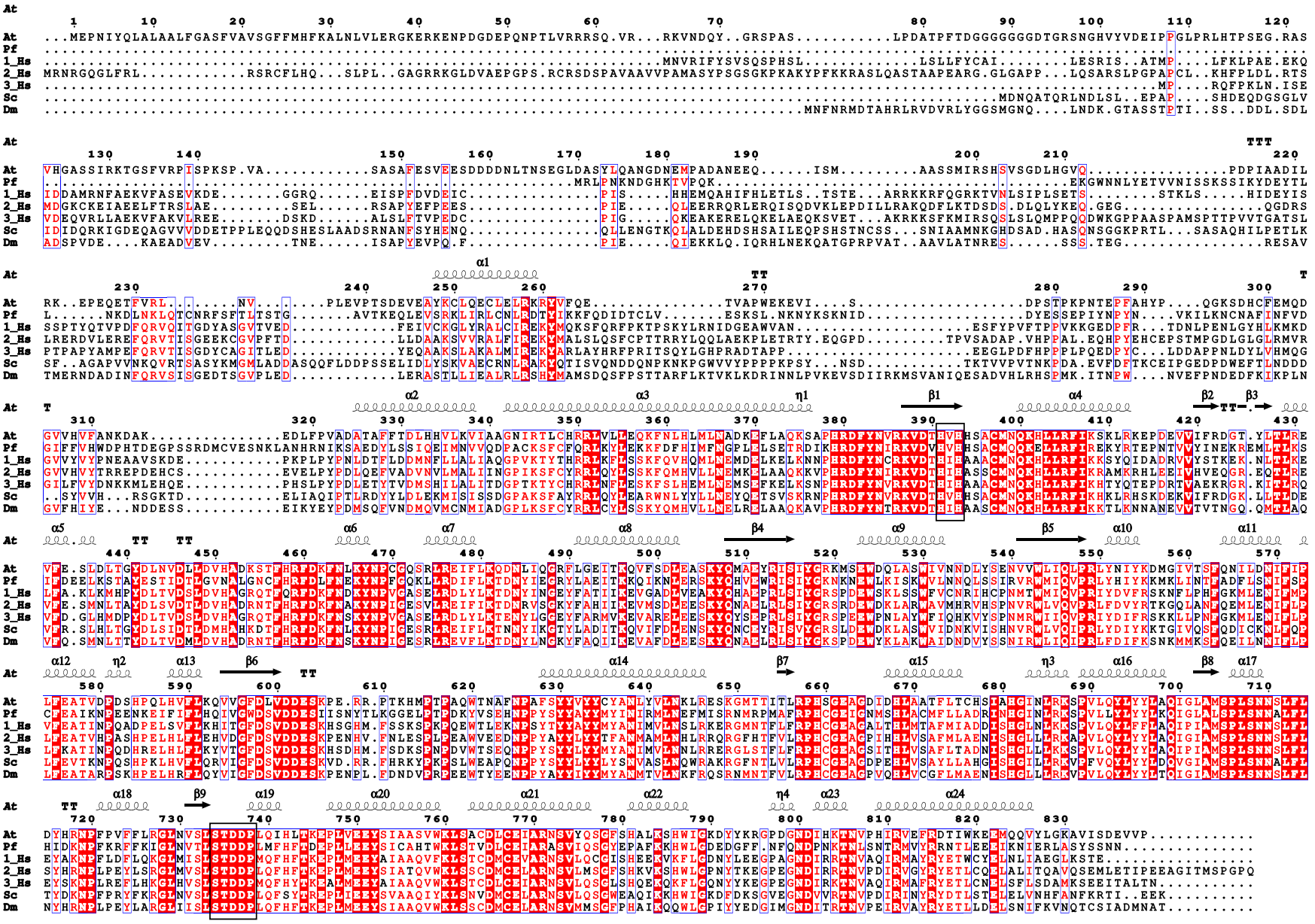

Figure 3.3: Multiple sequence alignment of AMPD sequences

Clustal omega alignment of AMP deaminase sequences from *Plasmodium* (Pf), yeast (Sc), *Arabidopsis* (At) and human (Hs2, Hs3) represented using ESpript 3.0. Secondary structure elements (helix and sheet) are represented on top of the sequence. 'HXH' and 'STDDP' motifs are indicated in black boxes.

AMPD from *Plasmodium* falciparum has 693 amino acids whereas the protein from other species of *Plasmodium* have around 693-698 amino acids. The PfAMPD protein sequence shows significant sequence identity with other well-characterized AMPDs (Fig. 3.4B) and also shows the presence of disordered segments when analyzed through disorder prediction tool PONDR (Xue et al., 2010)(Fig. 3.4C). While AMPD from other eukaryotes is around 800 amino acids in length, in some protozoan parasites it has been annotated to be even longer, with as many as 1500 amino acids (Fig. 3.4D). AMPD from plants such as *Arabidopsis thaliana* and *Oryza sativa* have a unique feature, that is, presence of an N-terminal trans-membrane helix that is not found in any other AMPD (Han et al., 2006). AMPD domain architecture comprises of a single domain characterized by an α8/β8 TIM barrel structure as shown in the crystal structure of *Arabidopsis thaliana* AMPD (PDB id: 2A3L). This domain organization is the most common form of domain organization in AMPD as shown in the Pfam database (Fig. 3.4D). But sequence analysis of AMPD from protozoan parasites such as *Acanthamoeba castellani* and *Entamoeba histolytica* etc. show whole domain duplication where one of the domains seems to be catalytically inactive as the critical residues in the 'HXH' motif and the 'STDDP' motif are mutated or absent (Fig. 3.4E). Nevertheless, none of the protozoan AMP deaminases is comprehensively characterized and the sequence, structure-function relation for these proteins remain elusive till date.

A

B

	1: At	2: Pf	3: 1_Hs	4: 2_Hs	5: 3_Hs	6: Sc	7: Dm
1: At	100	42.7	42.64	46.26	46.81	46.74	46.63
2: Pf	42.7	100	39.97	39.41	39.88	40.57	41.3
3: 1_Hs	42.64	39.97	100	49.15	60.86	39.78	47.75
4: 2_Hs	46.26	39.41	49.15	100	53.15	46.04	57.14
5: 3_Hs	46.81	39.88	60.86	53.15	100	41.92	49.79
6: Sc	46.74	40.57	39.78	46.04	41.92	100	46.02
7: Dm	46.63	41.3	47.75	57.14	49.79	46.02	100

C

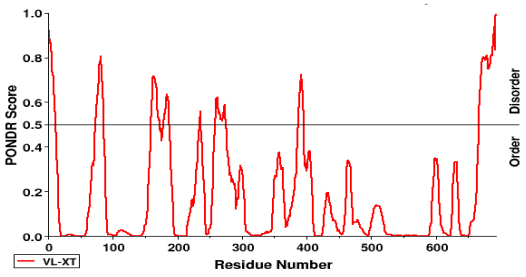

D

Sl. No	Id	Organism	Protein length	Domain 1	Domain 2
1	PF3D7_1329400	*P. falciparum*	693	238-648	-
2	P23109 (AMPD1)	*H. sapiens*	780	329-736	-
3	O80452	*A. thaliana*	839	384-790	-
4	P15274	*S. cerevisiae*	810	355-761	-
5	ACA1_248360	*A. castellanii*	1332	175-566	816-1222
6	EHI5A_063830	*E. histolytica*	1261	152-561	795-1207
7	TGGT1_234280	*T. gondii*	1159	359-769	-
8	Tb427tmp.211.1320	*T. brucei*	1417	196-591	818-1221
9	LdBPK_130870.1	*L. donovani*	1656	-	1093-1546

E

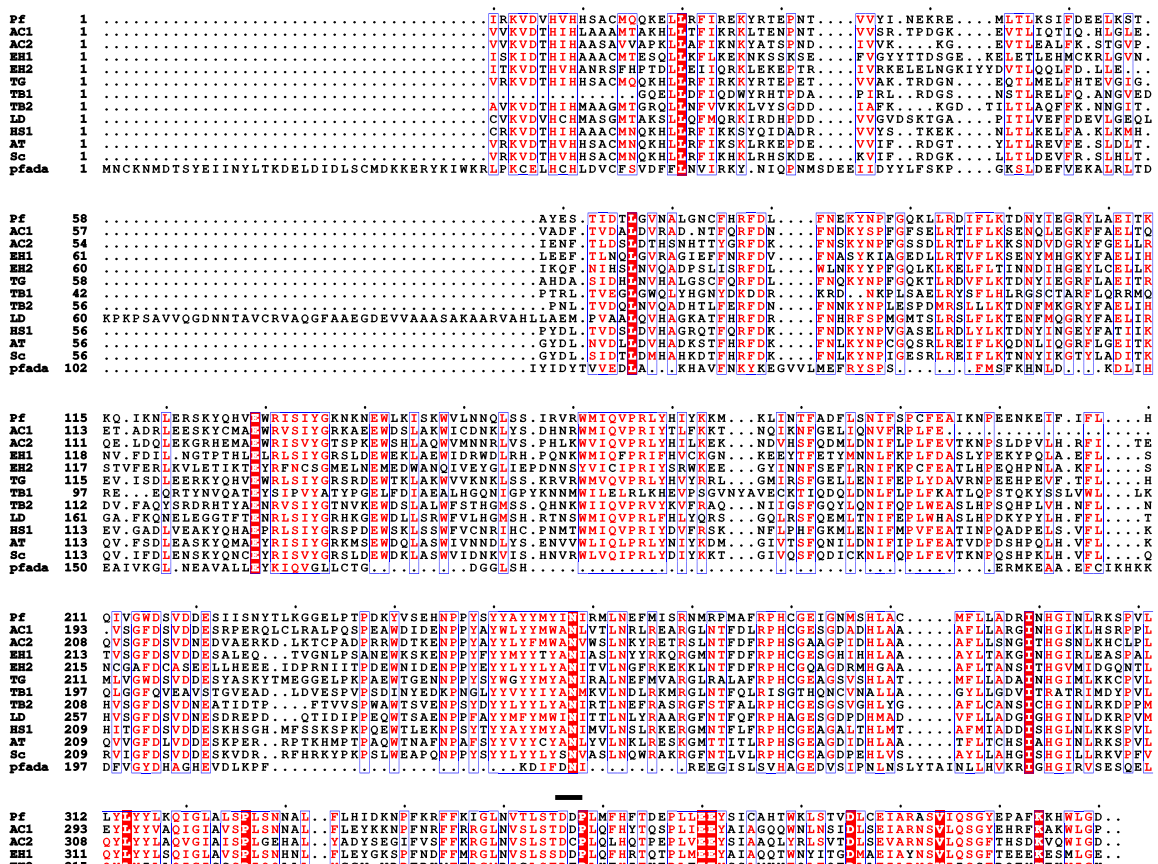

Figure 3.4: Domain organization in AMPD

(A) Crystal structure of AtAMPD (PDB ID: 2A3L). (B) Percentage identity matrix showing sequence identity across AMPD sequences from *Plasmodium* (Pf), yeast (Sc), *Arabidopsis* (At), human (Hs2, Hs3) and *Drosophila* (Dm). (C) Predictor of Natural Disordered Regions (PONDR) output for PfAMPD sequence. Peaks crossing the threshold line for PONDRscore indicate disordered segments. (D) Table of representative AMPD sequences indicating the total number of aminoacids. The sequences were subjected to Pfam analysis which identified the presence of either single or two AMP/adenosine deaminase domains. The location of these domains with respect to amino acid numbering is also indicated. (E) Multiple sequence alignment of only AMP/adenosine deaminase domains in AMPD sequences as annotated by Pfam database with that of adenosine deaminase. Pf (*Plasmodium falciparum*), AC (*Acanthamoeba castellani*), EH (*Entamoeba histolytica*), TG (*Toxoplasma gondii*), TB (*Trypanosoma brucei*), LD (*Leishmania donovani*), HS1 (Human AMPD1), AT (*Arabidopsis thaliana*), Sc (yeast) and pfada (*P. falciparum* adenosine deaminase). The key motifs 'HXH' and 'STDDP' are indicated with a black bar on top of the sequence. One of the domains in two domain AMPDs such as AC2, EH2, TB1 lack one or more critical residues in these key motifs.

AMP deaminase belongs to Amidohydrolase superfamily of enzymes that has diverse members such as phosphotriesterase, urease, dihydroorotase, isoaspartyl dipeptidase, D-hydantoinase, uronate isomerase, D-amino acid deacetylase. Amidohydrolase superfamily consists of members who share similarity in structure as well as the mechanism of action which involves metal-assisted hydrolysis of an amide or ester bond at a carbon or phosphorous atom. The members of the family have either one or two divalent metal ion centres which are involved in catalyzing diverse reactions such as deamination, decarboxylation, dechlorination, dephosphorylation and isomerisation. The proteins belonging to this family have an $\alpha 8/\beta 8$ TIM barrel structure, where most of the catalytic residues are clustered at the C–terminus. Structural characterization by X-Ray crystallography has revealed seven variations in this family based on the amino acid residues involved in the ligation of the metal ion. Divalent zinc is the predominantly found metal ion in this family, whereas there are examples containing zinc and nickel, zinc and iron or iron alone in the structure. Histidine, aspartate and glutamate residues from the beta strands are known to form a complex with the metal centre (Seibert and Raushel, 2005; Arbona, 2006; Marotta et al., 2009). Although the catalytic mechanism of AMPD is not understood in detail it might be similar to that of adenosine deaminase which is also a member of aminohydrolase superfamily. This has a mononuclear metal centre and its reaction follows nucleophilic substitution by water. The metal ion is coordinated by three histidines and an aspartate residue and another histidine residue seems to function as a general base in abstracting the proton from water bound to the metal centre. The hydroxide ion thus generated attacks the aromatic ring to form a tetrahedral intermediate. This event is primed by a proton donation by a glutamate residue which is three residue positions away from the conserved catalytic histidine. These structural features i.e. coordination of the metal ion by three histidines and an aspartate and the HXXE motif is seen in the crystal structure of AtAMPD (PDB id. 2A3L) also. Interestingly, it has been reviewed by Clara M. Seibert and Frank M. Raushel that this motif (HXXE) is absent in adenine deaminase (Seibert and Raushel, 2005). Finally, the tetrahedral intermediate is attacked by a proton from the

conserved histidine followed by proton transfer from the carbinol intermediate to the aspartate or glutamate residue (Fig. 3.5) (Seibert and Raushel, 2005).

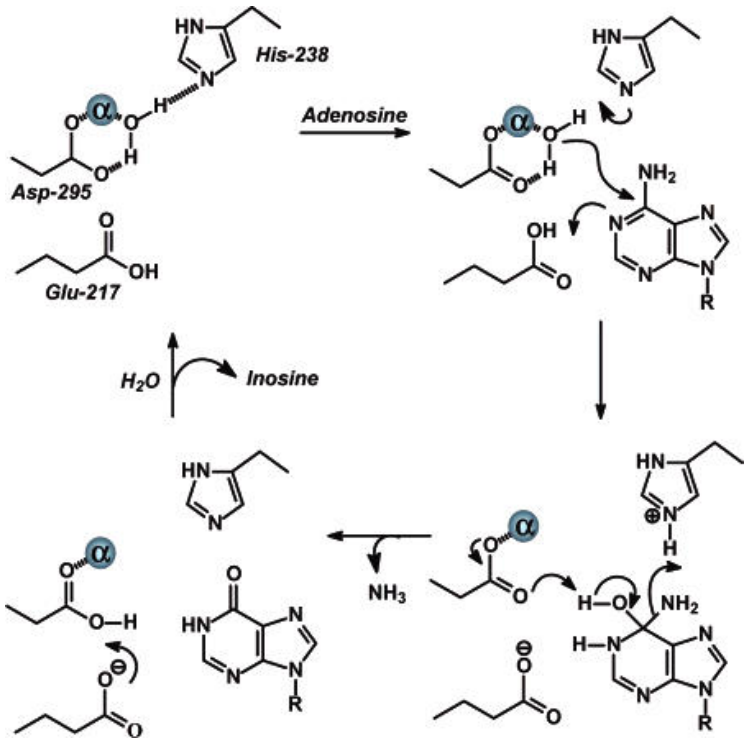

Figure 3.5: Reaction mechanism of adenosine deamination by adenosine deaminase

Reprinted (adapted) with permission from "Structural and catalytic diversity within the amidohydrolase superfamily", Clara M. Seibert and Frank M. Raushel, Copyright © 2005, American Chemical Society.

3.1.4 Summary of literature on AMPD

Salient features of AMPD in particular include, exclusive eukaryotic occurrence and a highly divergent N-terminus (Sabina and Mahnke-Zizelman, 2000; Marotta et al., 2009). Although detailed biochemical characterization of *S. cerevisiae* AMPD (ScAMPD) (Yoshino et al., 1979; Murakami, 1979; Murakami et al., 1980; Meyer et al., 1989; Merkler et al., 1989; Merkler and Schramm, 1990, 1993), and other AMPDs (from rabbit skeletal muscle, goldfish, sea scorpion etc.) have been carried out earlier (Marotta et al., 2009; Waarde and Kesbeke, 1981; Lushchak et al., 1998; Mangani et al., 2003; Martini et al., 2007), all studies have resorted to purifying the enzyme from native source and have faced the problem of protein degradation. Major findings include the presence of divalent zinc ion in the active site, tetrameric oligomeric state, activation by ATP and inhibition of enzyme activity by GTP and phosphate. Earlier reports have demonstrated the role of plasma histidine-proline-rich glycoprotein as a zinc chaperone involved in the assembly of AMPD1 (the skeletal muscle isoform) (Ranieri-Raggi et al., 2014). Till date, the only crystal structure available in the PDB database for this enzyme is from *Arabidopsis thaliana*, solved in

2006 by the group of Richard L Sabina (Han et al., 2006). Recombinant AtAMPD (N-terminal truncated version) like other AMPDs also exhibited allosteric activation by ATP (Han et al., 2006). Another crystal structure of rabbit muscle AMPD solved in the presence of the inhibitor coformycin 5' phosphate has been patented by the pharmaceutical company Pfizer (Bazin et al., 2003). Their rationale being, AMPD inhibition would lead to accumulation of AMP which can now be acted upon by nucleotidases to generate adenosine which is a potent vasodilator that would provide relief during myocardial infarction. AMP deaminase regulates intracellular AMP levels by catabolizing AMP to IMP. Impairment of this activity has physiological consequences. Accumulation of AMP leads to inhibition of the *de novo* purine biosynthetic pathway enzyme PRPP amidotransferase, thereby shutting off purine biosynthesis through this pathway. This leads to depletion in levels of IMP, which is a branch point metabolite that is needed for GMP production. Hence, intracellular GMP levels and in turn GTP levels fall below optimum. Lack of GTP impairs protein production as GTP is indispensable for translation initiation and elongation. As a consequence of this series of events, cells lacking AMPD activity show growth defect phenotype. This growth defect phenotype does not show up under normal conditions but reveals itself when cells are exposed to metabolite stress like the presence of adenine (in case of yeast) in the medium or adenosine circulating in the plasma (in case of mammalian cells). AMP deaminase deficiency has been implicated in genetic disorder like myoadenylate deaminase deficiency. Mutations in skeletal muscle AMP deaminase gene lead to premature termination of translation and due to lack of a functional enzyme causes severe fatigue, muscle cramps in the subjects after performing trivial tasks like climbing stairs or walking across the hall (Fishbein et al., 1978; Shumate et al., 1979; Sabina et al., 1984; Isackson et al., 2005). But evidence from literature also suggests a lack of AMPD is not the only reason for this consequence. Recently, Akizu *et al.* identified mutations in AMPD2 in families where individuals were found to be suffering from a neurodegenerative brainstem disorder termed 'pontocerebellar hypoplasia' (Akizu et al., 2013). In these subjects, neural cells in cerebellum and hippocampus die due to protein synthesis defect as a consequence of AMP accumulation caused by impairment in the activity of AMPD2 enzyme (Akizu et al., 2013). A sequencing study conducted on *Arabidopsis* mutants impaired in embryo development identified mutations in AMPD gene (Xu et al., 2005). Also, exposure of *Arabidopsis thaliana* seedlings to deaminoformycin (nucleoside analogue that would be taken up by plant cells and converted to a phosphorylated transition-state inhibitor of AMPD) showed a dose-dependent inhibition of plant growth (Sabina et al., 2007). In addition to this, a new mechanism of action for the anti-diabetic drug metformin has been proposed by Ouyang *et al.,* where it was shown that AMPD inhibition in L6 rat skeletal muscle cells by metformin, led to an increase in AMP levels which in-turn activated AMP-activated protein kinase (AMPK) (Ouyang et al., 2011), followed by downstream signalling events leading to glucose uptake. Also, AMPD and AMPK have been reported to counter-regulate each other and are implicated in hepatic steatosis (Lanaspa et al., 2012). Studies have documented an increase in AMPD activity in the soil-living amoeba *Dictyostelium discoidium* in response to nutrient starvation or treatment with hadacidin

(inhibitor of ADSS) (Jahngen and Rossomando, 1986). It was also found that loss of AMPD function in *Dictyostelium* resulted in increased AMP secretion, an impaired ratio of prestalk to prespore cells and reduced sporulation efficiency (Chae et al., 2002). In the context of malaria, a gain-of-function mutation in erythrocytic AMPD (AMPD3) was found to be associated with increased RBC turnover and conferred resistance in mice against *P. chabaudi* infection (Hortle et al., 2016). Also, an indirect piece of evidence for the presence of AMPD activity in *Plasmodium* was provided by Cassera *et al.,* where it was shown that erythrocytic AMP can be taken up by the parasite and converted to IMP by the action of AMPD (Cassera et al., 2008). But, a detailed biochemical and physiological characterization of this enzyme from the parasite has remained hitherto unavailable.

3.1.5 Objectives of the current study

AMPD enzyme from protozoan parasites has not been characterized till date. Since AMPD is a chief enzyme of purine nucleotide cycle and also a vital regulator of adenylate kinase activity, thereby regulating AEC of a cell; it would be very interesting to determine the role of AMPD enzyme in the apicomplexan parasite *P. falciparum*. In this regard following objectives were set for our study:

- Cloning, expression and purification of recombinant PfAMPD
- Biochemical and kinetic characterization of PfAMPD
- Elucidation of the physiological role of AMPD by reverse genetics approach

3.2 Results

3.2.1 Expression of recombinant PfAMPD

To facilitate biochemical characterization of AMP deaminase (AMPD) from *P. falciparum* (Pf), experiments were conducted to produce recombinant protein from heterologous expression systems. In this regard, RNA isolated from the parasite was used to synthesize cDNA that was subsequently used for cloning the complete ORF of AMPD gene (Fig. 3.6A) with an N-terminal hexahistidine tag in the expression vector, pETDuet-1. This construct was validated by sequencing and used for transforming expression strains Rosetta™(DE3)pLysS, and BL21 DE3 RIL. Upon induction with IPTG and analysis of expression by SDS-PAGE and Western blot, it was found that the protein underwent excessive degradation and moreover, was present completely in the insoluble fraction. From preliminary bioinformatics analyses, it was known that AMPD consists of a highly disordered N-terminus which undergoes degradation. Richard Sabina and co-workers were able to purify and crystallize a truncated version of AMPD from *Arabidopsis thaliana* (Han et al.,

2006). Hence, based on the sequence alignment of PfAMPD with AtAMPD, three N-terminal truncated constructs of PfAMPD namely- Δ59, Δ94 and Δ178 were made in pETDuet-1. But all three constructs showed expression profiles similar to that of the full length (Fig. 3.6B). In addition to this, a C-terminal hexahistidine tagged construct of full-length PfAMPD was made in pET23d, but degradation and insolubility of the protein was seen in this case also. To circumvent the problem of protein degradation and insolubility PfAMPD was co-expressed with various chaperone proteins. Even this approach proved futile and protein degradation was observed (Data shown in figure 1 of the appendix). In spite of these shortcomings, the protein was purified from the inclusion body by Ni-NTA affinity chromatography under denaturing conditions using 6 M guanidinium chloride as the chaotrophe. This purified protein was used as an antigen to immunize a rabbit for the purpose of generating polyclonal antibodies (Nagappa, 2014).

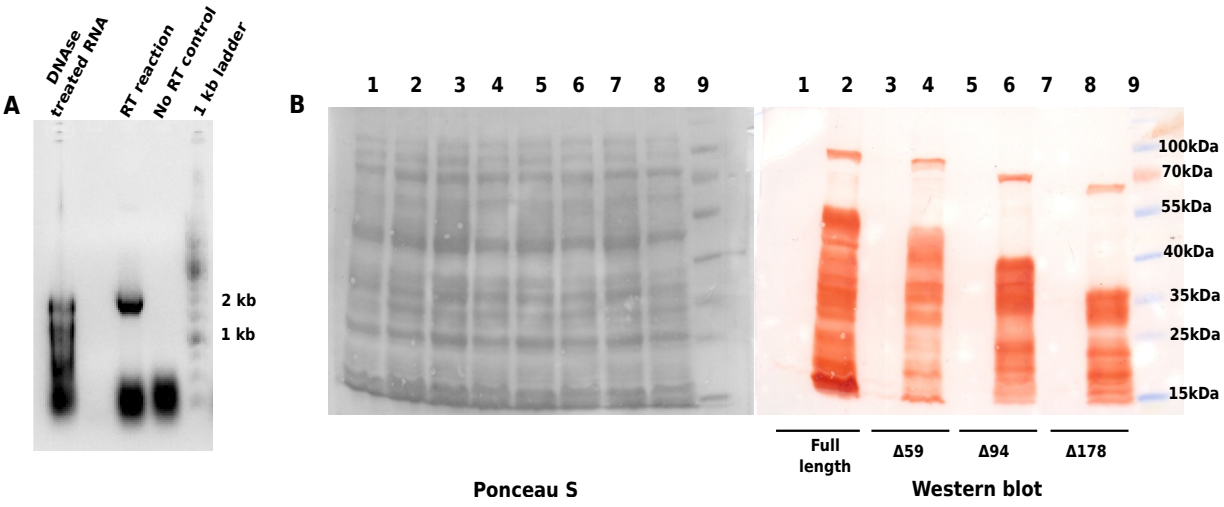

Figure 3.6: Expression of PfAMPD in *P. falciparum* and *E. coli*

(A) RT-PCR to determine the expression of AMPD in *P. falciparum*. Expected band of 2 kb was observed in the RT reaction lane. (B) Western blot analysis of full length and truncated versions of PfAMPD expressed in *E. coli* (lane 1, 3, 5 and 7 are lysates of uninduced culture and lane 2, 4, 6 and 8 are lysates of IPTG induced culture). The left panel is PonceauS stained blot and the right panel is blot developed by colorimetric method. Full-length protein and degradation bands for each construct of PfAMPD were observed. Figure reproduced with permission from "Biochemical and physiological investigations on adenosine 5' monophosphate deaminase from *Plasmodium spp*.", Kempaiah Nagappa et al, 2019, Copyright © Wiley Online Library.

Since stable and soluble protein was not obtained in the bacterial expression system, yeast expression system was adopted. The full-length gene cloned in pYES2/CT vector under GAL1 promoter was used to transform *S. cerevisiae* BY4742 strain. Upon induction with galactose and analysis by SDS-PAGE/Western blotting, it was found that PfAMPD was not expressed. Hence *in vitro* biochemical characterization of PfAMPD could not be carried out. Alternatively, the functionality of a protein can be determined by complementation experiments in heterologous systems like yeast, if a homolog is present. Yeast has single AMP deaminase gene, AMD1 encoding an 810 amino acid protein. AMPD knockout yeast strain grows normally in the regular growth medium,

but under metabolic stress, i.e. in the presence of S-adenosyl methionine (SAM)/adenine in the medium, it shows a growth defect phenotype. This is because SAM/adenine from the medium is taken up by the cells via transporters and converted to AMP by subsequent enzymatic reactions. Due to the absence of AMPD, AMP accumulates and inhibits the *de novo* pathway enzyme glutamine-PRPP-amidotransferase. This leads to a drop in the production of IMP; a common precursor that feeds into AMP and GMP synthesis. As a consequence of depleted GMP production, GTP levels are lowered and this, in turn, perturbs protein bio-synthesis that eventually manifests as a growth defect phenotype. This can be rescued by episomal expression of a functional AMPD from the yeast itself or any other organism. Metabolic rescue of this phenotype can be done by adding hypoxanthine to the medium which will form IMP upon phosphoribosylation by HGPRT or by adding aminoimidazole carboxamide ribonucleoside (AICAr) which will also form IMP via *de novo* pathway (Fig. 3.7) (Saint-Marc et al., 2009; Akizu et al., 2013). This principle was utilized to determine the functionality of PfAMPD.

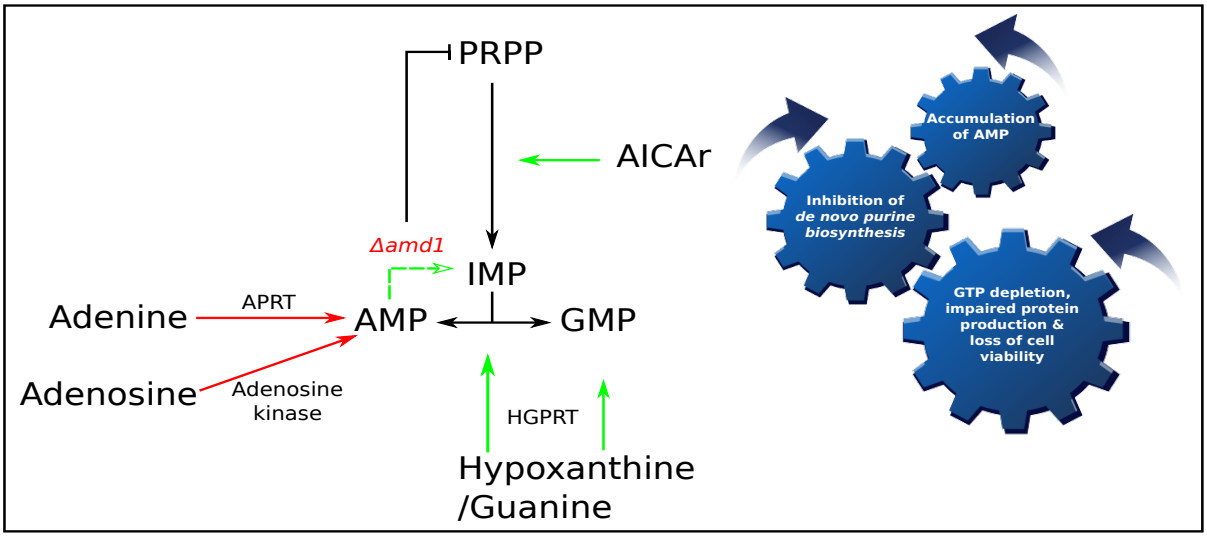

Figure 3.7: Principle of complementation assay

Schematic showing principle behind adenine toxicity in *Δamd1* yeast strains. Red arrows are possible modes of establishment of toxicity and green arrows are ways through which metabolite mediated rescue can be achieved. Dashed green arrow indicates the mode of rescue by expression of a functional AMPD. The interlocked gear represented on the right highlights the series of events that result from AMP accumulation. AMP accumulation leads to inhibition of *de novo* purine synthesis that in turn depletes GTP levels resulting in growth arrest.

Using *Δamd1* yeast strain (Fig. 3.8A and B) transformed with pYES2/CT_PfAMPD_$(His)_6$ (wildtype PfAMPD coding sequence cloned in pYES2/CT vector under GAL1 promoter) serial dilution and spotting assays were performed to check the functionality of PfAMPD. Rescue of the growth defect phenotype was not seen when compared to the control strain expressing ScAMPD (Fig. 3.8C). Upon performing RT-PCR on RNA isolated from galactose-induced $\Delta amd1$ cells con-

taining pYES2/CT_PfAMPD_$(His)_6$ vector, it was found that full-length transcript of PfAMPD gene was not formed. Instead, a product shorter than the expected size was observed (Fig. 3.8D). Upon sequencing, it was found that formation this shorter transcript was due to an aberrant processing/splicing event. Due to lack of full-length transcript, Δ*amd1* cells transformed with pYES2/CT_PfAMPD_$(His)_6$ failed to express recombinant protein and were not able to rescue the growth defect phenotype. Expression of PfAMPD was also attempted in *P. pastoris* using integrative plasmids (pGAPZαA and pGAPZ A) under the control of a constitutive promoter 'GAPDH'. Even in this system, protein expression was not observed by Western blotting. But by RT-PCR, the presence of a full-length transcript was seen (Fig. 3.8E) (Nagappa, 2014). Apart from these *in vivo* expression systems, cell-free expression system (TNT® Coupled Wheat Germ Extract Systems from Promega) was also employed to produce recombinant PfAMPD protein, but this approach also failed (Data shown in figure 1 of the appendix).

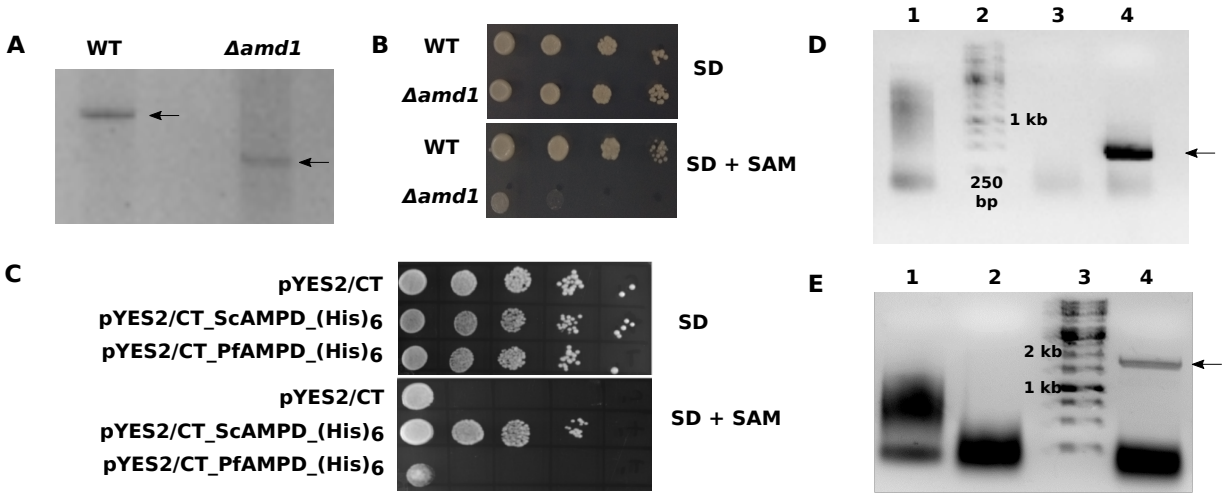

Figure 3.8: Genotype and phenotype of *Δamd1* yeast strain, complementation assay and expression analysis of PfAMPD in heterologous systems (*S. cerevisiae and P. Pastoris*) by RT-PCR

(A) PCR validation of *Δamd1* strain using 5' upstream and 3' downstream primers. Genomic DNA isolated from wild type and knockout yeast train was used as template. The difference in band size can be observed for AMPD loci between the two strains indicated by arrows. (B) *Δamd1* strain shows a growth defect phenotype in comparison to wildtype when grown on minimal medium containing SAM. (C) Rescue of growth defect was observed in cells carrying pYES2/CT_ScAMPD_$(His)_6$ (positive control) only and not in cells transformed with either pYES2/CT (vector control) or pYES2/CT_PfAMPD_$(His)_6$(test). (D) Agarose gel electropherogram of DNase treated RNA isolated from galactose-induced *Δamd1* cells carrying pYES2/CT_PfAMPD_$(His)_6$(lane1), molecular weight marker (lane 2), No RT control (lane 3) and test (RT sample) (lane 4). A band of 500 bp was obtained. Arrow mark indicates the band corresponding to an unexpected shorter transcript fragment. (E) Agarose gel electropherogram of DNase treated RNA isolated from *P. pastoris* cells carrying pGAPZαA_PfAMPD (lane1), No RT control (lane 2), molecular weight marker (lane 3) and test (RT sample) (lane 4). Arrow mark indicates the band corresponding to full-length transcript.

Heterologous systems expressing foreign genes have significant shortcomings such as transcript

instability, translational stalling, protein instability, toxicity associated with recombinant protein expression etc. and expressing a *Plasmodium* gene is no exception. Hence, functional complementation assay in Δ*amd1* yeast strain transformed with pYES2/CT plasmid containing wildtype PfAMPD gene had failed due to lack of production of full-length transcript. This might be due to the high AT content of the *Plasmodium* genome and presence of long stretches of continuous As and Ts which can often be recognized as terminator sequence by a heterologous system such as yeast. To circumvent this problem, the approach of codon harmonisation or codon optimization can be adopted. This involves redesigning of the gene where the existence of codon degeneracy is exploited and synonymous mutations are introduced in the gene *in silico,* keeping parameters such as codon adaptation index, the occurrence of repeats and GC% under consideration. Codon optimization majorly focuses on maintaining an optimum GC% as per the requirement of the expression host in addition to replacing low-frequency codons in a gene with synonymous high-frequency ones. One main aspect not taken into account by this approach is the pattern of usage of codons in a gene in its native context. For example, if a *Plasmodium* gene is analysed for its codon content with respect to *Plasmodium* codon usage we find that not all the codons in that gene are high-frequency codons and a significant number of low-frequency codons are observed. This pattern of occurrence of low-frequency codons has been attributed to be vital in regulating the rate of protein translation which in turn, facilitates proper folding of the protein. Codon harmonization approach takes this aspect also into consideration during redesigning the gene and tries to maintain the landscape of high and low-frequency codons for a given gene as seen in its native context, even in the heterologous system (Angov et al., 2008). The harmonised PfAMPD gene (hPfAMPD) was designed using the software EUGENE (Gaspar et al., 2012) (harmonised sequence provided in appendix) and the gene was synthesised by Shinegene, China and provided in the form of a plasmid construct (pMD19_hPfAMPD). Using codon harmonised PfAMPD gene, constructs were generated with various bacterial and yeast expression plasmids and tested for protein expression. The problem of protein degradation and insolubility persisted with the bacterial expression constructs containing codon harmonised PfAMPD gene, whereas protein expression was not observed by Western blotting of total protein extracts from the yeast expression systems (Data shown in figure 2 of the appendix).

3.2.2 PfAMPD functionally complements yeast AMPD deficiency

Complementation assay was repeated using *Δamd1* yeast strain transformed with vectors containing the codon harmonised PfAMPD gene. The assay was done by transforming *Δamd1* yeast strain with pCM189_hPfAMPD_$(His)_6$ (Tet-off system) and pYES2/CT_hPfAMPD_$(His)_6$ (Gal1 system) plasmids and transformants were selected on uracil deficient plates (SD-Ura) as both plasmids contain URA3 selection marker. pCM189 is a 'Tet-off' promotor based plasmid where the expression of foreign gene is constitutive and can be repressed only upon addition of tetracycline or its analogue doxycycline in the growth medium. This is contrary to the GAL1 promoter based plasmid pYES2/CT which requires the inducer galactose for gene expression and

gets repressed in the presence of glucose in the medium. Serial dilution and spotting of transformants was performed on plates containing glucose or galactose as carbon source with and without SAM and incubated for 48 hrs at 30 °C (Fig. 3.9).

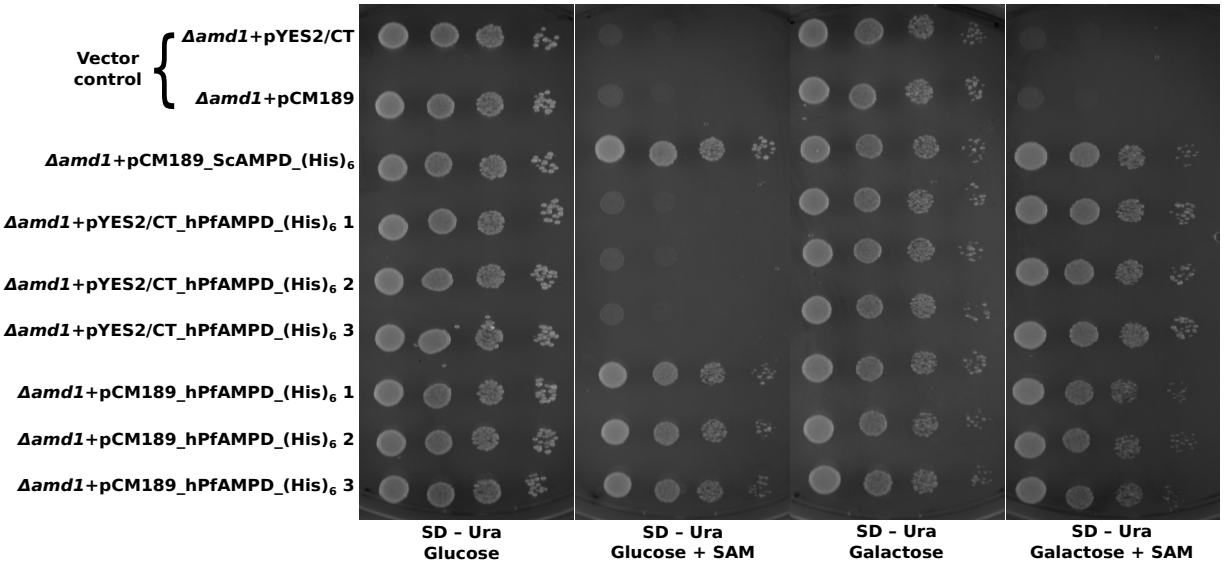

Figure 3.9: Serial dilution and spotting assay in *Δamd1* strain of yeast containing different plasmids showing the growth defect phenotype and its rescue

Transformants of *Δamd1* with either of the parent vectors i.e pYES2/CT or pCM189 (vector control) failed to show rescue of growth defect phenotype whereas, *Δamd1* cells with pCM189_ScAMPD_$(His)_6$(positive control) showed rescue of growth defect phenotype as expected. Cells carrying pYES2/CT_hPfAMPD_$(His)_6$ showed rescue of the growth defect phenotype only under galactose induction condition and not on SAM plates containing glucose as there would be repression of gene expression. Cells carrying pCM189_hPfAMPD_$(His)_6$ showed rescue of the growth defect phenotype on SAM plates containing either glucose or galactose as regulation of gene expression was not based on the carbon source.

Both vector controls i.e *Δamd1* yeast strain transformed with either pCM189 or pYES2/CT showed growth defect phenotype on plates containing SAM as expected, whereas, the knockout strain transformed with pCM189 expressing yeast AMPD (pCM189_ScAMPD_$(His)_6$) as positive control showed rescue of the growth defect phenotype. Yeast cells transformed with codon harmonised PfAMPD in pCM189 vector (pCM189_hPfAMPD_$(His)_6$) showed rescue of the growth defect phenotype in SAM containing glucose and galactose plates as there was no repression of gene expression. Also, cells containing codon harmonised PfAMPD gene in pYES2/CT vector (pYES2/CT_hPfAMPD_$(His)_6$) showed the rescue in the presence of SAM only on galactose (inducer) containing plate and not on glucose (repressor) containing plate, going to show that only upon galactose induction, functional PfAMPD was expressed and hence resulted in the rescue of the growth defect phenotype. This experiment proves that PfAMPD is a functional ortholog of ScAMPD. It has to be noted that functional complementation was observed even though we were not able to detect the protein by Western blotting. Nevertheless, this complementation assay served as the basis for further structure-function characterization of PfAMPD.

3.2.3 PfAMPD is stabilized by C-terminal GFP tag

Although codon harmonised PfAMPD with C-terminal $(His)_6$-tag showed functional complementation, full-length protein was not detected by Western blot probed with anti-$(His)_6$ antibody. Hence, a C-terminal GFP tagged construct (pYES2/CT_hPfAMPD_GFP) was generated so that it would simultaneously provide proof for the expression of the protein by microscopy and/or by Western blotting probed using anti-GFP antibody. The C-terminal GFP-tagged PfAMPD was also found to functionally complement yeast AMPD deficiency similar to the $(His)_6$-tagged protein going to show that GFP tagging did not affect enzyme activity. Moreover, GFP-tagged protein was also detected by Western blot when probed with anti-GFP antibody. Hence to determine if the GFP tag was conferring stability to the protein, dual-tagged PfAMPD constructs (i.e. pYES2/CT_$(His)_6$_hPfAMPD_GFP and pYES2/CT_hPfAMPD_GFP_$(His)_6$) were generated. Western blotting was performed using cells expressing various constructs of AMPD i.e. pYES2/CT_hPfAMPD_$(His)_6$, pYES2/CT_$(His)_6$_hPfAMPD_GFP and pYES2/CT_hPfAMPD_GFP_$(His)_6$ which were probed with anti-$(His)_6$ antibody and pYES2/CT_hPfAMPD_GFP, pYES2/CT_$(His)_6$_hPfAMPD_GFP and pYES2/CT_hPfAMPD_GFP_$(His)_6$ which were probed with anti-GFP antibody. All GFP tagged hPfAMPD constructs were detected by anti-GFP antibody whereas among $(His)_6$ tagged constructs pYES2/CT_$(His)_6$_hPfAMPD_GFP alone was detected by anti-$(His)_6$ antibody whereas, the other two constructs (pYES2/CT_hPfAMPD_$(His)_6$ and pYES2/CT_hPfAMPD_GFP_$(His)_6$) were not detected going to show that the presence of GFP tag at C-terminus confers stability to the protein (Fig. 3.10A). It was also observed that both the constructs (i.e. pYES2/CT_$(His)_6$_hPfAMPD_GFP and pYES2/CT_hPfAMPD_GFP_$(His)_6$) were able to functionally complement yeast AMPD deficiency (Fig. 3.10B).

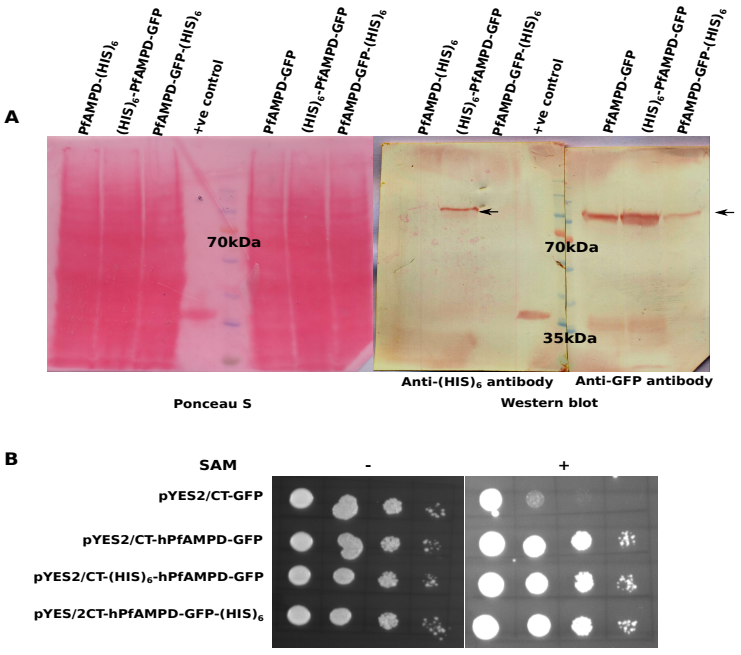

Figure 3.10: GFP tag confers stability to PfAMPD expressed in yeast

(A) Western blot analysis of Δ*amd1* yeast strain expressing $(His)_6$, GFP and dual-tagged PfAMPD. Full-length band was seen for only $(His)_6$-PfAMPD-GFP (arrowhead) when probed with anti-$(His)_6$ antibody, whereas, when probed with anti-GFP antibody full-length band was seen for all three versions of PfAMPD i.e GFP and dual-tagged versions (arrowhead). A previously purified $(His)_6$-tagged protein from the lab PfHADx, was used as positive control. (B) Complementation assay using Δ*amd1* yeast strain expressing GFP and dual-tagged PfAMPD. Both GFP and dual-tagged versions of PfAMPD were able to rescue the growth defect phenotype as compared to negative control (pYES2/CT_GFP) indicating that addition of GFP-tag does not affect the functionality of the protein. Figure reproduced with permission from "Biochemical and physiological investigations on adenosine 5' monophosphate deaminase from *Plasmodium spp*.", Kempaiah Nagappa et al, 2019, Copyright © Wiley Online Library. Western blot demonstrating specificity of anti-GFP antibody is provided in the appendix (Fig. A5)

3.2.4 Characterization of PfAMPD mutants

AMP deaminases are known to have a divergent N-termini that are prone to degradation. But, it has been reported that this proteolytic cleavage of the N-terminus does not have an impact on the activity or regulation of the enzyme's catalytic activity (Han et al., 2006; Saint-Marc et al., 2009). Full-length AtAMPD was found to be present in insoluble fraction upon heterologous expression using SF39 insect cell line. An N-terminal truncated version of *Arabidopsis thaliana* AMPD (AtAMPD) was expressed in soluble form and crystal structure was solved. Nevertheless, electron density was available for only the catalytic core. This structure showed the presence of a metal centre comprising of Zn^{2+} co-ordinated by H391, H393, H659 and D736 (Fig. 3.11A) (Han et al., 2006). In addition to this, the report also predicted the role of two hydrophobic residues F463 and Y467 (AtAMPD numbering) in displacement of the ribose ring (Fig. 3.11B) and identified E662 and H681 as putative catalytic residues (Fig. 3.11C) (Han et al., 2006). However, the contribution of these residues to catalysis/ structural stability was not experimentally validated. By forward genetics approach, residues critical for the functioning of the protein were identified in *Arabidopsis* (Xu et al., 2005) (D598 makes critical contacts with H659 and the mutant D598N was found to be embryonic lethal) and human (Akizu et al., 2013) (R674H, E778D and D793Y mutants were identified in an exome sequencing study on patients suffering from pontocerebellar hypoplasia) (Fig. 3.11D). These residues are highly conserved (Fig. 3.12) and using this information as a basis, site-directed mutagenesis was performed on PfAMPD gene. Mutants were validated by sequencing (Fig. 3.13) and examined for function by serial dilution and spotting assay (Fig. 3.14). It has to be noted that till date, no study using site-directed mutagenesis has been done to evaluate the role of different residues in PfAMPD.

In AtAMPD, deletion of N-terminal 139 residues yielded active enzyme and crystals of diffraction quality. Alignment of AMPD sequences shows that the catalytic core (180^{th} to 680^{th} residue, Pf numbering) is highly conserved (Fig. 3.12). Both *ΔN60* PfAMPD that corresponds to the truncated version of AtAMPD with 139 residues at N-terminus deleted (found to be soluble and used for crystallization), and *ΔN180* PfAMPD that corresponds to the catalytic core of the enzyme failed to functionally complement yeast AMPD deficiency (Fig. 3.14A) going to show

that in spite of the fact that AMPD sequences have a divergent N-termini, the N-terminus of PfAMPD contains critical residues which are indispensable for activity or structural integrity of the protein.

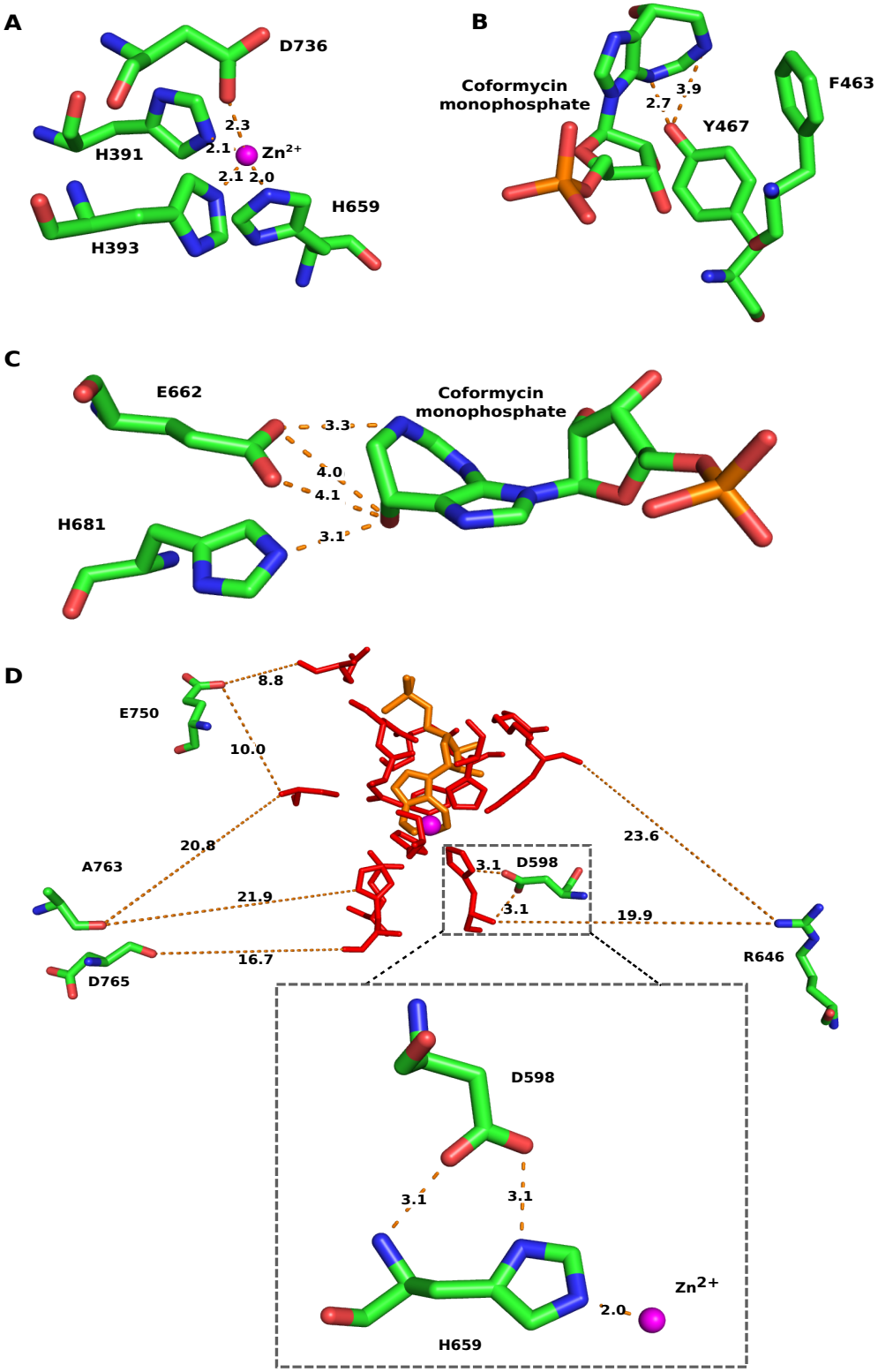

Figure 3.11: Contact-maps of functionally important residues in AtAMPD

Contact analysis was performed on AtAMPD crystal structure (PDB Id: 2A3L) to select residues for mutagenesis. Contacts of Zn^{2+} coordinating residues (A), hydrophobic residues interacting with ligand coformycin monophosphate (B), and contacts of putative catalytic residues (C) are shown. (D) Residues identified by forward genetics approach in AtAMPD and human AMPD2 have been represented in the context of the active site residues indicated by red lines. Residues that come within 4 Å cutoff of ligand coformycin monophosphate (orange sticks) and Zn^{2+}(magenta sphere) have been considered as active site residues. It should be noted that only D598 makes a critical contact with the active site residue H659 which is involved in Zn^{2+} co-ordination (zoomed image). All other residues are significantly far from the active site pocket. Figure reproduced with permission from "Biochemical and physiological investigations on adenosine 5' monophosphate deaminase from *Plasmodium spp*.", Kempaiah Nagappa et al, 2019, Copyright © Wiley Online Library.

Residues H245, H247, H517 and D594 of PfAMPD that correspond to the residues H391, H393, H659 and D736 of AtAMPD, that co-ordinate the divalent metal ion Zn^{2+} at the active site; upon mutation to alanine rendered the protein inactive as cells expressing the mutant protein failed to grow in the presence of SAM. In the report on AtAMPD structure (PDB id: 2A3L), it was proposed that the residues F463 and Y467 might be involved in displacing the ribose sugar of the ligand coformycin monophosphate (Han et al., 2006). In our study, we have found that mutating the corresponding residues in PfAMPD, F319 and Y323 to leucine did not result in loss of activity of the enzyme. Although F319L and Y323L mutants were active enough to support cell growth, the F319L mutant did show slightly reduced growth when compared with Y323L or the wild type. In the report by Han et al., (Han et al., 2006) it was proposed that H681 might be the catalytic base and in its absence, E662 might perform the same function although both these residues are conserved and are known to be required for catalysis by aminohydrolases in general. Hence, corresponding residues in PfAMPD i.e H539 and E520 were mutated to alanine and it was found that the cells expressing these mutants failed to grow on SAM indicating that both these residues are indispensable for the activity of the protein and both might be involved in the catalysis. The residue D595 (highlighted in bold) is present in the conserved motif 'STD**D**P' which is seen in all AMP/adenosine deaminases (Han et al., 2006). Mutating this residue to alanine also resulted in the loss of activity. A chemical mutagen screen and sequencing study conducted by Xu et al., (Xu et al., 2005) had identified a mutation (D598N) in AtAMPD that resulted in embryonic lethality (Xu et al., 2005). Mutation of the corresponding residue in PfAMPD D454 to asparagine resulted in loss of activity of the enzyme as observed by the lack of rescue of yeast growth defect phenotype. Akizu et al. had identified mutations in human AMPD2 (R674H, E778D and D793Y) which correlated with a neurological disorder called pontocerebellar hypoplasia (Akizu et al., 2013). R674 is conserved in human AMPD2, yeast and *Arabidopsis* AMPD but is a methionine in PfAMPD. This residue was mutated to arginine as well as histidine. Both M504R and M504H mutants were found to be active, but a slight growth defect was observed in M504H mutant compared to M504R and wildtype. E608D mutation in PfAMPD corresponding to E778 of human AMPD2 did not have any impact on the protein activity, whereas the D623Y mutant corresponding to D793 of human AMPD2 was inactive.

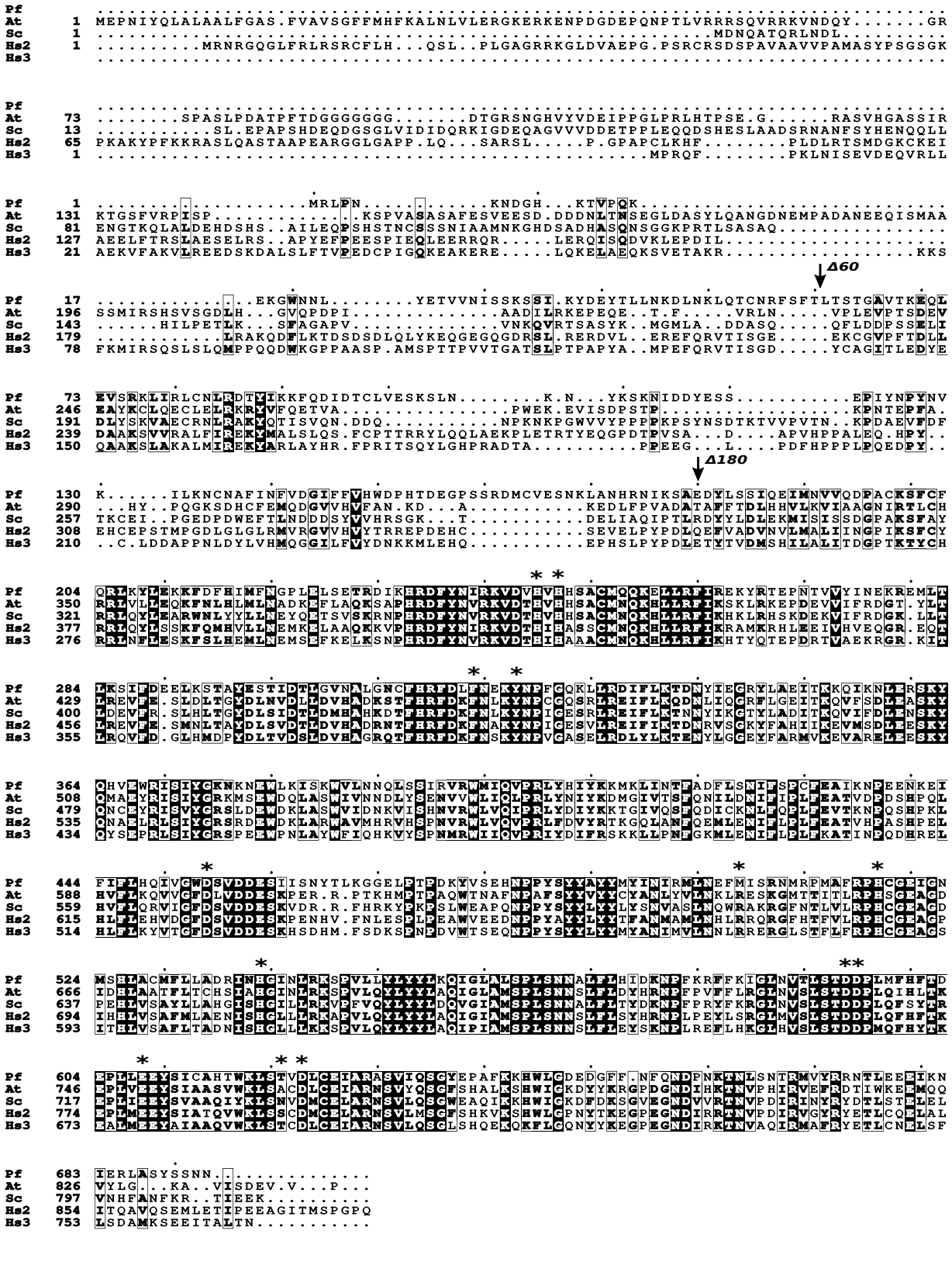
Δ60
Δ180

Figure 3.12: Multiple sequence alignment of AMP deaminase protein sequences

Clustal omega alignment of AMP deaminase sequences from *Plasmodium* (Pf), yeast (Sc), *Arabidopsis* (At) and human (Hs2, Hs3) represented using ESpript 3.0. * indicates residues selected for mutagenesis. Figure reproduced with permission from "Biochemical and physiological investigations on adenosine 5' monophosphate deaminase from *Plasmodium spp*.", Kempaiah Nagappa et al, 2019, Copyright © Wiley Online Library.

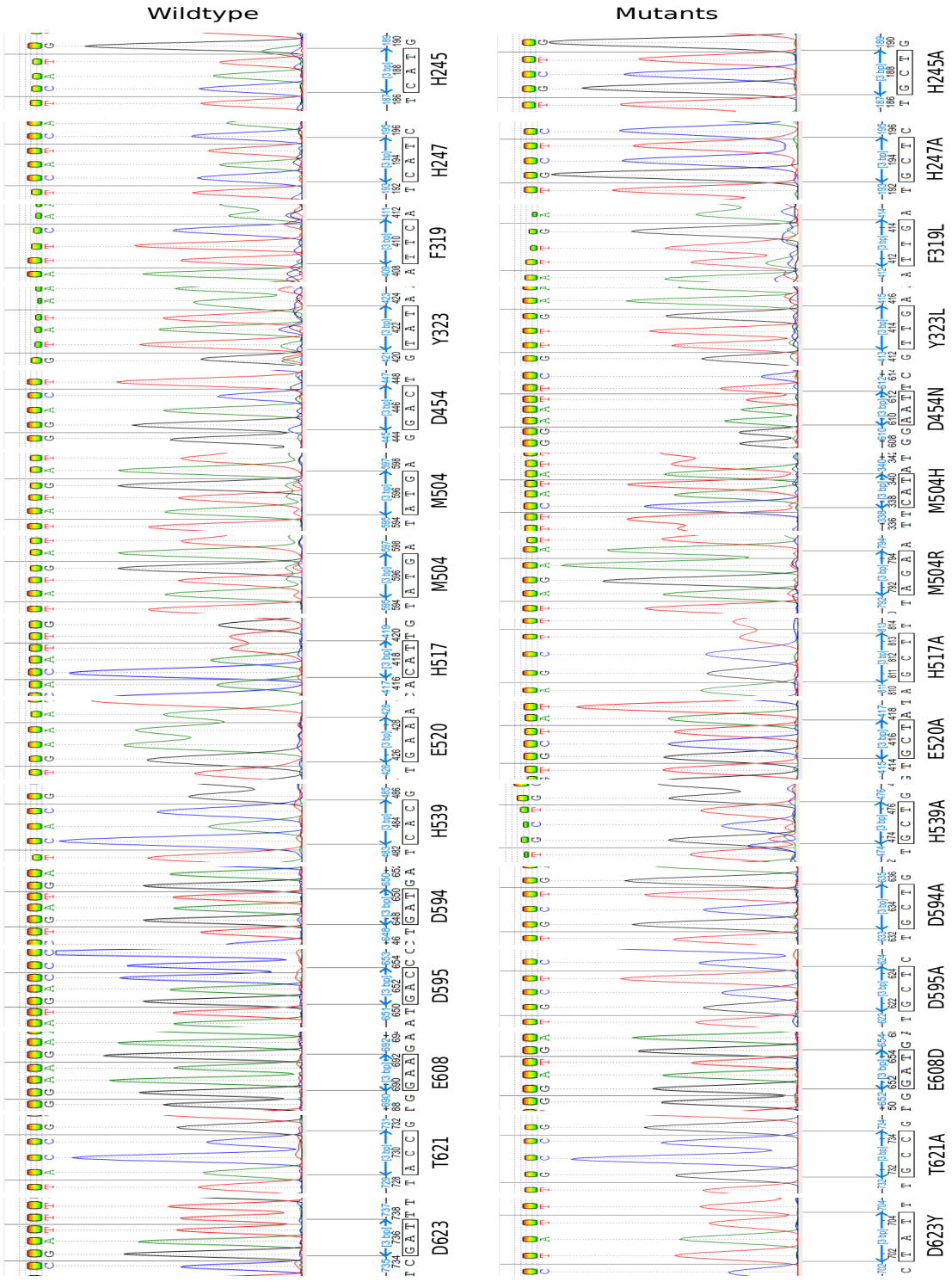

Figure 3.13: Sequencing of mutant PfAMPD constructs

DNA chromatograms validating PfAMPD mutant sequences by comparing with that of wildtype. The gene sequences had no other unwanted mutations. Figure reproduced with permission from "Biochemical and physiological investigations on adenosine 5' monophosphate deaminase from *Plasmodium spp*.", Kempaiah Nagappa et al, 2019, Copyright © Wiley Online Library.

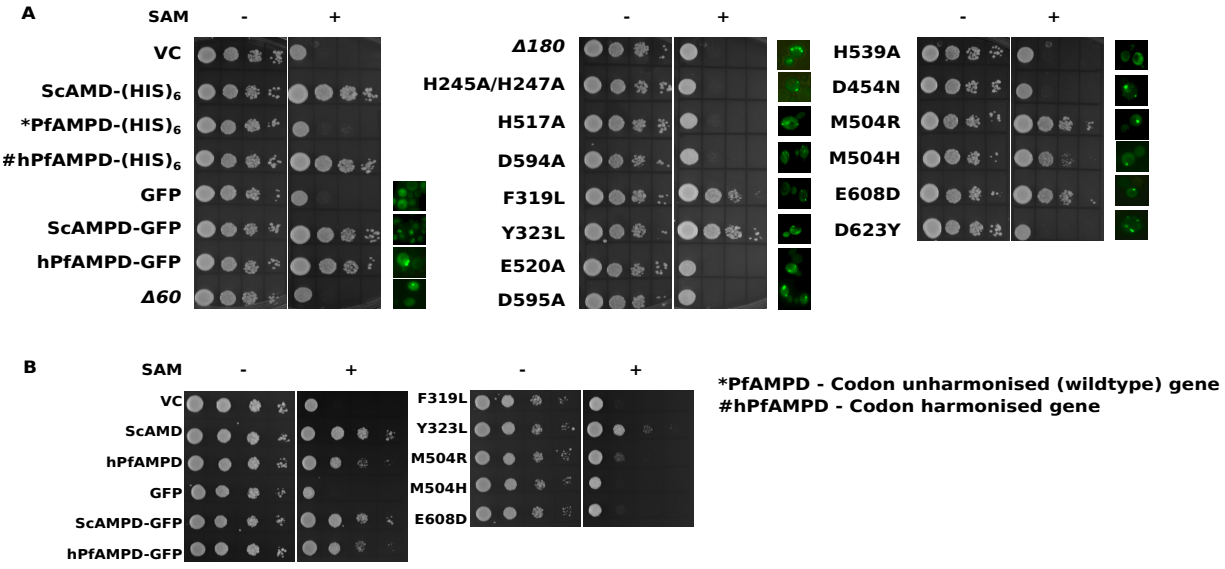

Figure 3.14: Complementation of AMPD deficiency in yeast

(A) The ability of truncated and mutant PfAMPDs to rescue the growth defect phenotype in *Δamd1* yeast strain grown in the presence of SAM was used as a reporter to identify the role of specific residues in enzyme function. Growth phenotype of mutants was compared to that of vector control (VC - strain containing either pYES2/CT or pYES2/CT_GFP), ScAMPD, and wildtype PfAMPD expressing cells. The functional complementation assay was performed at 30 ℃. Panel A also shows microscopic images of GFP fluorescence as evidence for protein expression. (B) Mutants that were able to rescue the growth defect phenotype at 30 ℃ were further investigated for their ability to complement at 37 ℃ and compared with that of wildtype ScAMPD and wildtype PfAMPD expressing cells. (Experiments have been performed in triplicates from two different batches of transformants and image from one experimental replicate is presented). Figure reproduced with permission from "Biochemical and physiological investigations on adenosine 5' monophosphate deaminase from *Plasmodium spp*.", Kempaiah Nagappa et al, 2019, Copyright © Wiley Online Library.

Complementation assays were also performed at 37 ℃ using wild type ($(His)_6$-tag and GFP-tag) yeast AMPD and PfAMPD and mutants of PfAMPD which had shown rescue of growth defect phenotype at 30 ℃ (Fig. 3.14B). Surprisingly wild type PfAMPD itself showed a minor yet observable reduction in the rescue of growth defect phenotype at 37 ℃ as compared to the yeast counterpart indicating sensitivity towards increased temperature. Among the mutants, only Y323L mutant of PfAMPD showed rescue of the growth defect phenotype similar to the wildtype, whereas the others completely failed to do so indicating that they might also be playing a role in stabilizing the structure of the protein that is affected at higher temperatures.

Expression of GFP-tagged PfAMPD and its mutants at the protein level was also determined

by Western blot (Fig. 3.15A and B) and microscopy. Both full-length band corresponding to PfAMPD-GFP fusion protein along with a band corresponding to free GFP were observed. Interestingly, GFP tagged PfAMPD showed varied localization patterns that included diffused cytosolic, cytoplasmic foci/punctate as well as a filamentous pattern (Fig. 3.15C-E). Even the mutants showed foci/punctate localization along with the diffused localization pattern. Earlier it has been reported that enzymes involved in glucose and nucleotide metabolism under nutrient starvation condition form multienzyme complexes which dissociate upon restoration of normal nutrient levels (Narayanaswamy et al., 2009). Although yeast AMPD was also mentioned to have such properties, in our experiments, altering nutrient state by growing cells in medium with/without purine bases did not affect localization pattern.

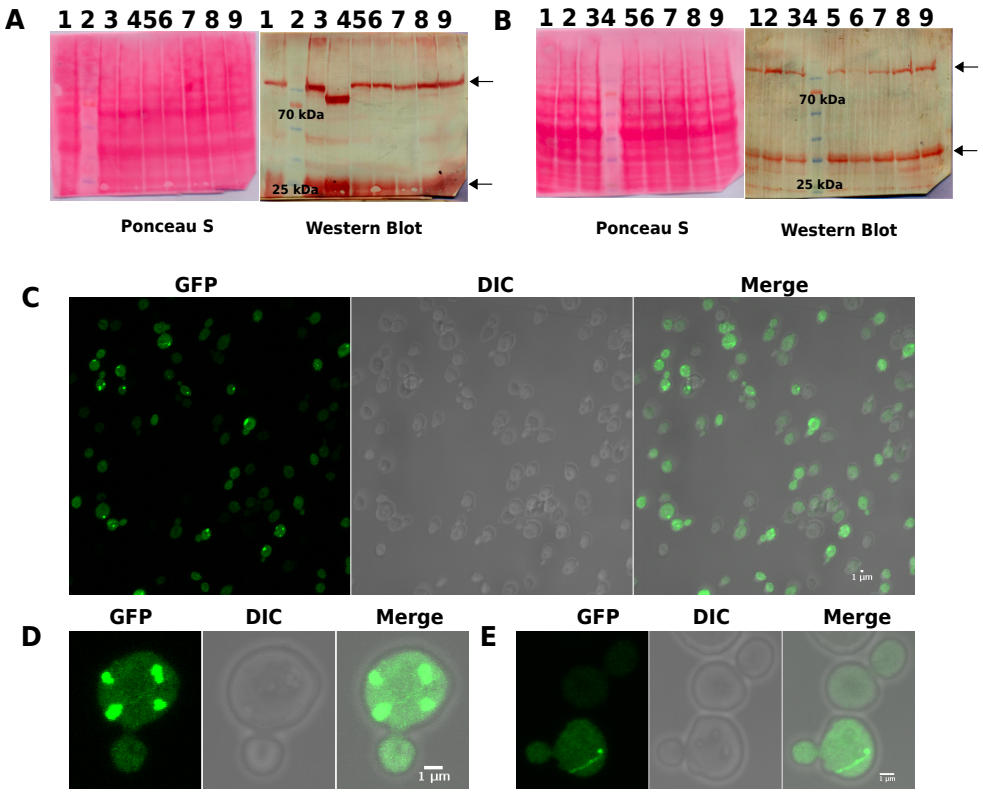

Figure 3.15: Episomal expression of PfAMPD-GFP in yeast

Lysates from cells expressing GFP tagged truncated or mutant version of PfAMPD were subjected to Western blot analysis to provide additional evidence for expression of protein. Panel A: 1, PfAMPD; 2, molecular weight marker; 3, Δ60; 4, Δ180; 5, H245A/H247A; 6, H517A; 7, D594A; 8, F319L; 9, Y323L. Panel B: 1, E520A; 2, H539A; 3, D595A; 4, molecular weight marker; 5, D454N; 6, M504A; 7, M504H; 8, E608D; 9, D623Y. Top arrow marks indicate the PfAMPD_GFP fusion protein whereas, the lower arrows indicate the degradation product of PfAMPD_GFP. (C-E) Microscopic images of yeast cells expressing C-terminal GFP tagged PfAMPD localized as cytosolic puncta or foci in most of the cells along with a diffused cytosolic pattern. Some cells showed multiple foci (D) and some showed a filamentous pattern (E) also. The images were captured under a 100x oil immersion objective of Ziess LSM 510 Meta confocal microscope. Figure reproduced with permission from "Biochemical and physiological investigations on adenosine 5' monophosphate deaminase from *Plasmodium spp*.", Kempaiah Nagappa et al, 2019, Copyright © Wiley Online Library.

3.2.5 Localization of AMPD in *Plasmodium*

3.2.5.1 Endogenous GFP tagging of PbAMPD

Parasites containing endogenously GFP-tagged AMPD gene were generated in *P. berghei* using linear vectors with homology arms, generated by recombineering strategy (Godiska et al., 2009; Pfander et al., 2011) and their genotype was confirmed by PCR (Fig. 3.16A-F). GFP signal was not seen upon microscopic examination of live cells. RT-PCR was done using GFP reverse primer for cDNA synthesis and gene-specific forward and GFP reverse primer for subsequent PCR which, confirmed the presence of the transcript from the GFP fused gene (Fig. 3.16H). Later it was found that the R6K_GFPmut3 plasmid which was used in the LR clonase reaction to generate the final tagging vector had a mutation in the GFP coding sequence which eventually might have lead to the production of a mutant version of GFPmut3 (L60P). This residue is located very close to the chromophore of GFP and the mutation might have affected the formation of the fluorophore.

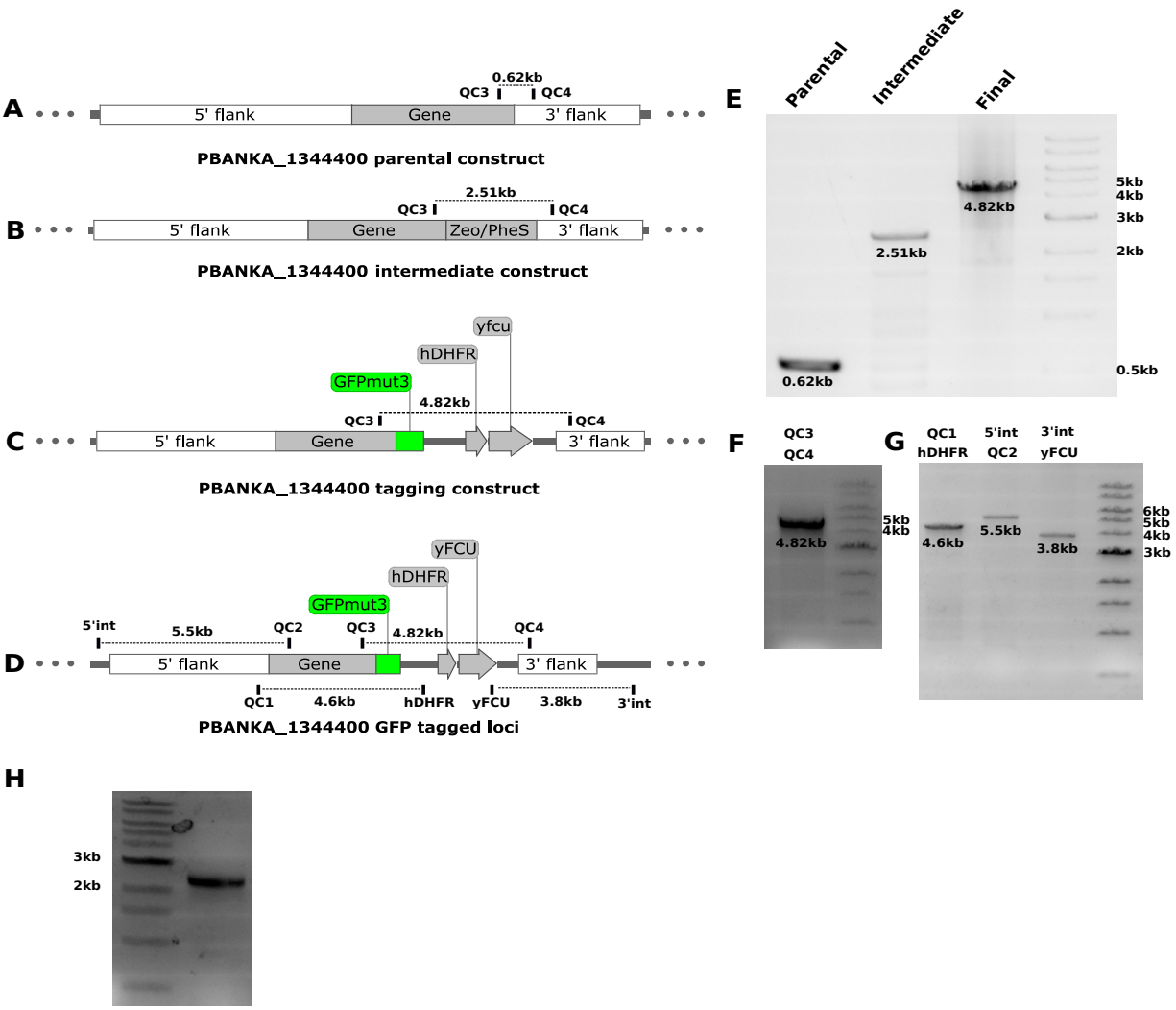

Figure 3.16: Generation of endogenous GFP-tagged PbAMPD parasites

(A-D) Schematic representation of PbAMPD parental, intermediate and final tagging constructs and PbAMPD loci after integration. Primers are indicated in the schematic by vertical bars and expected PCR product size is represented by the line between specific primer pairs. (E) PCR confirmation of parental, intermediate and final tagging constructs. Primers used were QC3 and QC4. (F and G) Genotyping of the transgenic strain for the integration of cassette in the correct locus. Primer pairs used are indicated on top of respective lanes. (H) RT-PCR to confirm the expression of the fusion gene. The last lane in panels E, F and G and the first lane in panel H have molecular weight marker loaded.

3.2.5.2 Episomal expression of PbAMPD using centromeric plasmid

As localization of PbAMPD could not be visualized in parasites due to the mutation in GFP used for tagging endogenous copy of AMPD, an over-expression construct (pBCEN5_PbAMPD_GFP) was used where the coding sequence of the gene for PbAMPD was cloned under PbEF1α promoter with a GFP tag at the C-terminus. When transfected with pBCEN5_PbAMPD_GFP, drug-resistant parasites were not obtained. As this result was reproducible with multiple transfection attempts we reasoned that increased expression of a stable AMPD over and above endogenous levels in *Plasmodium* might be toxic. Hence a catalytically inactive mutant (H245A/H247A) of PbAMPD was cloned in pBCEN5 with C-terminal GFP tag and transfected into *P. berghei*. Drug-resistant parasites were obtained, genotyped and a diffused cytosolic localization was observed (Fig. 3.17A and C). This localization pattern was similar to what was observed by immunofluorescence using anti-PfAMPD antibodies in *P. falciparum* (data in appendix). The GFP fusion protein was also detected by Western blotting (Fig. 3.17B).

As mentioned earlier, drug-resistant parasites were not obtained when wildtype *P. berghei* was transfected with pBCEN5 expressing PbAMPD-GFP wild type protein in spite of multiple attempts. Whereas, transfection with pBCEN5 expressing PbAMPD_H245A/H247A_GFP mutant protein yielded drug-resistant and GFP positive parasites. This prompted us to infer that increased levels of AMPD activity might be toxic to the cells and hence the inability to obtain drug-resistant parasites expressing active enzyme. To confirm this inference, pBCEN5_GFP (vector control), pBCEN5_PbAMPD_GFP and pBCEN5_PbAMPD_H245A/H247A_GFP were mixed in equal amounts (2.5 μg each) and co-transfected into wildtype *P. berghei* which resulted in a mixed population of drug-resistant parasites that were PCR positive for both vector control plasmid and plasmid containing either or both PbAMPD wildtype and mutant genes. Sequencing of the AMPD specific PCR product answered for the presence of only the plasmid carrying the mutant and that the plasmid carrying wildtype gene was not retained in the parasite (Fig. 3.17D-H). This confirms that the expression of functional PbAMPD in addition to endogenous levels is toxic to the parasites.

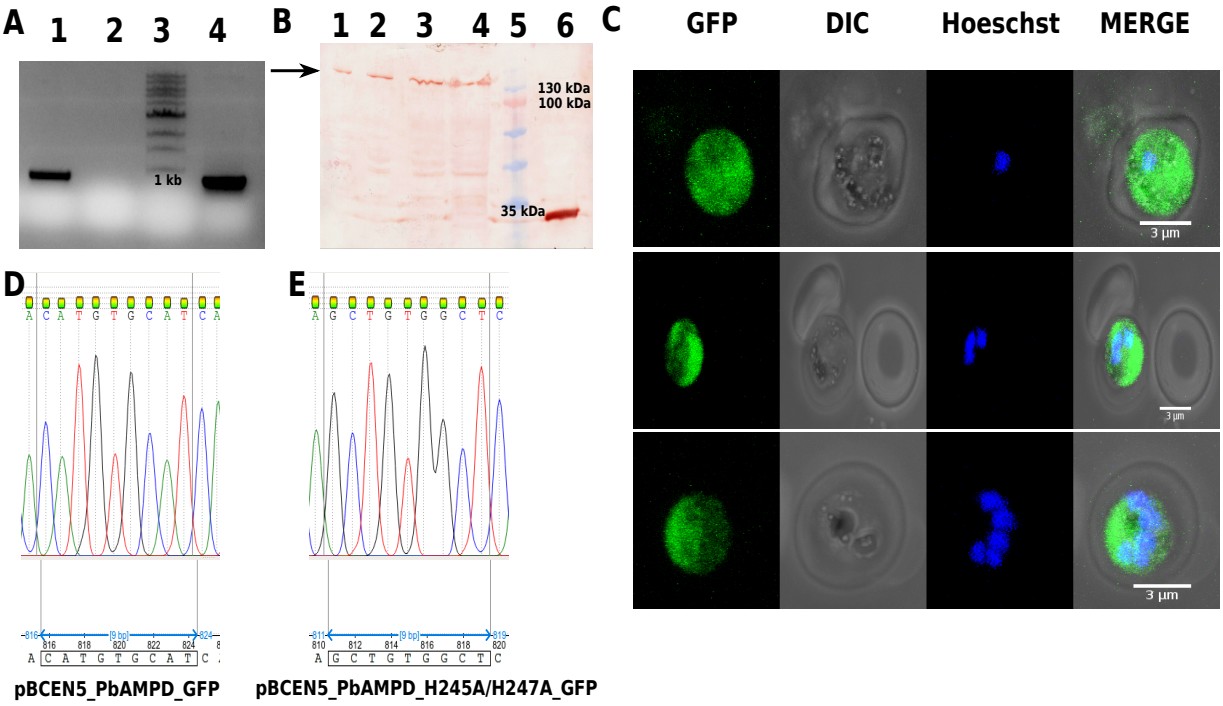

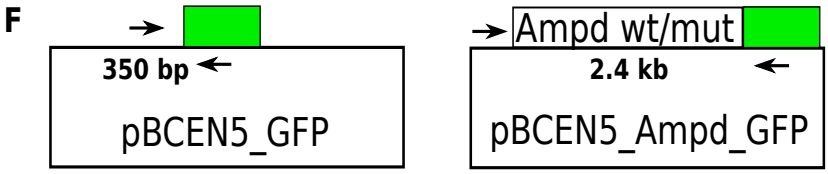

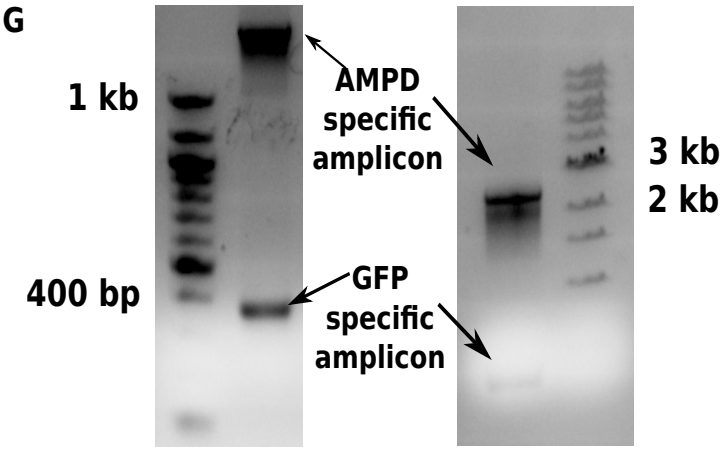

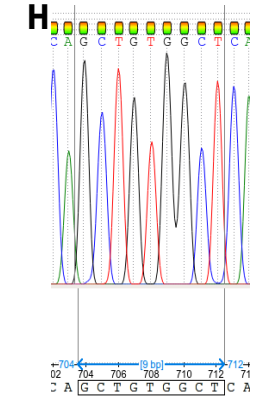

Sequencing result of AMPD specific amplicon obtained using DNA from co-transfectants as template

Figure 3.17: Episomal expression of PbAMPD in *P. berghei*

(A) PCR confirmation of pBCEN5_PbAMPD_H245A/H247A_GFP transfectants. Lane 1, DNA template isolated from transfectants; lane 2; no template control; lane 3, molecular weight marker; lane 4, +ve control (pBCEN5_PbAMPD_H245A/H247A_GFP). (B) Western blot showing the presence of full-length GFP fused PbAMPD_H245A/H247A protein (arrowhead) expressed through pBCEN5 in *P. berghei*. Lane 1 to 4, different volumes (5, 10, 20, 40 µL) of lysate from transfectants expressing PbAMPD_H245A/H247A_GFP fusion protein and lane 6, lysate from *P. berghei* strain expressing GFP alone. (C) Localization of episomally expressed PbAMPD_H245A/H247A_GFP in *P. berghei*. Images were acquired using Ziess LSM 510 META confocal microscope under 100 x oil immersion objective and maximum intensity projections obtained using ImageJ have been represented. (D-H) Results pertaining to co-transfection experiments. *P. berghei* was co-transfected with pBCEN5_GFP (vector control), pBCEN5_PbAMPD_GFP, pBCEN5_PbAMPD_H245A/H247A_GFP. Chromatogram D and E show the difference in DNA sequence between the wild type (**CAT** GTG **CAT**) and catalytically inactive mutant (**GCT** GTG **GCT**). (F) Schematic of the primers selected for genotyping the parasites by PCR. A primer that binds to vector backbone and a GFP internal reverse primer that would amplify the DNA segment present in both vector control and PbAMPD (both wildtype and mutant) were used. (G) PCR was performed on DNA isolated from drug-resistant parasites which turned out to be positive for both vector control and the gene of interest i.e PbAMPD (either wildtype or mutant or both). Bands corresponding to GFP alone and PbAMPD (wildtype or mutant or both) are indicated by arrow marks. The left image is of a 1 % agarose gel that was used to determine/resolve the presence lower molecular weight (vector control) PCR product and the right image is that of a 0.8 % agarose gel that was used to determine/resolve the presence of higher molecular weight (PbAMPD gene-specific) PCR product. The gene-specific PCR product was purified and sequenced to determine whether the sequence would correspond to wildtype PbAMPD or the mutant or a mixed population. As shown in the chromatogram (H) the DNA sequence of transfectants bearing pBCEN5 plasmid containing PbAMPD gene turned out to be the mutant version (**GCT** GTG **GCT**) and not the wildtype. Figure modified and reproduced with permission from "Biochemical and physiological investigations on adenosine 5' monophosphate deaminase from *Plasmodium spp*.", Kempaiah Nagappa et al, 2019, Copyright © Wiley Online Library.

Supporting evidence for the above mentioned inference was also observed in yeast strains lacking a functional *de novo* purine biosynthetic pathway. *Δade1* and *Δade2 yeast* strains are deficient in enzymes of *de novo* purine biosynthetic pathway (N-succinyl-5-aminoimidazole-4-carboxamide ribotide synthetase and phosphoribosylaminoimidazole carboxylase, respectively) and hence can be used as mimics of the *Plasmodium* parasite in the context of nucleotide metabolism (Fig. 3.18). These strains were obtained from EUROSCARF and genotyped by PCR. Survival of these strains is conditional to the presence of purine precursors such as hypoxanthine or adenine in the medium. Both *Δade1* and *Δade2 yeast* strains internalize purine bases (hypoxanthine or adenine) from the growth medium and convert to their respective mononucleotides (IMP or AMP) by the action of specific phosphoribosyltransferases (HGPRT or APRT). In such a scenario, where an enzyme that catabolizes these mononucleotides is over-expressed, it results in a futile cycle and compromises the cell viability that will manifest as a growth defect phenotype. Both *Δade1* and *Δade2* strains grown under purine limiting conditions showed growth defect phenotype upon episomal expression of ScAMPD. Interestingly, episomal expression of PfAMPD in *Δade1* and *Δade2* strains grown under similar conditions did not result in growth defect phenotype (Fig. 3.18D). Earlier Hortle et al. had identified a mutation in AMPD3 (erythrocytic isoform) and

identified that this mutation correlated with increased IMP levels (suggesting hyperactivity) in the RBCs leading to their reduced half-life. Mouse harbouring this mutation in AMPD3, displayed resistance to *P. chabaudi* infections and hence the authors hypothesized that AMPD activators could serve as potential antimalarials (Hortle et al., 2016). In addition to the expression of wildtype PfAMPD protein, the putative hyperactive mutant (T621A - corresponding to the mutation identified by Hortle et al.) was also expressed in *Δade1* and *Δade2* strains. Although found to be active, growth defect phenotype was not observed in the case of T621A mutant expressed in *Δade1* and *Δade2* strains. Although Hortle et al., have stated that this residue is conserved in AMPD sequences, independent sequence analysis showed the contrary (Fig. 3.12).

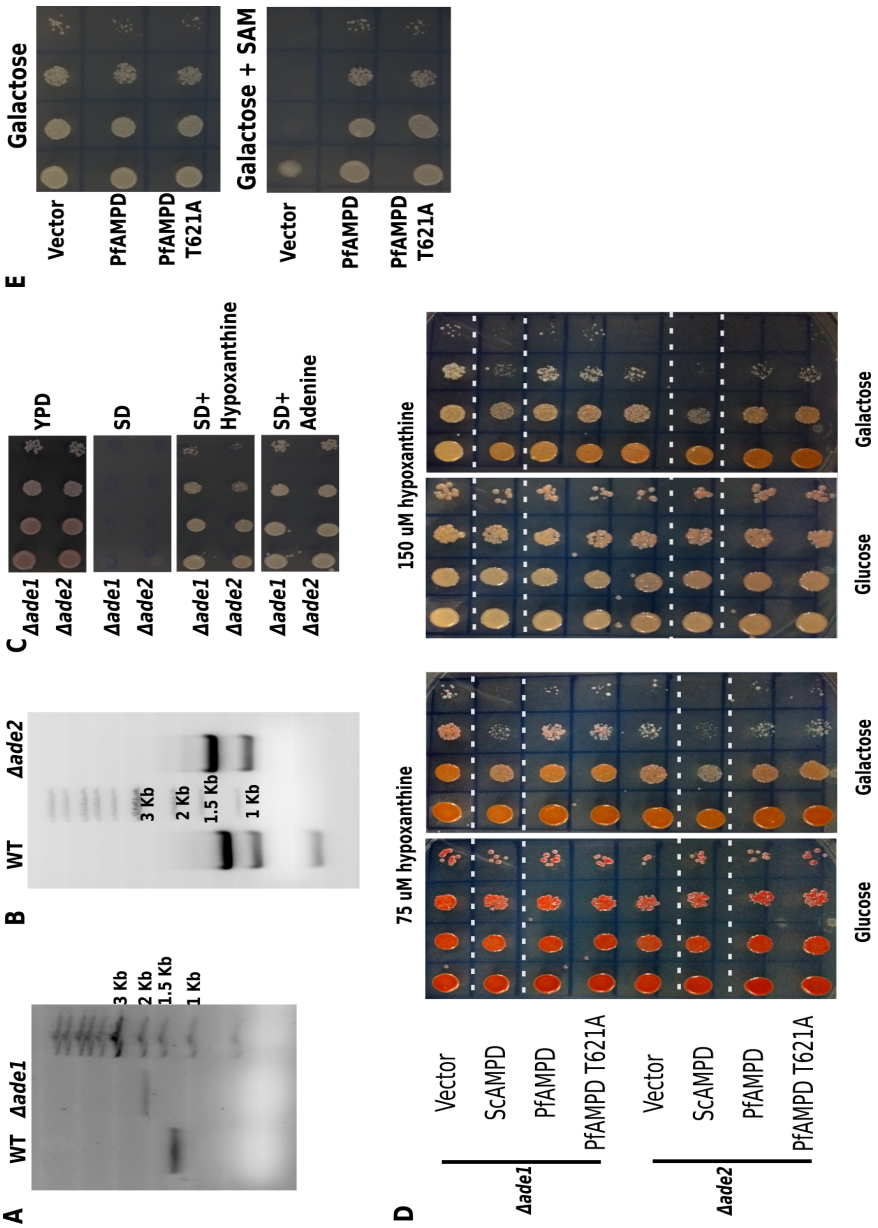

Figure 3.18: Genotype and phenotype of *Δade1* and *Δade2* strains and growth phenotype upon AMPD overexpression

(A and B) PCR validation of *Δade1* and *Δade2* strains. Using genomic DNA as template and 5' upstream and 3' downstream primers for the respective genes, PCR was performed. A difference in the size of the amplicon was observed for *Δade1* strain when compared with that of wildtype, validating the knockout. In the case of *Δade2*, PCR was followed by digestion of the PCR product with HindIII restriction enzyme. A difference in restriction digestion pattern was observed for *Δade2* in comparison to that of the wildtype. (C) Determination of growth phenotype of *Δade1* and *Δade2* strains on different growth medium. These strains grow only on rich medium (YPD) or minimal medium (SD) supplemented with purine source hypoxanthine or adenine and fail to grow in the absence of purine source. (D) *Δade1* and *Δade2* strains were transformed with vectors expressing ScAMPD or PfAMPD or PfAMPD-T621A mutant and grown on minimal medium containing 75 or 150 μM hypoxanthine as purine source. Cells episomally expressing ScAMPD displayed a growth defect phenotype when compared to vector control or PfAMPD (wildtype or mutant) in both strains and at both concentrations (highlighted in red dashed rectangle). The appearance of pink color in the colonies is due to the accumulation of P-ribosyl aminoimidazole under purine limiting conditions. (E) Growth phenotype of PfAMPD putative hyperactive mutant T621A when expressed in *Δamd1* strain. The mutant was found to be active and rescued the growth defect phenotype similar to the wildtype. Figure modified and reproduced with permission from "Biochemical and physiological investigations on adenosine 5' monophosphate deaminase from *Plasmodium spp.*", Kempaiah Nagappa et al, 2019, Copyright © Wiley Online Library.

3.2.6 AMPD is non-essential during asexual stages in *P. berghei*

Δampd P. berghei parasites were generated using linear pJAZZok vector with homology arms flanking the marker gene, generated by recombineering strategy (Godiska et al., 2009; Pfander et al., 2011). The knockout parasites were genotyped by PCR and Southern blotting, and by limiting dilution three clonal populations (C1, C2 and C3) were obtained that were genotyped by PCR (Fig. 3.19). One of the clonal populations (C1) was used for assessing the growth phenotype. Comparison of blood-stage growth rate measurements between wildtype and *Δampd P. berghei* parasites in mouse showed no significant difference (Fig. 3.20A and B), thus establishing that the gene is not essential for the parasite during the intra-erythrocytic stages.

Also, enumeration of gametocytes did not show any significant difference in the number of gametocytes as well as the ratio of female to male gametocytes between wildtype and *Δampd* parasites (Fig. 3.20C and D).

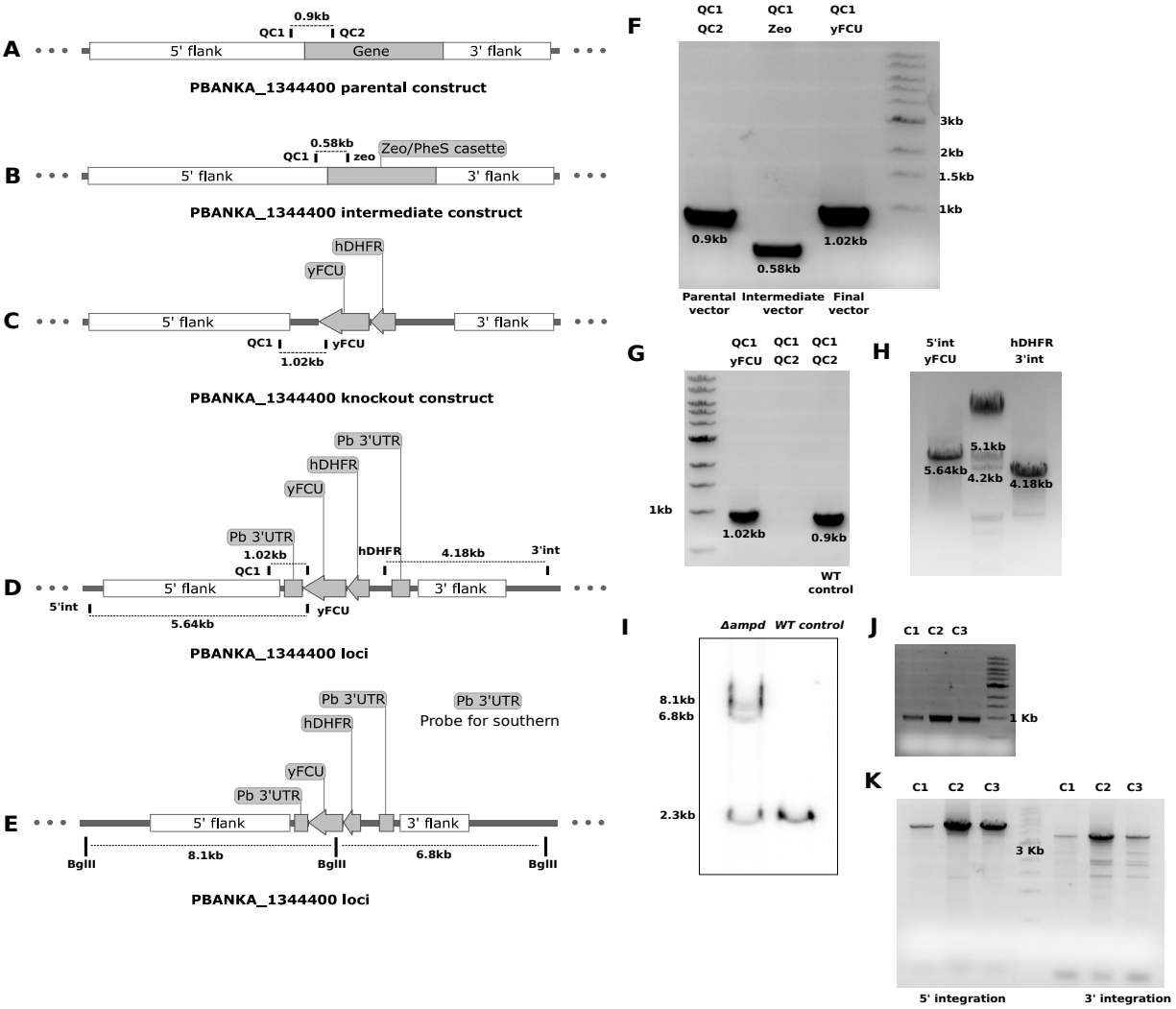

Figure 3.19: Generation of *P. berghei* Δ*ampd* parasites

(A-D) Schematic representation of PbAMPD parental, intermediate and final knockout constructs and PbAMPD loci after integration. Primers are indicated in the schematic by vertical bars and expected PCR product size is represented by the line between specif primer pairs. (E) Schematic representation of the restriction map of PbAMPD loci with BglII enzyme sites indicated by vertical bars. (F) PCR confirmation of parental, intermediate and final knockout constructs. (G and H) Genotyping of the *P. berghei* strain for the integration of cassette in the correct loci. (I) Genotyping of the strain by Southern blotting using Pb 3'UTR probe. Upon limiting dilution and cloning, three clonal lines (C1, C2 and C3) of Δampd *P. berghei* were obtained. The clones were genotyped by PCR using QC1, yFCU primer pair (J) as well as 5' and 3' integration confirmation primers (K). Bands corresponding to DNA fragments of expected sizes were obtained. Figure reproduced with permission from "Biochemical and physiological investigations on adenosine 5' monophosphate deaminase from *Plasmodium spp*.", Kempaiah Nagappa et al, 2019, Copyright © Wiley Online Library.

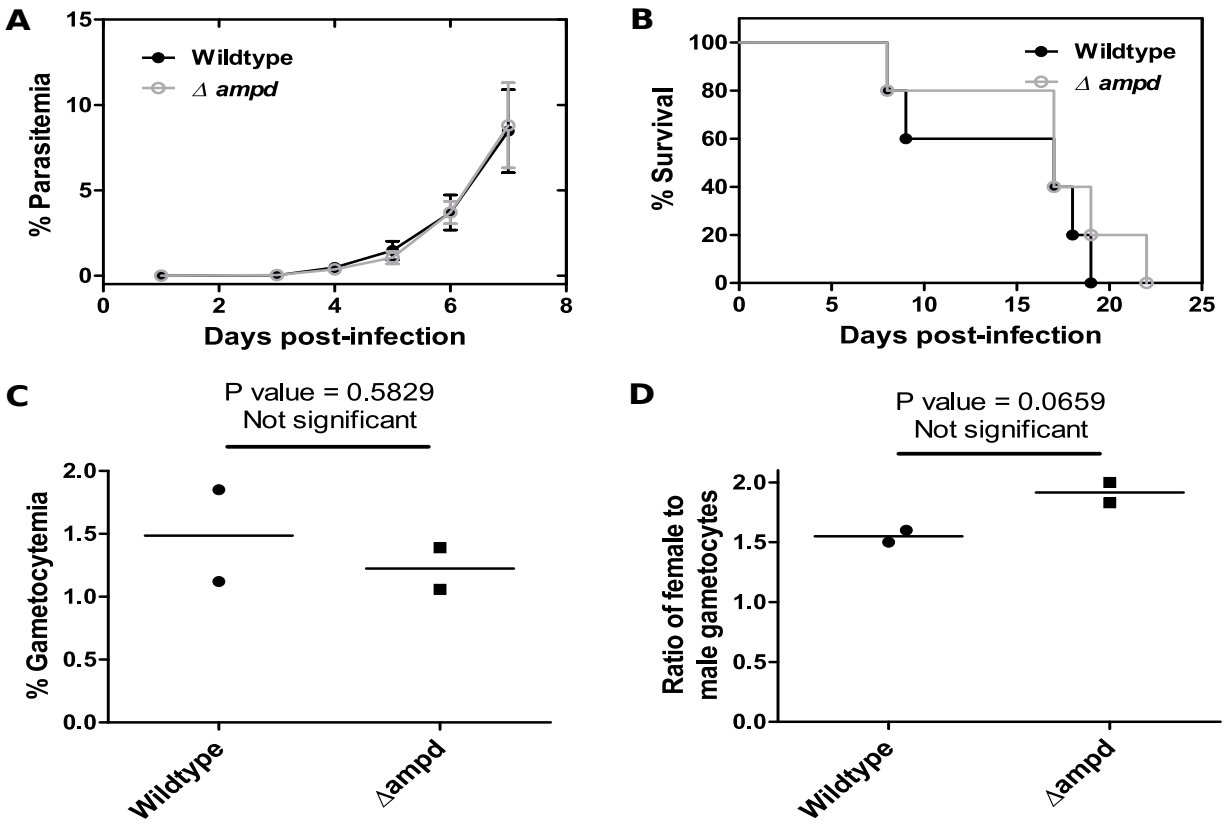

Figure 3.20: Phenotypic comparison of wildtype and *Δampd P. berghei* parasites

(A) Comparison of growth rates of intra-erythrocytic wildtype and *Δampd P. berghei* parasites in infected mice. The data represents the mean ± s.d. values obtained from five mice, each infected with 10^5 wildtype or *Δampd P. berghei* parasites. Statistical analysis was done using Student's unpaired t-test using GraphPad Prism V5. (B) Percentage survival of mice (n=5) infected with either wildtype or *Δampd P. berghei* parasites. (C) Comparison of the number of gametocytes formed in wildtype and *Δampd P. berghei* parasites. The data represents the mean ± s.d. values obtained from two mice, each infected with 4 * 10^6 wildtype or *Δampd P. berghei* parasites. (D) Comparison of female to male gametocyte ratio between wildtype or *Δampd P. berghei* parasites. Statistical analysis was done using Student's unpaired t-test using GraphPad Prism V5. Figure reproduced with permission from "Biochemical and physiological investigations on adenosine 5' monophosphate deaminase from *Plasmodium spp.*", Kempaiah Nagappa et al, 2019, Copyright © Wiley Online Library.

3.3 Discussion

AMPD belongs to amidohydrolase superfamily of enzymes and is part of purine nucleotide cycle involved in the cyclic interconversion of AMP and IMP. Studies on *Arabidopsis* and human AMPD have lead to the elucidation of the critical role of this enzyme in development, as impairment of its function affects AEC, as well as protein production. To our knowledge, till date, there were no reports on comprehensive characterization of any parasitic protozoan AMP deaminase. Previously, purine nucleotide cycle enzymes adenylosuccinate synthetase (ADSS) and adenylosuccinate lyase (ASL) from the malarial parasite *Plasmodium falciparum* have been characterized

(Jayalakshmi et al., 2002; Eaazhisai et al., 2004; Bulusu et al., 2009; Mehrotra et al., 2010). These two enzymes that constitute one arm of PNC and involved in AMP generation have been found to be essential for the parasite's survival (Sanderson and Rayner, 2017). AMPD constitutes the second arm of PNC, regenerating IMP from AMP and had remained unexplored. This prompted us to conduct investigations towards elucidating the physiological role of AMPD in *Plasmodium*.

Our prime objective of performing biochemical characterization on recombinant PfAMPD was met with numerous hurdles owing to its insoluble and unstable nature. When expressed in *E. coli,* full-length, as well as truncated versions of PfAMPD, showed a characteristic degradation pattern and all the fragments were present as inclusion bodies. Attempts to obtain soluble/stable protein by co-expressing with chaperones as well as refolding strategies were futile. Multiple expression systems and strategies were employed which included yeast (*S. cerevisiae* and *P. pastoris* using pYES2/CT and pGAPZ vectors, respectively), and *in vitro* cell-free protein synthesis system. None of these strategies was helpful in obtaining soluble and full-length PfAMPD (Data shown in the appendix). When expression was attempted in *S. cerevisiae* using a codon harmonised gene, the presence of a soluble and functional protein was established based on a growth phenotype readout in a functional complementation assay carried out using *Δamd1* yeast strain. Although we were able to express a functional PfAMPD in a heterologous system, the protein was not detected by Western blot when yeast cell lysates were probed with anti-$(His)_6$ antibodies. Hence to provide evidence for *'cause (protein expression) and consequence (functional complementation)'* correlation, we generated a PfAMPD-GFP fusion construct. Using this construct, the expression of protein was demonstrated by both microscopy and Western blot. The observation that only the GFP-tagged protein can be detected by Western blot and not the $(His)_6$-tagged counterpart indicated that the addition of GFP-tag had conferred stability to PfAMPD. To prove this, dual tag constructs (both $(His)_6$ and GFP) were generated and it was found that when probed with anti-$(His)_6$ antibody, the full-length protein was seen only when where there was an additional C-terminal GFP-tag (Fig. 3.10A). In spite of successfully detecting full-length protein on Western blot, we were unable to purify the protein in sufficient quantities for *in vitro* assays and hence had to rely on the use of functional complementation assay for further characterization of the protein.

The crystal structure of AtAMPD (PDB id. 2A3L) was used for addressing structure-function relationships in the *Plasmodium* enzyme. Our study provides a comparative analysis of similarities and differences between yeast, *Arabidopsis*, human and *P. falciparum* AMPD. Establishing the essentiality of the divergent N-terminus and identification of structurally and catalytically important residues was performed using functional complementation assay on truncated protein and site-directed mutants (Table 3.1). PfAMPD is different from any other AMPD as the N-terminal truncated version was found to be inactive, whereas N-terminal truncated versions of other AMPDs (yeast, *Arabidopsis*, human) have been reported to be active. In comparison to the yeast enzyme, PfAMPD shows a mild temperature-sensitive phenotype (when grown in the presence of SAM at 37 ℃) which becomes distinct in the mutants F319L, M504R, M504H and E608D

indicating the role of these residues in providing structural stability. Most residues identified as vital for functioning of human AMPD2 were found to be important for the Pf counterpart also.

Table 3.1: Residues selected for site-directed mutagenesis and their function

Sl. No.	Residue	Protein	Corresponding residue in PfAMPD	Mutation	Functional association of residue	Reference	Property of mutant PfAMPD *
1	H391	*A. thaliana* AMPD	H245	H245A/H247A	Zn^{2+} coordination	Han et al., 2006 Xu et al., 2005	Inactive
2	H393		H247				
3	H659		H517	H517A			Inactive
4	D736		D594	D594A			Inactive
5	F463		F319	F319L	Displacement of ribose ring		Active
6	Y467		Y323	Y323L			Active
7	E662		E520	E520A	Putative catalytic base		Inactive
8	H681		H539	H539A			Inactive
9	D737		D595	D595A	Present in STD'D'P motif		Inactive
10	D598		D454	D454N	Found in embryonic lethal mutant		Inactive
11	R674	*H. sapiens* AMPD2	M504	M504R & M504H	Identified in pontocerebellar hypoplasia	Akizu et al., 2013	Active
12	E778		E608	E608D			Active
13	D793		D623	D623Y			Inactive
14	T689	*H. sapiens* AMPD3	T621	T621A	Hyperactivity	Hortle et al., 2016	Active

***** results from this study. Table reproduced with permission from "Biochemical and physiological investigations on adenosine 5' monophosphate deaminase from *Plasmodium spp.*", Kempaiah Nagappa et al, 2019, Copyright © Wiley Online Library.

Unfortunately, although a transgenic strain of *P. berghei* where AMPD gene was endogenously tagged at the C-terminus with GFP was generated and expression was confirmed at the RNA level by RT-PCR, GFP fluorescence was not observed by microscopy owing to a mutation in the GFP gene located on the helix that carries the residues involved in the fluorophore formation. Attempts to express GFP-tagged PbAMPD from an episomal vector met with failure as multiple transfection attempts did not yield drug-resistant parasites. *Plasmodium* is completely dependent on the host for its purine source and operates predominantly via the HGPRT route for making IMP, which is then converted to AMP via the ADSS and ASL pathway and GMP via the IMPDH and GMPS reactions. AMP thus generated is utilized for various cellular processes including DNA synthesis during cell division. In such a metabolic context, increased expression of an enzyme that catabolizes AMP might result in the futile cycling of AMP/IMP interconversion probably

leading to a deficit of AMP that would have a deleterious effect on actively dividing cells. This explains our inability to get drug-resistant parasites when transfected with a vector expressing active AMPD that leads to higher levels of the enzyme in the cell. Whereas, drug-resistant parasites were obtained when transfection was done with pBCEN5 expressing catalytically inactive mutant of PbAMPD. In addition to this, when pBCEN5 plasmid expressing either GFP alone or GFP-tagged wildtype PbAMPD or GFP-tagged mutant PbAMPD were co-transfected into *P. berghei*, a mixed population of transfectants that were positive only for pBCEN5_GFP and pBCEN5_PbAMPD_H245A/H247A_GFP (inactive mutant) was obtained. This, adds credibility to our inference of cytotoxicity upon AMPD overexpression. Due to unavailability of inducible episomal expression systems in *Plasmodium,* we resorted to the yeast model to provide additional evidence for the detrimental nature of increased AMPD expression. We employed *Δade1* and *Δade2* strains which are very well characterized purine auxotrophs lacking functional *de novo* pathway and solely depend on purine salvage by APRT or adenosine kinase or HGPRT (Fig. 3.18). These cells were grown on minimal medium containing only hypoxanthine as purine source thereby, mimicking the *Plasmodium* parasite in the context of purine nucleotide salvage. In these growth conditions when AMPD was episomally expressed we observed growth defect when compared to the vector control or cells grown under repressive conditions (Fig. 3.18). Although growth defect was seen only in cells episomally expressing ScAMPD, the lack of this phenotype in cells expressing PfAMPD might reflect on the catalytic efficiencies of the two enzymes and heterologous context of the host expression system. The aforementioned observations in yeast and in *P. berghei* in conjunction with a study on a hyperactive mutation in erythrocyte isoform of AMPD resulting in decreased RBC half-life (Hortle et al., 2016) demonstrates that regulation of this enzyme activity is critical for the survival of cells incapable of *de novo* purine biosynthesis. It should be noted that the T621A mutation in PfAMPD which corresponds to the hyperactive mutation reported in erythrocytic isoform of AMPD, also failed to show growth defect phenotype when episomally expressed in *Δade1* and *Δade2* strains, although it was found to be active based on the complementation assay in AMPD knockout strain (Fig. 3.18). The critical aspect that determines the cell viability in this scenario would be the relative fluxes between AMP generating arm including HGPRT, ADSS and ASL and the AMP depleting arm of AMP deaminase. From our observation in the yeast model, it is evident that the AMPD arm dominates the other arm (HGPRT, ADSS and ASL), upon increased expression of AMPD. Therefore, we conclude that increased expression of AMPD in an organism solely dependent on hypoxanthine salvage might be toxic.

Plasmodium has two isoforms of adenylate kinase (AK1 and AK2) and two isoforms of adenylate kinase-like protein (ALP1 and ALP2). The loci of both AK and ALP were found to be refractory to deletion in *P. falciparum*, whereas in *P. berghei* AK1 was found to be essential while, AK2 was dispensable during asexual stages (Sanderson and Rayner, 2017). Since AMPD activity can in-turn modulate AK activity, essentiality of this gene was investigated in *P. berghei*. AMPD gene was successfully deleted in *P. berghei,* and the transgenic parasites did not show any difference

in phenotype from the wildtype during intra-erythrocytic growth and gametocyte development. Experiments pertaining to essentiality of AMPD in mosquito stages of the parasite life cycle (zygote, ookinete, oocyst and sporozoite), followed by determination of infectivity of sporozoites in liver cells and initiation of blood stage infection in C57BL6 mice were conducted in collaboration with Dr. Kota Arun Kumar's laboratory (Department of Animal Biology, School of Life Sciences, University of Hyderabad, Hyderabad, Telangana, India). Dipti Singh, Sandeep dey and Dr. Kota Arun Kumar conducted these experiments and found that *Δampd P. berghei* parasites exhibit normal development in the mosquito vector (Fig. 3.21), sporozoites display normal gliding motility and transform into EEFs (exo-erythrocytic forms) in HepG2 cells (Fig. 3.22) and initiate a timely blood stage infection in C57BL6 mice (Table 3.2). Hence, AMPD is not essential for the parasite's survival. It has to be noted that in a recent study by Zhang et al, the gene locus was found to amenable for disruption using piggy-bac transposon-mediated saturation mutagenesis (Zhang et al., 2018) during erythocytic asexual stages.

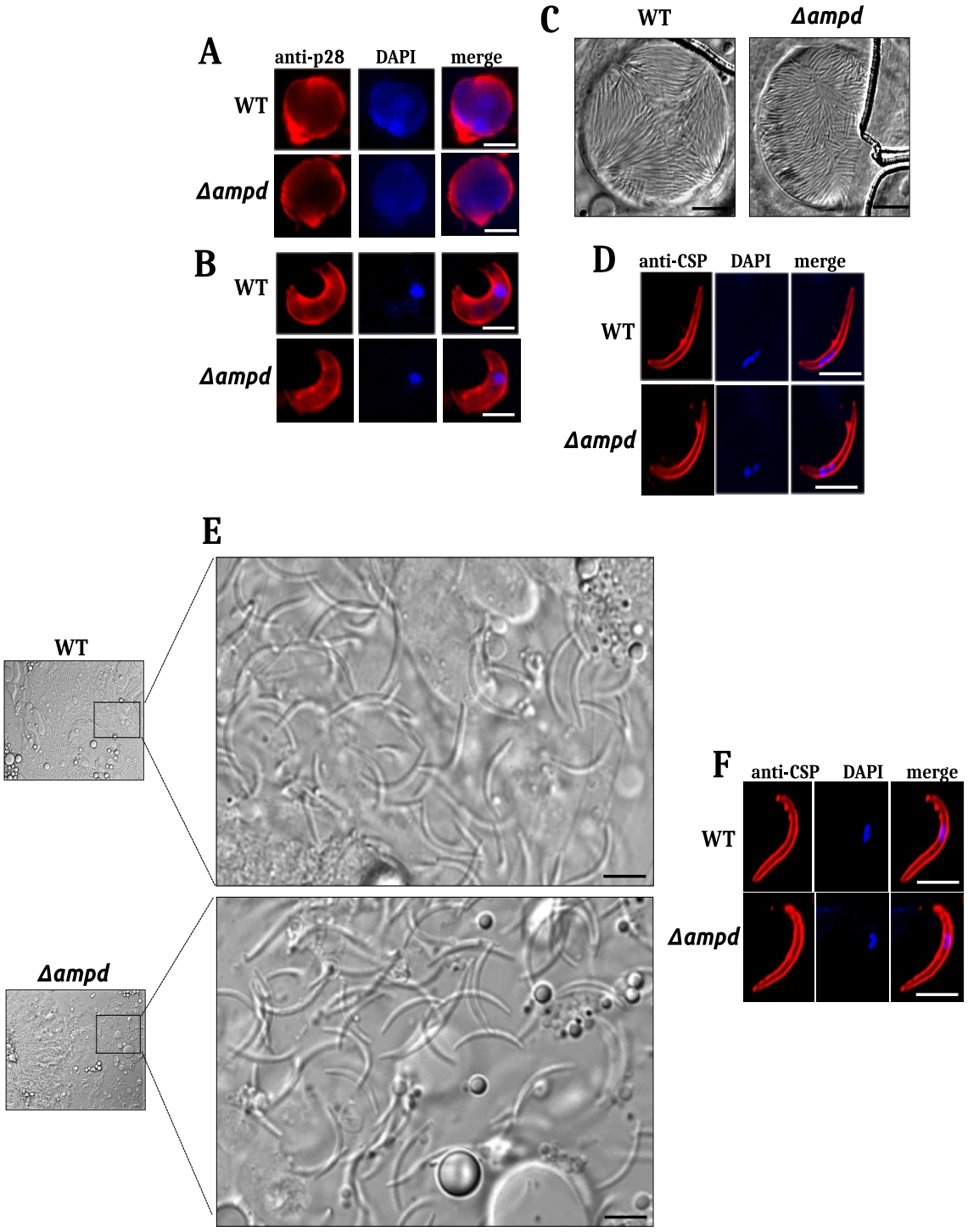
A
anti-p28
DAPI
merge
WT
Δampd
B
WT
Δampd
C
WT
Δampd
D
anti-CSP
DAPI
merge
WT
Δampd
E
WT
Δampd
F
anti-CSP
DAPI
merge
WT
Δampd

Figure 3.21: Examination of wildtype and *Δampd P. berghei* parasites in mosquito stages

Sexual stages were stained with anti-p28 antibody. (A) Zygote (B) Ookinete. Scale 5 μm (C) D14 Oocyst showing sporulation. Scale 20 μm. (D) D14 midgut sporozoite stained with anti-CSP antibody and nuclei with DAPI. Scale 5 μm. (E) Whole mount of D19-20 infected salivary glands. A small area is magnified to show sporozoites. (F) Day 19-20 salivary gland sporozoites stained with anti-CSP antibody and nuclei with DAPI. Scale 5 μm. Figure reproduced with permission from "Biochemical and physiological investigations on adenosine 5' monophosphate deaminase from *Plasmodium spp.*", Kempaiah Nagappa et al, 2019, Copyright © Wiley Online Library.

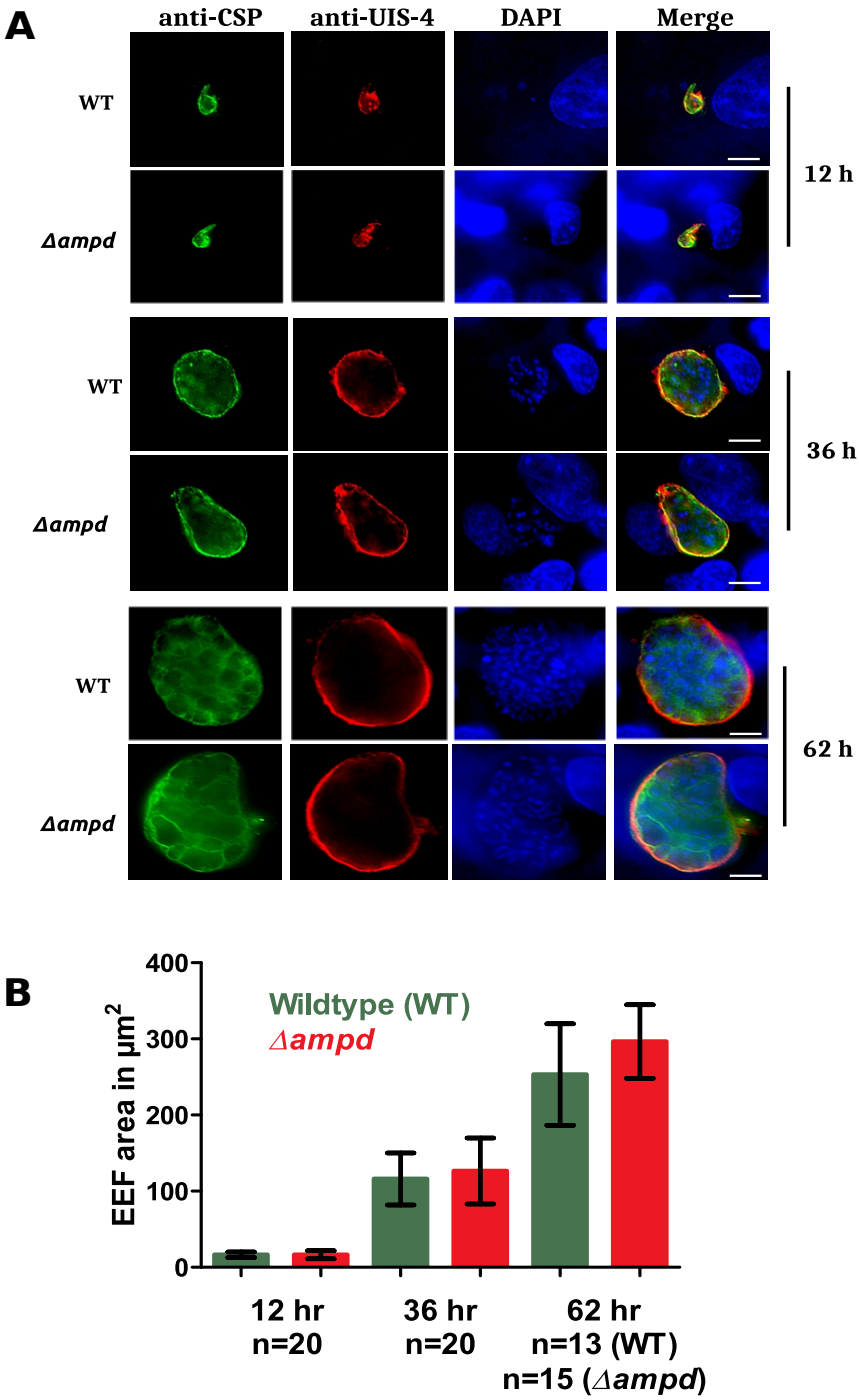

Figure 3.22: *In vitro* liver stage development of wildtype (WT) and *Δampd P. berghei* parasites

(A) *In vitro* liver stage development of wildtype and *Δampd P. berghei* parasites at 12, 36 and 62 hours time points. The developing EEFs were stained with anti-CSP and anti-UIS-4 antibodies that are markers for parasite membrane and parasitophorous vacuole, respectively. The parasite and host nuclei were stained with DAPI. Scale 10 μm. (B) Quantification of EEF size in wildtype and *Δampd P. berghei* parasites at 12, 36 and 62 hours time points. Figure reproduced with permission from "Biochemical and physiological investigations on adenosine 5' monophosphate deaminase from *Plasmodium spp*.", Kempaiah Nagappa et al, 2019, Copyright © Wiley Online Library.

Table 3.2: Analysis of pre-patency in *Δampd P. berghei* sporozoites

Experiment number	Parasite strain	Number of animals used for intravenous injection	Number of sporozoites injected per animal	Number of animals positive for blood stage infection	Pre-patent period (days)
Experiment 1	Wildtype	3	3×10^3	3/3	3.5
	Δ*ampd*	3	3×10^3	3/3	3.5
Experiment 2	Wildtype	2	1×10^4	2/2	3
	Δ*ampd*	2	1×10^4	2/2	3

Table reproduced with permission from "Biochemical and physiological investigations on adenosine 5' monophosphate deaminase from *Plasmodium spp*.", Kempaiah Nagappa et al, 2019, Copyright © Wiley Online Library.

The growth defect seen in *Δamd1* yeast strain manifests only in the presence of adenine or adenosine source (SAM) in the external medium, which results in the build-up of intracellular AMP levels by the action of APRT or adenosine kinase. This can be relieved only by expressing a functional AMPD or by supplementing hypoxanthine or guanine in the media. In mammalian systems, it is the circulating adenosine levels that cause the defective phenotype in Δ*ampd* cells. But for the *Plasmodium* parasite that is harboured inside the erythrocyte, the enzymes APRT and adenosine kinase, which would add to AMP pools are absent. Even though the erythrocyte compartment has both APRT and adenosine kinase, and AMP generated via this route can enter the parasite (Cassera et al., 2008); hypoxanthine is the key precursor for purines in *Plasmodium*. Interestingly, in *Dictyostelium* that has adenosine kinase and APRT and *Toxoplasma gondii* that has adenosine kinase, loss of AMPD results in a developmental/growth defect phenotype (Chae et al., 2002; Sidik et al., 2016). Also, both adenosine kinase and APRT genes are present in *Chromera velia* which is a free-living ancestor of *Plasmodium* (Aurrecoechea et al., 2016). An inherently advantageous metabolic wiring that is deficient of adenosine kinase and APRT seems to have enabled the parasite to survive even in the absence of AMPD in all stages (Fig. 3.23).

However, it is also possible that upon deletion of AMPD gene in *Plasmodium*, AMP levels are not perturbed significantly and this might reflect the sluggish nature of the enzyme. Alternatively, even if significant amount of AMP is accumulated, adenylate kinase might be non-responsive to these levels of AMP thereby, resulting in no phenotype change in *Δampd* parasites as compared to wildtype. A detailed metabolomics study evaluating the levels of AMP in AMPD knockout as well as over-expression conditions might throw more light in this context..

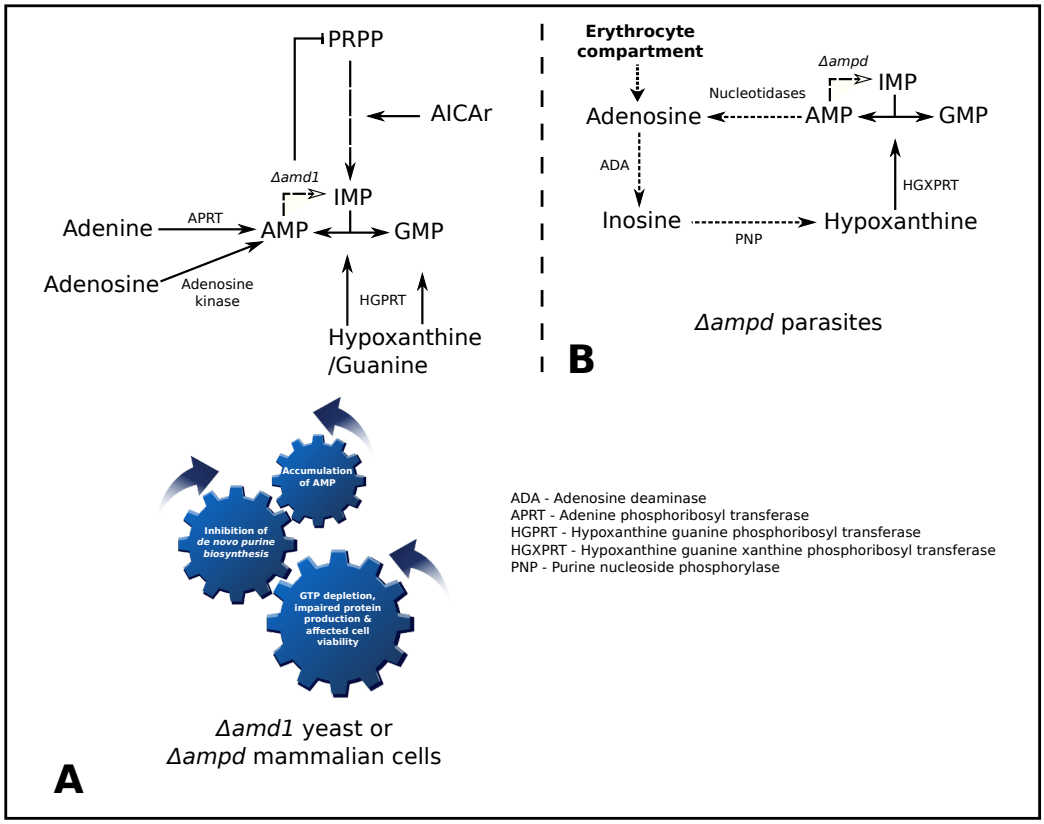

Figure 3.23: Schematic of AMP metabolism in yeast, mammalian cells and *Plasmodium*

(A) Mode of AMP accumulation (APRT and adenosine kinase pathways) and its consequences in AMPD knockout yeast or mammalian cells and mode of metabolite mediated rescue (HGPRT pathway). (B) Mode of AMP metabolism in Δ*ampd* parasites (note: enzymes APRT and adenosine kinase which would have lead to AMP accumulation are absent in the parasite). In addition to the salvage of hypoxanthine by HGXPRT, another possible route for IMP generation from AMP is also shown (dashed arrow). Figure modified and reproduced with permission from "Biochemical and physiological investigations on adenosine 5' monophosphate deaminase from *Plasmodium spp*", Kempaiah Nagappa et al, Copyright © Wiley Online Library.

In summary, this study is the first report on the comprehensive biochemical and physiological characterization of AMPD from an apicomplexan parasite. Apart from providing evidence for the expression of the AMPD gene in *Plasmodium* by RT-PCR, we have also demonstrated that the protein is functional by making use of complementation assay in an AMPD knockout yeast strain. In addition, critical residues have been identified that are required for the functionality

of this protein and the dispensable nature of this enzyme function in all stages of the parasite's life cycle has been determined. Having demonstrated that overexpression of AMPD is toxic, one can ascertain that regulation of its activity is vital and it would be interesting to investigate the mode of regulation of this enzyme, employed by the parasite.

Chapter 4

Studies on haloacid dehalogenase superfamily members

This chapter provides a brief introduction to nucleotidases and haloacid dehalogenase superfamily (HADSF) of proteins. Key roles of this class of enzymes in cellular physiology are discussed in a concise manner. Apart from summarizing the role of HADSF members in metabolism in *Plasmodium,* sequence analysis on the candidate HADSF members under investigation is also provided. *Plasmodium* HADSF members were expressed in *E. coli* heterologous system and two HADSF members (PbPGP and PfHADx) were purified to homogeneity. Extended substrate screen was performed using various phosphorylated substrates such as nucleotide phosphates, sugar phosphates, phosphorylated amino acids and co-factors etc. Parasites with the endogenous copy of PGP tagged with GFP were used to determine the localization of PbPGP whereas, localization of PfHADx was determined by indirect immunofluorescence using antigen-specific polyclonal antibodies raised in rabbit. Both proteins were found to be in the cytosol. In addition, gene ablation studies were conducted using linear pJAZZ vectors containing 5' and 3' UTRs as homology arms and gene of interest replaced by selection marker to determine the essentiality of HADSF members in *P. berghei.* PbPGP was found to be essential as it is involved in 'metabolic proof-reading'. The study on PbPGP has been published in 'The Journal of Biological Chemistry' (Nagappa et al., 2019a).

4.1 Introduction

4.1.1 Phosphate – A brief overview

Phosphate is present in biological systems as both organic and inorganic forms. Phosphorylated metabolites in the form of esters or anhydrides contribute to a major proportion of an organism's metabolome (30-40%) (Westheimer, 1987). It is found in DNA, RNA, phosphorylated forms of sugars, lipids and co-enzymes. Phosphorylation is one of the common post-translational modifications seen in proteins as well. The phopho-metabolome/proteome of an organism is maintained by an interplay of kinases and phosphatases. The phosphate moiety has versatile chemistry which makes it such a favourable group in nature. It is a good leaving group, can form esters (mono, di and tri) with alkyl-OH or aryl–OH groups and also form acid anhydrides in addition to phosphoramidate (P-N), phosphorothioate (P-S) and phosphonate (P-C) bonds. Phosphoryl group transfer reactions are vital in biological systems as they are ubiquitously found in signalling and metabolic pathways (Bowler et al., 2010; Hunter, 2012). Under physiological conditions, phosphate esters are formed with ease by kinases and are maintained stably unless catalytically acted upon by phosphatases. A simple molecule like methyl phosphate dianion in solution has a half-life of one trillion years, however alkaline phosphatase catalyses the hydrolysis with a rate enhancement of more than 10^{27} fold (Lassila et al., 2011). Kinases and phosphatases act on a broad spectrum of substrates ranging from small molecules such as sugars, amino acids and lipids to large proteins. Hence a good understanding of the phosphate chemistry is needed to gain insight into the regulatory aspects of cell physiology.

4.1.2 Nucleotidases and regulation of AEC

As discussed in the first section, AMP deaminase reaction is vital in regulating adenylate energy charge-ratio of a cell as it can deplete AMP levels and hence drive the adenylate kinase reaction forward. An alternative way to catabolise AMP would be by means of AMP-specific or broad specificity nucleotidases which will dephosphorylate AMP to adenosine. Adenosine can be acted upon by adenosine deaminase to give inosine which will be used as a substrate by purine nucleoside phosphorylase to give hypoxanthine and ribose phosphate. HGPRT catalyses the formation of IMP (from hypoxanthine) which can be used to generate AMP or GMP depending on the cellular requirement. Adenosine generated from AMP can be phosphorylated to AMP by adenosine kinase, but this enzyme is not present in the malaria parasite *Plasmodium*. Studies on *P. falciparum* HGXPRT, ADSS, ASL and GMPS have been conducted in the laboratory and have provided valuable insight into the purine metabolism of the parasite (Raman et al., 2004; Bhat et al., 2008; Bulusu et al., 2009; Mehrotra et al., 2010; Bhat et al., 2011a,b; Mehrotra et al., 2012; Ballut et al., 2015). We extended our study by attempting to characterize recombinant PfAMPD but were rendered unable by the unstable and insoluble nature of the protein. Meanwhile, we took a detour in our line of study where we intended to characterize the nucleotidases in the par-

asite. These enzymes, like AMPD, can contribute to the regulation of AEC by depleting AMP levels.

4.1.3 HAD superfamily

Haloacid dehalogenase superfamily is a group of enzymes whose name is derived from a microbial detoxifying enzyme, 2-haloacid dehalogenase, which was the first ever characterised enzyme in the superfamily. The members of this family perform characteristic chemistry involving metal ion assisted nucleophilic attack acting on a broad spectrum of substrates. The members have an α/β Rossmanoid core domain and a cap domain between which the catalytic residues reside. The cap is known to contribute to the substrate specificity as well as protect the active site. HAD family members are found in prokaryotes, eukaryotes and archaea with ~80000 proteins identified till date. Most of them (~80%) are known to perform phosphoryl group transfer by acting as phosphatases/phosphotransferases/phosphomutases. HAD members occur in large number within an individual organism – *E. coli* (28), *Mycobacterium tuberculosis* (30), *Caenorhabditis elegans* (84), *H. sapiens* (183), *A. thaliana* (169), *P. falciparum* (20). These proteins are also found as fusions with other proteins giving rise to complex domain organizations (Allen and Dunaway-Mariano, 2004; Burroughs et al., 2006; Allen and Dunaway-Mariano, 2009; Srinivasan, 2011).

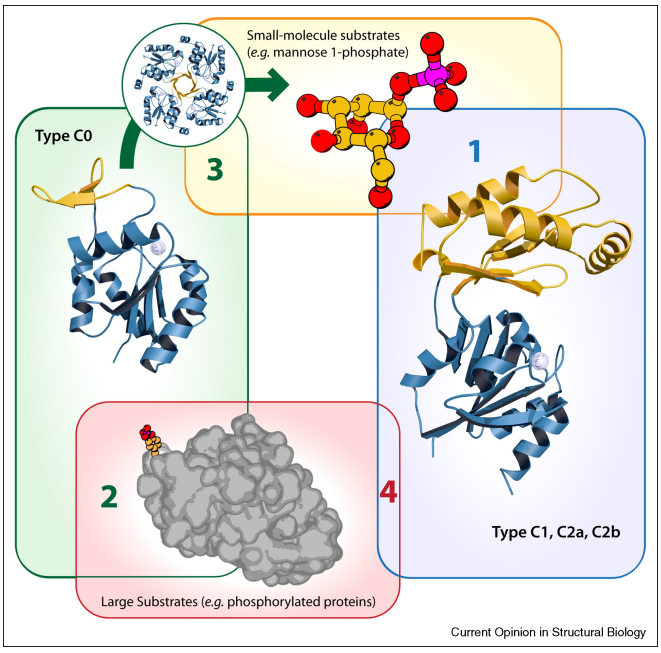

Figure 4.1: Representation of the substrate range and types of HADSF members

HADSF members with C1 or C2 caps are known to act on small molecules (1) or termini of macromolecules (4). Capless HADS act on phosphorylated proteins (2). Oligomerization of C0 HADS can render the ability to act on small molecules (3). Figure reproduced with permission from "Markers of fitness in a successful enzyme superfamily", Karen N Allen and Debra Dunaway-Mariano, Copyright © 2009 Elsevier Ltd.

HAD family members have been classified into three subgroups based on the nature and position of the cap domain (Fig. 4.1). Insertion of the cap in C1 class of HADs is found after the first β strand of the core and after third β strand in case of C2a and C2b class. C0 class members have the shortest of caps or no cap at all. Capped HADs are involved in catalysis using small molecules as substrates whereas the C0 or capless HADs are known to act on large proteins. In HADs acting on small molecules the cap helps in occlusion of bulk solvent from the active site and in C0 HADs the substrate itself performs this role. Examples are also found where C0 HADs oligomerize in such a way that the subunits perform the role of cap themselves enabling them to process small molecules (Rangarajan et al., 2006). The HAD superfamily members have four characteristic motifs comprising of the core catalytic residues (Fig. 4.2). They are loop 1 DXDXT motif, loop 2 S/T motif, loop 3 K/R motif and loop 4 D/E motif where two aspartate residues are separated by 3 or 4 hydrophobic amino acids (Allen and Dunaway-Mariano, 2004; Calderone et al., 2004; Burroughs et al., 2006; Allen and Dunaway-Mariano, 2009).

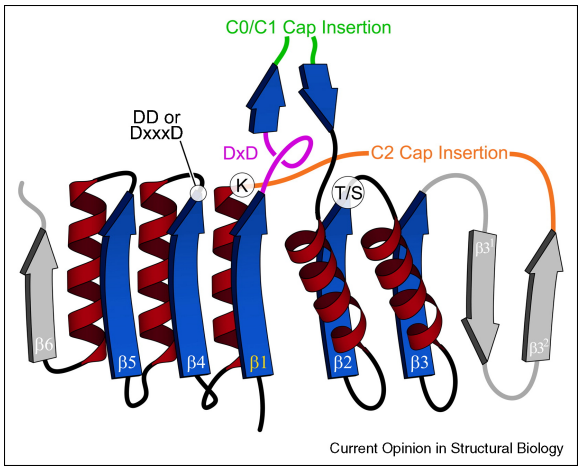

Figure 4.2: Topology diagram of HADSF Rossmann fold

The insertion points of HAD C0/C1 and C2 cap are labelled. The conserved HAD motifs are also indicated. Figure reproduced with permission from "Markers of fitness in a successful enzyme superfamily", Karen N Allen and Debra Dunaway-Mariano, Copyright © 2009 Elsevier Ltd.

Catalysis by HAD members involves a nucleophilic attack by the conserved aspartate in motif I on the electrophile (phosphorous) resulting in the formation of a covalent enzyme-bound intermediate (phosphor-enzyme intermediate), which is attacked by water or the acceptor group resulting in the hydrolysis of the intermediate (Fig. 4.3). Most HAD members make use of Mg^{2+} ion co-ordinated through the nucleophilic aspartate and the phosphate of the substrate neutralizing the negative charge and also stabilizing the structure (Allen and Dunaway-Mariano, 2004). HAD members are involved in various aspects of cellular physiology such as intermediary and secondary metabolism, housekeeping/ house cleaning reactions, nutrient uptake, stress resistance, cell wall biosynthesis etc (Proudfoot et al., 2004; Kuznetsova et al., 2006; Caparrós-Martín et al., 2007; Titz et al., 2007; Weiss, 2007; Taylor et al., 2010; Guggisberg et al., 2014b; Kuznetsova et al.,

2015; Guggisberg et al., 2018). Hence it is necessary to characterize the repertoire of HADs in an organism to obtain a holistic picture of their physiological role and significance.

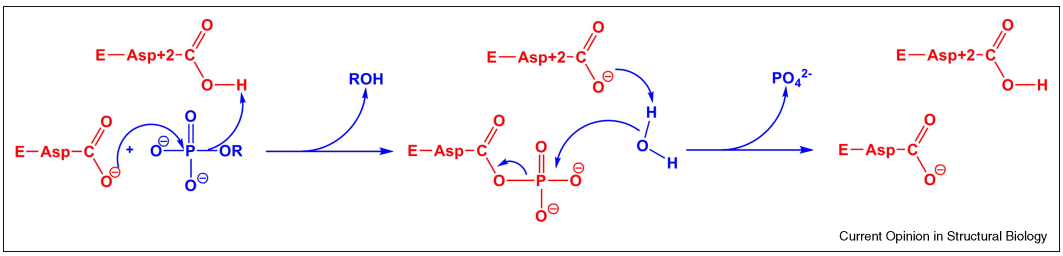

Figure 4.3: Catalytic mechanism of HADSF members

HADSF members follow a ping-pong mechanism involving a phosphor-enzyme intermediate formation followed by a hydrolytic attack in case of phosphatases or transfer to an acceptor group in case of phosphotransferases. Figure reproduced with permission from "Markers of fitness in a successful enzyme superfamily", Karen N Allen and Debra Dunaway-Mariano, Copyright © 2009 Elsevier Ltd.

Haloacid dehalogenase superfamily (HADSF) is a large family of enzymes consisting mainly of phosphatases and phosphotransferases, that are both intracellular and extracellular in nature. These enzymes are characterized by the presence of a core Rossmanoid-fold and a cap-domain (Allen and Dunaway-Mariano, 2004, 2009). Studies on HADSF members have focused on identifying their physiological substrates by screening a wide range of metabolites that include sugar phosphates, lipid phosphates, nucleotides as well as phosphorylated amino acids and co-factors. This approach has helped understand the physiological relevance of these enzymes in various cellular processes such as cell wall synthesis, catabolic and anabolic pathways, salvage pathways, signaling pathways and detoxification (Burroughs et al., 2006; Guggisberg et al., 2014b; Huang et al., 2015; Kuznetsova et al., 2006, 2015; Proudfoot et al., 2004; Roberts et al., 2005; Srinivasan et al., 2015; Titz et al., 2007; Weiss, 2007; Guggisberg et al., 2018). Apart from dephosphorylating metabolites, HADSF members have also been known to dephosphorylate proteins and such members are characterized by the absence of the cap domain (Allen and Dunaway-Mariano, 2004, 2009). A large scale study reported by Huang *et al.* has identified a HADSF member from *Salmonella enterica* that catalyzes the dephosphorylation of more than 100 phosphorylated substrates (Huang et al., 2015). This extended substrate specificity is a common observation in HADSF members and often leads to a confounding situation where, determining the physiological substrate of such promiscuous enzymes becomes a challenging task.

Recent studies have identified and characterised HADSF members from the apicomplexan parasite, *Plasmodium* (Srinivasan and Balaram, 2007; Knöckel et al., 2008; Guggisberg et al., 2014b; Srinivasan et al., 2015; Guggisberg et al., 2018; Dumont et al., 2018). HADSF members from *Plasmodium* have been found to be involved in processes that lead to the development of resistance to the drug fosmidomycin, which inhibits isoprenoid biosynthesis (Guggisberg et al., 2014b). Also, these enzymes show considerable activity towards nucleotide monophosphates and phosphorylated co-factors, and generic substrates such as p-nitrophenyl phosphate (pNPP) and

β-glycerophosphate. Earlier studies have been conducted in the laboratory on *Legionella pneumophila* cN-II (Srinivasan et al., 2014), *P. vivax* broad specificity phosphatase (PvHAD2) (Srinivasan et al., 2015) and *P. falciparum* IMP specific nucleotidase - 1 (ISN1) (Prakashkumar, 2018). PvHAD2 is a monomer with high catalytic efficiency for β-glycerophosphate followed by pyridoxal 5´-phosphate in addition to having moderate activity towards α-glycerophosphate, xanthosine 5´-monophosphate, adenosine 5´-monophosphate and the artificial substrate p-nitrophenyl phosphate. The preferred divalent cation for PvHAD2 was Mg^{2+} and its activity was inhibited by phosphate (Srinivasan et al., 2015). PfISN1 is a tetrameric enzyme exhibiting high catalytic efficiency towards IMP. The protein also displays allosteric activation in the presence of ATP and is inhibited by phosphocholine. ISN1, that is predominantly found in fungi, is interestingly not present in the rodent malaria species of *Plasmodium* (Prakashkumar, 2018).

4.1.4 Objectives of the current study

There are numerous proteins which are not functionally annotated in the PlasmoDB database and this holds true for HADs as well. In the context of regulation of AEC by depleting AMP levels, we intended to characterise putative HADs in *Plasmodium*, assign a functional role and explore whether they have any possible role in regulating the adenylate energy charge of the parasite. In this regard the following objectives are set for our study:

1. Cloning, expression and purification of *Plasmodium* HADs in a heterologous system

2. Biochemical and biophysical characterization of *Plasmodium* HADs

3. Elucidation of the physiological role of *Plasmodium* HADs by performing knockout and knockdown studies and determination of localization

4.2 Studies on PGP

4.2.1 Introduction

A HADSF member that was annotated as 4-nitrophenylphosphatase from *P. falciparum* (gene id. PF3D7_0715000) was characterized by Knöckel *et al.,* and was proposed to be involved in dephosphorylation of thiamine monophosphate, the precursor of the active form of vitamin B1 (thiamine pyrophosphate). *In vitro* assays on the purified recombinant enzyme showed that this protein displayed similar specific activities towards thiamine monophosphate and other substrates (ADP, ATP, CTP, G-6-P, F-6-P and PLP) (Knöckel et al., 2008). An independent BLASTp search conducted by us revealed that this protein sequence has significant homology (28-30 %) with phosphoglycolate phosphatase (PGP) from yeast, human and mouse (Fig. 4.4). The $(His)_6$-tagged recombinant *P. falciparum* (Pf) 4-nitrophenylphosphatase when expressed in *Escherichia coli,* was found to be completely insoluble. However, *P. berghei* (Pb) 4-nitrophenylphosphatase

(gene id. PBANKA_1421300) (referred to as PbPGP here onwards) that shares 69.6 % identity (Fig. 4.4B) with its *Pf* homolog, expressed in the soluble form in *E. coli* and could be purified to homogeneity. Here, we report on the biochemical characterization and essentiality of PbPGP. An extended substrate screen identified 2-phosphoglycolate and 2-phospho L-lactate as relevant physiological substrates in addition to the generic substrates pNPP and β-glycerophosphate. Attempts at gene ablation showed that PbPGP gene cannot be disrupted in *P. berghei*, despite the locus being non-refractory for genetic recombination. Our findings emphasize the importance of the 'metabolic proof-reading' process, which involves clearance or modification of toxic cellular metabolites generated as a consequence of error in substrate recognition by enzymes of intermediary metabolism. This process is universal and is analogous to proof-reading observed in DNA polymerases and aminoacyl-tRNA synthetases (Van Schaftingen et al., 2013). Other examples of metabolic errors and associated proof-reading enzymes are listed below (Table 4.1).

Table 4.1: List of error-prone enzymes and associated metabolic proof-reading enzymes

Data compiled from Van Schaftingen et al. (2013).

Enzyme	Main reaction	Side reaction	Proof-reading enzyme	Proof-reading reaction
Malate dehrdrogenase	Oxaloacetate to Malate	α-ketoglutarate to L-2-hydroxyglutarate	L-2-hydroxyglutarate dehydrogenase	L-2-hydroxyglutarate to α-ketoglutarate
Glyceraldehyde 3-phosphate dehydrogenase	NAD^+ to NADH (reduction) during conversion of Glyceraldehyde 3-phosphate to 1,3 bis-P-glycerate	NAD^+ to NADHX (hydration) during conversion of Glyceraldehyde 3-phosphate to 1,3 bis-P-glycerate	NAD(P)HX dehydratase	NAD(P)HX to NAD(P)H
Acetyl-CoA carboxylase	Acetyl-CoA to Malonyl-CoA	Butyryl-CoA to Ethylmalonyl-CoA	Ethylmalonyl-CoA decarboxylase	Ethylmalonyl-CoA to Butyryl-CoA
Carnosine synthase	β-alanyl-L-histidine synthesis	β-alanyl-L-lysine and β-alanyl-L-ornithine production	β-alanyl-L-lysine and β-alanyl-L-ornithine dipeptidase	Hydrolysis of β-alanyl-L-lysine and β-alanyl-L-ornithine
3-phosphoglycerate dehydrogenase	3-phosphoglycerate to 3-phosphooxypyruvate	α-ketoglutarate to D-2-hydroxyglutarate	D-2-hydroxyglutarate dehydrogenase	D-2-hydroxyglutarate to α-ketoglutarate

A recent addition to this list is pyruvate kinase whose main reaction is the conversion of phosphoenol pyruvate to pyruvate. But it also catalyses the conversion of L-lactate to 2-phospho L-lactate that gets hydrolyzed back to L-lactate by a phosphatase (PGP) belonging to HAD superfamily. This enzyme acts on other substrates such as 2-phosphoglycolate and 4-phospho D-erythronate also (Collard et al., 2016). Our studies on the *P. berghei* homolog of PGP establish the essential physiological nature and biochemical function of this conserved cytosolic enzyme and suggest that drugs that specifically inhibit parasite phosphoglycolate phosphatase can be promising anti-malarial agents.

4.2.2 Results

4.2.2.1 Biochemical characterization of recombinant PbPGP

BLASTp analysis of Pf and Pb PGP protein sequences showed 28-30 % sequence homology with phosphoglycolate phosphatase, a conserved protein, present across eukaryotes from yeast to mouse including humans, involved in metabolic proof-reading (Fig. 4.4A). The Pf and Pb protein sequences show 69.6 % identity (Fig. 4.4B).

A

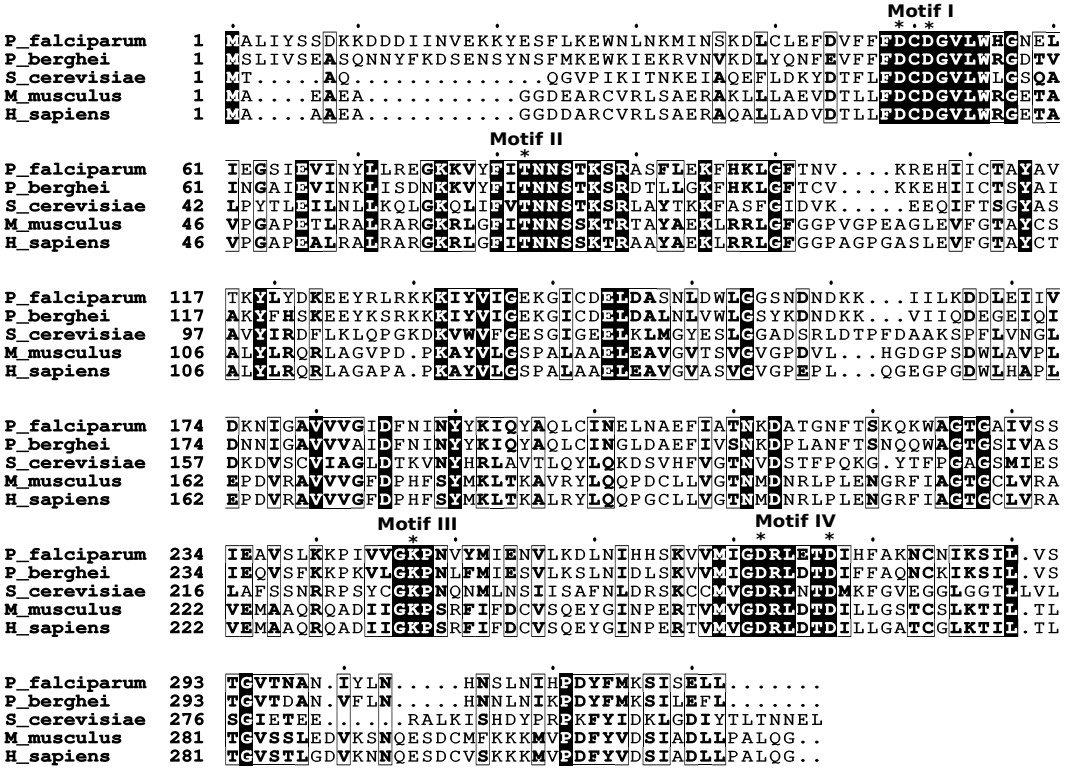

B

Organism	*P. falciparum*	*P. berghei*	*S. cerevisiae*	*M. musculus*	*H. sapiens*
P. falciparum	100	69.57	28.62	31.25	30.59
P. berghei	69.57	100	27.42	30.03	28.71
S. cerevisiae	28.62	27.42	100	31.8	32.46
M. musculus	31.25	30.03	31.8	100	90.65
H. sapiens	30.59	28.71	32.46	90.65	100

Figure 4.4: Multiple sequence alignment of phosphoglycolate phosphatase protein sequences

(A) Clustal omega alignment of phosphoglycolate phosphatase from *Plasmodium falciparum* (P_falciparum), *Plasmodium berghei* (P_berghei), *Saccharomyces cerevisiae* (S_*cerevisiae*), *Mus musculus* (M_musculus) and human (H_sapiens). Residues of the conserved HAD motifs involved in catalysis are indicated by *****. (B) Percentage identity matrix showing the extent of homology between the sequences. Figure reproduced with permission from "Phosphoglycolate phosphatase is a metabolic proofreading enzyme essential for cellular function in *Plasmodium berghei*", Kempaiah Nagappa et al, 2019, Copyright © The American Society for Biochemistry and Molecular Biology, Inc.

Upon expression of C-terminal $(His)_6$-tagged PfPGP in Rosetta DE3 pLysS strain of *E. coli*, the protein was found to be present completely in the insoluble fraction (Fig. 4.5A). This was unlike the strep-tagged PfPGP that was reported to be present in small quantities in the soluble fraction and hence amenable to purification. Therefore, we made use of the protein solubility prediction software PROSOII and found that homologues of PfPGP from other *Plasmodium* species were predicted to be soluble (Fig. 4.5B). Hence, the previously uncharacterized *P. berghei* homolog was chosen for further biochemical studies and physiological investigations. PbPGP was expressed in the *E. coli* strain Rosetta DE3 pLysS and purified to homogeneity by Ni-NTA affinity chromatography (Fig. 4.5C) followed by size-exclusion chromatography (Fig. 4.6D).

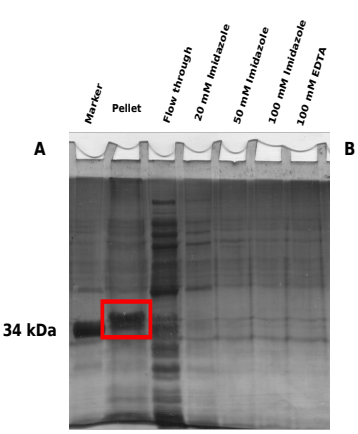

B

Gene Id	Predicted class	Solubility score
PF3D7_0715000	Insoluble	0.33
PKNH_1424000	Soluble	0.745
PVX_122960	Soluble	0.689
PBANKA_1421300	Soluble	0.648
PY17X_1423300	Soluble	0.608
PCHAS_1423100	Soluble	0.652
PCYB_143210	Soluble	0.719

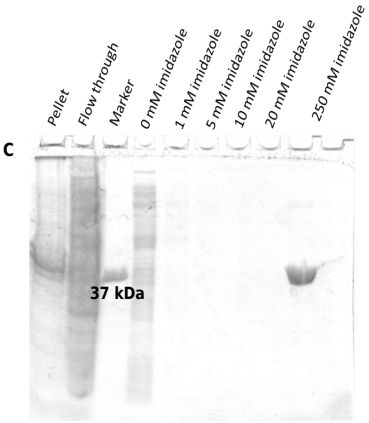

Figure 4.5: Purification of *Plasmodium* PGP

(A) Purification of recombinant *P. falciparum* PGP using Ni-NTA agarose, analysed by SDS-PAGE. The expressed protein is only in the insoluble fraction. *Methanocaldococcus jannaschii* ATPPase (34 kDa) that was earlier purified in the laboratory was used as a molecular mass marker. (B) Solubility indices for PGP homologues from different *Plasmodium* species as predicted by PROSOII. (C) Purification of recombinant *P. berghei* PGP using Ni-NTA agarose, analysed by SDS-PAGE. Soluble protein was eluted with buffer containing 250 mM imidazole. *Plasmodium falciparum* haloacid dehalogenase-like hydrolase (PlasmoDB gene id: PF3D7_1118400) (37 kDa) that was earlier purified in the laboratory was used as a molecular mass marker. Figure reproduced with permission from "Phosphoglycolate phosphatase is a metabolic proofreading enzyme essential for cellular function in *Plasmodium berghei*", Kempaiah Nagappa et al, 2019, Copyright © The American Society for Biochemistry and Molecular Biology, Inc.

PbPGP on analytical gel filtration using Sephacryl S-200 column showed a mass of about 78 kDa, whereas the theoretical mass is 37 kDa, indicating that the protein is a dimer (Fig. 4.6B and C). When further analyzed in the presence of 1 M NaCl, there was a shift in oligomeric state of the protein from dimer, towards monomer suggesting that the oligomers are held by electrostatic interactions (Fig. 4.6B and C).

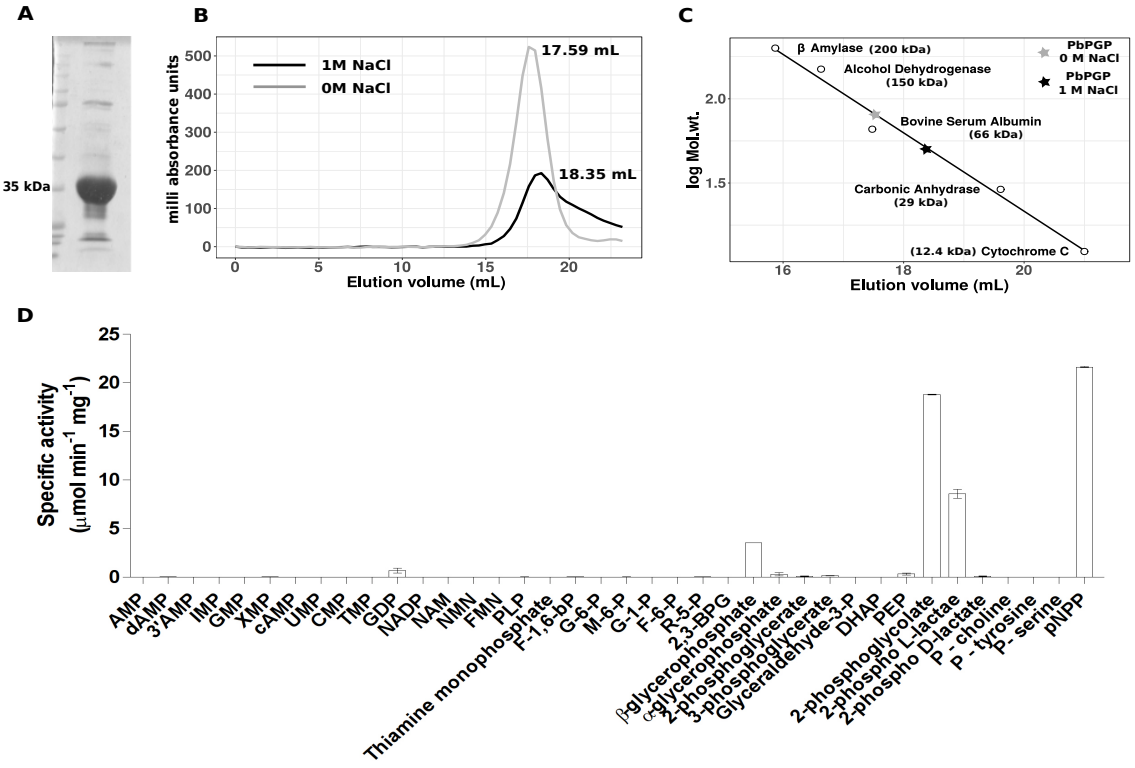

Figure 4.6: Purification and identification of physiological substrates of PbPGP

(A) SDS-PAGE of PbPGP purified using Ni-NTA affinity followed by size-exclusion chromatography. (B and C) Determination of the oligomeric state of PbPGP. (B) Elution profile of PbPGP in the presence and absence of 1 M NaCl and (C) molecular mass calibration curve with elution volumes of PbPGP in the absence and presence of NaCl interpolated. (D) Screen for potential substrates of PbPGP. Mean specific activity values are provided for each substrate and error bars represent SD (n=2). AMP, adenosine 5' monophosphate; dAMP, deoxyadenosine 5' monophosphate; 3'AMP, adenosine 3' monophosphate; IMP, inosine 5' monophosphate; GMP, guanosine 5' monophosphate; XMP, xanthosine 5' monophosphate; cAMP, 3' 5' cyclic AMP; UMP, uridine 5' monophosphate; CMP, cytidine 5' monophosphate; TMP, thymidine 5' monophosphate; GDP, guanosine diphosphate; NADP, nicotinamide adenine dinucleotide phosphate; NAM, nicotinic acid mononucleotide; NMN, nicotinamide mononucleotide; FMN, flavin mononucleotide; F-1,6-bp, fructose 1,6-bisphosphate; G-6-P, glucose 6-phosphate; M-6-P, mannose 6-phosphate; G-1-P, glucose 1-phosphate; F-6-P, fructose 6-phosphate; R-5-P, ribose 5-phosphate; 2,3-BPG, 2,3-bisphosphoglycerate; DHAP, dihydroxyacetone phosphate; PEP, phosphoenolpyruvate. Figure reproduced with permission from "Phosphoglycolate phosphatase is a metabolic proofreading enzyme essential for cellular function in *Plasmodium berghei*", Kempaiah Nagappa et al, 2019, Copyright © The American Society for Biochemistry and Molecular Biology, Inc.

A total of 38 compounds were screened as possible substrates for PbPGP. Although the enzyme displayed very low activity towards nucleotides and sugar phosphates as reported for PfPGP by Knöckel *et al.*, (Knöckel et al., 2008) a novel observation was made as a consequence of our extended substrate screen. PbPGP showed very high activity on 2-phosphoglycolate and 2-phospho L-lactate in addition to the generic substrates pNPP and β-glycerophosphate (Fig. 4.6D). It should be noted that the enzyme was stereospecific for 2-phospho L-lactate and showed no activity on 2-phospho D-lactate.

4.2.2.2 Kinetic studies on PbPGP

PbPGP showed maximum activity at pH 7.0 and preferred Mg^{2+} as co-factor over other divalent cations (Fig. 4.7B and C). The substrate saturation plots for β-glycerophosphate, 2-phosphoglycolate and 2-phospho L-lactate were hyperbolic (Fig. 4.7D-F) and were fit to Michaelis-Menten equation to obtain the kinetic parameters, such as K_{m} and V_{max} (Table 4.2). PbPGP has higher K_{m} value for 2-phosphoglycolate (3.3 and 11.4 fold) and 2-phospho L-lactate (27.4 and 6.4 fold) when compared with that of murine PGP and yeast Pho13. The k_{cat} value for PbPGP for 2-phosphoglycolate is 11.4 and 3.9 fold higher and for 2-phospho L-lactate is 37 and 8.9 fold higher when compared to that of murine and yeast homologs, respectively. The catalytic efficiency ($k_{\mathrm{cat}}/K_{\mathrm{m}}$) for 2-phosphoglycolate is 3.5 fold higher and 2.9 fold lower when compared with its murine and yeast homologs respectively. With 2-phospho L-lactate as substrate, the parasite enzyme has similar catalytic efficiency as its murine and yeast homologs.

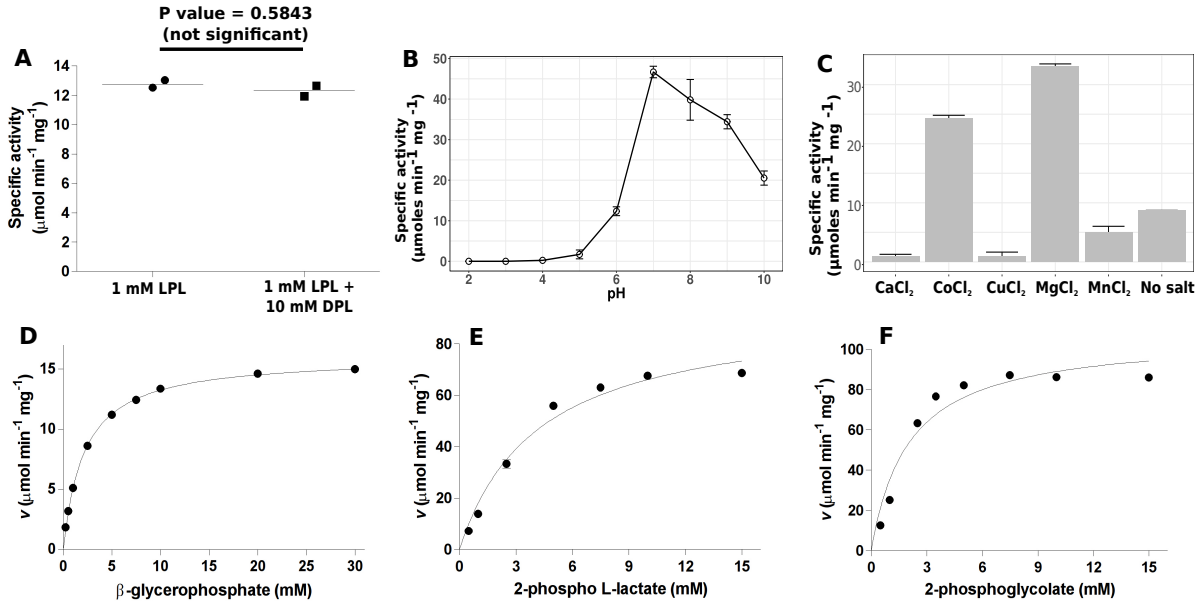

Figure 4.7: Biochemical and kinetic characterization of PbPGP

(A) PbPGP assay performed using 1 mM 2-phospho L-lactate (LPL) as substrate with and without 10 mM 2-phospho D-lactate (DPL). The assay conditions used were 5 mM $MgCl_2$, 200 mM Tricine-NaOH, pH 7.4, in a total volume of 100 µL, and at 37 °C. The reaction was initiated with 1.89 µg of enzyme and incubated for 2 minutes. Horizontal bars represent mean and circles and squares represent individual data points. Statistical analysis was done using paired t-test. (B) pH optimum of PbPGP. (C) Histogram showing activity of PbPGP in the presence of salts of various divalent cations using pNPP as substrate. (D-F) Substrate concentration vs. specific activity plots fit to Michaelis–Menten equation for β-glycerophosphate, 2-phospho L-lactate and 2-phosphoglycolate. Substrate titration experiment was conducted in two technical replicates containing two biological replicates each. Plots from one technical replicate are shown. Each data point represents mean specific activity value and error bars represent SD (n=2). Figure reproduced with permission from "Phosphoglycolate phosphatase is a metabolic proofreading enzyme essential for cellular function in *Plasmodium berghei*", Kempaiah Nagappa et al, 2019, Copyright © The American Society for Biochemistry and Molecular Biology, Inc.

Table 4.2: Kinetic parameters of *P. berghei* PGP compared with that of homologs from yeast and mouse

Substrate	Kinetic parameters of PbPGP			
	K_m (µM)	V_{max} (µmol min^{-1} mg^{-1})	k_{cat} (s^{-1})	k_{cat}/K_m (M^{-1} s^{-1})
β - glycerophosphate	2110 ± 11	16.2 ± 0.14	10.18 ± 0.08	4827
2 - phosphoglycolate	2526 ± 494	119.5 ± 12.5	75.15 ± 7.86	29747
2 - phospho L - lactate	4773 ± 574	107 ± 13.2	67.34 ± 8.31	14108
Kinetic parameters of Murine PGP #				
2 - phosphoglycolate	766 ± 68	11.34 *	6.56 ± 0.44	8564
2 - phospho L - lactate	174 ± 55	3.14 *	1.82 ± 0.34	10480
Kinetic parameters of *S. cerevisiae* Pho13 #				
2 - phosphoglycolate	221 ± 13	32.87 *	19.0 ± 0.44	85700
2 - phospho L - lactate	747 ± 135	13.09 *	7.57 ± 1.04	10113

Data represents mean ± S.E.M (N=2), Nagappa et al, (2019).

#Values taken from Collard et al., 2016

* V_{max} was calculated using k_{cat} values from Collard et al., 2016. Molecular mass values of 34540.68 Da and 34624.58 Da for murine PGP and Pho13, respectively was used in the calculation.

4.2.2.3 Generation of active site mutants for PbPGP

Active site mutants PbPGP_D49N was generated and the mutant was confirmed by sequencing (Fig. 4.8A). The mutant was expressed, purified (Fig. 4.8B) and assayed for activity with pNPP as substrate and was found to be inactive as compared to control (Fig. 4.8C). The mutant will be used to solve the structure of protein coupled to 2-phospho L-lactate or 2-phosphoglycolate.

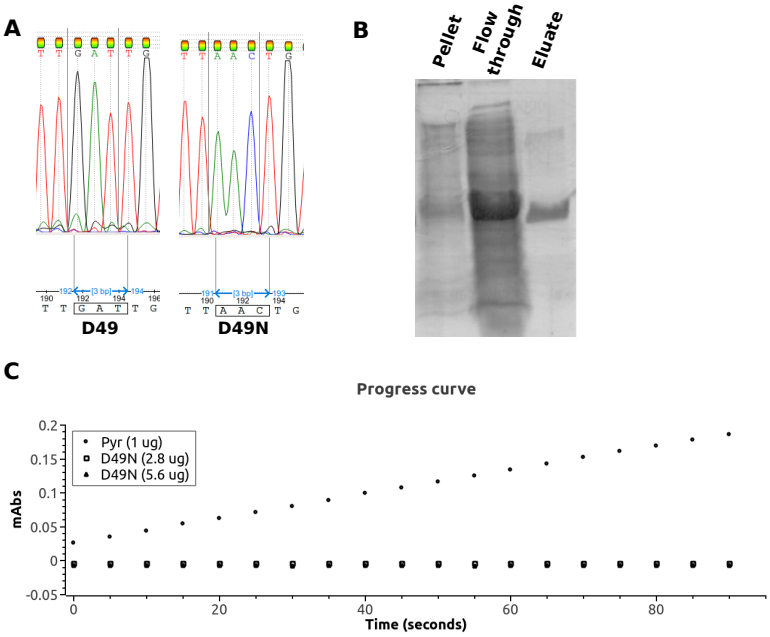

Figure 4.8: Generation, purification and activity measurement of PbPGP active site mutant

(A) Chromatogram showing the peaks corresponding to the desired mutation, PbPGP_D49N. (B) SDS-PAGE gel showing Ni-NTA purified PbPGP_D49N. (C) Progress curve of the assay for pNPP hydrolysis performed on mutants with wild type PfHADx (Pyr) as control.

4.2.2.4 Probing the essentiality of PbPGP and localization in *P. berghei*

pJAZZ linear knockout vector for PbPGP was generated by following the strategy described by Pfander *et al.* (Pfander et al., 2011). Drug-resistant parasites were not obtained in the first transfection attempt. In the second attempt, though drug-resistant parasites were obtained, genotyping by PCR revealed non-specific integration of the marker cassette. These parasites were positive by PCR for both the PbPGP gene and the hDHFR marker but were negative for specific 5' and 3' integration PCRs (Fig. 4.9).

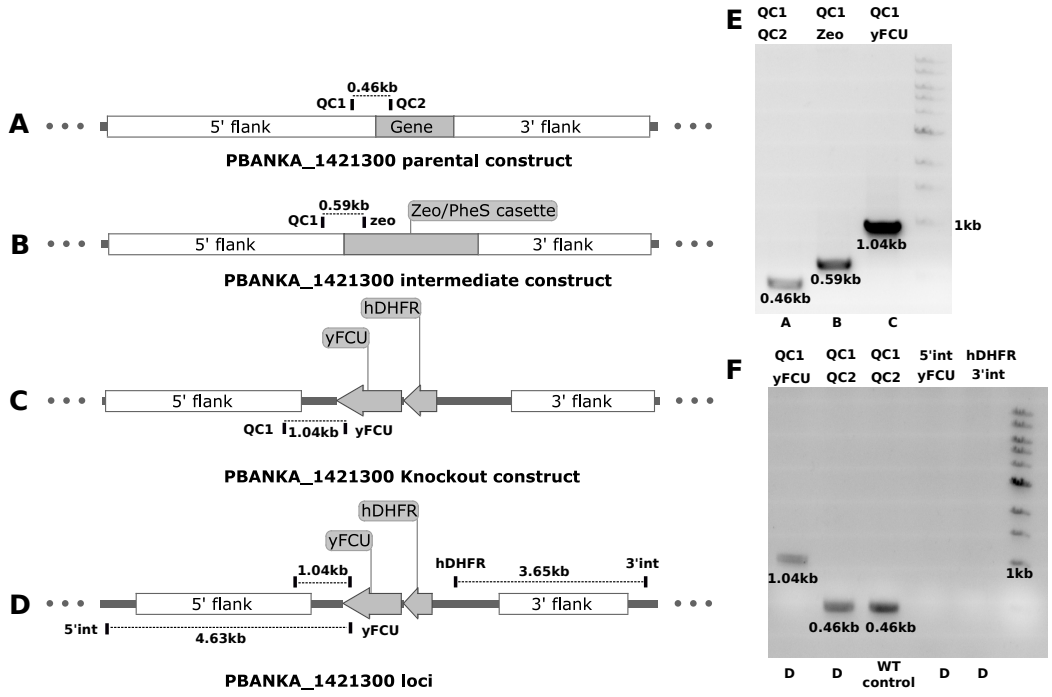

Figure 4.9: Generation of PbPGP knockout construct and knockout parasites

(A-D) Schematic representation of PbPGP parental, intermediate and final knockout constructs and PbPGP loci after integration. Primers are indicated in the schematic by vertical bars and expected PCR product size is represented by a line between specific primer pairs. (E) PCR confirmation of parental, intermediate and final knockout construct. Primer pairs used are indicated on top of the panel. A, B, and C below the panel refer to panels A-C in the figure. (F) Genotyping of the strain for the integration of cassette in the correct loci. D refers to the schematic of the loci of the transfectants from which the genomic DNA was isolated and 'WT control' refers to genomic DNA template isolated from untransfected parasites. Figure reproduced with permission from "Phosphoglycolate phosphatase is a metabolic proofreading enzyme essential for cellular function in *Plasmodium berghei*", Kempaiah Nagappa et al, 2019, Copyright © The American Society for Biochemistry and Molecular Biology, Inc.

To rule out that the locus is not refractory for recombination, parasites containing endogenously GFP-tagged PbPGP gene were generated in *P. berghei* using linear vectors with homology arms, generated by recombineering strategy (Godiska et al., 2009; Pfander et al., 2011) and their genotype was confirmed by PCR (Fig. 4.10). GFP signal was not seen upon microscopic examination of live cells due to a mutation in the GFP protein sequence close to the chromophore which rendered the tag non-fluorescent.

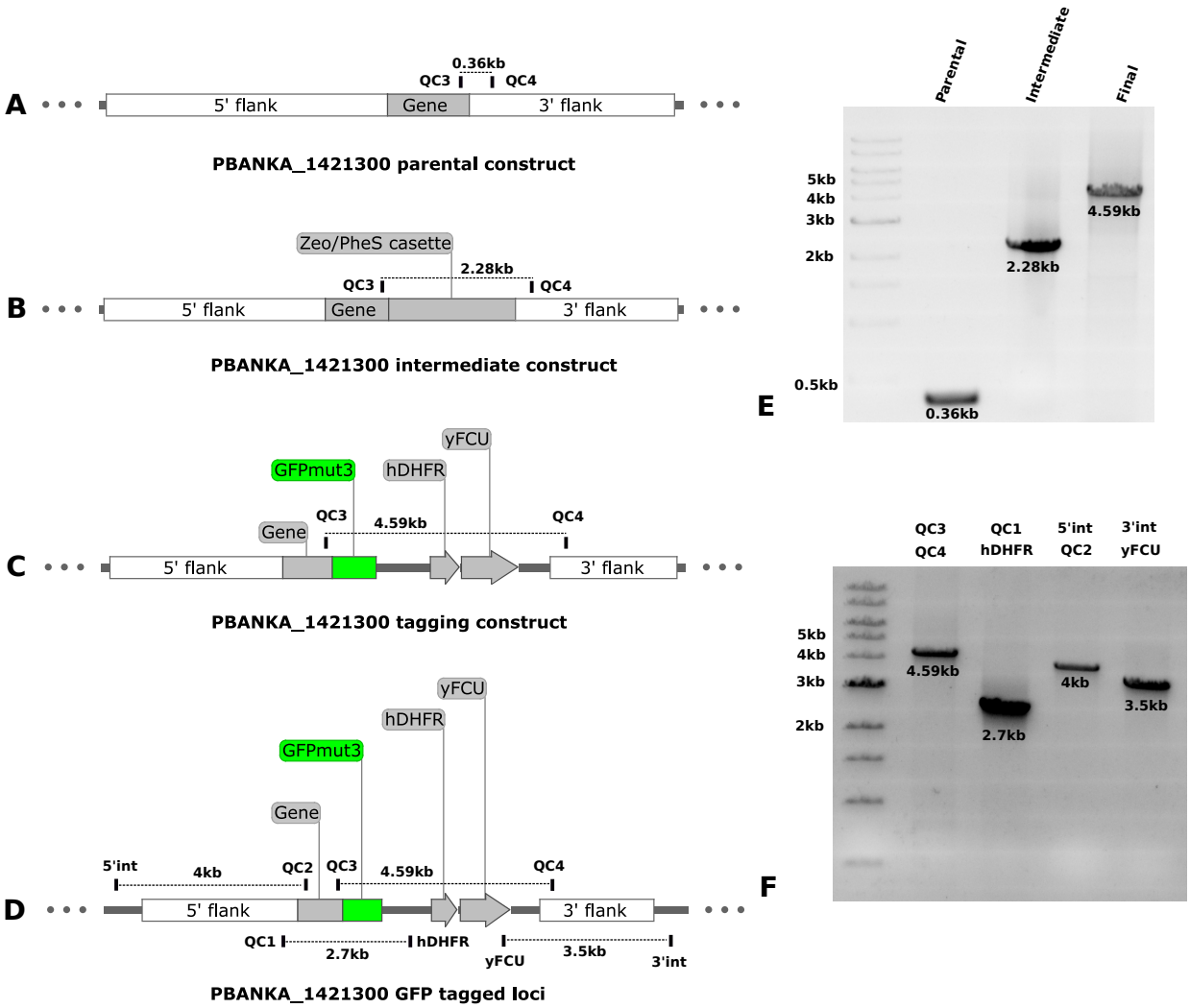

Figure 4.10: Generation of PbPGP GFP-tag construct and parasite

(A-D) Schematic representation of PbPGP parental, intermediate and final GFP-tagging constructs and PbPGP loci after integration. Oligonucleotide primers are indicated by vertical bars and expected PCR-product size is represented by a line between specific primer pairs. (E) PCR confirmation of parental, intermediate and final GFP-tagging construct. (F) Genotyping of the strain for the integration of cassette in the correct loci. Primer pairs used are mentioned on top of the panel.

Since it was not possible to obtain knockout parasites, a conditional knockdown (at the protein

level) strategy was employed by tagging the gene for PbPGP with a regulatable fluorescent affinity tag (RFA) where the stability of the fusion protein is conditional to the binding of the small molecule trimethoprim. The conditional knockdown vector was also generated by following the recombineering strategy and validated by PCR (Fig. 4.11). Transgenic parasites were obtained in the first transfection attempt itself and genotyping by PCR showed the presence of a single homogenous population with the correct insertion of RFA tag (Fig. 4.11F). Nevertheless, it was observed that the reduction in the levels of RFA-tagged protein upon removal of TMP, varied between 30-60 % across experiments and complete knockdown could not be achieved (Fig. 4.12A-C). As a consequence, there was no significant difference in growth rate between parasites grown in mice fed with or without trimethoprim (Fig. 4.12D and E). The transgenic RFA-tagged *P. berghei* parasites were also employed to determine the localization of PbPGP and upon microscopic observation, a cytosolic GFP signal was observed in all the intra-erythrocytic stages (Fig. 4.12F).

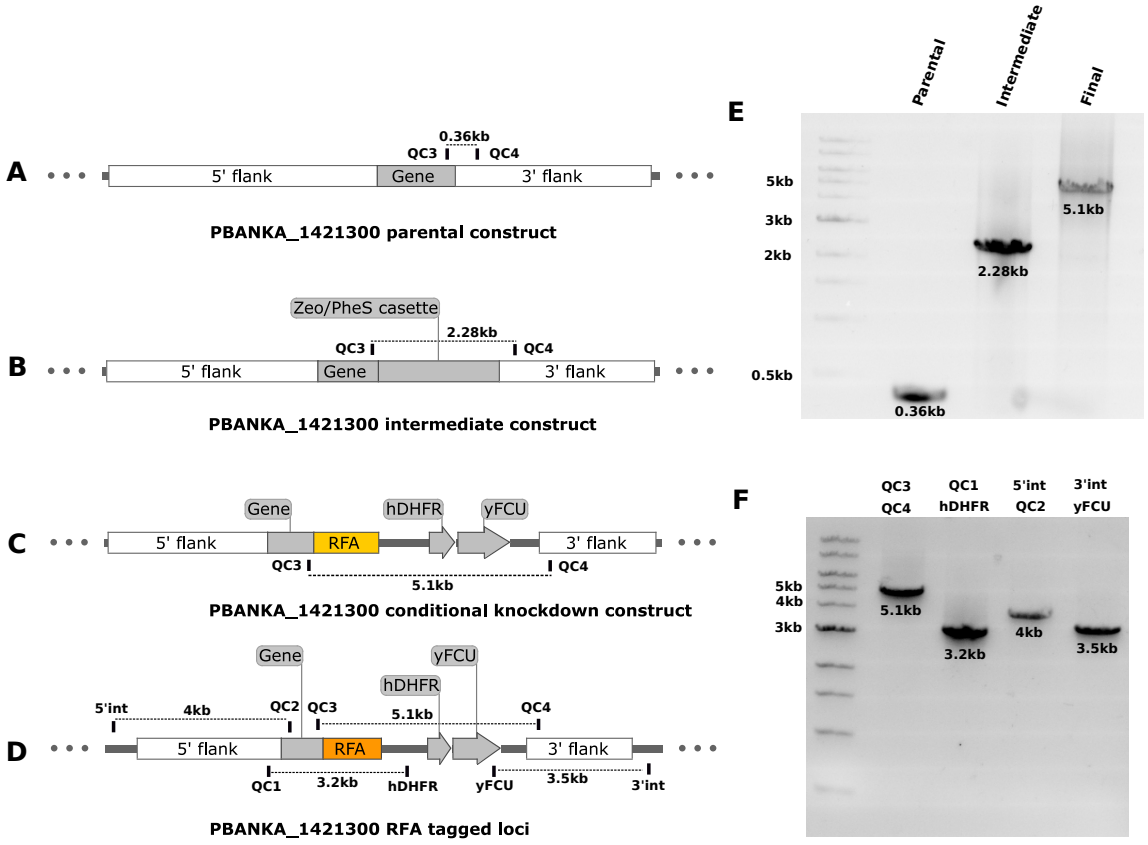

Figure 4.11: Generation of PbPGP conditional knockdown construct and parasite

(A-D) Schematic representation of PbPGP parental, intermediate and final RFA tagging constructs and PbPGP loci after integration. Oligonucleotide primers are indicated by vertical bars and expected PCR-product size is represented by a line between specific primer pairs. (E) PCR confirmation of parental, intermediate and final RFA-tagging construct. (F) Genotyping of the strain for the integration of cassette in the correct loci. Primer pairs used are mentioned on top of the panel. Figure reproduced with permission from "Phosphoglycolate phosphatase is a metabolic proofreading enzyme essential for cellular function in *Plasmodium berghei*", Kempaiah Nagappa et al, 2019, Copyright © The American Society for Biochemistry and Molecular Biology, Inc.

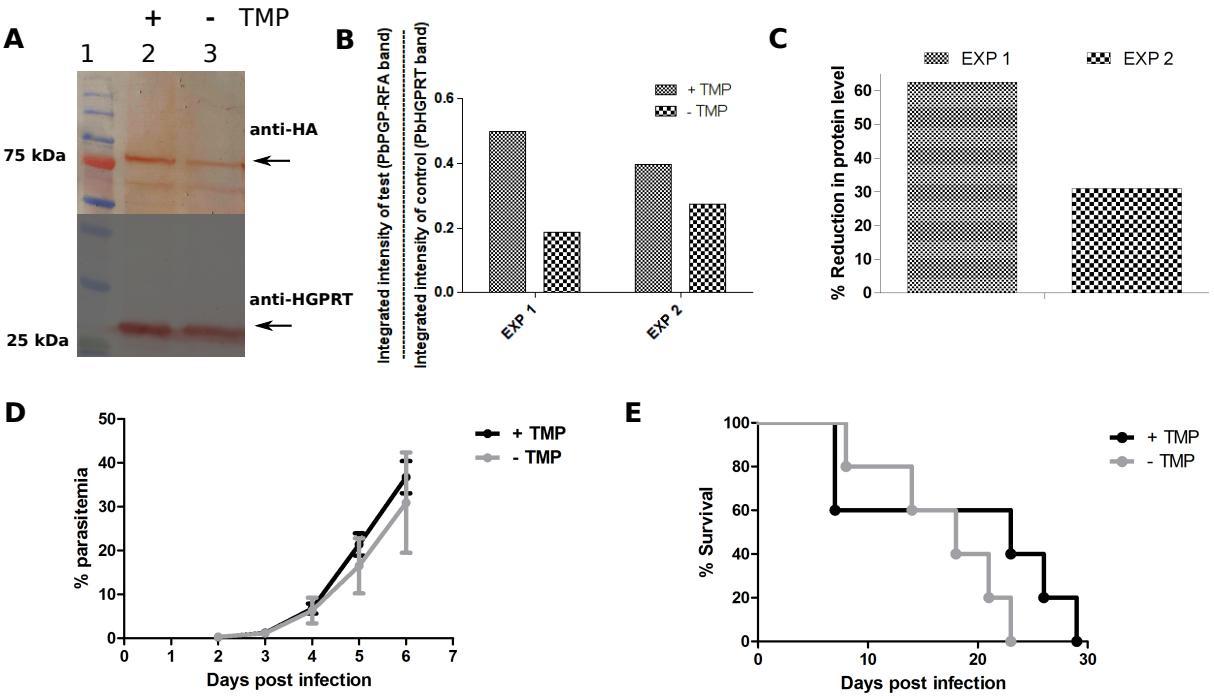

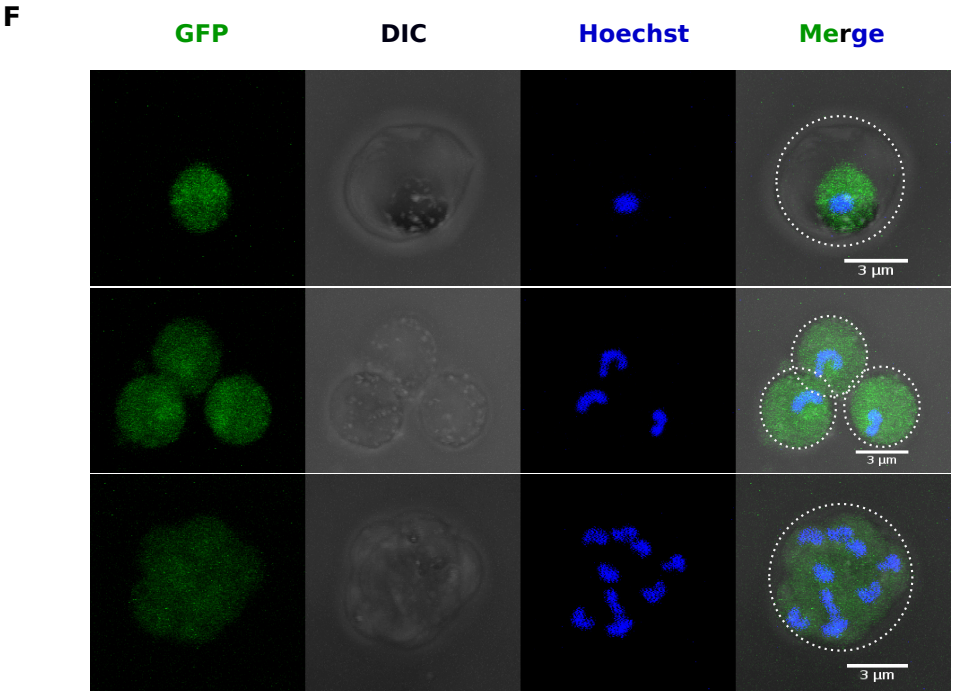

Figure 4.12: Phenotypic characterization of PbPGP conditional knockdown parasites and localization of PbPGP

(A) Western blot analysis of cell lysates of RFA-tagged parasites from mice fed with/without trimethoprim (TMP) (30 mg in 100 mL) for 6 days. The experiment was performed twice (Exp1 and Exp2) and blot from one experimental replicate is shown. The top panel is the blot probed with anti-HA antibody and the arrow mark indicates the RFA tagged PbPGP protein. The bottom panel was probed with anti-PfHGPRT antibody. (B) Ratio of the intensity of RFA tagged PbPGP to the intensity of control HGPRT. (C) Reduction in PbPGP levels upon removal of TMP relative to the levels in the presence of TMP. Protein levels under '+ TMP' condition was taken as 100 %. (D) Comparison of growth rates of PbPGP conditional knockdown *P. berghei* parasites grown in mice fed with or without trimethoprim (TMP). The data represents the mean ± s.d. values obtained from five mice each infected with 1.7 * 10^5 parasites. Statistical analysis was done using paired t-test using Graph Pad Prism V5 (P value = 0.1560, not significant). (E) Percentage survival of mice (n=5) infected with PbPGP RFA-tagged *P. berghei* parasites and fed with or without trimethoprim. The survival curves were found to be not significantly different according to the Log-rank (Mantel-cox) test (P value = 0.2765) and Gehen-Breslow-Wilcoxon test (P value = 0.6740). (F) Localization of PbPGP in PbPGP RFA-tagged parasites grown in '+ TMP' condition. The erythrocyte boundary is indicated by a white dotted line in the merge panel. Figure reproduced with permission from "Phosphoglycolate phosphatase is a metabolic proofreading enzyme essential for cellular function in *Plasmodium berghei*", Kempaiah Nagappa et al, 2019, Copyright © The American Society for Biochemistry and Molecular Biology, Inc.

4.2.3 Discussion

Earlier Knöckel *et al.* had performed a TBLASTN search and identified a potential 4-nitrophenylphosphatase in *P. falciparum*. The authors had proposed a novel role for this HADSF member and suggested involvement in vitamin B1 homeostasis (Knöckel et al., 2008). We found the *P. falciparum* 4-nitrophenylphosphatase sequence to have homology with human, mouse and yeast phosphoglycolate phosphatases. An extended substrate specificity screen of the recombinant *P. berghei* enzyme revealed that indeed this protein is phosphoglycolate phosphatase, which is mainly involved in detoxification, having very high activity on 2-phosphoglycolate and 2-phospho L-lactate with no activity on thiamine monophosphate. 2-phosphoglycolate is reported to be formed during repair of free radical mediated damage of DNA ends (Pellicer et al., 2003) and accumulation of this metabolite in the cell, leads to inhibition of the key glycolytic enzyme triosephosphate isomerase (TIM) (Fig. 4.13). Studies on phosphoglycolic acid phosphatases from yeast and mouse have demonstrated that this enzyme also performs metabolic proof-reading by catabolizing the substrates 2-phospho L-lactate and 4-phosphoerythronate which are products of enzymatic side reactions. The activity of PbPGP on 4-phosphoerythronate could not be tested due to the non-availability of the compound. 2-phospho L-lactate, generated by phosphorylation of L-lactate by pyruvate kinase, is known to inhibit phosphofructokinase and 4-phosphoerythronate, which is a product of GAPDH side reaction, is known to inhibit 6-phosphogluconate dehydrogenase (Fig. 4.13) (Collard et al., 2016). Due to the detrimental effect of these metabolites, it becomes essential to clear the cell of these metabolic toxins. This is reflected upon by the fact that phosphoglycolate phosphatase is an essential gene in mouse (Segerer et al., 2016). Also,

in *Arabidopsis*, knockout of PGLP1 isoform leads to impaired post-germination development of primary leaves (Schwarte and Bauwe, 2007).

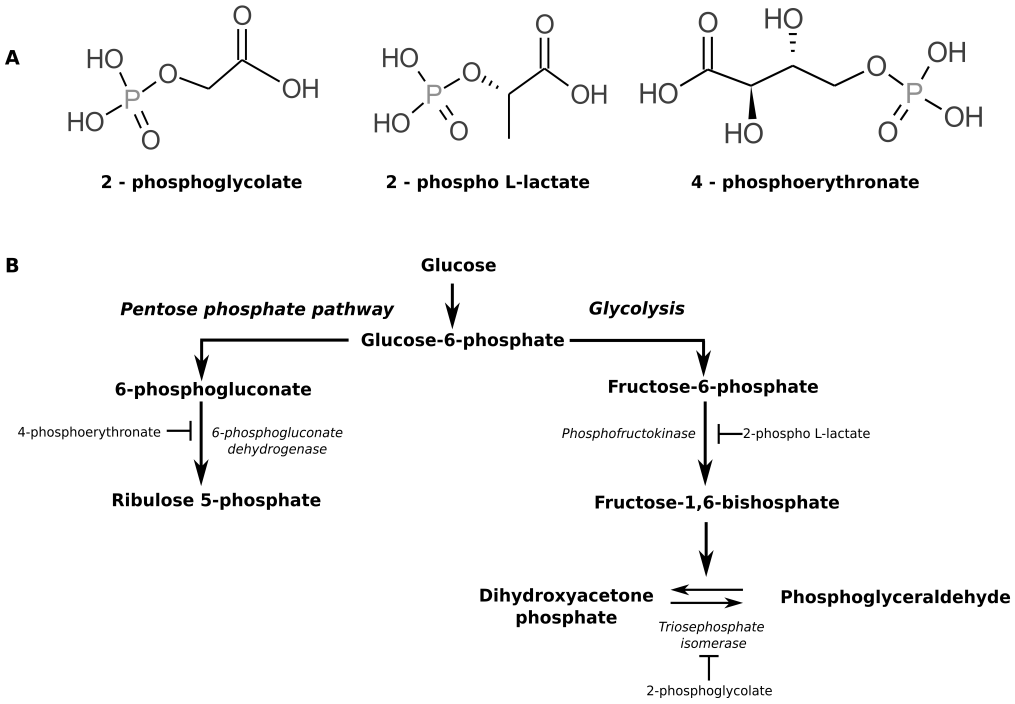

Figure 4.13: Metabolites that are substrates for phosphoglycolate phosphatase (A) and their inhibition of key metabolic pathways (B)

Figure reproduced with permission from "Phosphoglycolate phosphatase is a metabolic proofreading enzyme essential for cellular function in *Plasmodium berghei*", Kempaiah Nagappa et al, 2019, Copyright © The American Society for Biochemistry and Molecular Biology, Inc.

Plasmodium in its intra-erythrocytic stages experiences very high levels of oxidative stress (Atamna and Ginsburg, 1993) leading to an increased ROS production that can damage its DNA, the repair of which will result in generation and accumulation of 2-phosphoglycolate. The parasite performs lactic acid fermentation and secretes large amounts of lactate into the medium, most of which is L-lactate (93-94 %), in addition to a small proportion of D-lactate (6-7 %) that is known to be produced through the methylglyoxal pathway (Vander Jagt et al., 1990). This lactate can accumulate and be phosphorylated in the cell to give rise to 2-phospholactate. In a recent study, *Dumont et al.,* through metabolite profiling of wild type and *Δpfpgp P. falciparum* concluded that PfPGP has specificity for 2-phospho D-lactate while our studies contradict this inference and provide direct evidence for the sole substrate specificity for the L-isomer. In their experiment, *Δpfpgp* parasites when grown under normal culture conditions or in the presence of 2 mM L-lactate showed a similar 12 fold higher accumulation of phospholactate when compared with wildtype parasites grown under the same culture conditions. However, in the presence of increasing concentrations of D-lactate in the culture medium, they observed a dose-dependent increase in the accumulation of phospholactate that is not significantly different between wild type

and *Δpfpgp* parasites. Although this rules out the absence of PfPGP activity being the cause for 2-phospho D-lactate accumulation, the authors have concluded that PfPGP utilizes 2-phospho D-lactate as a substrate (Dumont et al., 2018). The physiological reasons for these observations of Dumont *et al.,* can be rationalized in the following manner. As L-lactate is the predominant isomer produced in high concentrations in the cell, externally added L-lactate may not be taken up inside the cell or even if taken up, might not significantly perturb intracellular L-lactate concentration. Therefore, in the experiment of Dumont *et al.,* the addition of L-lactate to the culture medium did not lead to an increase in levels of phospholactate in wild type or *Δpfpgp* parasites (Dumont et al., 2018). Whereas, D-lactate is produced in the parasite at very low levels and exogenously added D-lactate might be acted upon by pyruvate kinase to form 2-phospho D-lactate. This can happen in both wild type and *Δpfpgp* parasites and the absence of significant difference in levels of phospholactate accumulation between wild type and *Δpfpgp* parasites when grown in the presence of D-lactate (Dumont et al., 2018) is expected as our studies show that PGP is specific for only 2-phospho L-lactate. Further, Dumont *et al.* perform metabolite profiling of wt and *Δglo1* (impaired in D-lactate production) parasites in the presence of methyl glyoxal in the culture medium and observe similar levels of phospholactate accumulation in both parasites. The authors justify this observation by speculating that either methly glyoxal is converted to D-lactate by the erythrocyte and then transported to the parasite or is directly converted to D-lactate in the parasite by the involvement of apicoplast glyoxalase-1 (Dumont et al., 2018). Either way, D-lactate levels in the parasite increase, gets phosphorylated and accumulates in both wildtype and *Δglo1* parasites as phospholactate, in-spite of the presence of PGP gene. This again goes to show that PGP does not act on the D-isomer. As pyruvate kinase is known to have a higher binding affinity for D-lactate when compared to that for L-lactate (Nowak and Mildvan, 1972), accumulation of phospholactate in wildtype and *Δpfpgp* parasites grown on D-lactate and parasites grown on methylglyoxal could be a consequence of the preferential activity of pyruvate kinase on D-lactate. The indirect inferences provided by Dumont *et al.*, are akin to a 'phenocopy' witnessed as a consequence of pyruvate kinase activity on D-lactate, rather than a true phenotype associated with phosphoglycolate phosphatase deficiency. Our results on the purified enzyme directly show that PbPGP acts only on 2-phospho L-lactate and not on 2-phospho D-lactate (Fig. 4.6A). We further validated this by performing enzyme assays with 1 mM 2-phospho L-lactate in the presence or absence of 10 mM 2-phospho D-lactate. The absence of a significant change in specific activity clearly shows that 2-phospho D-lactate does not bind to the enzyme (Fig. 4.7D). This observation is consistent with that of the murine homolog of PbPGP that also acts only on 2-phospho L-lactate (Collard et al., 2016). In addition to the above evidence, the possible difference in substrate specificity across the enzymes from the two *Plasmodium* species, *P. falciparum* and *P. berghei* was also addressed by taking recourse to sequence and structural analysis of the proteins. Both proteins are highly identical and residues around the four HAD motifs are highly conserved (Fig. 4.14A). Both protein sequences were subjected to homology modelling and both modelled structures aligned without any gross structural differences (Fig.

4.14B and C). This strongly suggests that PfPGP like PbPGP would also have specificity for only 2-phospho L-lactate.

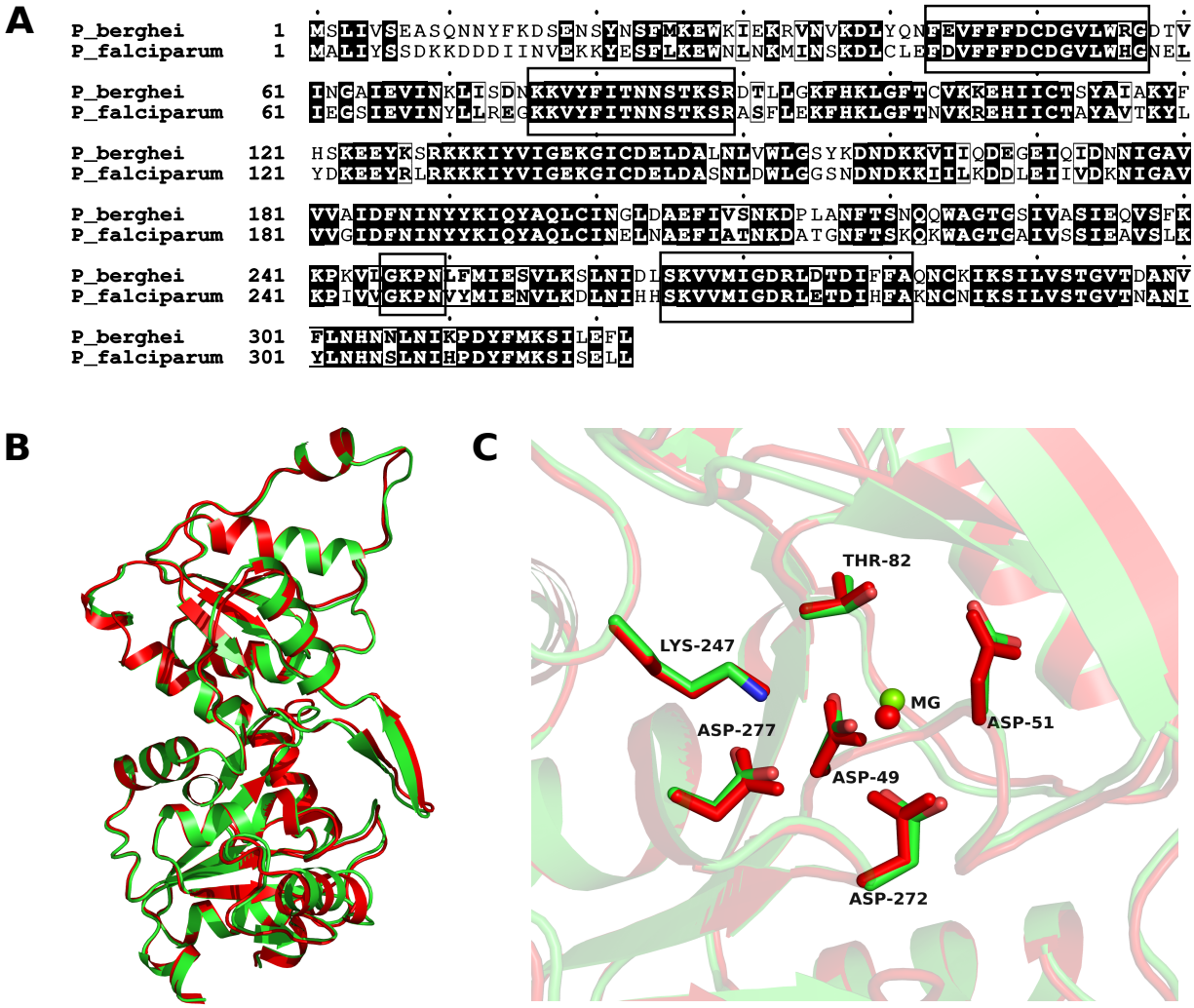

Figure 4.14: Sequence analysis and homology modelling of phosphoglycolate phosphatase

(A) Pair-wise alignment of Pf and Pb phosphoglycolate phosphatase protein sequences. Residues around the conserved HAD motifs are enclosed in black boxes. (B) Superposition of PfPGP and PbPGP structures modelled using SWISS-MODEL and 4BKM (PDB id.) as template. PfPGP is colored green and PbPGP is colored red. (C) Zoomed in view of the active site pocket showing key residues of the HAD motifs. Figure reproduced with permission from "Phosphoglycolate phosphatase is a metabolic proofreading enzyme essential for cellular function in *Plasmodium berghei*", Kempaiah Nagappa et al, 2019, Copyright © The American Society for Biochemistry and Molecular Biology, Inc.

Recombinant human pyruvate kinase M2 isoform has been shown to phosphorylate L-lactate leading to the production of 2-phospho L-lactate that was in turn, shown to inhibit phosphofructokinase-2 activity in crude lysates of HCT116 cells and activity of recombinant phosphofructokinase-fructose 1,6-bisphosphatase (PFKFB) isozymes, PFKFB3 and PFKFB4 (Collard et al., 2016).

Interestingly, in yeast, knockout of PHO13 (PGP homolog) is viable as yeast performs alcohol fermentation instead of lactate fermentation and hence does not accumulate phospholactate. Also, the inhibition of pentose-phosphate pathway caused by accumulation of 4-phospho D-erythronate is countered by transcriptional up-regulation of pentose-phosphate pathway enzymes (Collard et al., 2016). *Plasmodium* has two genes coding for phosphofructokinase, one on chromosome 9 (PfPFK9) and the other on 11 (PfPFK11) and only PfPFK9 has been shown to be functional. It has been reported that unlike the host enzyme, PfPFK9 lacks regulation by fructose 1,6-bisphosphate, phosphoenolpyruvate and citrate (Mony et al., 2009). In such a scenario, we speculate that 2-phospho L-lactate might directly inhibit PfPFK9 to regulate glycolysis as knockout of PbPGP is not possible. This selective mode of regulation might be unique to *Plasmodium*.

In *Plasmodium*, where glycolysis is the sole source of ATP in asexual stages (Mehta et al., 2006), the parasite cannot afford inhibition of its critical enzymes such as PFK and TIM arising from accumulation of toxic metabolites. Hence, having a metabolic proof-reading/detoxifying enzyme becomes vital for its survival. Inability to obtain knockout parasites indicates essentiality of this protein for parasite survival during asexual stages. Regulatable fluorescent affinity (RFA) tagging was attempted and a homogenous population of transfectants with RFA-tag integrated at the right loci was obtained. Having established that the locus is amenable for genetic manipulation, conditional knockdown strategy at protein level making use of the RFA tag (Muralidharan et al., 2011) was adopted. Conditional knockdown at the protein level showed only 30-60 % reduction and hence parasites were viable (Fig. 4.12A-E). A similar observation has been described for yoelipain where the authors were neither able to knockout nor achieve significant knockdown of protein levels to see growth difference. Therefore, it was concluded that the gene was essential during intra-erythrocytic stages (Pei et al., 2013). Our results are similar and indicate essentiality of PbPGP in asexual stages. This conclusion on the gene essentiality of PbPGP is in agreement with the findings of Dumont *et al.,* on PfPGP where, *Δpfpgp* parasites show growth defect (Dumont et al., 2018). Further biochemical and structural studies on PGP could pave the way for rational design of inhibitors with potent antimalarial activity.

4.3 Studies on HAD2, HADx and HAD3

4.3.1 Introduction

PvHAD2 is a type IIb member of HAD superfamily with all the conserved catalytic motifs (Srinivasan et al., 2015). The crystal structure of PvHAD2 was solved and deposited (PDB id. 2B30) in PDB database by Structural Genomics of Pathogenic Protozoa Consortium (SGPP). Biochemical characterization of this protein revealed it to be a dimer acting on β-glycerophosphate and pyridoxal 5´-phosphate in addition to AMP, XMP and dAMP (Srinivasan et al., 2015). Recently it has been shown that mutations in PfHAD2 lead to the development of fosmidomycin resistance in *in vitro* cultured *P. falciparum*. Since PfHAD2 was shown to be hydrolyzing nucleotide monophosphates it has been proposed that mutation in this enzyme rendering it inactive might increase intracellular levels of nucleotides that can activate phosphofructokinase-9, thereby increasing the flux through MEP pathway and resulting in fosmidomycin resistance (Guggisberg et al., 2018). Nevertheless, the essentiality of HAD2 was not determined. In the current study, this question has been answered. HADx is a type Ia member of HAD superfamily that was previously uncharacterized while, HAD3 is a type IIb member of HAD superfamily. Although PfHAD3 protein sequence has been reported to possess 30% identity and approximately 50% similarity with PfHAD1 its function remains unknown (Guggisberg et al., 2014a). Due to low sequence conservation among HADSF members (Fig. 4.15) its highly challenging to predict function based on sequence homology alone. Adding to this difficulty is the broad substrate specificity of HADSF members which, renders the task of assigning physiological role an elaborate one. Screening a huge number of compounds to identify relevant physiological substrates becomes imperative to understand structure-function of HADSF members and the same approach has been adopted in the current study.

A

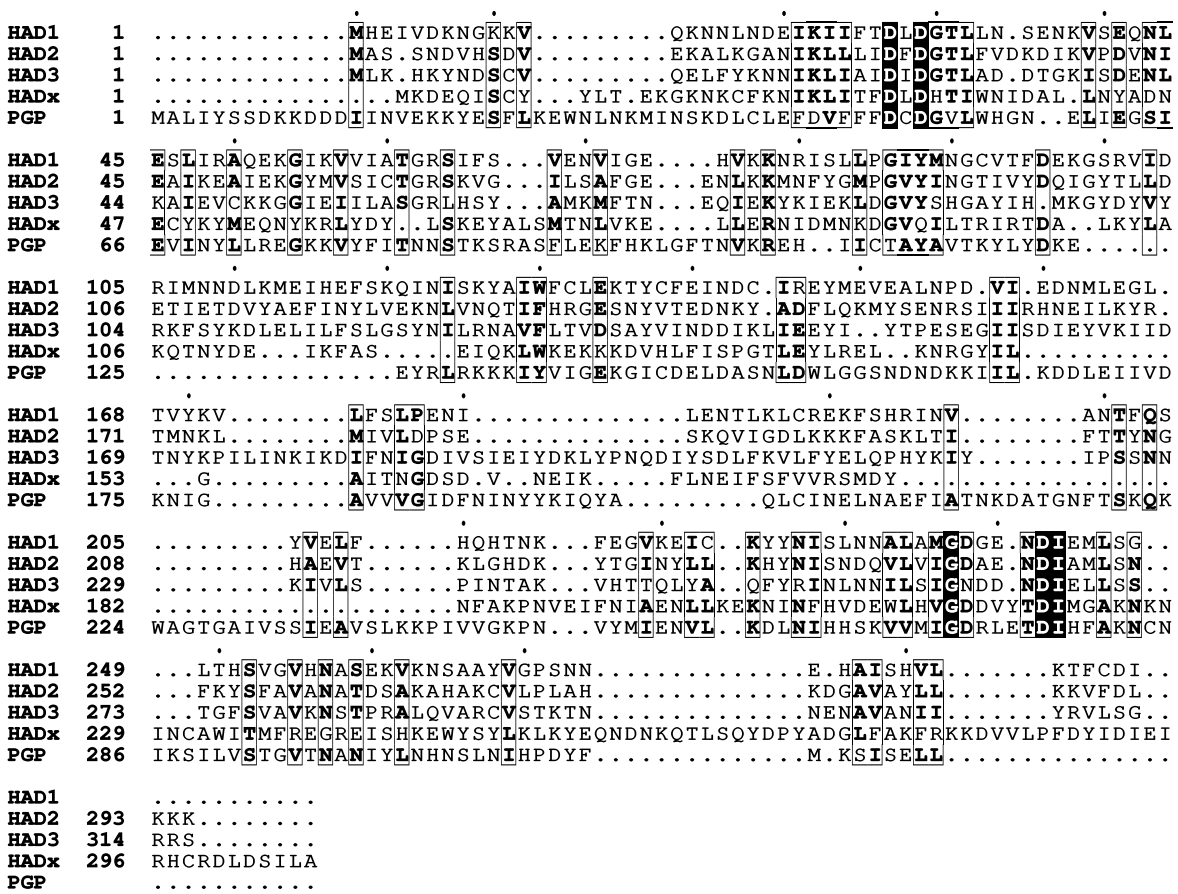

B

	HAD1	HAD2	HAD3	HADx	PGP
HAD1	100	28.92	23.94	16.46	18.80
HAD2	28.92	100	24.40	18.55	21.03
HAD3	23.94	24.40	100	13.15	13.03
HADx	16.46	18.55	13.15	100	20.17
PGP	18.80	21.03	13.03	20.17	100

Figure 4.15: Multiple sequence alignment of PfHAD 1-3, HADx and PGP protein sequences

(A) Clustal omega alignment of HADSF members from *Plasmodium*. (B) Percentage identity matrix showing the extent of homology between the sequences.

4.3.2 Results

4.3.2.1 Expression and purification of recombinant PfHADx

The HAD family members PfHAD3 and PfHADx were cloned in pET vectors by the restriction digestion and ligation strategy. The clones were confirmed by PCR, restriction mapping

and sequencing. Upon expression in Rosetta DE3 pLysS strain of *E. coli,* followed by Ni-NTA chromatography it was found that only PfHADx was soluble and PfHAD3 was completely in the insoluble fraction (Fig. 4.16A and B). Using protein solubility prediction software PROSOII we found that homologues of PfHAD3 from other *Plasmodium* species were also predicted insoluble (Fig. 4.16C). Hence HAD3 could not be biochemically characterised.

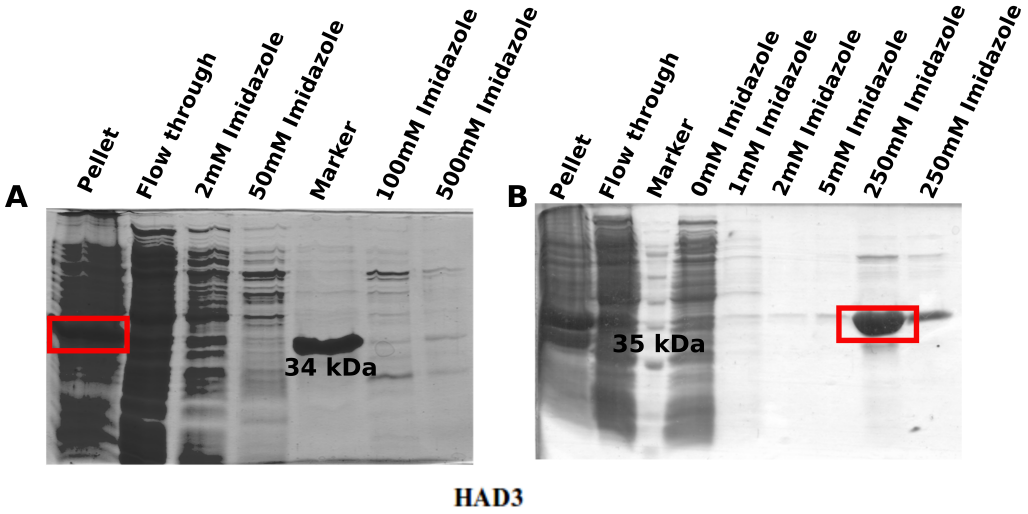

C

Gene Id	Predicted class	Solubility score
PF3D7_1226100	Insoluble	0.262
PKNH_1445500	Insoluble	0.472
PVX_123935	Insoluble	0.302
PBANKA_1441000	Insoluble	0.293
PY17X_1443500	Insoluble	0.312
PCHAS_1443000	Insoluble	0.22
PCYB_145180	Insoluble	0.475

Figure 4.16: Purification of *Plasmodium* HADSF members

(A) Purification of recombinant PfHAD3 using Ni-NTA agarose, analysed by SDS-PAGE. (B) Purification of recombinant PfHADx using Ni-NTA agarose, analysed by SDS-PAGE. *Methanocaldococcus jannaschii* ATPPase (34 kDa) that was earlier purified in the laboratory was used as a molecular mass marker in panel A. Protein present in insoluble fraction or soluble fraction is indicated in the red box. (C) Solubility indices for HAD3 homologues from different *Plasmodium* species as predicted by PROSOII.

PfHADx was further purified by anion-exchange chromatography using Q-sepharose beads (Fig. 4.17). The fractions obtained after anion-exchange chromatography were pooled and dialysed against 20 mM Tris HCl, pH 8 containing 10 % glycerol and 1 mM DTT.

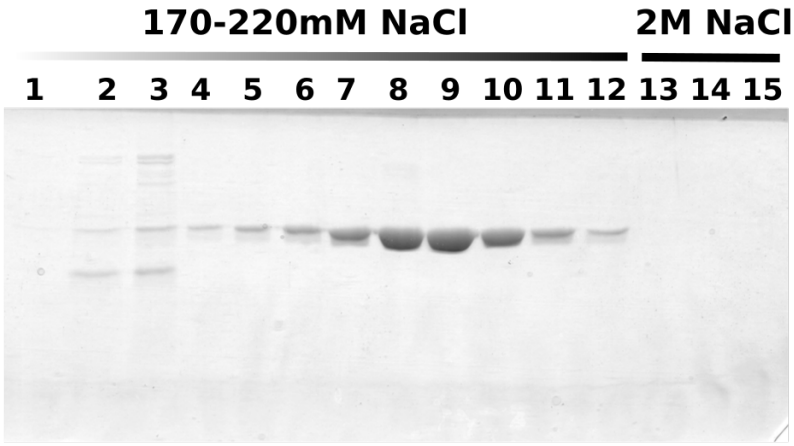

Figure 4.17: Elution profile of PfHADx after Q-sepharose anion exchange chromatography, analysed by SDS-PAGE

Fractions from anion-exchange chromatography analysed on SDS-PAGE. PfHADx eluted in buffer containing 170-220 mM NaCl.

4.3.2.2 Far-UV CD spectra of PfHADx

The circular dichroism spectrum of PfHADx was acquired using Jasco J - 810 spectropolarimeter (Fig. 4.18). The spectrum was analysed using K2D2 server and the protein was found to be comprised of 30 % α – helix.

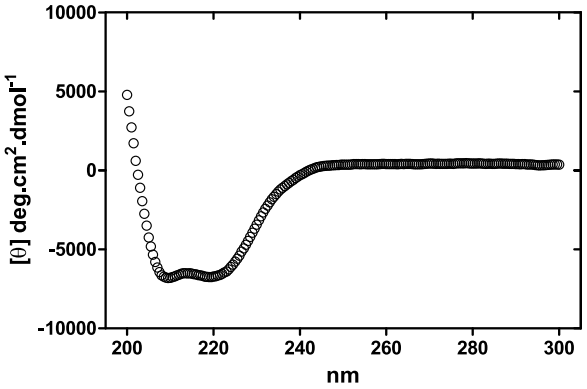

Figure 4.18: Far-UV CD spectrum of PfHADx

Analysis of the secondary structure of PfHADx by far-UV CD spectroscopy.

4.3.2.3 Determination of oligomeric status of PfHADx by analytical size-exclusion chromatography

PfHADx on analytical gel filtration using Sephacryl S-200 column showed a mass of about 42.5 kDa, whereas the theoretical mass is 37 kDa, indicating that the protein is a monomer (Fig.

4.19A and B).

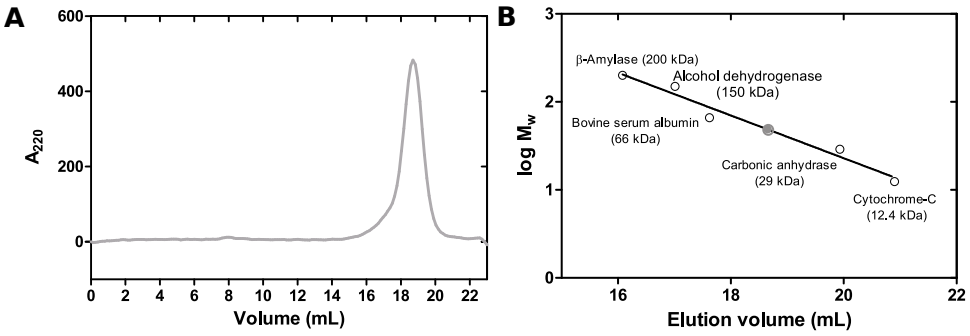

Figure 4.19: Analytical size-exclusion chromatography

Determination of the oligomeric state of PfHADx. (A) Elution profile of PfHADx. (B) Molecular mass calibration curve with elution volume of PfHADx interpolated.

4.3.2.4 Biochemical characterization of PfHADx

A total of 36 compounds were used for the substrate screen for PfHADx, that showed high activity for purine nucleotides followed by a significant activity on pyrimidine nucleotides and co-enzymes such as PLP and FMN. The protein also showed weak activity on sugar phosphates indicating that it has broad substrate specificity (Fig. 4.20). The protein did not show activity on 3´ nucleotides, amino acid phosphates etc.

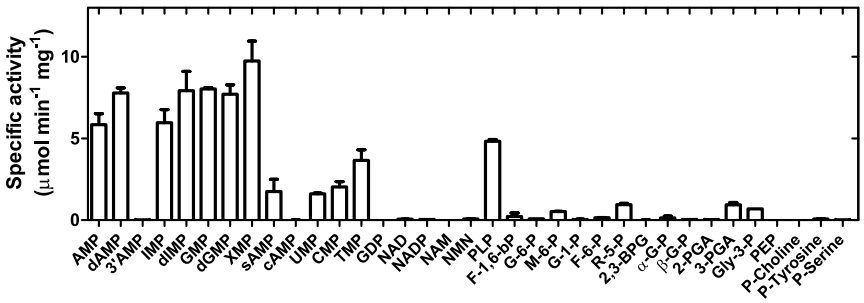

Figure 4.20: Identification of physiological substrates

Screen for potential substrates of PfHADx. Mean specific activity values are provided for each substrate and error bars represent SD (n=2). AMP, adenosine 5' monophosphate; dAMP, deoxy adenosine 5' monophosphate; 3'AMP, adenosine 3' monophosphate; IMP, inosine 5' monophosphate; GMP, guanosine 5' monophosphate; XMP, xanthosine 5' monophosphate; cAMP, 3' 5' cyclic AMP; UMP, uridine 5' monophosphate; CMP, cytidine 5' monophosphate; TMP, thymidine 5' monophosphate; GDP, guanosine diphosphate; NADP, nicotinamide adenine dinucleotide phosphate; NAM, nicotinic acid mononucleotide; NMN, nicotinamide mononucleotide; FMN, flavin mononucleotide; F-1,6-bp, fructose 1,6-bisphosphate; G-6-P, glucose 6-phosphate; M-6-P, mannose 6-phosphate; G-1-P, glucose 1-phosphate; F-6-P, fructose 6-phosphate; R-5-P, ribose 5-phosphate; 2,3-BPG, 2,3-bisphosphoglycerate; DHAP, dihydroxyacetone phosphate; PEP, phosphoenolpyruvate.

Among the five salts screened, $MgCl_2$ was found to be the most preferred salt for PfHADx (Fig.4.21A) using GMP as substrate. This was also repeated using pNPP as substrate (Fig. 4.21B).

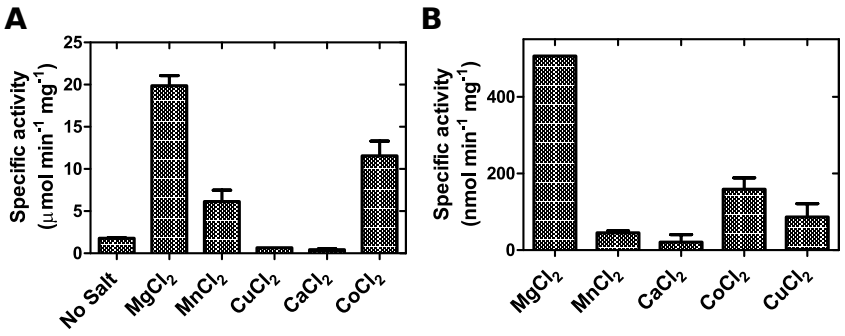

Figure 4.21: Screening for preferred divalent metal ion

Histogram showing the activity of PfHADx in the presence of salts of various divalent cations using GMP (A) and pNPP (B) as substrates.

PfHADx was found to have an optimum pH of 6.5 when GMP was used as substrate (Fig. 4.22A). Also, it was found that when pH exceeded 6.5, the drop in activity was due to change in ionization status of the enzyme and drop in the activity below pH 6.5 was due to irreversible structural changes in the protein as shown by pH stability experiments (Fig. 4.22G). pH titration plots for substrates other than GMP are also provided (Fig. 4.22B-F).

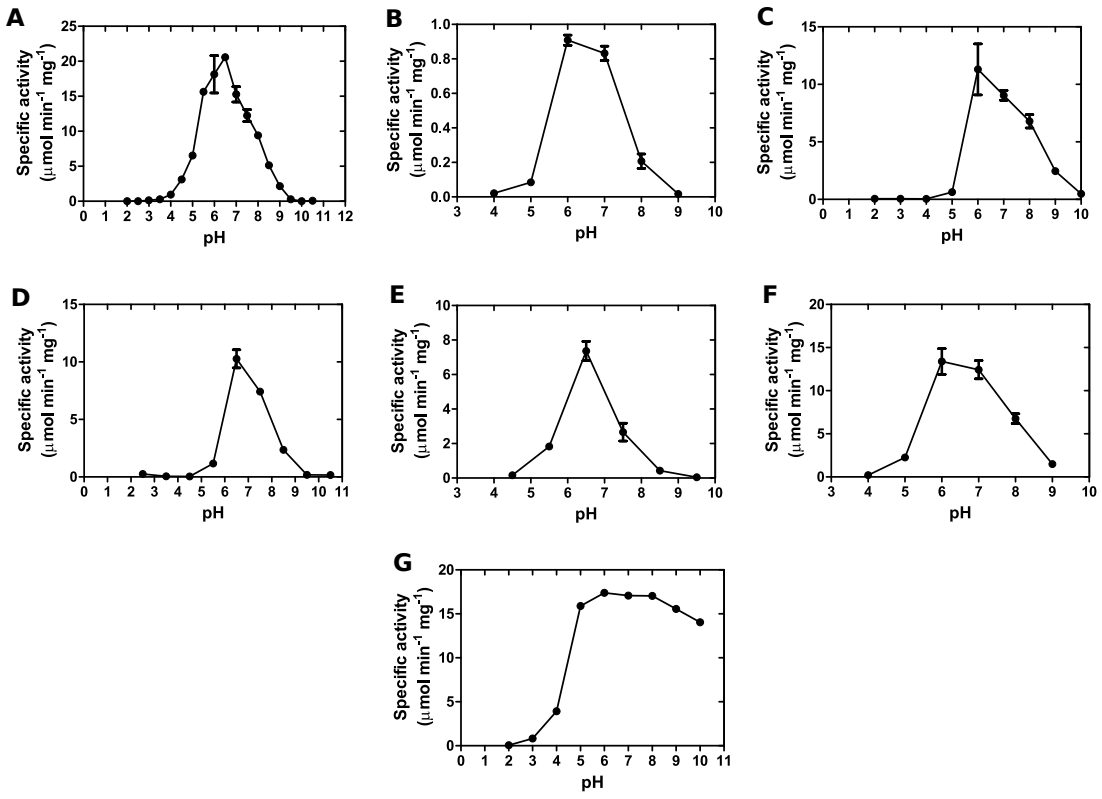

Figure 4.22: pH profile of PfHADx

pH titration plots for PfHADx using different substrates (A) GMP (B) 3-phosphoglyceric acid, (C) IMP, (D) PLP, (E) UMP and (F) XMP. (G) Determination of pH-dependent enzyme stability. Activity measurement of PfHADx incubated at different pH followed by assay at optimum pH.

Substrate titrations were carried out using purine and pyrimidine nucleotides and sugar-phosphate to determine K_{m}, V_{max} and catalytic efficiency of PfHADx towards different substrates. PfHADx displayed the highest catalytic efficiency towards purine nucleotides followed by pyrimidine nucleotides. The substrate vs activity plots for various substrates are shown below (Fig. 4.23). A histogram has been provided for comparison of catalytic efficiency of the enzyme with various substrates (Fig. 4.24). It was found that the enzyme showed a hyperbolic profile for all the substrates except IMP and pNPP which showed substrate inhibition pattern. Interestingly, dIMP showed hyperbolic pattern unlike, IMP.

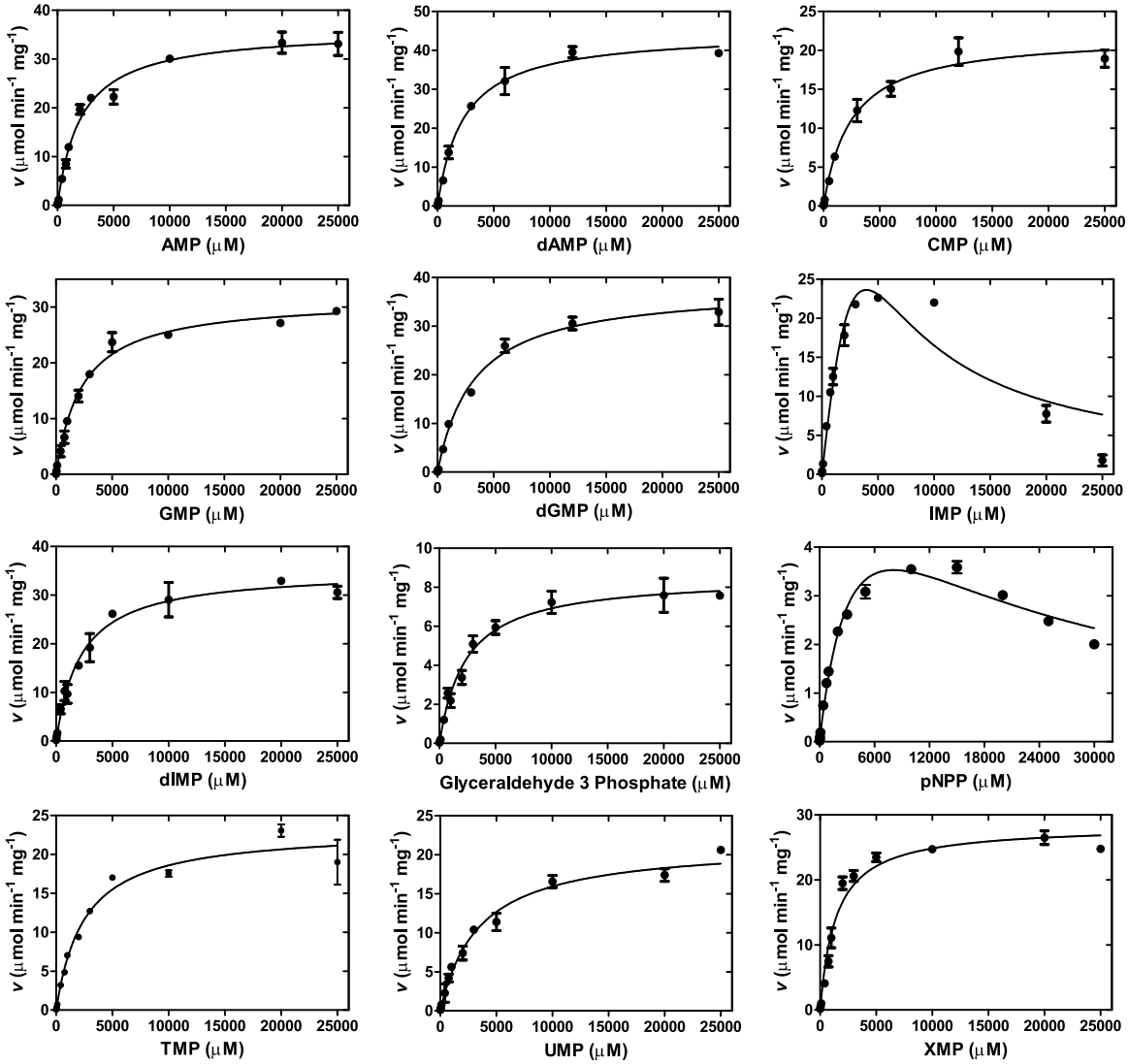

Figure 4.23: Substrate *vs* initial velocity plots for PfHADx with different substrates

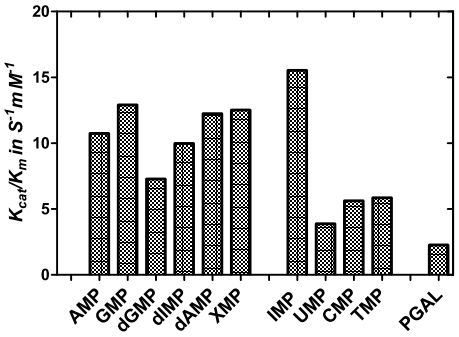

Figure 4.24: Comparison of the catalytic efficiency of PfHADx towards various substrates

Phosphate was found to be a competitive inhibitor for PfHADx with a K_i value of 20 μM (Fig. 4.25). The plots were fitted to the equation for competitive inhibition.

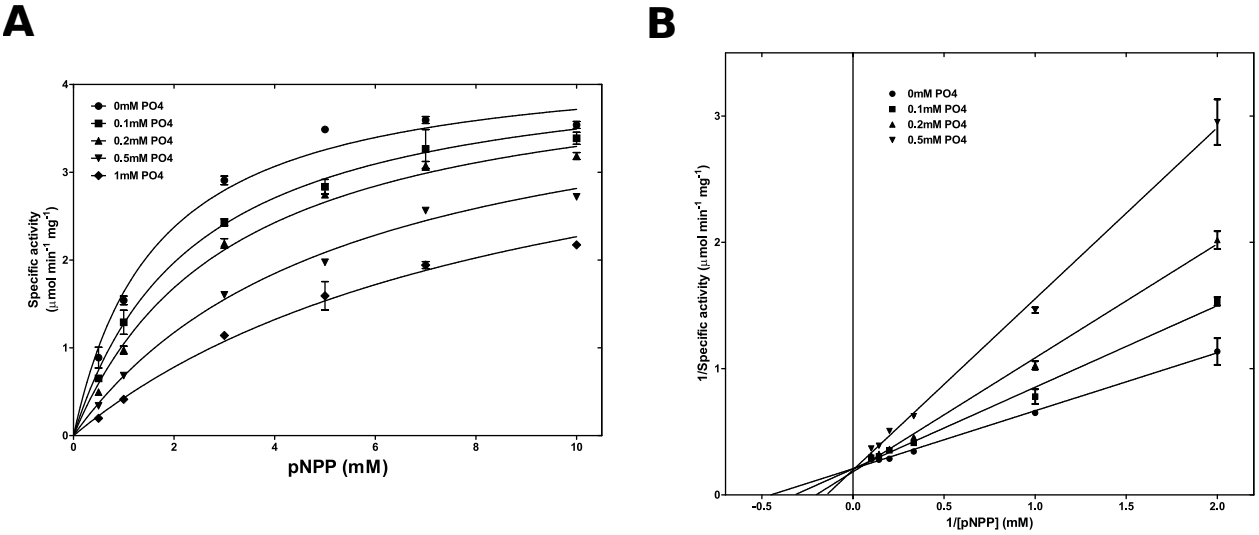

Figure 4.25: Inhibition kinetics on PfHADx

Substrate concentration vs. specific activity plots at different fixed inhibitor concentration fit to competitive inhibition model (A) and double reciprocal plot of the same data (B)

4.3.2.5 Generation of active site mutants for PfHADx

Active site mutants PfHADx_D29N was generated and the mutant was confirmed by sequencing (Fig. 4.26A). The mutant was expressed, purified (Fig. 4.26B) and assayed for activity with pNPP as substrate and was found to be inactive even after using 10 times the amount of enzyme

used for wildtype (Fig. 4.26C). This mutant will be used to obtain the structure of the ligand-bound enzyme.

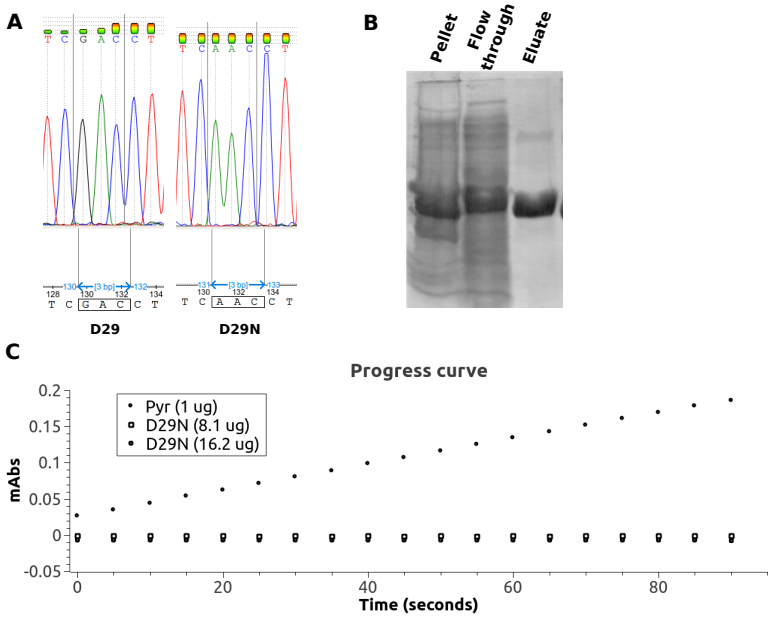

Figure 4.26: Generation, purification and activity measurement of PfHADx active site mutant

(A) Chromatogram showing the peaks corresponding to the desired mutation, PfHADx_D29N. (B) SDS-PAGE gel showing Ni-NTA purified PfHADx_D29N. (C) Progress curve of the assay for pNPP hydrolysis performed on mutants with wild type PfHADx (Pyr) as control.

4.3.2.6 Antibody generation and indirect immunofluorescence to determine the localization of PfHADx

Antibody raised in rabbit was used to determine the titre by dot blot (Fig. 4.27A). The pre-immune serum did not give any signal whereas immune serum gave a significant signal even at a dilution of 1:20000. *P. falciparum* parasites at early trophozoite to schizont stage were harvested and immunofluorescence microscopy was performed. Antibody concentration and dilution were normalized across pre-immune control and antigen-specific antibody. Secondary antibody was goat anti-rabbit which was coupled to the fluorophore Alexa488 (excitation 495 nm and emission 519 nm). DAPI (excitation 358 nm and emission 461 nm) was used for nuclear staining. In pre-immune control, the signal was not seen in the parasitized erythrocytes. Whereas with the immune serum diffused cytosolic signal was seen in parasitized erythrocytes and not in uninfected erythrocytes (Fig.4.27B).

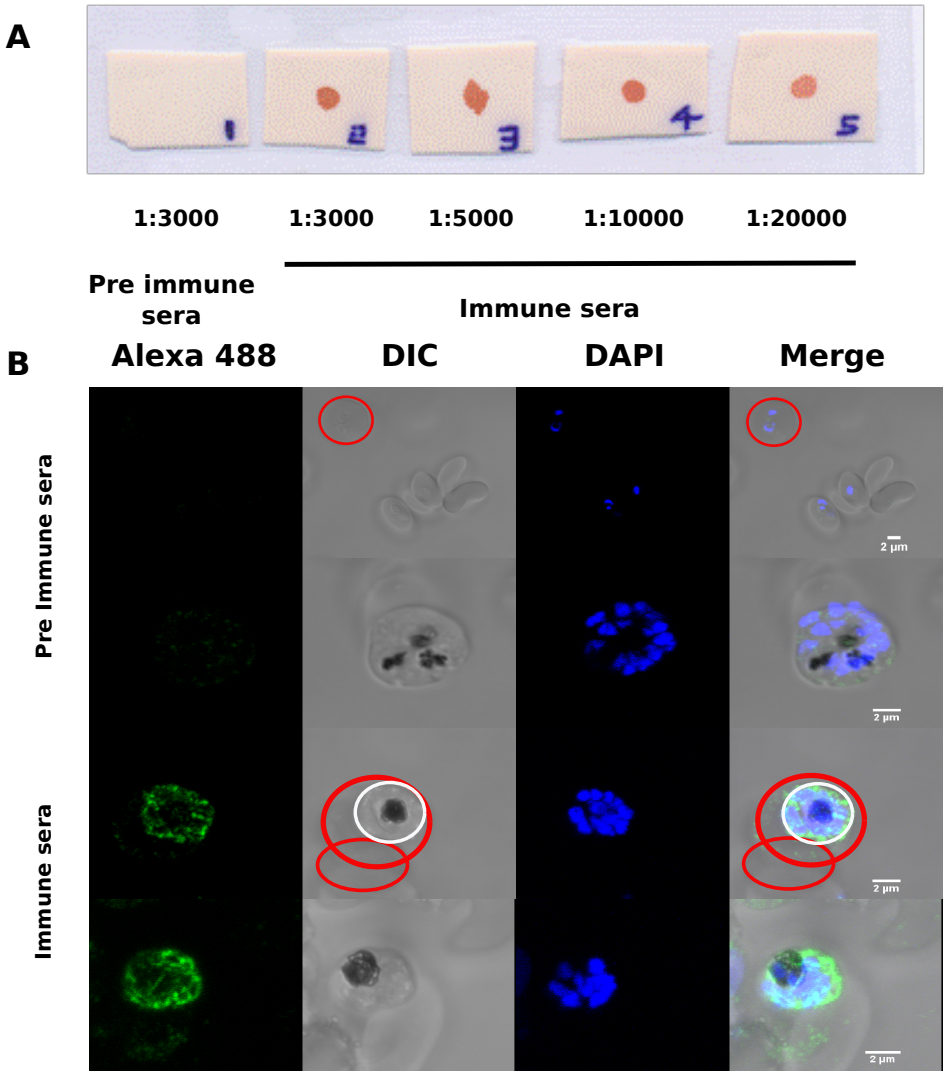

Figure 4.27: Antibody generation and localization of PfHADx

(A) Determination of antibody titre by dot blot. The dilutions are as mentioned in the figure. (B) Parasite culture probed with pre-immune antibody and immune antibody. Red circle corresponds to the RBC boundary, whereas the white circle demarcates parasite boundary.

4.3.2.7 Probing essentiality of HADSF members

Linear vectors with homology arms flanking *Plasmodium* selection marker were generated for all HADSF members by following the strategy described by Pfander *et al.*, (Pfander et al., 2011). Drug-resistant parasites were obtained for all three genes (PbHADx, PbHAD2 and PbHAD3). The genotype of all the constructs and transgenic parasites was validated by PCR (Fig. 4.28, 4.29 and 4.30). A homogenous knockout population was obtained for PbHAD2, PbHADx and PbHAD3 genes.

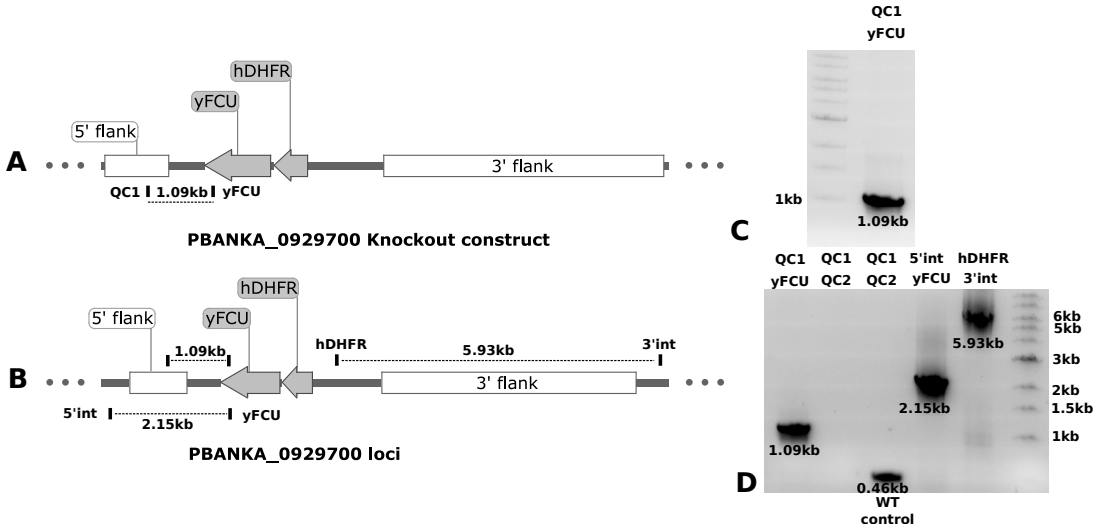

Figure 4.28: Generation of PbHADx knockout construct and knockout parasites

(A and B) Schematic representation of PbHADx final knockout constructs and PbHADx loci after integration. Primers are indicated in the schematic by vertical bars and expected PCR product size is represented by a line between specific primer pairs. (C) PCR confirmation of final knockout construct. Primer pairs used are indicated on top of the panel. (D) Genotyping of the strain for the integration of cassette in the correct loci. 'WT control' refers to the genomic DNA template isolated from untransfected parasites.

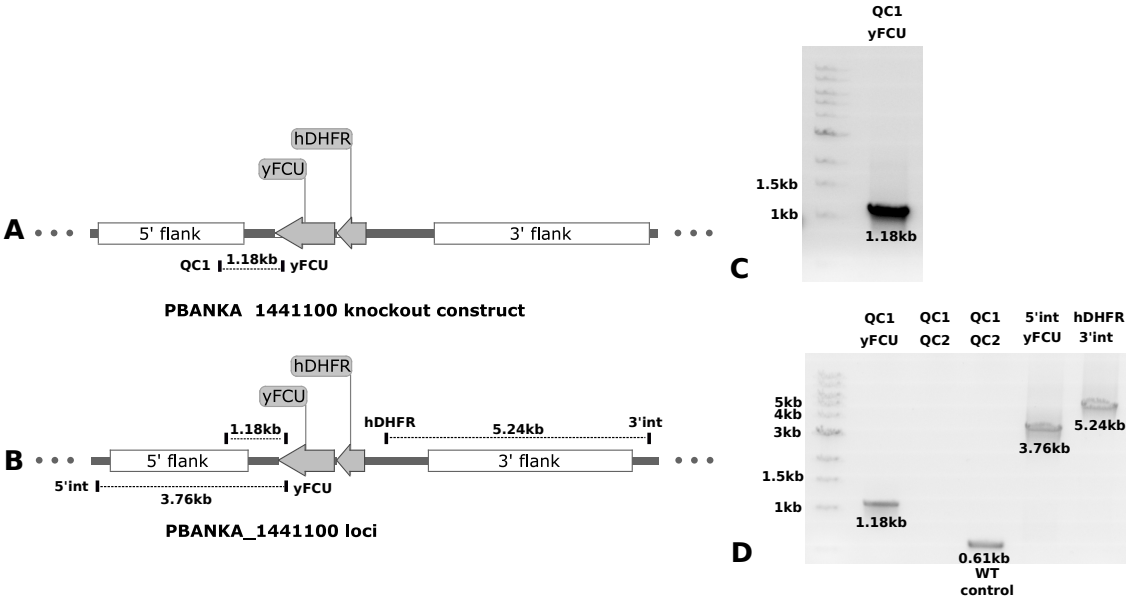

Figure 4.29: Generation of PbHAD2 knockout construct and knockout parasites

(A and B) Schematic representation of PbHAD2 final knockout constructs and PbHAD2 loci after integration. Primers are indicated in the schematic by vertical bars and expected PCR product size is represented by a line between specific primer pairs. (C) PCR confirmation of final knockout construct. Primer pairs used are indicated on top of the panel. (D) Genotyping of the strain for the integration of cassette in the correct loci. 'WT control' refers to the genomic DNA template isolated from untransfected parasites.

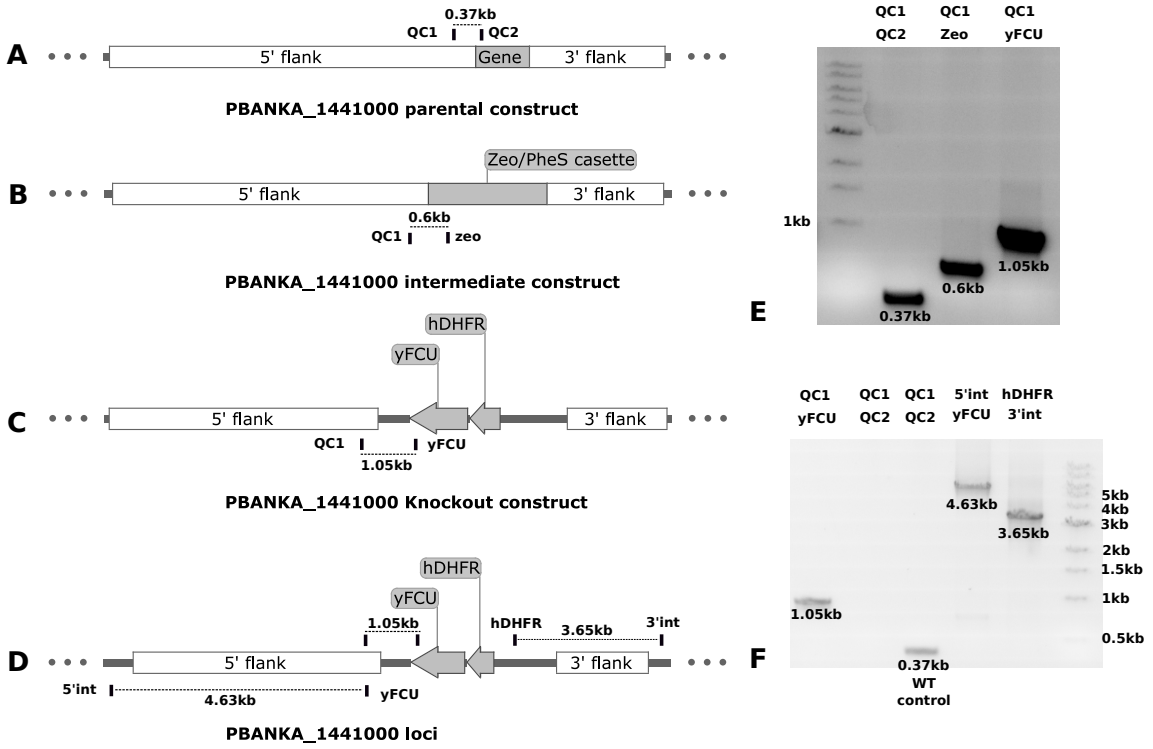

Figure 4.30: Generation of PbHAD3 knockout construct and knockout parasites

(A-D) Schematic representation of PbHAD3 parental, intermediate and final knockout constructs and PbHAD3 loci after integration. Primers are indicated in the schematic by vertical bars and expected PCR product size is represented by a line between specific primer pairs. (E) PCR confirmation of parental, intermediate and final knockout construct. Primer pairs used are indicated on top of the panel. A, B, and C below the panel refer to panels A-C in the figure. (F) Genotyping of the strain for the integration of cassette in the correct loci. D refers to the schematic of the loci of the transfectants from which the genomic DNA was isolated and 'WT control' refers to the genomic DNA template isolated from untransfected parasites.

4.3.3 Discussion

Due to a high extent of sequence diversity in HADSF members, it is extremely challenging to predict the functionality of proteins based on sequence similarity alone. Hence it becomes imperative to perform an unbiased substrate screen to identify relevant physiological substrates for characterization of HADSF members. In our study we have employed a combination of *in vitro* biochemical assays and *in vivo* gene ablation studies to understand the biochemical function and physiological relevance of individual HADSF members. Our findings are summarized below.

4.3.3.1 Studies on HADx

PfHADx, a previously uncharacterized HADSF member from *Plasmodium* was recombinantly expressed in soluble form and further taken up for comprehensive biochemical characterization. The protein displayed broad substrate specificity and acted on purine and pyrimidine nucleotide

monophosphates, phosphorylated small molecules, sugars and co-factors. Although we have identified several substrates for PfHADx, further expansion of the repertoire of substrates in the screening assay might reveal new candidates which can be physiological substrates for this enzyme. Interestingly, substrate vs initial velocity plots for all substrates tested showed hyperbolic pattern except the plots for pNPP and IMP which showed substrate inhibition pattern. As this pattern was not seen in case of dIMP we speculate that the enzyme might have a second binding site and binding of IMP to this site is mediated through the 2' oxygen atom. Apart from determining the cytosolic localization of this monomeric enzyme, we have also successfully deleted its homolog in rodent malaria model *P. berghei*, going to show that this catabolic enzyme is not essential in intra-erythrocytic stages of the parasite. While the essentiality of this HADSF member remains to be determined in other stages of the parasite life cycle, the recombinant protein serves as an ideal candidate for structure-function studies aimed at elucidation of features contributing to its promiscuous nature pertaining to substrate recognition.

4.3.3.2 Studies on HAD2 and HAD3

PvHAD2 was earlier characterized and reported to be acting on pyridoxal phosphate, β-glycerophosphate, AMP, XMP and several sugar phosphates, while its homolog from *P. falciparum,* PfHAD2 had also displayed substrate specificity towards sugar phosphates (Srinivasan et al., 2015; Guggisberg et al., 2018). Mutations inactivating PfHAD2 have been identified in *in vitro* cultured *P. falciparum* parasites that had developed resistance to the drug fosmidomycin and hence this gene was implicated in the emergence of drug resistance (Guggisberg et al., 2018). In the current study, we have extended investigations on HAD2 and were successful in ablating this gene in *P. berghei*, hence proving its dispensable nature for the parasite intra-erythrocytic stages. Although we were not able to characterize HAD3 due to its insoluble nature, the gene could be deleted in *P. berghei*, showing that it is not essential. Further studies determining the essentiality of PbHAD2 and PbHAD3 in other stages of the parasite life cycle will provide a comprehensive understanding of the role of these proteins in parasite physiology.

The study on HADSF members is summarized in Fig. 4.31. Four HADSF members were selected for characterization out of which *in vitro* biochemical assays could not be performed on HAD3 as the protein was insoluble. The function of PGP was annotated and the discrepancy regarding its substrate specificity existing in the literature was resolved through our investigations. PGP is involved in metabolic proof-reading in the parasite and is a potential drug target due to its essentiality. HADx was found to be acting on various substrates including purine, pyrimidine and co-factor phosphates some of which were substrates for HAD2 also. Further extension of substrate screening might result in more hits as relevant physiological substrates for these two enzymes. Though transgenic *P. berghei* parasites were obtained with either HAD2, HAD3 or HADx gene deleted, the phenotype of these parasites need to be accessed and compared to that of the wildtype.

PGP	HADx	HAD2	HAD3
322 amino acids	306 amino acids	295 amino acids	316 amino acids
Motif I - DCDGV	Motif I - DLDHT	Motif I - DFDGT	Motif I - DIDGT
Dimer	Monomer	Monomer	?
2, 3 and 4 carbon sugar phosphates are substrates	Purines, pyrimidines nucleotides and phosphorylated co-factors	Pyridoxal phosphate	??????
Detoxification	Nucleotide metabolism?	Vitamin metabolism?	??????
Cannot be knocked out	Can be knocked out	Can be knocked out	Can be knocked out
Vital for parasite survival	???	???	???
Structural investigation will help in inhibitor design	Structural investigation will help understand substrate specificity		

Figure 4.31: Summary of study on HADSF members

Conclusions and future prospects

Enzymes involved in *Plasmodium* purine nucleotide metabolism have been extensively studied by groups all over the world including ours as this pathway is an important drug target. This thesis titled "Biochemical and Physiological Investigations on Adenosine Monophosphate Deaminase and Haloacid Dehalogenase Superfamily Members from *Plasmodium spp.*" focuses on the preliminary characterization of a purine nucleotide cycle enzyme, AMP deaminase (AMPD) and members of the Haloacid Dehalogenase superfamily (HADSF) from *Plasmodium falciparum* and *Plasmodium berghei*. Purine nucleotide cycle performs inter-conversion of IMP and AMP with the release of fumarate and ammonia as by-products, that have physiological consequences. The pathway also plays a chief role in maintaining the adenylate energy charge (AEC) ratio, which is critical for cell survival (Chapman and Atkinson, 1973). This is achieved by regulating the levels of AMP. AMPD is a catabolic enzyme which deaminates AMP to IMP that can be further channelized to GMP production or AMP synthesis depending on the cellular requirement for respective mononucleotides. AMP can also be catabolized to adenosine and inorganic phosphate by specific/promiscuous 5´ nucleotidases, which are a common occurrence in the HAD superfamily. In a cellular context, AMP can be regarded as the central hub for the regulation of AEC. AMP deaminase, as well as nucleotidases, play a key role in maintaining the levels of this metabolite. Failure in the regulation of AMP levels results in accumulation of this metabolite which has been shown to inhibit the *de novo* purine biosynthetic pathway that subsequently leads to defective protein synthesis (Akizu et al., 2013). AMP accumulation also drives the adenylate kinase reaction in the direction towards ATP depletion, which is physiologically not productive. Given the importance of nucleotide metabolism in the malaria parasite, it becomes imperative to have a substantial understanding of the modes and players involved in the regulation of nucleotide levels. Here, I have made an attempt to understand the role of AMPD and putative nucleotidases belonging to HAD superfamily from the parasitic protozoan *Plasmodium*.

Characterization of PfAMPD was performed by evaluating the ability of wildtype and mutant forms of PfAMPD to complement the deficiency of its homologue in a knockout yeast strain ($\Delta amd1$). Importance of various residues in the functionality of PfAMPD protein based on analysis of sequence, structure and literature available on AMPD from other organisms and evidence from our complementation assay was utilized to bring forth the similarities and key differences between PfAMPD and its homologues from *S. cerevisiae*, *Arabidopsis* and human. The AMPD

gene was deleted in the murine malaria parasite *P. berghei* and was found to be non-essential for intra-erythrocytic growth of the knockout parasites. Through a collaborative effort, essentiality of AMPD in other stages of the parasite life cycle was also examined. This included phenotypic analysis of *Δampd P. berghei* parasites in the mosquito vector, immunofluorescence assay for the zygote, ookinete and sporozoites, gliding motility assay on salivary gland sporozoites, in vitro development of *Δampd P. berghei* exo-erythrocytic forms (EEFs) and infection of C57BL6 mice with *Δampd P. berghei* sporozoites. *Δampd P. berghei* parasites exhibited normal development in the mosquito vector. Sporozoites displayed normal gliding motility and transformed into EEFs in HepG2 cells and initiated a timely blood stage infection in C57BL6 mice. Hence AMPD is not essential for parasite survival even in mosquito and liver stages. However, when episomal expression was attempted, viable parasites were not obtained, suggesting that perturbing AMP homeostasis by over-expressing AMPD might be lethal. Additional evidence was obtained to support this hypothesis by recreating this metabolic context in yeast. *Δade1* and *Δade2* yeast strains that are purine auxotrophs were grown in the presence of hypoxanthine, mimicking *Plasmodium* nucleotide metabolism. Upon over-expression of AMPD using a GAL1 promoter based system, growth defect was observed; thus validating the hypothesis. As AMPD is known to be allosterically modulated by ATP, GTP and phosphate, allosteric activators of PfAMPD could be developed as anti-parasitic agents (Nagappa et al., 2019b). **Since regulation of AMPD activity is critical it would be interesting to investigate the mode of regulation of this enzyme, employed by the parasite. In this regard, anti-GFP antibody was used to pull-down PbAMPD-GFP (inactive mutant) from *P. berghei* lysate and was detected by Western blot. Further studies involving mass spectrometric analysis will provide the identity of interacting partners of AMPD, revealing more information about its regulation**.

All the HAD members in the current study were expressed and purified using the *E. coli* expression system. Identification of physiologically relevant substrates by an unbiased substrate screen and determination of oligomeric state, optimum pH, preferred divalent metal ion were the key features that were determined. One of the HADSF members, *Plasmodium falciparum* (Pf) 4-nitrophenylphosphatase was previously shown to be involved in vitamin B1 metabolism (Knöckel et al., 2008). By conducting a BLASTp search, it was found that 4-nitrophenylphosphatase from Pf has significant homology with phosphoglycolate phosphatase (PGP) from mouse, human, and yeast, prompting us to re-investigate the biochemical properties of the *Plasmodium* enzyme. Because the recombinant PfPGP enzyme was insoluble, extensive biochemical characterization of the recombinantly expressed and purified homolog from *Plasmodium berghei* (Pb) was conducted, leading to the identification of 2-phosphoglycolate and 2-phospho-L-lactate as the relevant physiological substrates of PbPGP. 2-Phosphoglycolate is generated during repair of damaged DNA ends, 2-phospho-L-lactate is a product of pyruvate kinase side reaction, and both potently inhibit two key glycolytic enzymes, triosephosphate isomerase and phosphofructokinase. Hence, PGP-mediated clearance of these toxic metabolites is vital for cell survival and functioning. These

results differ significantly from those in a previous study wherein the PfPGP enzyme has been inferred to act on 2-phospho-D-lactate and not on the L isomer (Dumont et al., 2018). Apart from resolving the substrate specificity conflict through direct *in vitro* enzyme assays, PGP gene-knockout studies in *P. berghei*, confirm that this conserved metabolic proof-reading enzyme is essential in *Plasmodium*. These findings establish PbPGP as an essential enzyme for normal physiological function in *P. berghei* and suggest that drugs that specifically inhibit *Plasmodium* PGP may hold promise for use in anti-malarial therapies (Nagappa et al., 2019a). **Crystallization attempts made using the D49N inactive mutant of PbPGP resulted in the formation of gels, phase transitions and precipitations and proper crystals were not obtained. Further optimization of crystallization conditions is required in this direction**.

The other HADSF member, PfHADx was found to be acting on a broad category of monophosphates such as purine/pyrimidine monophosphates as well as phosphorylated cofactors and sugar phosphates. **Further extension of substrate screen might reveal more physiologically relevant substrates. The inactive mutant of PfHADx, D29N will be used for crystallization studies that will address the issue of substrate specificity in this HADSF member.** The third HAD member PfHAD3 turned out to be completely insoluble when expressed in *E. coli* and hence could not be characterized biochemically. **Knockout parasite lines were generated in *P. berghei* for HADx and HAD3 in addition to HAD2. Further studies accessing the growth phenotype of the knockout parasites in intra-erythrocytic, mosquito and liver stages will provide a holistic picture regarding the role of HADSF members in parasite physiology. Also, episomal over-expression constructs will be used to determine the effect of over-expression of individual HADSF members in *P. berghei*. HADx that is involved in catabolism of various nucleotides, phosphorylated co-factors and sugar phosphates might result in toxicity when over expressed, as it will perturb homeostasis of various metabolite levels. Alternatively this hypothesis can also be validated by developing a tet-repressor based inducible over-expression system in *P. berghei*. Upon induction of HADSF members from the episomal copy, targeted metabolomics can be conducted to determine the levels of key metabolites that have already been identified as relevant substrate through *in vitro* substrate screening experiments. If over-expression of HAD3 is not toxic then the transfectants can be used to purify the protein and perform substrate screen to identify relevant physiological substrates.** As far as, understanding *Plasmodium* nucleotide and central carbon metabolism are concerned, this study contributes a significant piece of information to further our knowledge on parasite biochemistry.

Appendix

Studies on AMPD

Expression of PfAMPD in heterologous expression systems

One of the approaches that were employed to obtain soluble protein was to co-express PfAMPD with chaperones which would assist in the proper folding of PfAMPD. For this purpose TaKaRa plasmid kit containing plasmids encoding different combination of chaperones such as pG-KJE8 (dnaK, dnaJ, grpE, groES and groEL), pGro7 (groES-groEL), pKJE7 (dnaK, dnaJ and grpE), pG-Tf2 (groES-groEL and tig) and pTf16 (tig) was used. BL21 DE3 *E. coli* strain was transformed with pETDuet-1_PfAMPD and selected on LB-ampicillin agar plate. A single colony was picked and was used to prepare chemically competent cells as described earlier (Chung et al., 1989). These cells were now transformed individually with each of the five plasmids from the chaperone kit and selected on LB-ampicillin-chloramphenicol plates. Induction of chaperones was carried out by the addition of tetracycline or arabinose according to the manufacturer's protocol and induction of PfAMPD was carried out using 0.5 mM IPTG. Samples were collected after 6 hours of induction and were analysed by SDS-PAGE and Western blotting where the expression was checked by probing the blot with anti-PfAMPD antibody raised in rabbit as primary and anti-rabbit IgG raised in goat conjugated with HRP as the secondary. Co-expression with chaperones neither helped in enhancing protein solubility nor in preventing degradation.

Methylotrophic yeast *Pichia pastoris* is also widely used as an expression system for heterologous protein expression. The *Pichia pastoris* system provides an option for both secretory and intracellular expression of recombinant proteins. PfAMPD cloned in pGAPZαA consists of an N-terminal α-mating factor signal peptide from yeast which facilitates the recombinant protein to be secreted out into the medium. After the translation the protein is exported form endoplasmic reticulum to golgi apparatus where it is subjected to proteolytic processing by Ste13 and Kex2 proteases which cleave-off the signal peptide. The rest of the protein is packed inside a vesicle which gets exocytosed. Both spent medium and cells were examined by SDS-PAGE and Western blotting for expression. On the other hand, plasmid pGAPZ A lacks this signal sequence and hence the expressed protein remains inside the cell. Both these expression systems did not show expression of the protein.

One of the major hurdles faced by structural genomics initiatives is non-availability of soluble and stable proteins. Various expression systems and numerous solubility enhancing tags are commercially available to aid the researcher but many a time even these strategies are met with failure. In recent times one platform which has gained increased application is the cell free system which employs partially or fully purified cellular components for the purpose of protein production in vitro (Shimizu et al., 2001; Rui et al., 2011; Mudeppa and Rathod, 2013). Various sources include extract from *E. coli*, rabbit reticulocyte, wheat germ etc. Most of these reagents are commercially available and protocols to prepare them in-house are also available. For expressing PfAMPD we employed TNT® T7 coupled wheat germ extract from Promega to

achieve recombinant protein production. The kit was used as per the manufacturer's instruction. The template was PfAMPD cloned in pET23d vector. The luciferase construct supplied with the kit was used as control. The samples were analysed by Western blotting using anti-$(His)_6$ antibodies. Protein expression was not observed.

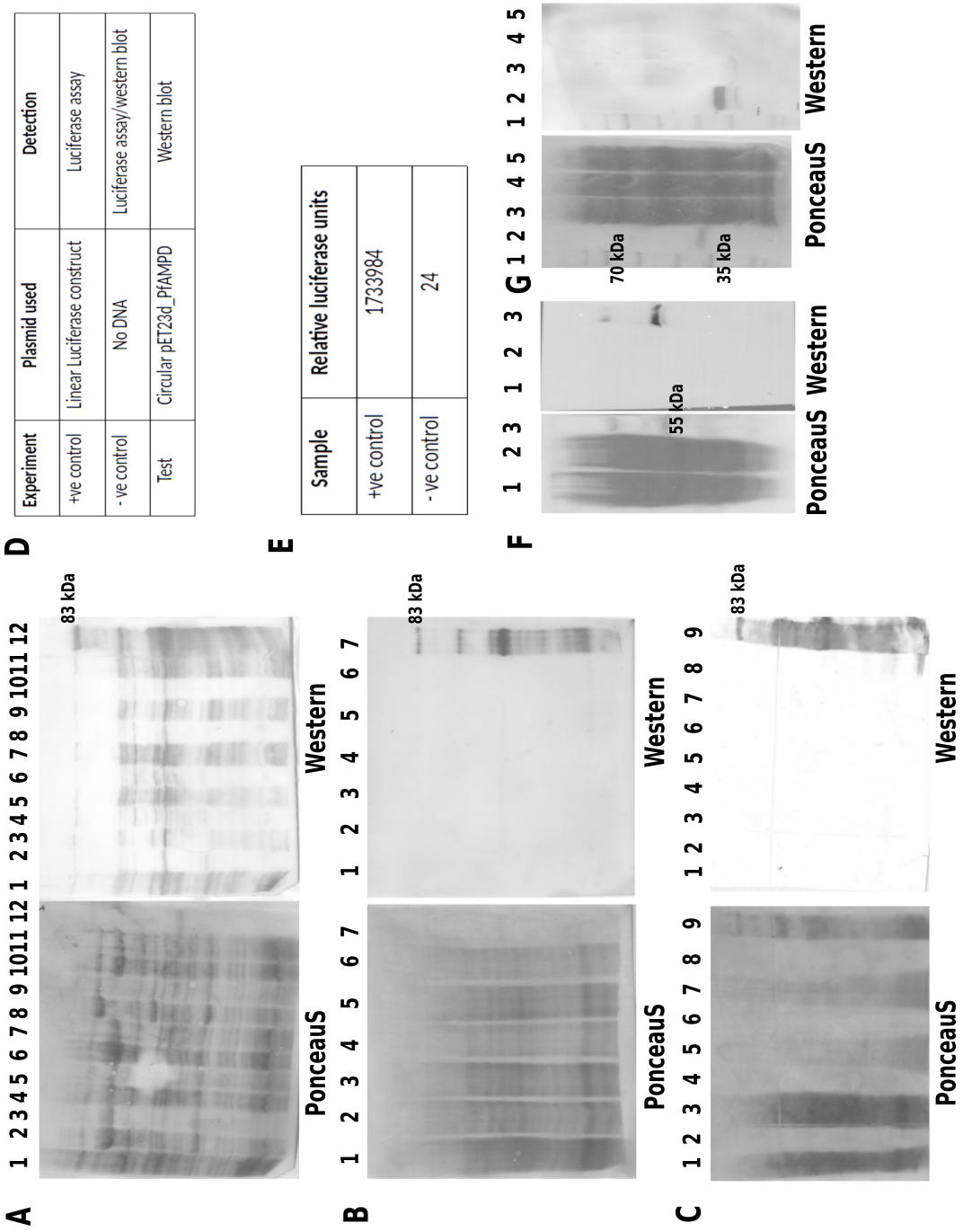

Figure A.1: Expression of PfAMPD in heterologous expression systems

Left panels are Ponceau S stained blots and right panels are the blots after development. (A) Co-expression of PfAMPD with chaperone proteins. Lane 1, lysate of BL 21DE3 strain expressing PfAMPD without chaperones; lanes 2 and 3, lysate of cells expressing PfAMPD with groES-groEL and tig; lanes 4 and 5, lysate of cells expressing PfAMPD with tig; lanes 6 and 7, lysate of cells expressing PfAMPD with groES-groEL; lanes 8 and 9, lysate of cells expressing PfAMPD with dnaK, dnaJ and grpE; lanes 10 and 11, lysate of cells expressing PfAMPD with dnaK, dnaJ, grpE, groES and groEL. Lanes 3, 5, 7, 9 and 11 have 0.5mM IPTG induced samples. Lane 12 has purified $(His)_6$-PfAMPD from bacteria as positive control. (B) Secretory expression of PfAMPDA in *P. pastoris*. lane 1 and 5, processed cell lysate from vector control transformants; lane 2 and 6, processed media from vector control transformants; lane 3 and 7, processed cell lysate from pGAPZαA_PfAMPD transformants; lane 4 and 8, processed media from pGAPZαA_PfAMPD transformants and lane 9 – $(His)_6$-PfAMPD purified from bacteria as a positive control; samples in lanes 1, 2, 3, and 4 were obtained after 60 hrs of induction and samples in lanes 5, 6, 7, and 8 were obtained after 72 hrs of induction. The left panel is the Ponceau S stained blot right panel is the blot after development. (C) Intra-cellular expression of PfAMPDA in *P. pastoris*. lane 1, lysate of vector control transformant cells; lane 2 to 6, lysate of pGAPZ A_PfAMPD transformants and lane 7, $(His)_6$-PfAMPD purified from bacteria as a positive control. The cells were induced for 40 hrs. Left panel is the Ponceau S stained blot right panel is the blot after development. (D-G) Expression of PfAMPD using a cell-free system. (D) Outline of experimental conditions and vectors used in a tabular form. (E) Result of luciferase assay after the *in vitro* cell-free synthesis reaction. (F) Western blot analysis of the wheat germ extract system used for expression of PfAMPD. Lane 1, the sample from *in vitro* cell-free synthesis reaction containing pET23d_PfAMPD_$(His)_6$ as DNA template; lane 2, the sample from *in vitro* cell-free synthesis reaction containing no DNA template and lane 3, $(His)_6$-PfHAD purified protein as a positive control. The left panel is the Ponceau stained blot. The right panel is the blot developed using ECL kit from Thermo Scientific. (G) Western blot analysis of the wheat germ extract system used for expression of PfAMPD using linearized vectors. Lane 1, molecular weight marker; lane 2, $(His)_6$-PfHAD purified protein as positive control; lane 3, sample from *in vitro* cell-free synthesis reaction containing pET21b_$(His)_6$_hPfAMPD_$(His)_6$ as DNA template; lane 4, sample from *in vitro* cell-free synthesis reaction containing pYES2/CT_hPfAMPD_$(His)_6$ as DNA template; and lane 5, sample from *in vitro* cell-free synthesis reaction containing pETDuet-1_$(His)_6$PfAMPD_GFP as DNA template.

Codon harmonised Pf AMPD sequence

AAGCTTGATATCGGATCCGGTACCGAATTCATGCGCTTACCAAACAAGAATGATGGTCAT
AAAACCGTTCCACAAAAAGAAAAAGGTTGGAATAATTTGTATGAAACTGTTGTTAATATC
TCTTCCAAGTCCTCCATTAAATATGATGAATATACCCTATTAAACAAGGATCTGAACAAA
TTACAGACTTGTAATCGTTTTTCTTTTACCTTAACCAGCACCGGGGCTGTTACTAAAGAA
CAGCTCGAAGTCAGCAGGAAACTAATTAGACTATGTAATCTAAGAGATACCTATATTAAA
AAGTTTCAAGATATAGACACCTGCCTGGTTGAATCTAAATCTTTAAACAAGAATTACAAG
TCGAAAAATATTGATGATTATGAATCCTCTGAACCAATCTATAATCCATATAATGTCAAA
ATTTTAAAGAATTGTAATGCCTTCATCAATTTTGTCGACGGGATTTTCTTTGTTCATTGG
GACCCGCATACCGATGAAGGTCCATCTTCGAGGGATATGTGCGTCGAATCTAACAAACTT
GCAAACCATCGCAACATTAAATCTGCTGAAGATTACTTGTCCTCGATTCAAGAAATCATG
AATGTTGTCCAAGACCCAGCTTGCAAATCTTTTTGCTTTCAACGCCTAAAATACTTGGAA
AAGAAATTTGATTTCCATATTATGTTTAATGGTCCATTAGAGTTAAGCGAAACCAGAGAC
ATCAAGCATCGCGATTTTTATAATATTAGAAAAGTTGATGTTCATGTTCATCATTCGGCA
TGCATGCAACAAAAAGAACTATTACGTTTTATTAGAGAGAAATATAGAACTGAACCGAAT
ACTGTCGTTTATATTAATGAAAAGAGAGAGATGTTAACTTTAAAATCTATTTTTGATGAA
GAACTAAAGTCTACTGCTTATGAAAGCACGATTGATACCTTAGGTGTTAATGCGTTAGGT
AATTGTTTTCATAGATTTGATCTATTCAATGAAAAGTATAATCCCTTTGGTCAGAAATTA
TTAAGAGATATTTTCTTGAAGACCGACAATTATATCGAAGGTAGATACTTAGCGGAAATC
ACTAAAAAGCAAATCAAGAATCTGGAACGTTCTAAATATCAACATGTTGAATGGAGAATT
TCTATCTATGGTAAAAACAAGAATGAGTGGTTAAAAATTTCCAAATGGGTTCTGAATAAT
CAACTGTCTTCTATTAGAGTTCGTTGGATGATTCAAGTTCCCAGATTATATCATATTTAT
AAGAAAATGAAACTAATTAATACCTTTGCTGATTTTCTATCTAATATTTTCTCTCCATGT
TTTGAAGCAATCAAAAATCCCGAAGAAAATAAGGAAATTTTTATTTTCTTACATCAAATC
GTTGGTTGGGACTCTGTTGATGATGAATCCATCATCTCGAATTATACTTTAAAGGGTGGG
GAGCTACCCACTCCAGATAAATATGTTTCTGAACATAATCCACCCTATTCCTACTATGCA
TATTATATGTATATTAATATTCGTATGCTAAATGAGTTTATGATTTCAAGAAATATGAGA
CCGATGGCTTTCAGGCCACATTGTGGTGAAATCGGTAATATGTCTCACCTAGCTTGTATG
TTTTTATTAGCCGATAGGATTAATCACGGTATCAACTTGAGGAAATCTCCAGTTTTATTA
TACTTGTATTATCTAAAGCAAATTGGGTTAGCTTTATCCCCACTATCTAATAATGCACTA
TTCTTACATATCGATAAAAACCCGTTCAAGCGTTTCTTTAAAATCGGGCTAAACGTTACT
CTAAGCACTGATGACCCACTAATGTTTCATTTTACGGATGAACCATTACTGGAAGAATAT
AGCATTTGTGCCCATACTTGGAAATTATCTACCGTCGATTTGTGCGAAATCGCTAGGGCC
TCTGTTATCCAATCTGGTTATGAGCCCGCTTTTAAGAAACATTGGTTAGGTGACGAGGAC
GGTTTCTTTAACTTTCAAAATGACCCGAATAAGACTAACTTATCTAATACTAGGATGGTT
TATAGGAGGAATACCTTAGAGGAGGAAATTAAAAATATCGAACGCCTAGCATCGTATTCT
TCTAACAATCACCACCACCACCACTAACTCGAGTCTAGAGCGGCCGCCTGCAG

Expression of codon harmonised PfAMPD gene in heterologous expression system

The PfAMPD gene was harmonised for yeast codon usage using Eugene codon optimization tool (Gaspar et al., 2012). This synthesised gene was subcloned into *E. coli*, *S. cerevisiae* and *P. pastoris* expression vectors and checked for expression and solubility of the protein. Various *E. coli* strains were also employed for this purpose. Expression in bacterial culture was carried out in 5 mL culture induced at 0.6 OD_{600} using 1 mM IPTG for 3 hours at 30 °C, 180 rpm. For expression check 250 µL culture equivalent of cell lysate was analysed by SDS-PAGE/Western blotting. Solubility check was done in bacterial system using 800 mL culture lysed by French pressure cell followed by Ni-NTA chromatography. In yeast, induction was carried out in a 1 litre culture for 24 hrs in SD-Ura with galactose for pYES2/CT_hPfAMPD_$(His)_6$ transformants, SD-Ura with glucose for pCM189_hPfAMPD_$(His)_6$ transformants and YPD for pGAPZ A_hPfAMPD_$(His)_6$ transformants.

Table A.1: List of constructs containing codon harmonised PfAMPD gene used for recombinant protein production

Expression system	Vector
E. coli	pQE30_$(His)_6$_hPfAMPD_$(His)_6$
	pET22b_PelB_hPfAMPD_$(His)_6$
	pET21b_$(His)_6$_hPfAMPD_$(His)_6$
	pET21b_MBP_hPfAMPD_$(His)_6$
P. pastoris	pGAPZ A_hPfAMPD_$(His)_6$
S. cerevisiae	pYES2/CT_hPfAMPD_$(His)_6$
	pCM189_hPfAMPD_$(His)_6$

None of the above-mentioned expression systems and constructs consisting of harmonised PfAMPD gene helped in obtaining stable/soluble protein.

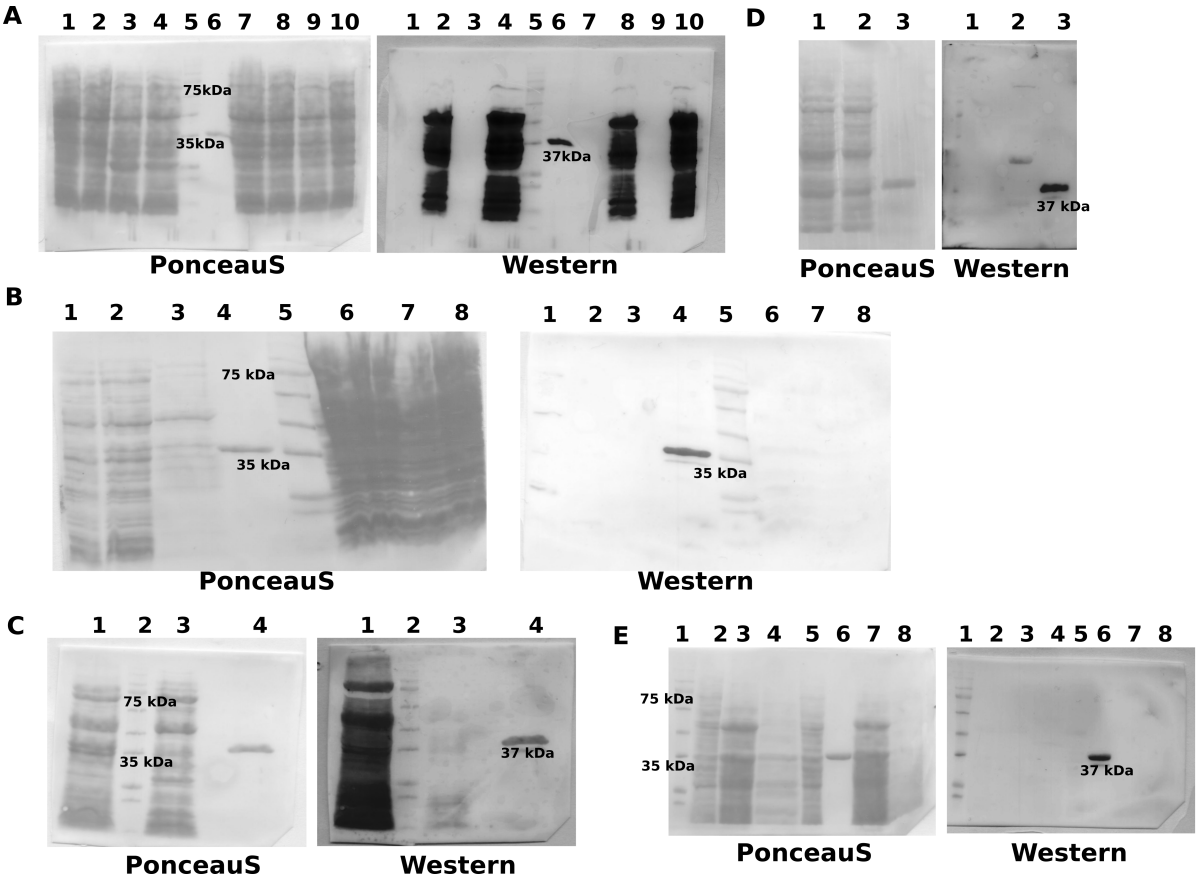

Figure A.2: Expression of codon harmonised PfAMPD gene in heterologous expression system

Left panels are the Ponceau S stained blots and right panels are the blots after development. (A) Expression of PfAMPD cloned in pQE30 vector using various bacterial strains. Lane 1, lysate of uninduced BL21 DE3 cells; lane 2, lysate of IPTG induced BL21 DE3 cells; lane 3, lysate of uninduced BL21 DE3 RIL cells; lane 4, lysate of IPTG induced BL21 DE3 RIL cells; lane 5, molecular weight marker; lane 6, $(His)_6$-tagged PfHAD purified from bacteria as a positive control; lane 7, lysate of uninduced C41 DE3 cells; lane 8, lysate of IPTG induced BL21 DE3 RIL cells; lane 9, lysate of uninduced Rosetta DE3 cells; lane 10, lysate of IPTG induced Rosetta DE3 RIL cells. (B) Expression of PfAMPD cloned in pET22b vector. Lane 1, pellet fraction; lane 2, wash fraction; lane 3, soluble fraction; lane 4, $(His)_6$-tagged PfHAD purified from bacteria as positive control; lane 5, molecular weight marker. Expression of PfAMPD cloned in pGAPZ A. Lanes 6-8, lysates of three induces transformants. (C) Expression of PfAMPD cloned in pET21b vector. Lane 1, pellet fraction; lane 2, molecular weight marker; lane 3, soluble fraction; lane 4, $(His)_6$-tagged PfHAD purified from bacteria as a positive control. (D) Expression of PfAMPD cloned in pET21b vector with MBP tag at N-terminus. Lane 1, lysate of uninduced cells; lane 2, Lane 1, lysate of IPTG induced cells; lane 3, $(His)_6$-tagged PfHAD purified from bacteria as a positive control. (E) Expression of PfAMPD cloned in pYES2/CT and pCM189. Lane 1, molecular weight marker; lane 2, pellet fraction; lane 3, soluble fraction; lane 4, fraction bound to Ni-NTA beads; lane 5, pellet fraction; lane 6, $(His)_6$-tagged PfHAD purified from bacteria as positive control; lane 7, soluble fraction; lane 8, fraction bound to Ni-NTA beads; lanes 2, 3 and 4 correspond to samples from cells transformed with pYES2/CT_hPfAMPD_$(His)_6$; lanes 5, 7 and 8 correspond to samples from cells transformed with pCM189_hPfAMPD_$(His)_6$.

Attempts towards the purification of PfAMPD from yeast

Using *Δamd1* yeast cells transformed with pYES2/CT_$(His)_6$_hPfAMPD_GFP, purification of PfAMPD was attempted. A single colony was inoculated into 10 mL SD-Ura medium with 2 % glucose as carbon source and grown for 12 hrs at 30 ℃, 180 rpm. This overnight culture was transferred to fresh 500 mL medium and further grown for 16 hrs at 30 ℃, 180 rpm. The cells were harvested under sterile conditions and washed with sterile water once and resuspended in 1 L SD-Ura medium with 2 % galactose as carbon source. The cells were further grown for 8 hrs at 30 ℃, 180 rpm. The cells were harvested by centrifugation and resuspended in 20 mL of lysis buffer (50 mM Tris HCl, pH 8, 100 mM NaCl, 10 % w/v glycerol, 1 mM DTT, 0.1 mM PMSF) and subjected to lysis by passing through a homogenizer at 40000 psi. The lysis was confirmed by microscopy. The cell lysate was centrifuged at 18000 x g, 4 ℃, 30 min. The supernatant was mixed with 500 µL Ni-NTA agarose beads and incubated on a rotating rod at 4 ℃ for 3 hrs. The lysate along with the beads was poured into a glass column and subjected to immobilized metal affinity chromatography. The fractions from the column were analysed by SDS-PAGE followed by Western blotting.

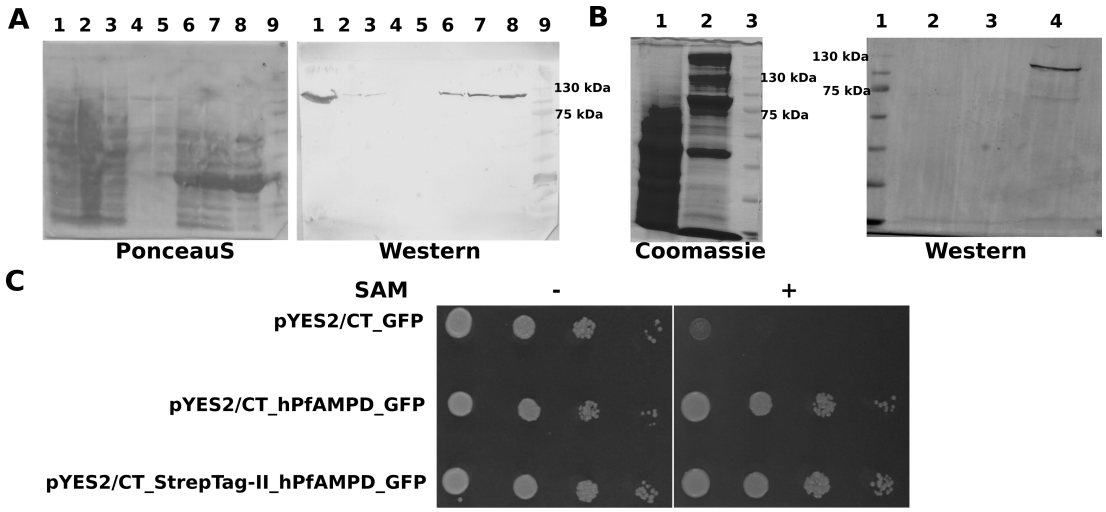

Figure A.3: Purification of PfAMPD from yeast

(A) Purification of $(His)_6$_hPfAMPD_GFP fusion protein from yeast. Lane 1, pellet fraction; lane 2, flow through fraction; lane 3, 0 mM imidazole fraction; lane 4, wash fraction; lane 5, wash fraction; lane 6 and 7, 250 mM imidazole fraction; lane 8, beads fraction and lane 9, molecular weight marker. The left panel is PonceauS stained blot and the right panel is the blot after development. Anti-$(His)_6$ antibody raised in mouse was used to detect the protein (B) Purification of StrepTag-II_hPfAMPD_GFP fusion protein from yeast. The left panel is the Coomassie-stained gel. Lane 1, unbound fraction; lane 2, bead fraction and lane 3, molecular weight marker. The right panel is the Western blot probed with anti-GFP antibody raised in mouse. Lane 1, molecular weight marker; lane 2, unbound fraction; lane 3, wash fraction and lane 4, bead fraction. (C) Complementation assay to determine the functionality of StrepTag-II_hPfAMPD_GFP fusion protein. *Δamd1* yeast cells expressing StrepTag-II_hPfAMPD_GFP fusion protein show rescue of growth defect phenotype similar to the positive control (*Δamd1* yeast cell expressing hPfAMPD_GFP fusion protein).

As the imidazole eluted fractions were very impure and the amount of protein was so low that it could only be detected by Western blotting, purification was also attempted using *Δamd1* yeast cells transformed with pYES2/CT_StrepTag-II_hPfAMPD_GFP vector. A single colony was inoculated into 10 mL SD-Ura medium with 2 % glucose as carbon source and grown for 12 hrs at 30 ℃, 180 rpm. This overnight culture was transferred to fresh 50 mL media and grown for further 16 hrs at 30 ℃, 180 rpm. The cells were harvested under sterile conditions and washed with sterile water once and resuspended in 100 mL SD-Ura medium with 2 % galactose as carbon source. The cells were further grown for 8 hrs at 30 ℃, 180 rpm. The cells were harvested by centrifugation and resuspended in 0.5 mL lysis buffer (50 mM Tris HCl, pH 8, 100 mM NaCl, 10 % w/v glycerol, 1 mM DTT, 0.1 mM PMSF) and subjected to lysis by vortexing with glass beads multiple times (30 seconds vortexing followed by 30 seconds on ice). The lysate was diluted to 5 mL with lysis buffer and centrifuged at 18000 x g, 4 ℃, 30 min. The supernatant was mixed with 50 µL Streptactin beads and incubated on a rotating rod at 4 ℃ for 3 hrs. The lysate along with the beads was poured on to a glass column and flow through was collected. The beads were washed with 1 mL lysis buffer. The fractions were analysed by SDS-PAGE followed by Western blotting. Although the Strep-tagged protein was detected by Western blotting, the problem of low yield persisted. Nevertheless, it was observed that even this protein was functional as *Δamd1* yeast cells transformed with pYES2/CT_StrepTag-II_hPfAMPD_GFP displayed rescue of growth defect phenotype.

Localization of PfAMPD by immunofluorescence

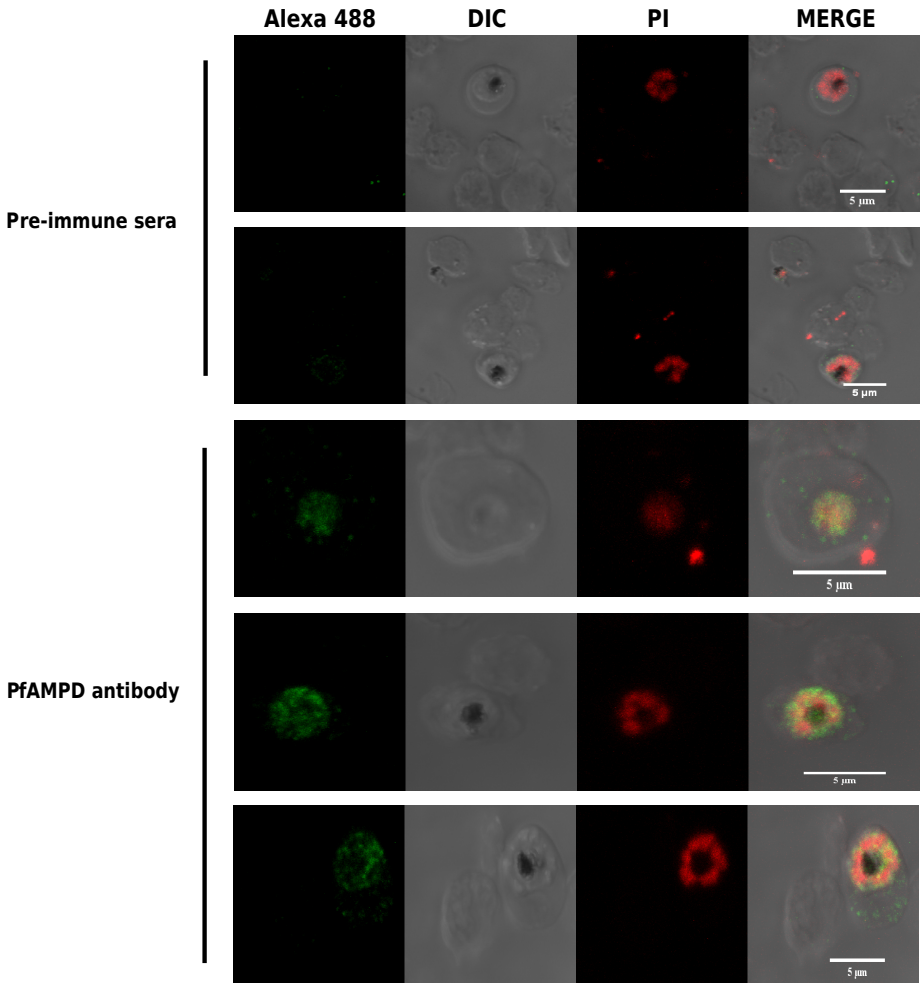

Figure A.4: Localization of PfAMPD by immunofluorescence

PfAMPD was localized by immunofluorescence using anti-PfAMPD antibodies generated in rabbit.

PfAMPD was found to be localized in the cytosol as observed by immunofluorescence microscopy. This result is similar to that observed in *P. berghei* where C-terminal GFP-tagged catalytically inactive PbAMPD was episomally expressed.

Western blotting of yeast lysates

Yeast cells transformed with empty pYES2CT plasmid (negative control) and plasmid encoding GFP, ScAMPD_GFP, PfAMPD_GFP or Δ60_GFP were induced and samples were analysed by SDS-PAGE and Western blotting. In spite of loading significant amounts of cell lysates, anti-GFP antibody did not recognize any non-specific antigen.

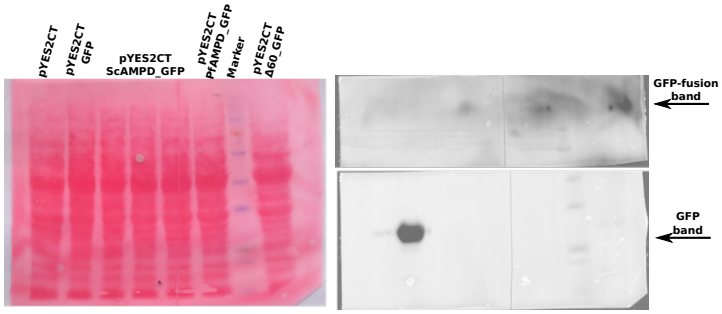

Figure A.5: SDS-PAGE analysis of yeast lysates obtained after galactose induction

Transfection of *P. falciparum*

P. falciparum parasites were transfected with pGDB_PfAMPD for the purpose of generating a conditional knockdown strain. Both exponential wave and square wave protocol were followed. A time constant of 20.2 ms and a droop percentage of 3 % were achieved, which were well within the permissible range. The culture was maintained for 40 days, but parasites resistant to drug blasticidin were not observed. Hence the culture was terminated.

General protocols used

* *Yeast gDNA isolation protocol.* Single colonies of *Saccharomyces cerevisiae* were picked from a YPD plate and suspended in 100 µl of 200 mM LiOAc, 1 % SDS solution and were incubated at 70 °C for 15 minutes. After incubation, 300 µl of 96 % ethanol was added for DNA precipitation, samples were mixed by brief vortexing and DNA was collected by centrifugation at 15000 × g for 3 minutes. Precipitated DNA was dissolved in 100 µl of TE, cell debris was spun down by brief centrifugation (15000 × g, 1 minute) and 1 µl of the supernatant was used for PCR.

* *Yeast transformation protocol.* A single colony was inoculated in YPD medium and grown at 30 °C, 250 rpm overnight. The A_{600} was checked and 1 O.D of cells were transferred to 5 ml YPD medium and grown further (4 hrs -5 hrs) to get a final A_{600} of 4.Transformation mix consisted of 240 µL of 50 % PEG 3350, (added at the end using cut tips), 50 µL of 2 mg ml-1 Carrier DNA (boiled before adding), 36 µL, 1 M Li acetate, 10-15 µL PCR product/Plasmid (1µg) and water 24-19 µL. The cells were harvested by centrifugation and supernatant was discarded. Transformation mix was added to the cell pellet and mixed thoroughly avoiding any clump formation. Cells were subjected to heat shock at 42 °C for 40 mins following which, they were harvested and plated on selection medium and incubated at 30 °C for two days.

* *CF11 purification of parasitized RBCs.* Cellulose (fibrous) was packed up to 3 mL volume in a 20 mL syringe and autoclaved. Blood collected from a mouse was diluted in 15 mL RPMI-1640 medium and loaded on to the CF11 column and passed through the packed cellulose by

pushing the plunger gently. The filtrate was collected and centrifuged at 400 × g to harvest the parasitized erythrocytes devoid of WBCs. This pellet can now be used for erythrocyte lysis and further processing.

** Alkaline transfer protocol for Southern transfer.* Restriction enzyme digested DNA sample was separated on 0.7 % agarose gel. The DNA was subjected to depurination using 0.25 M HCl until the bromophenol blue dye turned yellow in colour. This was followed by treatment with alkaline transfer buffer till the colour of the dye turned back to blue. The gel was now placed on the transfer set up which consisted of blotting papers soaked in alkaline transfer buffer. The Zeta probe membrane pre-soaked in transfer buffer was placed on top of the gel followed by stacking of blotting sheets on top. A weight was placed on the top and transfer was allowed to happen for 20 hours. The membrane was then subjected to UV cross-linking using 'auto crosslink' programme of Stratagene UV cross-linker. Thereafter the blot was treated with pre-hybridization buffer for 90 minutes in roller bottle at 65 °C. The blot was then treated with pre-heated hybridization buffer for 24 hours in roller bottle at 65 °C. Washes were given using wash buffer A (20 minutes) and B (30 minutes, 3 times) in roller bottle at 65 °C. The washed blot was air dried and exposed to a phosphor screen for 12 hours.

Composition of Reagents and media used

*1 x PBS (1 Litre)

8 g NaCl, 0.2 g KCl, 1.44 g Na_2HPO_4, and 0.24 g KH_2PO_4

*1 x PBST (1 Litre)

8 g NaCl, 0.2 g KCl, 1.44 g Na_2HPO_4, 0.24 g KH_2PO_4 and 1 mL Tween 20

*TSS buffer (5 mL)

2 x LB 500 µL, 25 % PEG 3350 400 µL, 1 M $MgCl_2$ and DMSO 50 µL

* Erythrocyte lysis buffer

155 mM NH_4Cl, 10 mM $KHCO_3$ and 0.1 mM EDTA

* TNE buffer

10 mM Tris HCl, pH 8, 0.5 mM EDTA and 100 mM NaCl

* Cytomix

120 mM KCl, 0.2 mM $CaCl_2$, 2 mM EGTA, 10 mM $MgCl_2$, 25 mM HEPES, 5 mM K_2HPO_4 and 5 mM KH_2PO_4 adjusted to pH 7.6

* Alkaline transfer buffer

0.4 N NaOH and 1 M NaCl

* Pre-hybridization solution

5 % SDS, 0.5 M NaCl, 6 mM EDTA and 0.1 M Sodium phosphate pH 7

* Hybridization solution

30 µL ssDNA (provided in the random primer kit from BRIT), 100 µL radiolabelled probe added to 20 mL pre-hybridization solution and boiled for 10 min.

* Wash buffer A

2x SSC and 1 % SDS

* Wash buffer B

0.5x SSC and 0.1 % SDS

* 20x SSC (standard sodium citrate) (for 200 mL)

35.06 g NaCl and 17.74 g sodium citrate adjusted to pH 7 using concentrated HCl

* YPD (1000 mL)

Yeast extract – 10 g Peptone – 20 g Dextrose – 20 g. Make up the volume and autoclave & store at room temperature.

* SD – N (100 mL)

20x YNB (without amino acids and ammonium sulphate) – 5 mL 20x Dextrose – 5 mL 20x Dextrose is 40 % D – Glucose. 20x YNB is 3.4 % YNB (w/o amino acids and w/o ammonium sulphate or just w/o amino acids as per requirements) Filter sterilize using 0.2 micron filter & store at 4 degrees.

* Amino acid solutions

His – 2 % stock solution - stored in al foil in fridge (filter sterilized) and working solution - 0.2 mL/200 mL medium.

Leu – 1 % stock solution - stored in fridge (autoclaved) and working solution - 1.2 mL/200 mL medium.

Met – 2 % stock solution - stored in fridge (autoclaved) and working solution - 0.2 mL/200 mL medium.

Ura – 0.2 % stock solution made in 1 % sodium carbonate, stored in fridge (autoclaved) and working solution – 2 mL/200 mL medium.

Lys – 1.5 % stock solution - stored in fridge (autoclaved) and working solution - 0.4 mL/200 mL medium.

Ade – 20 mg ml^{-1} stock solution made in 1 M HCl and working solution - 300 µM i.e. 0.2 mL/100 mL medium.

* G418 stock 50 mg mL^{-1} & working 200 µg mL^{-1}

* SAM stock 200 mg mL^{-1} & working 50 µg mL^{-1}

List of primers

AMPD cDNA synthesis from *P. falciparum* total RNA		
P1	ATACCC**AAGCTT**TTAATTGTTTGATGAATAGCTAGCTAGTCG	
Cloning of wild type PfAMPD in pETDuet-1		
P2	TTTCCG**GAATTC**ACGGTTACCTAATAAAAATGATGGTC	
P3	ATACCC**AAGCTT**TTAATTGTTTGATGAATAGCTAGCTAGTCG	
Cloning of *Δ59* PfAMPD in pETDuet-1		
P4	TTTCCG**GAATTC**AACTTTAACGTCCACGGGG	
P5	ATACCC**AAGCTT**TTAATTGTTTGATGAATAGCTAGCTAGTCG	
Cloning of *Δ94* PfAMPD in pETDuet-1		
P6	TTTCCG**GAATTC**AATCGACACTTGCCTTGTAGAAAG	
P7	ATACCC**AAGCTT**TTAATTGTTTGATGAATAGCTAGCTAGTCG	
Cloning of *Δ178* PfAMPD in pETDuet-1		
P8	TTTCCG**GAATTC**AGCAGAAGATTATTTATCTAGCATACAAGAAATTATG	
P9	ATACCC**AAGCTT**TTAATTGTTTGATGAATAGCTAGCTAGTCG	
Cloning of PfAMPD in pET23d		
P10	AACTTG**CCATGG**CACGGTTACCTAATAAAAATGATGGTC	
P11	GAGGCCTGAATGCCATTGGTCTCATATTTCTAC	
P12	GTAGAAATATGAGACCAATGGCATTCAGGCCTC	
P13	ATACCG**CTCGAG**ATTGTTTGATGAATAGCTAGCTAGTCG	
Cloning of ScAMPD in pYES2/CT		
P14	TGT**GAGCTC**ATGGACAATCAGGCTACACAGAGGC	
P15	CAT**CTCGAGGGCGCC**CTTTTCTTCAATGGTTCTCTTGAAATTGGC	
Cloning of ScAMPD in pCM189		
P16	TATTGAA**GGCCT**ATGGACAATCAGGCTACACAGAG	
P17	ATAA**CTGCAG**TCACTTTTCTTCAATGGTTCTCTTG	
Cloning of wild type PfAMPD in pYES2/CT		
P18	ATCGG**GGTACC**ATGTCTCGGTTACCTAATAAAAATGATGGTCATAAAACTG	
P19	GGCTAG**TCTAGA**TCACTTTGTTAGCAGCCGGATCTCAGTG	
Cloning of wild type PfAMPD in pGAPZαA		
P20	AGC**CTCGAG**AAAAGAGAGGCTGAAGCTATGAGATTACCTAATAAAAATGATGGTCATAAAACTGT TCCTC	
P21	GGCTAG**TCTAGA**TTAATTGTTTGATGAATAGCTAGCTAGTCGTTCG	
P22	GCTAGCTAACCATAGAAACATAAAATCAGCAGAAG	
P23	CTTCTGCTGATTTTATGTTTCTATGGTTAGCTAGC	
Cloning of eGFP in pYES2/CT		
P24	TGC**GGATCCTCTAGA**ATGGTGAGCAAGGGCGAGG	
P25	AAA**CTGCAGCTCGAG**TTACTTGTACAGCTCGTCCATGCCG	
Cloning of ScAMPD - GFP in pYES2/CT		
P26	Amplification of	TGT**GAGCTC**ATGGACAATCAGGCTACACAGAGGC

P27	ScAMPD segment	CAT**CTCGAG**<u>**GGCGCC**</u>CTTTTCTTCAATGGTTCTCTTGAAATTGGC
P28	Amplification of GFP segment	ATA**GGCGCC**ATGGTGAGCAAGGGCGAGGAGCTG
P29		AAA**CTGCAG**<u>**CTCGAG**</u>TTACTTGTACAGCTCGTCCATGCCG
Cloning of harmonised PfAMPD - GFP in pYES2/CT		
P30	Amplification of PfAMPD segment	CCAGTGAATTAGAACTCGGTACG
P31		TCA**TCTAGA**ATTGTTAGAAGAATACGATGCTAGGCGTTCG
P32	Amplification of GFP segment	TGC**GGATCC**<u>**TCTAGA**</u>ATGGTGAGCAAGGGCGAGG
P33		AAA**CTGCAG**<u>**CTCGAG**</u>TTACTTGTACAGCTCGTCCATGCCG
Cloning of truncated versions of PfAMPD in pYES2/CT		
P34	Δ60FP	TGC**GGATCCGGTACC**ATGTTAACCAGCACCGGGGCTGTTACTAAAG
P35	Δ180FP	TGC**GGATCCGGTACC**ATGTTAACCAGCACCGGGGCTGTTACTAAAG
Cloning of PfAMPD mutants in pYES2/CT		
P36	H245A/H247AFP	TTATAATATTAGAAAAGTTGATGTT**GCT**GTT**GCT**CATTCGGCATGCATGCAA CAAAAAG
P37	H245A/H247ARP	CTTTTTGTTGCATGCATGCCGAATGAGCAACAGCAACATCAACTTTTCTAAT ATTATAA
P38	F319LFP	GTTTTCATAGATTTGATCTA**TTG**AATGAAAAGTATAATCCC
P39	F319LRP	GGGATTATACTTTTCATTCAATAGATCAAATCTATGAAAAC
P40	Y323LFP	GATTTGATCTATTCAATGAAAAG**TTG**AATCCCTTTGGTCAGAAATTATTAAG
P41	Y323LRP	CTTAATAATTTCTGACCAAAGGGATTCAACTTTTCATTGAATAGATCAAATC
P42	D454NFP	CATCAAATCGTTGGTTGG**AAT**TCTGTTGATGATGAATCCATC
P43	D454NRP	GATGGATTCATCATCAACAGAATTCCAACCAACGATTTGATG
P44	M504RFP	CGTATGCTAAATGAGTTT**AGA**ATTTCAAGAAATATGAGACCG
P45	M504RRP	CGGTCTCATATTTCTTGAAATTCTAAACTCATTTAGCATACG
P46	M504HFP	CGTATGCTAAATGAGTTT**CAT**ATTTCAAGAAATATGAGACCG
P47	M504HRP	CGGTCTCATATTTCTTGAAATATGAAACTCATTTAGCATACG
P48	H517AFP	CCGATGGCTTTCAGGCCA**GCT**TGTGGTGAAATCGGTAATATG
P49	H517ARP	CATATTACCGATTTCACCACAAGCTGGCCTGAAAGCCATCGG
P50	E520AFP	CAGGCCACATTGTGGT**GCT**ATCGGTAATATGTCTCACC
P51	E520ARP	GGTGAGACATATTACCGATAGCACCACAATGTGGCCTG
P52	H539AFP	GTTTTTATTAGCCGATAGGATTAAT**GCT**GGTATCAACTTGAGGAAATCTCC
P53	H539ARP	GGAGATTTCCTCAAGTTGATACCAGCATTAATCCTATCGGCTAATAAAAAC
P54	D594AFP	GCTAAACGTTACTCTAAGCACT**GCT**GACCCACTAATGTTTCATTTTACGG
P55	D594ARP	CCGTAAAATGAAACATTAGTGGGTCAGCAGTGCTTAGAGTAACGTTTAGC
P56	D595AFP	CGTTACTCTAAGCACTGAT**GCT**CCACTAATGTTTCATTTTACG
P57	D595ARP	CGTAAAATGAAACATTAGTGGAGCATCAGTGCTTAGAGTAACG
P58	E608DFP	CGGATGAACCATTACTG**GAT**GAATATAGCATTTGTGCCC
P59	E608DRP	GGGCACAAATGCTATATTCATCCAGTAATGGTTCATCCG
P60	T621A FP	CCCATACTTGGAAATTATCT**GCC**GTCGATTTGTGCGAAATCGC
P61	T621A RP	GCGATTTCGCACAAATCGACGGCAGATAATTTCCAAGTATGGG
P62	D623YFP	CTTGGAAATTATCTACCGTC**TAT**TTGTGCGAAATCGCTAGGGC

P63	D623YRP	GCCCTAGCGATTTCGCACAAATAGACGGTAGATAATTTCCAAG
Common primers for pYES2/CT		
P64	Gal forward	AATATACCTCTATACTTTAACGTCAAGG
P65	Cyc reverse	GCGTGAATGTAAGCGTGAC
Cloning of dual tagged PfAMPD in pYES2/CT		
P66	$(His)_6$-AMPD-GFP	CTT**GGTACC**ATGCACCACCACCACCACCACCGCTTACCAAACAAGAATGATGGTC
		Cyc reverse
	AMPD-GFP-$(His)_6$	Gal forward
P67		ATT**CTCGAG**TTAGTGGTGGTGGTGGTGGTGCTTGTACAGCTCGTCCATGCCGAG
Generation of GFP tagging and knockout vectors for PbAMPD by recombineering		
P68	QC1	CGCACATGTGTATGTAATACTACTTC
P69	QC2	GAAGTAATGAAGCGAGTACTTTG
P70	QC3	GGGGAGAAAACAGCTCACCC
P71	QC4	AATGCGCAAACTCGAGCTCG
P72	Knockout recup	GTTTATATGTCTTTAAAAAAAATTTATATACTTATAAATATATAAAAATA**CCGCCTACTGCGACTATAGA**
P73	Knockout recdown	CCCATTTTATAAAAATTCAAATTGTCACTGAATTATAAAAATGTGAACAT**AAGGCGCATAACGATACCAC**
P74	Tag recup	ATGAAGAAAATGAAAATATCATAAGGCTTGCTAATTATTTTAATAAATCA**AAGGCGCATAACGATACCAC**
P75	Tag recdown	CCCATTTTATAAAAATTCAAATTGTCACTGAATTATAAAAATGTGAACAT**CCGCCTACTGCGACTATAGA**
P76	Zeo	TCATTCTTCGAAAACGATCTGCG
P77	yFCU	GTGGATGAAAATATTACTGGTGCTTTGAGGGGTGAGC
P78	hDHFR	ACTTCTTAAACCTAATCTGTAGTAAGGAAGGGATTG
P79	5’ integration	TTACACAAATCAGTGTGTCTAAGCCAG
P80	3’ integration	CTATGTGGCATTACCTCACAATAGTTCGGCG
Generation of probe for Southern blot		
P81	CATGCACATGCATGTAAATAGCTAAAATTATGAAC	
P82	CAAGTCCAACTATTTATGAATCATTGAAGAGACAAC	
AMPD cDNA synthesis from GFP tagged AMPD *P. berghei* parasite		
P83	CATATGATCTGGGTATCTCGCAAAGCATTG	
Cloning of GFP tagged PbAMPD in PbCEN5		
P84	TTATAAATAAATAAAAAATTTTATAAAACATAGGG**ATGAATGATCAAAAAAATGAAGGC**	
P85	ACAACTCCAGTGAAAAGTTCTTCTCCTTTACTCAT**TGATTTATTAAAATAATTAGCAAGCCTTATG**	
Cloning of GFP tagged PbAMPD mutant in PbCEN5		
P86	PbCEN5 bacbone FP	GCCTTCAAAATTTAAATTTATTTTAATATTTCC
P87	GFP internal RP	CATATGATCTGGGTATCTCGCAAAGCATTG
P88	H245A/H247A FP	CATAAGGAAAGTGGATGCA**GCT**GTG**GCT**CATTCAGCATGTATGCAAC

P89	H245A/H247A RP	GTTGCATACATGCTGAATG**AGC**CAC**AGC**TGCATCCACTTTCCTTATG
Genotyping of yeast knockout strains		
P90	amd1fp	AACTTTATTTTAGGGCACGTGG
P91	amd1rp	ATTCGAGGTAAAAACTTCAACAGC
P92	ade1fp	TTCTTTGAGGTAAGACGGTTGGG
P93	ade1rp	AGCCAGGGAAGTAATTAGCGG
P94	ade2fp	TATTAGTGAGAAGCCGAGAATTTTG
P95	ade2fp	ACTACAAAGATATCCTGACGTAGCG
Cloning of N-terminal Strep and C-terminal GFP tagged PfAMPD in pYES2/CT		
P96	CTT**GGTACC**ATGTGGTCTCATCCACAATTTGAGAAGCGCTTACCAAACAAGAATGATGGTC	
Cloning of conditional knockdown construct for PfAMPD in pGDB		
P97	AAAGC**CTCGAG**GAAATATGAGACCCATGGCATTCAG	
P98	GCAC**CCTAGG**ATTGTTTGATGAATAGCTAGCTAGTCGTTCG	

Studies on HADSF members

Synthesis of 2-phospholactate

Both D and L isomers of 2-phospholactate were synthesized according to the protocol described in 'Chapter 2'. The molecules were characterized by NMR and mass spectrometry.

2-phospho L-lactate. ^{1}H NMR (600 MHz, D_2O): δ 4.75 (m, 1H), 1.50 (d, 3H); ^{13}C NMR (150 MHz): δ 175.9, 70.6, 18.8; ^{31}P NMR (243 MHz): δ -0.33; HRMS (ESI-TOF, $\{M + H\}^+$) calcd.for $(C_3H_7O_6P + H)^+$ 171.0014 found 171.0041. Number of scans: 16 (^{1}H NMR), 256 (^{31}P NMR), and 512 (^{13}C NMR).

2-phospho D-lactate. ^{1}H NMR (600 MHz, D_2O): δ 4.71 (m, 1H), 1.49 (d, 3H); ^{13}C NMR (150 MHz): δ 176.5, 70.2, 19.0; ^{31}P NMR (243 MHz): δ -0.07; HRMS (ESI-TOF, $\{M + H\}^+$) calcd.for $(C_3H_7O_6P + H)^+$ 171.0014 found 171.0059. Number of scans: 16 (^{1}H NMR), 256 (^{31}P NMR), and 6144 (^{13}C NMR).

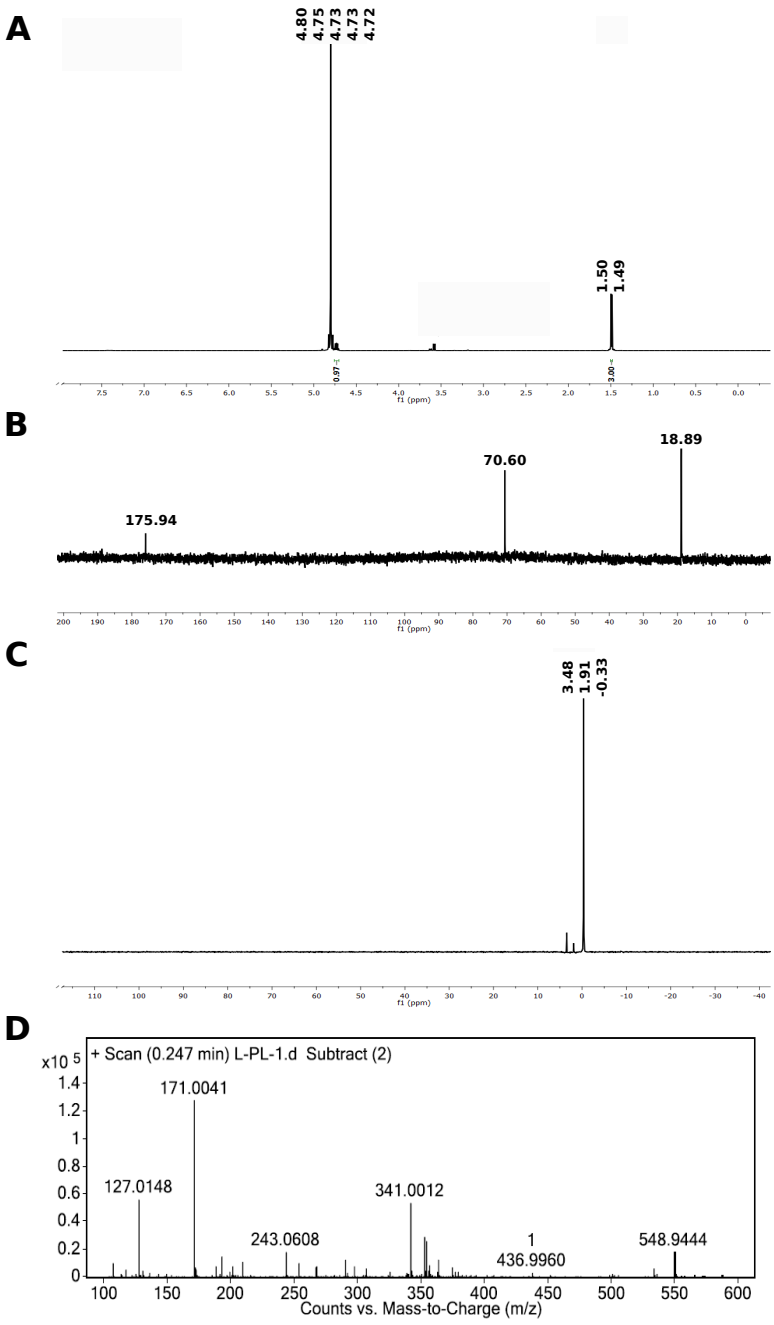

Figure A.6: Characterization of 2-Phospho L-lactate

(A) ^{1}H NMR of 2-Phospho L-lactate in D_2O. (B) ^{13}C NMR of 2-Phospho L-lactate in D_2O. (C) ^{31}P NMR of 2-Phospho L-lactate in D_2O. (D) HRMS (ESI-TOF) spectra of 2-Phospho L-lactate.

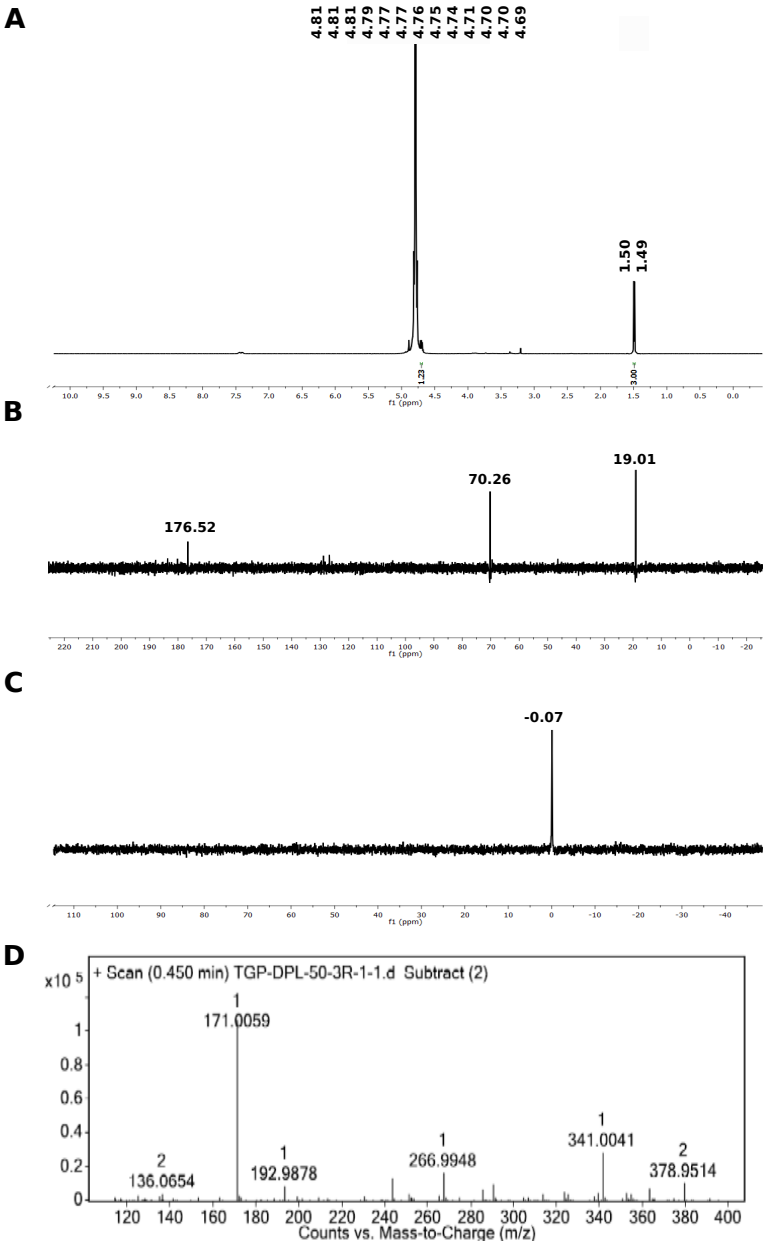

Figure A.7: Characterization of 2-Phospho D-lactate

(A) ^{1}H NMR of 2-Phospho D-lactate in D_2O. (B) ^{13}C NMR of 2-Phospho D-lactate in D_2O. (C) ^{31}P NMR of 2-Phospho D-lactate in D_2O. (D) HRMS (ESI-TOF) spectra of 2-Phospho D-lactate.

List of primers

Cloning of PfHAD3 in pET23d		
P1	CATG**GCTAGC**TTAAAACACAAATATAACGATTCATGTGTAC	
P2	CTTT**CTCGAG**AGAGCGCCTTCCAGATAAAACTC	
Cloning of PfHADx in pET22b		
P3	AGCC**CATATG**AAAGATGAACAAATATCATGTTATTATCTTAC	
P4	ACCG**CTCGAG**TGCAAGTATACTATCTAGATCTCGACAG	
Cloning of PfPGP in pET23d		
P5	CAAG**CCATGG**CTTTAATTTATTCGAGTGATAAAAAAGATG	
P6	ACCG**CTCGAG**TAATTCCGATATGGATTTCATAAAATAATCAGG	
Cloning of PbPGP in pET22b		
P7	AGCC**CATATG**TCATTAATCGTTTCTGAAGCTAGCC	
P8	ACCG**CTCGAG**AAATTCCAAAATAGACTTCATAAAATAATCAG	
Cloning of PfHADx D29N in pET22b		
P9	TAAAATTGATAACGTTCAACCTTGACCATACGATATG	
P10	CATATCGTATGGTCAAGGTTGAACGTTATCAATTTTA	
Cloning of PbPGP D49N in pET22b		
P11	GAAGTTTTTTTTTTTAACTGTGATGGGGTTTTATGG	
P12	CCATAAAACCCCATCACAGTTAAAAAAAAAAACTTC	
Common T7 primers		
P13	TAATACGACTCACTATAGGG	
P14	GCTAGTTATTGCTCAGCGG	
PBANKA_1441100 (PbHAD2) knockout		
P15	QC1	GCTTATTTTTTCCTGTGCATTGCTTGGAC
P16	QC2	CCAACCTTAGATCTTCCTGTGCATATACTTACC
P17	5' integration	GCCATAGATATCGATGGAACGTTAGCAG
P18	3' integration	CACGCACACATGTGCAGGTATTATGTTAGTTAC
PBANKA_0929700 (PbHADx) knockout		
P19	QC1	GTCTTTGTCATTGCTGTGTAAATTGAAATATATGGG
P20	QC2	CGGCATAATTAAGTAATGCATTTATATTCCATAAAGTATC
P21	5' integration	GTATATAATTCAGGGAGGATTAACGATGC
P22	3' integration	CACGCACACATGTGCAGGTATTATGTTAGTTAC
PBANKA_1441000 (PbHAD3) knockout		
P23	QC1	CCCCATTAACGAAGGATCAATACACTCG
P24	QC2	GCATATGCCCCATGAGAATATATTCCATCC
P25	recup	AATTAGGGATTAAAGTTATATTAGCTACTGGTAGACTACAACCATATGCTccgcctactgcgactataga
P26	recdw	ATGATAGAAAATTTATATTTATTGGTGTAAATAAATATATATATATATATAaaggcgcataacgataccac
P27	5' integration	GCTTTATAGTGGTCAAACTAGCTAAATACGAAC

P28	3' integration	CCATCGAAATCAATTAGGAGTAGTTTAATATCTGC
PBANKA_1421300 (PbPGP) knockout and tagging		
P29	QC1	ACTCGGGCACGTTATCTCAATGG
P29	QC2	CTCCTCTCCATAAAACCCCATCACAATC
P30	QC3	TGGAGTTACCGATGCGAATGTG
P31	QC4	AGCGATAATGAGGCATCAGAAGC
P32	recup	ATATCTTATTTTAAAATAAAATATTTTGAAAAAGGAAAAAAAAAGAAAAAccgcctactgcgactataga
P33	recdw	ACTGAAATATATATATATATATGTATATATCCACATGTTATATGCATCATaaggcgcataacgataccac
P34	tagrecup	ATTTAAATATTAAACCTGATTATTTTATGAAGTCTATTTTGGAATTTTTAaaggcgcataacgataccac
P35	tagrecdw	ACTGAAATATATATATATATATGTATATATCCACATGTTATATGCATCATccgcctactgcgactataga
P36	5' integration	CCATCAAAAGTGATAGATCGTCTAGCAATAGTAG
P37	3' integration	GATTTAATCCCCAATTATATGAACAAATCGAAAACGG
Common primers		
P38	ZEO	TCATTCTTCGAAAACGATCTGCG
P39	yFCU	GTGGATGAAAATATTACTGGTGCTTTGAGGGGTGAGC
P40	hDHFR	ACTTCTTAAACCTAATCTGTAGTAAGGAAGGGATTG
PCR amplification of GFP-DDD-HA (RFA)		
P41	TGTACAAAAAAGCAGGCTTG**CCGCGG**ATGAGTAAAGGAGAAGAACTTTTCACTGG	
P42	ATATATAAGTAAGAAAAACG**GGGCCC**TCAAGCGTAATCTGGAACATCG	

Rights and permissions

SPRINGER NATURE LICENSE TERMS AND CONDITIONS

Jun 06, 2019

This Agreement between Mr. Lakshmeesha Nagappa ("You") and Springer Nature ("Springer Nature") consists of your license details and the terms and conditions provided by Springer Nature and Copyright Clearance Center.

License Number	4603100657822
License date	Jun 06, 2019
Licensed Content Publisher	Springer Nature
Licensed Content Publication	Nature Reviews Disease Primers
Licensed Content Title	Malaria
Licensed Content Author	Margaret A. Phillips, Jeremy N. Burrows, Christine Manyando, Rob Hooft van Huijsduijnen, Wesley C. Van Voorhis et al.
Licensed Content Date	Aug 3, 2017
Licensed Content Volume	3
Type of Use	Thesis/Dissertation
Requestor type	non-commercial (non-profit)
Format	print and electronic
Portion	figures/tables/illustrations
Number of figures/tables/illustrations	1
High-res required	no
Will you be translating?	no
Circulation/distribution	<501
Author of this Springer Nature content	no
Title	Biochemical and Physiological Investigations on Adenosine Monophosphate Deaminase and Haloacid Dehalogenase Superfamily Members from Plasmodium spp.
Institution name	n/a
Expected presentation date	Jun 2019
Portions	Figure 1
Requestor Location	Mr. Lakshmeesha Nagappa JNCASR Bangalore, Karnataka 560064 India Attn: Mr. Lakshmeesha Nagappa
Total	0.00 USD

Terms and Conditions

Springer Nature Terms and Conditions for RightsLink Permissions
Springer Nature Customer Service Centre GmbH (the Licensor) hereby grants you a non-exclusive, world-wide licence to reproduce the

Copyright Clearance Center

Confirmation Number: 11828725
Order Date: 07/02/2019

Customer Information

Customer: Lakshmeesha Nagappa
Account Number: 3001339173
Organization: Lakshmeesha Nagappa
Email: lakshmeeshakn@jncasr.ac.in
Phone: +91 8105084052
Payment Method: Invoice

This is not an invoice

Order Details

Mini reviews in medicinal chemistry

Billing Status: **N/A**

Order detail ID: 71937265
ISSN: 1389-5575
Publication Type: Journal
Volume:
Issue:
Start page:
Publisher: BENTHAM SCIENCE PUBLISHERS LTD.

Permission Status: **Granted**
Permission type: Republish or display content
Type of use: Thesis/Dissertation
Order License Id: 4621120432746

Requestor type	Academic institution
Format	Print, Electronic
Portion	chart/graph/table/figure
Number of charts/graphs/tables/figures	1
The requesting person/organization	Lakshmeesha K N
Title or numeric reference of the portion(s)	Table 1
Title of the article or chapter the portion is from	Drug Targets for Plasmodium falciparum: A Post-Genomic Review/Survey
Editor of portion(s)	N/A
Author of portion(s)	Altman, Russ B. ; Yeh, Iwei
Volume of serial or monograph	6
Issue, if republishing an article from a serial	2
Page range of portion	179-182
Publication date of portion	Feb 1, 2006
Rights for	Main product
Duration of use	Life of current edition
Creation of copies for the disabled	no
With minor editing privileges	no
For distribution to	Worldwide
In the following language(s)	Original language of publication
With incidental promotional use	no

Bentham Science Publishers Ltd. LICENSE TERMS AND CONDITIONS

Jun 06, 2019

This is a License Agreement between Mr. Lakshmeesha Nagappa ("You") and Bentham Science Publishers Ltd. ("Bentham Science Publishers Ltd.") provided by Copyright Clearance Center ("CCC"). The license consists of your order details, the terms and conditions provided by Bentham Science Publishers Ltd., and the payment terms and conditions.

All payments must be made in full to CCC. For payment instructions, please see information listed at the bottom of this form.

License Number	4603110712456
License date	Jun 06, 2019
Licensed content publisher	Bentham Science Publishers Ltd.
Licensed content title	CURRENT TOPICS IN MEDICINAL CHEMISTRY -HILVERSUM-
Licensed content date	Jan 1, 2001
Type of Use	Thesis/Dissertation
Requestor type	Academic institution
Format	Print, Electronic
Portion	image/photo
Number of images/photos requested	1
The requesting person/organization is:	Lakshmeesha K N
Title or numeric reference of the portion(s)	Figure 1
Title of the article or chapter the portion is from	Purine and Pyrimidine Pathways as Targets in Plasmodium falciparum
Editor of portion(s)	N/A
Author of portion(s)	L. Schramm, Vern ; et al
Volume of serial or monograph.	11
Issue, if republishing an article from a serial	16
Page range of the portion	2103-2115
Publication date of portion	Aug 1, 2011
Rights for	Main product
Duration of use	Life of current and all future editions
Creation of copies for the disabled	no
With minor editing privileges	no
For distribution to	Worldwide
In the following language(s)	Original language of publication
With incidental promotional use	no

ELSEVIER LICENSE
TERMS AND CONDITIONS

Jun 06, 2019

This Agreement between Mr. Lakshmeesha Nagappa ("You") and Elsevier ("Elsevier") consists of your license details and the terms and conditions provided by Elsevier and Copyright Clearance Center.

License Number	4603191402601
License date	Jun 06, 2019
Licensed Content Publisher	Elsevier
Licensed Content Publication	Molecular and Biochemical Parasitology
Licensed Content Title	Central carbon metabolism of Plasmodium parasites
Licensed Content Author	Kellen L. Olszewski,Manuel Llinás
Licensed Content Date	Feb 1, 2011
Licensed Content Volume	175
Licensed Content Issue	2
Licensed Content Pages	9
Start Page	95
End Page	103
Type of Use	reuse in a thesis/dissertation
Intended publisher of new work	other
Portion	figures/tables/illustrations
Number of figures/tables/illustrations	1
Format	both print and electronic
Are you the author of this Elsevier article?	No
Will you be translating?	No
Original figure numbers	Figure 1
Title of your thesis/dissertation	Biochemical and Physiological Investigations on Adenosine Monophosphate Deaminase and Haloacid Dehalogenase Superfamily Members from Plasmodium spp.
Expected completion date	Jun 2019
Estimated size (number of pages)	150
Requestor Location	Mr. Lakshmeesha Nagappa JNCASR Bangalore, Karnataka 560064 India Attn: Mr. Lakshmeesha Nagappa
Publisher Tax ID	GB 494 6272 12
Total	0.00 USD
Terms and Conditions	

JOHN WILEY AND SONS LICENSE TERMS AND CONDITIONS

Jul 08, 2019

This Agreement between Mr. Lakshmeesha Nagappa ("You") and John Wiley and Sons ("John Wiley and Sons") consists of your license details and the terms and conditions provided by John Wiley and Sons and Copyright Clearance Center.

License Number	4624300499721
License date	Jul 08, 2019
Licensed Content Publisher	John Wiley and Sons
Licensed Content Publication	Molecular Microbiology
Licensed Content Title	Biochemical and physiological investigations on adenosine 5′ monophosphate deaminase from Plasmodium spp.
Licensed Content Author	Lakshmeesha Kempaiah Nagappa, Dipti Singh, Sandeep Dey, et al
Licensed Content Date	Jul 5, 2019
Licensed Content Volume	0
Licensed Content Issue	0
Licensed Content Pages	20
Type of use	Dissertation/Thesis
Requestor type	Author of this Wiley article
Format	Print and electronic
Portion	Full article
Will you be translating?	No
Title of your thesis / dissertation	Biochemical and Physiological Investigations on Adenosine Monophosphate Deaminase and Haloacid Dehalogenase Superfamily Members from Plasmodium spp.
Expected completion date	Jul 2019
Expected size (number of pages)	150
Requestor Location	Mr. Lakshmeesha Nagappa JNCASR Bangalore, Karnataka 560064 India Attn: Mr. Lakshmeesha Nagappa
Publisher Tax ID	EU826007151
Total	0.00 USD
Terms and Conditions	

TERMS AND CONDITIONS

This copyrighted material is owned by or exclusively licensed to John Wiley & Sons, Inc. or one of its group companies (each a"Wiley Company") or handled on behalf of a society with which a Wiley Company has exclusive publishing rights in relation to a particular work

INTRODUCTION

Copyright Clearance Center

Confirmation Number: 11813662
Order Date: 05/09/2019

Customer Information

Customer: Lakshmeesha Nagappa
Account Number: 3001339173
Organization: Lakshmeesha Nagappa
Email: lakshmeeshakn@jncasr.ac.in
Phone: +91 8105084052
Payment Method: Invoice

This is not an invoice

Order Details

Journal of biological chemistry

Billing Status: **N/A**

Order detail ID:	71894998
ISSN:	1083-351X
Publication Type:	e-Journal
Volume:	
Issue:	
Start page:	
Publisher:	AMERICAN SOCIETY FOR BIOCHEMISTRY AND MOLECULAR BI
Author/Editor:	AMERICAN SOCIETY FOR BIOCHEMISTRY & MOLECULAR BIOL

Permission Status: **Granted**

Permission type: Republish or display content
Type of use: Thesis/Dissertation
Order License Id: 4584590115688

Requestor type	Academic institution
Format	Print, Electronic
Portion	chapter/article
The requesting person/organization	Lakshmeesha K N
Title or numeric reference of the portion(s)	Article
Title of the article or chapter the portion is from	Phosphoglycolate phosphatase is a metabolic proofreading enzyme essential for cellular function in Plasmodium berghei
Editor of portion(s)	Ruma Banerjee
Author of portion(s)	N/A
Volume of serial or monograph	294
Issue, if republishing an article from a serial	13
Page range of portion	
Publication date of portion	January 30, 2019
Rights for	Main product
Duration of use	Life of current edition
Creation of copies for the disabled	no
With minor editing privileges	no
For distribution to	Worldwide
In the following language(s)	Original language of publication
With incidental promotional use	no
Lifetime unit quantity of new product	Up to 499

Bibliography

Akizu N, Cantagrel V, Schroth J, Cai N, Vaux K, et al. (2013) AMPD2 regulates GTP synthesis and is mutated in a potentially treatable neurodegenerative brainstem disorder. Cell **154**: 505–517.

Allen KN, Dunaway-Mariano D (2004) Phosphoryl group transfer: evolution of a catalytic scaffold. Trends Biochem Sci **29**: 495–503.

Allen KN, Dunaway-Mariano D (2009) Markers of fitness in a successful enzyme superfamily. Curr Opin Struct Biol **19**: 658–665.

Angov E, Hillier CJ, Kincaid RL, Lyon JA (2008) Heterologous protein expression is enhanced by harmonizing the codon usage frequencies of the target gene with those of the expression host. PloS one **3**: e2189.

Antony HA, Parija SC (2016) Antimalarial drug resistance: an overview. Trop Parasitol **6**: 30–41.

Aparicio IM, Marín-Menéndez A, Bell A, Engel PC (2010) Susceptibility of *Plasmodium falciparum* to glutamate dehydrogenase inhibitors–A possible new antimalarial target. Mol Biochem Parasitol **172**: 152–155.

Arbona RM (2006) Mechanistic characterization of members of the amidohydrolase superfamily. Ph.D. thesis, Texas A&M University.

Armstrong CM, Goldberg DE (2007) An FKBP destabilization domain modulates protein levels in *Plasmodium falciparum*. Nat Methods **4**: 1007–1009.

Atamna H, Ginsburg H (1993) Origin of reactive oxygen species in erythrocytes infected with *Plasmodium falciparum*. Mol Biochem Parasitol **61**: 231–241.

Atkinson DE (1968) Energy charge of the adenylate pool as a regulatory parameter. Interaction with feedback modifiers. Biochemistry **7**: 4030–4034.

Aurrecoechea C, Barreto A, Basenko EY, Brestelli J, Brunk BP, et al. (2016) EuPathDB: the eukaryotic pathogen genomics database resource. Nucleic Acids Res **45**: D581–D591.

Ballut L, Violot S, Shivakumaraswamy S, Thota LP, Sathya M, et al. (2015) Active site coupling in *Plasmodium falciparum* GMP synthetase is triggered by domain rotation. Nat Commun **6**: 8930.

Balu B, Shoue DA, Fraser MJ, Adams JH (2005) High-efficiency transformation of *Plasmodium falciparum* by the lepidopteran transposable element piggyBac. Proc Natl Acad Sci USA **102**: 16391–16396.

Bauschjurken MT, Sabina RL (1995) Divergent N-terminal regions in AMP deaminase and isoform-specific catalytic properties of the enzyme. Arch Biochem Biophys **321**: 372–380.

Bazin RJ, McDonald GA, Phillips C (2003) UK Patent GB2373504 .

Belen Cassera M, Zhang Y, Z Hazleton K, L Schramm V (2011) Purine and pyrimidine pathways as targets in *Plasmodium falciparum*. Curr Top Med Chem **11**: 2103–2115.

Beyer HM, Gonschorek P, Samodelov SL, Meier M, Weber W, et al. (2015) AQUA cloning: a versatile and simple enzyme-free cloning approach. PloS one **10**: e0137652.

Bhat JY, Shastri BG, Balaram H (2008) Kinetic and biochemical characterization of *Plasmodium falciparum* GMP synthetase. Biochem J **409**: 263–273.

Bhat JY, Venkatachala R, Balaram H (2011a) Substrate-induced conformational changes in *Plasmodium falciparum* guanosine monophosphate synthetase. The FEBS J **278**: 3756–3768.

Bhat JY, Venkatachala R, Singh K, Gupta K, Sarma SP, et al. (2011b) Ammonia channeling in *Plasmodium falciparum* GMP synthetase: investigation by NMR spectroscopy and biochemical assays. Biochemistry **50**: 3346–3356.

Bianchi-Smiraglia A, Wawrzyniak J, Bagati A, Marvin E, Ackroyd J, et al. (2015) Pharmacological targeting of guanosine monophosphate synthase suppresses melanoma cell invasion and tumorigenicity. Cell Death Differ **22**: 1858–1864.

Bowler MW, Cliff MJ, Waltho JP, Blackburn GM (2010) Why did Nature select phosphate for its dominant roles in biology? New J Chem **34**: 784–794.

Bulusu V, Jayaraman V, Balaram H (2011a) Metabolic fate of fumarate, a side product of the purine salvage pathway in the intraerythrocytic stages of *Plasmodium falciparum*. J Biol Chem **286**: 9236–9245.

Bulusu V, Srinivasan B, Bopanna MP, Balaram H (2009) Elucidation of the substrate specificity, kinetic and catalytic mechanism of adenylosuccinate lyase from *Plasmodium falciparum*. Biochim Biophys Acta **1794**: 642–654.

Bulusu V, Thakur SS, Venkatachala R, Balaram H (2011b) Mechanism of growth inhibition of intraerythrocytic stages of *Plasmodium falciparum* by 5-aminoimidazole-4-carboxamide ribonucleoside (AICAR). Mol Biochem Parasitol **177**: 1–11.

Burroughs AM, Allen KN, Dunaway-Mariano D, Aravind L (2006) Evolutionary genomics of the HAD superfamily: understanding the structural adaptations and catalytic diversity in a superfamily of phosphoesterases and allied enzymes. J Mol Biol **361**: 1003–1034.

Bushell E, Gomes AR, Sanderson T, Anar B, Girling G, et al. (2017) Functional profiling of a *Plasmodium* genome reveals an abundance of essential genes. Cell **170**: 260–272.

Calderone V, Forleo C, Benvenuti M, Thaller MC, Rossolini GM, et al. (2004) The first structure of a bacterial class B acid phosphatase reveals further structural heterogeneity among phosphatases of the haloacid dehalogenase fold. J Mol Biol **335**: 761–773.

Caparrós-Martín JA, Reiland S, Köchert K, Cutanda MC, Culiánez-Macia FA (2007) *Arabidopsis thaliana* AtGpp1 and AtGpp2: two novel low molecular weight phosphatases involved in plant glycerol metabolism. Plant Mol Biol **63**: 505–517.

Carballar-Lejarazú R, James AA (2017) Population modification of Anopheline species to control malaria transmission. Pathog Glob Health **111**: 424–435.

Carter R, Mendis KN (2002) Evolutionary and historical aspects of the burden of malaria. Clin Microbiol Rev **15**: 564–594.

Cassera MB, Hazleton KZ, Riegelhaupt PM, Merino EF, Luo M, et al. (2008) Erythrocytic adenosine monophosphate as an alternative purine source in *Plasmodium falciparum*. J Biol Chem **283**: 32889–32899.

Chae SC, Fuller D, Loomis WF (2002) Altered cell-type proportioning in *Dictyostelium* lacking adenosine monophosphate deaminase. Dev Biol **241**: 183–194.

Chapman AG, Atkinson DE (1973) Stabilization of adenylate energy charge by the adenylate deaminase reaction. J Biol Chem **248**: 8309–8312.

Chapman AG, Fall L, Atkinson DE (1971) Adenylate energy charge in *Escherichia coli* during growth and starvation. J Bacteriol **108**: 1072–1086.

Chen P, Toribara Tt, Warner H (1956) Microdetermination of phosphorus. Anal Chem **28**: 1756–1758.

Chung C, Niemela SL, Miller RH (1989) One-step preparation of competent *Escherichia coli*: transformation and storage of bacterial cells in the same solution. Proc Natl Acad Sci USA **86**: 2172–2175.

Collard F, Baldin F, Gerin I, Bolsée J, Noël G, et al. (2016) A conserved phosphatase destroys toxic glycolytic side products in mammals and yeast. Nat Chem Biol **12**: 601.

Collart F, Chubb C, Mirkin B, Huberman E (1992) Increased inosine-5'-phosphate dehydrogenase gene expression in solid tumor tissues and tumor cell lines. Cancer Res **52**: 5826–5828.

Collart FR, Huberman E (1990) Expression of IMP dehydrogenase in differentiating HL-60 cells. Blood **75**: 570–576.

Cowman AF, Healer J, Marapana D, Marsh K (2016) Malaria: biology and disease. Cell **167**: 610–624.

Crabb BS, Cowman AF (1996) Characterization of promoters and stable transfection by homologous and nonhomologous recombination in *Plasmodium falciparum*. Proc Natl Acad Sci USA **93**: 7289–7294.

Crowther GJ, Napuli AJ, Gilligan JH, Gagaring K, Borboa R, et al. (2011) Identification of inhibitors for putative malaria drug targets among novel antimalarial compounds. Mol Biochem Parasitol **175**: 21–29.

de Koning-Ward TF, Gilson PR, Crabb BS (2015) Advances in molecular genetic systems in malaria. Nat Rev Microbiol **13**: 373–387.

DeFronzo RA, Tripathy D (2009) Skeletal muscle insulin resistance is the primary defect in type 2 diabetes. Diabetes Care **32**: S157–S163.

del Prado GRL, García CH, Cea LM, Espinilla VF, Moreno MFM, et al. (2014) Malaria in developing countries. J Infect Dev Ctries **8**: 001–004.

Dondorp AM, Nosten F, Yi P, Das D, Phyo AP, et al. (2009) Artemisinin resistance in *Plasmodium falciparum* malaria. N Engl J Med **361**: 455–467.

Downie MJ, Kirk K, Mamoun CB (2008) Purine salvage pathways in the intraerythrocytic malaria parasite *Plasmodium falciparum*. Eukaryot Cell **7**: 1231–1237.

Dumont L, Richardson MB, van der Peet P, Dixon MW, Williams SJ, et al. (2018) The metabolic repair enzyme phospho-glycolate phosphatase regulates central carbon metabolism and fosmidomycin sensitivity in *Plasmodium falciparum*. bioRxiv p. 415505.

Eaazhisai K, Jayalakshmi R, Gayathri P, Anand R, Sumathy K, et al. (2004) Crystal structure of fully ligated adenylosuccinate synthetase from *Plasmodium falciparum*. J Mol Biol **335**: 1251–1264.

Eastman RT, Fidock DA (2009) Artemisinin-based combination therapies: a vital tool in efforts to eliminate malaria. Nat Rev Microbiol **7**: 864–874.

Elford BC, Haynes JD, Chulay JD, Wilson RJ (1985) Selective stage-specific changes in the permeability to small hydrophilic solutes of human erythrocytes infected with *Plasmodium falciparum*. Mol Biochem Parasitol **16**: 43–60.

Fishbein WN, Armbrustmacher VW, Griffin JL (1978) Myoadenylate deaminase deficiency: a new disease of muscle. Science **200**: 545–548.

Fuhrmann M, Hausherr A, Ferbitz L, Schödl T, Heitzer M, et al. (2004) Monitoring dynamic expression of nuclear genes in *Chlamydomonas reinhardtii* by using a synthetic luciferase reporter gene. Plant Mol Biol **55**: 869–881.

Gardner MJ, Hall N, Fung E, White O, Berriman M, et al. (2002) Genome sequence of the human malaria parasite *Plasmodium falciparum*. Nature **419**: 498.

Gaspar P, Oliveira JL, Frommlet J, Santos MA, Moura G (2012) EuGene: maximizing synthetic gene design for heterologous expression. Bioinformatics **28**: 2683–2684.

Ghorbal M, Gorman M, Macpherson CR, Martins RM, Scherf A, et al. (2014) Genome editing in the human malaria parasite *Plasmodium falciparum* using the CRISPR-Cas9 system. Nat Biotechnol **32**: 819–821.

Giacomello A, Salerno C (1978) Human hypoxanthine-guanine phosphoribosyltransferase. Steady state kinetics of the forward and reverse reactions. J Biol Chem **253**: 6038–6044.

Gietz RD, Schiestl RH (2007) High-efficiency yeast transformation using the LiAc/SS carrier DNA/PEG method. Nat Protoc **2**: 31–34.

Godiska R, Mead D, Dhodda V, Wu C, Hochstein R, et al. (2009) Linear plasmid vector for cloning of repetitive or unstable sequences in *Escherichia coli*. Nucleic Acids Res **38**: e88–e88.

Gomes AR, Bushell E, Schwach F, Girling G, Anar B, et al. (2015) A genome-scale vector resource enables high-throughput reverse genetic screening in a malaria parasite. Cell host & microbe **17**: 404–413.

Goonewardene R, Daily J, Kaslow D, Sullivan TJ, Duffy P, et al. (1993) Transfection of the malaria parasite and expression of firefly luciferase. Proc Natl Acad Sci USA **90**: 5234–5236.

Greenwood B, Mutabingwa T (2002) Malaria in 2002. Nature **415**: 670–672.

Guggisberg AM, Amthor RE, Odom AR (2014a) Isoprenoid biosynthesis in *Plasmodium falciparum*. Eukaryot Cell **13**: 1348–1359.

Guggisberg AM, Frasse PM, Jezewski AJ, Kafai NM, Gandhi AY, et al. (2018) Suppression of drug resistance reveals a genetic mechanism of metabolic plasticity in malaria parasites. mBio **9**: e01193–18.

Guggisberg AM, Park J, Edwards RL, Kelly ML, Hodge DM, et al. (2014b) A sugar phosphatase regulates the methylerythritol phosphate (MEP) pathway in malaria parasites. Nat Comm **5**: 4467.

Guiguemde WA, Shelat AA, Bouck D, Duffy S, Crowther GJ, et al. (2010) Chemical genetics of *Plasmodium falciparum*. Nature **465**: 311–315.

Han BW, Bingman CA, Mahnke DK, Bannen RM, Bednarek SY, et al. (2006) Membrane association, mechanism of action, and structure of *Arabidopsis* embryonic factor 1 (FAC1). J Biol Chem **281**: 14939–14947.

Hazleton KZ, Ho MC, Cassera MB, Clinch K, Crump DR, et al. (2012) Acyclic immucillin phosphonates: second-generation inhibitors of *Plasmodium falciparum* hypoxanthine-guanine-xanthine phosphoribosyltransferase. Chemistry & biology **19**: 721–730.

Hellsten Y, Richter E, Kiens B, Bangsbo J (1999) AMP deamination and purine exchange in human skeletal muscle during and after intense exercise. J Physiol **520**: 909–920.

Hortle E, Nijagal B, Bauer DC, Jensen LM, Ahn SB, et al. (2016) Adenosine monophosphate deaminase 3 activation shortens erythrocyte half-life and provides malaria resistance in mice. Blood **128**: 1290–1301.

Huang H, Pandya C, Liu C, Al-Obaidi NF, Wang M, et al. (2015) Panoramic view of a superfamily of phosphatases through substrate profiling. Proc Natl Acad Sci USA **112**: E1974–E1983.

Hunter T (2012) Why nature chose phosphate to modify proteins. Philos Trans Royal Soc B **367**: 2513–2516.

Huthmacher C, Hoppe A, Bulik S, Holzhütter HG (2010) Antimalarial drug targets in *Plasmodium falciparum* predicted by stage-specific metabolic network analysis. BMC Syst Biol **4**: 120.

Isackson PJ, Bujnicki H, Harding CO, Vladutiu GD (2005) Myoadenylate deaminase deficiency caused by alternative splicing due to a novel intronic mutation in the AMPD1 gene. Mol Genet Metab **86**: 250–256.

Iwanaga S, Khan SM, Kaneko I, Christodoulou Z, Newbold C, et al. (2010) Functional identification of the *Plasmodium* centromere and generation of a *Plasmodium* artificial chromosome. Cell Host & Microbe **7**: 245–255.

Jahngen EG, Rossomando EF (1986) AMP deaminase in *Dictycostelium discoideum*: Increase in activity following nutrient deprivation induced by starvation or hadacidin. Mol Cell Biochem **71**: 71–78.

James S, Collins FH, Welkhoff PA, Emerson C, Godfray HCJ, et al. (2018) Pathway to deployment of gene drive mosquitoes as a potential biocontrol tool for elimination of malaria in sub-Saharan Africa: recommendations of a scientific working group. Am J Trop Med Hyg **98**: 1–49.

Janse CJ, Ramesar J, Waters AP (2006) High-efficiency transfection and drug selection of genetically transformed blood stages of the rodent malaria parasite *Plasmodium berghei*. Nat Protoc **1**: 346–356.

Jayalakshmi R, Sumathy K, Balaram H (2002) Purification and characterization of recombinant *Plasmodium falciparum* adenylosuccinate synthetase expressed in *Escherichia coli*. Protein Expr Purif **25**: 65–72.

Jensen MD, Conley M, Helstowski LD (1983) Culture of *Plasmodium falciparum*: the role of pH, glucose, and lactate. J Parasitol **69**: 1060–1067.

Kalsi KK, Yuen AH, Rybakowska IM, Johnson PH, Slominska E, et al. (2003) Decreased cardiac activity of AMP deaminase in subjects with the AMPD1 mutation - a potential mechanism of protection in heart failure. Cardiovasc Res **59**: 678–684.

Ke H, Lewis IA, Morrisey JM, McLean KJ, Ganesan SM, et al. (2015) Genetic investigation of tricarboxylic acid metabolism during the *Plasmodium falciparum* life cycle. Cell Rep **11**: 164–174.

Knöckel J, Bergmann B, Müller IB, Rathaur S, Walter RD, et al. (2008) Filling the gap of intracellular dephosphorylation in the *Plasmodium falciparum* vitamin B1 biosynthesis. Mol Biochem Parasitol **157**: 241–243.

Konno Y, Natsumeda Y, Nagai M, Yamaji Y, Ohno S, et al. (1991) Expression of human IMP dehydrogenase types I and II in *Escherichia coli* and distribution in human normal lymphocytes and leukemic cell lines. J Biol Chem **266**: 506–509.

Kuznetsova E, Nocek B, Brown G, Makarova KS, Flick R, et al. (2015) Functional diversity of haloacid dehalogenase superfamily phosphatases from *Saccharomyces cerevisiae*: biochemical, structural, and evolutionary insights. J Biol Chem **290**: 18678–18698.

Kuznetsova E, Proudfoot M, Gonzalez CF, Brown G, Omelchenko MV, et al. (2006) Genome-wide analysis of substrate specificities of the *Escherichia coli* haloacid dehalogenase-like phosphatase family. J Biol Chem **281**: 36149–36161.

Kyrou K, Hammond AM, Galizi R, Kranjc N, Burt A, et al. (2018) A CRISPR–Cas9 gene drive targeting doublesex causes complete population suppression in caged *Anopheles gambiae* mosquitoes. Nat Biotechnol **36**: 1062–1066.

Lanaspa MA, Cicerchi C, Garcia G, Li N, Roncal-Jimenez CA, et al. (2012) Counteracting roles of AMP deaminase and AMP kinase in the development of fatty liver. PloS one **7**: e48801.

Lassila JK, Zalatan JG, Herschlag D (2011) Biological phosphoryl-transfer reactions: understanding mechanism and catalysis. Annu Rev Biochem **80**: 669–702.

Li CM, Tyler PC, Furneaux RH, Kicska G, Xu Y, et al. (1999) Transition-state analogs as inhibitors of human and malarial hypoxanthine-guanine phosphoribosyltransferases. Nat Struct Mol Biol **6**: 582–587.

Li P, Ogino K, Hoshikawa Y, Morisaki H, Toyama K, et al. (2013) AMP deaminase 3 plays a critical role in remote reperfusion lung injury. Biochem Biophys Res Commun **434**: 131–136.

Liehl P, Meireles P, Albuquerque IS, Pinkevych M, Baptista F, et al. (2015) Innate immunity induced by *Plasmodium* liver infection inhibits malaria reinfections. Infect Immun **83**: 1172–1180.

Lin-Cereghino J, Wong WW, Xiong S, Giang W, Luong LT, et al. (2005) Condensed protocol for competent cell preparation and transformation of the methylotrophic yeast *Pichia pastoris*. Biotechniques **38**: 44–48.

Lowenstein J (1972) Ammonia production in muscle and other tissues: the purine nucleotide cycle. Physiol Rev **52**: 382–414.

Lushchak VI, Smirnova YD, Storey KB (1998) AMP-deaminase from sea scorpion white muscle: properties and redistribution under hypoxia. Comp Biochem Physiol **119**: 611–618.

Madrid DC, Ting LM, Waller KL, Schramm VL, Kim K (2008) *Plasmodium falciparum* purine nucleoside phosphorylase is critical for viability of malaria parasites. J Biol Chem **283**: 35899–35907.

Mahmoudi S, Keshavarz H (2017) Efficacy of phase 3 trial of RTS, S/AS01 malaria vaccine: the need for an alternative development plan. Hum Vaccin Immunother **13**: 2098–2101.

Mangani S, Meyer-Klaucke W, Moir AJ, Ranieri-Raggi M, Martini D, et al. (2003) Characterization of the zinc-binding site of the histidine-proline-rich glycoprotein associated with rabbit skeletal muscle AMP deaminase. J Biol Chem **278**: 3176–3184.

Marotta R, Parry BR, Shain DH (2009) Divergence of AMP deaminase in the ice worm *Mesenchytraeus solifugus* (Annelida, Clitellata, Enchytraeidae). Int J Evol Biol **2009**.

Martini D, Ranieri-Raggi M, Sabbatini AR, Moir AJ, Polizzi E, et al. (2007) Characterization of the metallocenter of rabbit skeletal muscle AMP deaminase. A new model for substrate interactions at a dinuclear cocatalytic Zn site. Biochim Biophys Acta **1774**: 1508–1518.

Mehrotra S, Mylarappa B, Iyengar P, Balaram H (2010) Studies on active site mutants of *P. falciparum* adenylosuccinate synthetase: insights into enzyme catalysis and activation. Biochim Biophys Acta **1804**: 1996–2002.

Mehrotra S, Ningappa MB, Raman J, Anand RP, Balaram H (2012) Mutational analysis of cysteine 328 and cysteine 368 at the interface of *Plasmodium falciparum* adenylosuccinate synthetase. Biochim Biophys Acta **1824**: 589–597.

Mehta M, Sonawat HM, Sharma S (2006) Glycolysis in *Plasmodium falciparum* results in modulation of host enzyme activities. J Vector Borne Dis **43**: 95–103.

Merkler DJ, Schramm VL (1990) Catalytic and regulatory site composition of yeast AMP deaminase by comparative binding and rate studies. Resolution of the cooperative mechanism. J Biol Chem **265**: 4420–4426.

Merkler DJ, Schramm VL (1993) Catalytic mechanism of yeast adenosine 5'-monophosphate deaminase. Zinc content, substrate specificity, pH studies, and solvent isotope effects. Biochemistry **32**: 5792–5799.

Merkler DJ, Wali AS, Taylor J, Schramm VL (1989) AMP deaminase from yeast. Role in AMP degradation, large scale purification, and properties of the native and proteolyzed enzyme. J Biol Chem **264**: 21422–21430.

Meyer SL, Kvalnes-Krick KL, Schramm VL (1989) Characterization of AMD, the AMP deaminase gene in yeast. Production of amd strain, cloning, nucleotide sequence, and properties of the protein. Biochemistry **28**: 8734–8743.

Mikolajczak SA, Vaughan AM, Kangwanrangsan N, Roobsoong W, Fishbaugher M, et al. (2015) *Plasmodium vivax* liver stage development and hypnozoite persistence in human liver-chimeric mice. Cell host & microbe **17**: 526–535.

Mineo I, Kono N, Shimizu T, Hara N, Yamada Y, et al. (1985) Excess purine degradation in exercising muscles of patients with glycogen storage disease types V and VII. J Clin Invest **76**: 556–560.

Mony BM, Mehta M, Jarori GK, Sharma S (2009) Plant-like phosphofructokinase from *Plasmodium falciparum* belongs to a novel class of ATP-dependent enzymes. Int J Parasitol **39**: 1441–1453.

Mudeppa DG, Rathod PK (2013) Expression of functional *Plasmodium falciparum* enzymes using a wheat germ cell-free system. Eukaryot Cell **12**: 1653–1663.

Murakami K (1979) AMP Deaminase from Baker's Yeast: Kinetic and Molecular Properties. J Biochem **86**: 1331–1336.

Murakami K, Nagura H, Yoshino M (1980) Permeabilization of yeast cells: application to study on the regulation of AMP deaminase activity *in situ*. Anal Biochem **105**: 407–413.

Muralidharan V, Oksman A, Iwamoto M, Wandless TJ, Goldberg DE (2011) Asparagine repeat function in a *Plasmodium falciparum* protein assessed via a regulatable fluorescent affinity tag. Proc Natl Acad Sci USA **108**: 4411–4416.

Nagai M, Natsumeda Y, Weber G (1992) Proliferation-linked regulation of type II IMP dehydrogenase gene in human normal lymphocytes and HL-60 leukemic cells. Cancer Res **52**: 258–261.

Nagappa LK (2014) Preliminary Studies on *Plasmodium falciparum* adenosine 5' monophosphate deaminase. Master's thesis, Jawaharlal Nehru Centre for Advanced Scientific Research.

Nagappa LK, Satha P, Govindaraju T, Balaram H (2019a) Phosphoglycolate phosphatase is a metabolic proof-reading enzyme essential for cellular function in *Plasmodium berghei*. J Biol Chem **294**: 4997–5007.

Nagappa LK, Singh D, Dey S, Kumar KA, Balaram H (2019b) Biochemical and physiological investigations on adenosine 5' monophosphate deaminase from *Plasmodium spp.* Mol Microbiol **Manuscript accepted**.

Narayanaswamy R, Levy M, Tsechansky M, Stovall GM, O'Connell JD, et al. (2009) Widespread reorganization of metabolic enzymes into reversible assemblies upon nutrient starvation. Proc Natl Acad Sci USA **106**: 10147–10152.

Nowak T, Mildvan AS (1972) Nuclear magnetic resonance studies of the function of potassium in the mechanism of pyruvate kinase. Biochemistry **11**: 2819–2828.

Olotu A, Fegan G, Wambua J, Nyangweso G, Leach A, et al. (2016) Seven-year efficacy of RTS, S/AS01 malaria vaccine among young African children. N Engl J Med **374**: 2519–2529.

Olszewski KL, Llinás M (2011) Central carbon metabolism of *Plasmodium* parasites. Mol Biochem Parasitol **175**: 95–103.

Oppenheim RD, Creek DJ, Macrae JI, Modrzynska KK, Pino P, et al. (2014) BCKDH: the missing link in apicomplexan mitochondrial metabolism is required for full virulence of *Toxoplasma gondii* and *Plasmodium berghei*. PLoS Pathog **10**: e1004263.

Orr RY, Philip N, Waters AP (2012) Improved negative selection protocol for *Plasmodium berghei* in the rodent malarial model. Malar J **11**: 103.

Ouyang J, Parakhia RA, Ochs RS (2011) Metformin activates AMP kinase through inhibition of AMP deaminase. J Biol Chem **286**: 1–11.

Pei Y, Miller JL, Lindner SE, Vaughan AM, Torii M, et al. (2013) *Plasmodium yoelii* inhibitor of cysteine proteases is exported to exomembrane structures and interacts with yoelipain-2 during asexual blood-stage development. Cell Microbiol **15**: 1508–1526.

Pellicer MT, Nunez MF, Aguilar J, Badia J, Baldoma L (2003) Role of 2-phosphoglycolate phosphatase of *Escherichia coli* in metabolism of the 2-phosphoglycolate formed in DNA repair. J Bacteriol **185**: 5815–5821.

Pfander C, Anar B, Schwach F, Otto TD, Brochet M, et al. (2011) A scalable pipeline for highly effective genetic modification of a malaria parasite. Nat Methods **8**: 1078–1082.

Phillips M, Burrows J, Manyando C, van Huijsduijnen RH, WC VV, et al. (2017) Malaria. Nat Rev Dis Primers **3**: 17050.

Prakashkumar SA (2018) Structure-function study of an imp-specific 5'-nucleotidase from *Plasmodium falciparum*. Ph.D. thesis, Jawaharlal Nehru Centre for Advanced Scientific Research.

Proudfoot M, Kuznetsova E, Brown G, Rao NN, Kitagawa M, et al. (2004) General enzymatic screens identify three new nucleotidases in *Escherichia coli*: Biochemical characterization of SurE, YfbR, and YjjG. J Biol Chem **279**: 54687–54694.

Raman J, Mehrotra S, Anand RP, Balaram H (2004) Unique kinetic mechanism of *Plasmodium falciparum* adenylosuccinate synthetase. Mol Biochem Parasitol **138**: 1–8.

Rangarajan ES, Proteau A, Wagner J, Hung MN, Matte A, et al. (2006) Structural snapshots of *Escherichia coli* histidinol phosphate phosphatase along the reaction pathway. J Biol Chem **281**: 37930–37941.

Ranieri-Raggi M, Moir A, Raggi A (2014) The role of histidine-proline-rich glycoprotein as zinc chaperone for skeletal muscle AMP deaminase. Biomolecules **4**: 474–497.

Roberts A, Lee SY, McCullagh E, Silversmith RE, Wemmer DE (2005) YbiV from *Escherichia coli* K12 is a HAD phosphatase. Proteins: Struct, Funct, Bioinf **58**: 790–801.

Rodriguez-Suarez R, Xu D, Veillette K, Davison J, Sillaots S, et al. (2007) Mechanism-of-action determination of GMP synthase inhibitors and target validation in *Candida albicans* and *Aspergillus fumigatus*. Chemistry & biology **14**: 1163–1175.

Roth JE (1990) *Plasmodium falciparum* carbohydrate metabolism: a connection between host cell and parasite. Blood cells **16**: 453–60.

Roy S, Karmakar T, Rao VSP, Nagappa LK, Balasubramanian S, et al. (2015a) Slow ligand-induced conformational switch increases the catalytic rate in *Plasmodium falciparum* hypoxanthine guanine xanthine phosphoribosyltransferase. Mol Biosyst **11**: 1410–1424.

Roy S, Nagappa LK, Prahladarao VS, Balaram H (2015b) Kinetic mechanism of *Plasmodium falciparum* hypoxanthine-guanine-xanthine phosphoribosyltransferase. Mol Biochem Parasitol **204**: 111–120.

RTS SCTP (2015) Efficacy and safety of RTS, S/AS01 malaria vaccine with or without a booster dose in infants and children in Africa: final results of a phase 3, individually randomised, controlled trial. The Lancet **386**: 31–45.

Rui E, Fernandez-Becerra C, Takeo S, Sanz S, Lacerda MV, et al. (2011) *Plasmodium vivax*: comparison of immunogenicity among proteins expressed in the cell-free systems of *Escherichia coli* and wheat germ by suspension array assays. Malar J **10**: 192.

Sabina R, Swain J, Olanow C, Bradley WG, Fishbein W, et al. (1984) Myoadenylate deaminase deficiency. Functional and metabolic abnormalities associated with disruption of the purine nucleotide cycle. J Clin Invest **73**: 720–730.

Sabina RL, Mahnke-Zizelman DK (2000) Towards an understanding of the functional significance of N-terminal domain divergence in human AMP deaminase isoforms. Pharmacol Ther **87**: 279–283.

Sabina RL, Paul AL, Ferl RJ, Laber B, Lindell SD (2007) Adenine nucleotide pool perturbation is a metabolic trigger for AMP deaminase inhibitor-based herbicide toxicity. Plant Physiol **143**: 1752–1760.

Saint-Marc C, Pinson B, Coulpier F, Jourdren L, Lisova O, et al. (2009) Phenotypic consequences of purine nucleotide imbalance in *Saccharomyces cerevisiae*. Genetics **183**: 529–538.

Sambrook J, Russell DW (2001) Molecular cloning: a laboratory manual (3-volume set), vol. 999. Cold spring harbor laboratory press New York.

Sanderson T, Rayner JC (2017) PhenoPlasm: a database of disruption phenotypes for malaria parasite genes. Wellcome Open Res **2**.

Scheibel LW, Ashton SH, Trager W (1979) *Plasmodium falciparum*: microaerophilic requirements in human red blood cells. Exp Parasitol **47**: 410–418.

Schwach F, Bushell E, Gomes AR, Anar B, Girling G, et al. (2015) Plasmo GEM, a database supporting a community resource for large-scale experimental genetics in malaria parasites. Nucleic Acids Res **43**: D1176–D1182.

Schwarte S, Bauwe H (2007) Identification of the photorespiratory 2-phosphoglycolate phosphatase, PGLP1, in *Arabidopsis*. Plant Physiol **144**: 1580–1586.

Segerer G, Hadamek K, Zundler M, Fekete A, Seifried A, et al. (2016) An essential developmental function for murine phosphoglycolate phosphatase in safeguarding cell proliferation. Sci Rep **6**: 35160.

Seibert CM, Raushel FM (2005) Structural and catalytic diversity within the amidohydrolase superfamily. Biochemistry **44**: 6383–6391.

Shimizu Y, Inoue A, Tomari Y, Suzuki T, Yokogawa T, et al. (2001) Cell-free translation reconstituted with purified components. Nat Biotechnol **19**: 751–755.

Shu Q, Nair V (2008) Inosine monophosphate dehydrogenase (IMPDH) as a target in drug discovery. Med Res Rev **28**: 219–232.

Shumate JB, Katnik R, Ruiz M, Kaiser K, Frieden C, et al. (1979) Myoadenylate deaminase deficiency. Muscle & Nerve **2**: 213–216.

Sidik SM, Huet D, Ganesan SM, Huynh MH, Wang T, et al. (2016) A genome-wide CRISPR screen in *Toxoplasma* identifies essential apicomplexan genes. Cell **166**: 1423–1435.

Soga A, Ko-ketsu M, Fukumoto S (2018) Development of a bsd-blasticidin selection system in *Plasmodium berghei*. FEBS Lett **592**: 1847–1855.

Srinivasan B (2011) Structure function studies on three members of the haloacid dehalogenase (HAD) superfamily of enzymes. Ph.D. thesis, Jawaharlal Nehru Centre for Advanced Scientific.

Srinivasan B, Balaram H (2007) ISN1 nucleotidases and HAD superfamily protein fold: *in silico* sequence and structure analysis. In Silico Biol **7**: 187–193.

Srinivasan B, Nagappa LK, Shukla A, Balaram H (2015) Prediction of substrate specificity and preliminary kinetic characterization of the hypothetical protein PVX_123945 from *Plasmodium vivax*. Exp Parasitol **151**: 56–63.

Straimer J, Lee MC, Lee AH, Zeitler B, Williams AE, et al. (2012) Site-specific genome editing in *Plasmodium falciparum* using engineered zinc-finger nucleases. Nat Methods **9**: 993–998.

Sultan AA, Thathy V, de Koning-Ward TF, Nussenzweig V (2001) Complementation of *Plasmodium berghei* TRAP knockout parasites using human dihydrofolate reductase gene as a selectable marker. Mol Biochem Parasitol **113**: 151–156.

Taylor PL, Sugiman-Marangos S, Zhang K, Valvano MA, Wright GD, et al. (2010) Structural and kinetic characterization of the LPS biosynthetic enzyme d-α, β-d-heptose-1, 7-bisphosphate phosphatase (GmhB) from *Escherichia coli*. Biochemistry **49**: 1033–1041.

Timón-Gómez A, Proft M, Pascual-Ahuir A (2013) Differential regulation of mitochondrial pyruvate carrier genes modulates respiratory capacity and stress tolerance in yeast. PLoS One **8**: e79405.

Ting LM, Gissot M, Coppi A, Sinnis P, Kim K (2008) Attenuated *Plasmodium yoelii* lacking purine nucleoside phosphorylase confer protective immunity. Nat Med **14**: 954–958.

Titz B, Häuser R, Engelbrecher A, Uetz P (2007) The *Escherichia coli* protein YjjG is a house-cleaning nucleotidase *in vivo*. FEMS Microbiol Lett **270**: 49–57.

Trager W, Jensen JB (1976) Human malaria parasites in continuous culture. Science **193**: 673–675.

Van Schaftingen E, Rzem R, Marbaix A, Collard F, Veiga-da Cunha M, et al. (2013) Metabolite proofreading, a neglected aspect of intermediary metabolism. J Inherit Metab Dis **36**: 427–434.

Vander Jagt DL, Hunsaker LA, Campos NM, Baack BR (1990) D-lactate production in erythrocytes infected with *Plasmodium falciparum*. Mol Biochem Parasitol **42**: 277–284.

VanWye JD, Haldar K (1997) Expression of green fluorescent protein in *Plasmodium falciparum*. Mol Biochem Parasitol **2**: 225–229.

Waarde AV, Kesbeke F (1981) Regulatory properties of AMP-deaminase from lateral red muscle and dorsal white muscle of goldfish, Carassius auratus (L.). Comp Biochem Physiol **69**: 413–423.

Waters A, Thomas A, Van Dijk M, Janse C (1997) Transfection of malaria parasites. Methods **13**: 134–147.

Weiss B (2007) YjjG, a dUMP phosphatase, is critical for thymine utilization by *Escherichia coli* K-12. J Bacteriol **189**: 2186–2189.

Westheimer FH (1987) Why nature chose phosphates. Science **235**: 1173–1178.

WHO (2018) Fact Sheet: World Malaria Report. World Health Organization .

Wu Y, Kirkman LA, Wellems TE (1996) Transformation of *Plasmodium falciparum* malaria parasites by homologous integration of plasmids that confer resistance to pyrimethamine. Proc Natl Acad Sci USA **93**: 1130–1134.

Xu J, Zhang HY, Xie CH, Xue HW, Dijkhuis P, et al. (2005) Embryonic factor 1 encodes an AMP deaminase and is essential for the zygote to embryo transition in *Arabidopsis*. Plant J **42**: 743–758.

Xu Y, Eads J, Sacchettini JC, Grubmeyer C (1997) Kinetic mechanism of human hypoxanthine- guanine phosphoribosyltransferase: rapid phosphoribosyl transfer chemistry. Biochemistry **36**: 3700–3712.

Xue B, Dunbrack RL, Williams RW, Dunker AK, Uversky VN (2010) PONDR-FIT: a meta-predictor of intrinsically disordered amino acids. Biochim Biophys Acta **1804**: 996–1010.

Yeh I, Altman RB (2006) Drug Targets for *Plasmodium falciparum*: a post-genomic review/survey. Mini Rev Med Chem **6**: 177–202.

Yoshino M, Murakami K, Tsushima K (1979) AMP deaminase from baker's yeast. Purification and some regulatory properties. Biochim Biophys Acta **570**: 157–166.

Zhang M, Wang C, Otto TD, Oberstaller J, Liao X, et al. (2018) Uncovering the essential genes of the human malaria parasite *Plasmodium falciparum* by saturation mutagenesis. Science **360**: eaap7847.

Addendum to bibliography

Phillips MA, Rathod PK (2010) *Plasmodium* dihydroorotate dehydrogenase: a promising target for novel anti-malarial chemotherapy. Infect Disord Drug Targets **10:** 226–239.

Belen Cassera M, Zhang Y, Hazleton KZ, Schramm VL (2011) Purine and pyrimidine pathways as targets in *Plasmodium falciparum*. Curr Top Med Chem **11:** 2103–2115.

Gero AM, Dunn CG, Brown DM, Pulenthiran K, Gorovits EL, et al. (2003) New malaria chemotherapy developed by utilization of a unique parasite transport system. Curr Pharm Des **9:** 867–877.

Jiang L, Lee PC, White J, Rathod PK (2000) Potent and selective activity of a combination of thymidine and 1843U89, a folate-based thymidylate synthase inhibitor, against *Plasmodium falciparum*. Antimicrob Agents Chemother **44:** 1047–1050.

Kaiser MM, Baszczyňski O, Hocková D, Poštová-Slavětínská L, Dračínskỳ M, et al. (2017) Acyclic nucleoside phosphonates containing 9-deazahypoxanthine and a five-membered heterocycle as selective inhibitors of plasmodial 6-oxopurine phosphoribosyltransferases. ChemMedChem **12:** 1133–1141.

Keough DT, Hocková D, Holy A, Naesens LM, Skinner-Adams TS, et al. (2009) Inhibition of hypoxanthine-guanine phosphoribosyltransferase by acyclic nucleoside phosphonates: a new class of antimalarial therapeutics. J Med Chem **52:** 4391–4399.

Madrid DC, Ting LM, Waller KL, Schramm VL, Kim K (2008) *Plasmodium falciparum* purine nucleoside phosphorylase is critical for viability of malaria parasites. J Biol Chem **283:** 35899–35907.

McConkey GA (2000) *Plasmodium falciparum*: isolation and characterisation of a gene encoding protozoan GMP synthase. Exp Parasitol **94:** 23–32.

Seymour KK, Yeo A, Rieckmann KH, Christopherson RI (1997) dCTP levels are maintained in *Plasmodium falciparum* subjected to pyrimidine deficiency or excess. Ann Trop Med Parasit **91:** 603–609.

Seymour KK, Lyons SD, Phillips L, Rieckmann KH, Christopherson RI (1994) Cytotoxic effects of inhibitors of *de novo* pyrimidine biosynthesis upon *Plasmodium falciparum*. Biochemistry **33:** 5268–5274.

Slavic K, Krishna S, Derbyshire ET, Staines HM (2011) Plasmodial sugar transporters as anti-malarial drug targets and comparisons with other protozoa. Malar J **10:** 165.

Spacek P, Keough DT, Chavchich M, Dracinsky M, Janeba Z, et al. (2017) Synthesis and evaluation of asymmetric acyclic nucleoside bisphosphonates as inhibitors of *Plasmodium falciparum* and human hypoxanthine-guanine-xanthine phosphoribosyltransferase. J Med Chem **60:** 7539–7554.

Veletzky L, Rehman K, Lingscheid T, Poeppl W, Loetsch F, et al. (2014) *In vitro* activity of immunosuppressive drugs against *Plasmodium falciparum*. Malar J **13:** 476.

Webster H, Whaun J (1982) Antimalarial properties of bredinin. Prediction based on identification of differences in human host-parasite purine metabolism. J Clin Invest **70:** 461–469.